

NASA CONTRACTOR
REPORT



NASA CR-406

NASA CR-406

N66-23406
528
CR-406

27 ~~27~~ ~~27~~

GPO PRICE \$ _____

CFSTI PRICE(S) \$ 1.25

Hard copy (HC) _____

Microfiche (MF) 1.25

ff 653 July 65

SLOSH DESIGN HANDBOOK I

by James R. Roberts, Eduardo R. Basurto, and Pei-Ying Chen

Prepared under Contract No. NAS 8-11111 by
NORTHROP SPACE LABORATORIES
Huntsville, Ala.
for George C. Marshall Space Flight Center

SLOSH DESIGN HANDBOOK I

By James R. Roberts, Eduardo R. Basurto, and Pei-Ying Chen

Distribution of this report is provided in the interest of information exchange. Responsibility for the contents resides in the author or organization that prepared it.

Prepared under Contract No. NAS 8-11111 by
NORTHROP SPACE LABORATORIES
Huntsville, Ala.

for George C. Marshall Space Flight Center

NATIONAL AERONAUTICS AND SPACE ADMINISTRATION

For sale by the Clearinghouse for Federal Scientific and Technical Information
Springfield, Virginia 22151 - Price \$3.25

Foreword

This Handbook was prepared by Northrop Space Laboratories, Huntsville, Alabama, for the Dynamics and Analysis Section of the Aero-Astrodynamic Laboratory of the George C. Marshall Space Flight Center. Its contents represent a partial fulfillment of the project since additional topics are forthcoming which, upon completion, will be integrated into the Handbook.

Abstract

23466

Design information related to the effects of propellant sloshing is presented for use in both control and structural problems. Both analytical and experimental results are given and all pertinent material is referenced. Graphs have been included, whenever possible, to expedite preliminary design calculations. The areas covered are: (1) linearized fluid theory, (2) equivalent mechanical model theory, (3) results of analytical studies of liquid oscillations in variously shaped containers when subjected to different types of excitation, i.e., boundary conditions, fluid velocity potentials, natural frequencies, liquid force and moment resultants and equivalent mechanical models, and (4) results of both analytical and experimental studies concerned with propellant slosh suppression, with particular emphasis on fixed-ring baffles.

Author

SLOSH DESIGN HANDBOOK

Table of Contents

Foreword.....	iii
Abstract.....	iv
Definition of Symbols and Parameters.....	vi
I. Introduction.....	1-1
II. Linearized Fluid Theory.....	2-1
III. Equivalent Mechanical Model Theory.....	3-1
IV. Rigid Tanks.....	4-1
4.1 Introduction.....	4-1
4.2 Circular Cylindrical Tank.....	4-3
4.3 Sector Tank.....	4-37
4.4 Quarter-Sectored Tank.....	4-49
4.5 Eighth-Sectored Tank.....	4-76
4.6 Annular Tank.....	4-86
4.7 Annular-Sector Tank.....	4-112
4.8 Rectangular Tank.....	4-126
V. Propellant Slosh Suppression.....	5-1
5.1 Anti-Slosh Devices.....	5-1
Appendix.....	A-1
References.....	B-1

NOTATION

a	-	Radius of circular cylindrical tank Outer radius of annular or annular-sector tank Length of rectangular tank in x-direction
a_o	-	Inner radius of ring baffle
b	-	Inner radius of annular or annular-sector tank
C_D	-	Local drag coefficient
c	-	Radial clearance between tank wall and ring baffle
\bar{c}	-	Effective damping coefficient
c_d	-	Damping coefficient of disc
c_n	-	Damping coefficient of n^{th} slosh mass
$c.g.$	-	Center of gravity of undisturbed liquid
D	-	Baffle spacing Tank diameter
d	-	Tank diameter Depth of baffle below undisturbed free surface
d_s	-	Depth of baffle below undisturbed free surface
d^*	-	Distance of baffle above the undisturbed free surface, $D - d$
F_{q_i}	-	Force in q_i -direction
\bar{F}	-	Dimensionless liquid force, $F/\rho g a^3$
$F(s)$	-	Laplace transform of the force F
$F(t)$	-	Arbitrary function of time
g	-	Acceleration due to gravity
\bar{g}_n	-	Damping factor of n^{th} liquid mode
H_n	-	z-coordinate for point of attachment of n^{th} pendulum
h	-	Depth of liquid measured from tank bottom
h_n	-	z-coordinate of n^{th} slosh mass
I	-	Mass moment of inertia of fixed mass

NOTATION (continued)

\bar{I}	-	Effective mass moment of inertia of fluid
I_d	-	Mass moment of inertia of disc
I_{mn}	-	Mass moment of inertia of mn^{th} slosh mass
I_s	-	Mass moment of inertia of solidified fluid
i	-	Imaginary unit
\hat{i}	-	Unit vector in x-direction
J	-	Mass moment of inertia of fixed mass
\bar{J}	-	Effective mass moment of inertia of fluid
J_{mn}	-	Mass moment of inertia of mn^{th} slosh mass
$J_\nu(\beta)$	-	Bessel function of the 1^{st} kind of order ν and argument β
$J'_\nu(\beta)$	-	First derivative of $J_\nu(\beta)$ with respect to the argument β
\hat{j}	-	Unit vector in y-direction
K_{mn}	-	Torsional stiffness coefficient of shaft
k	-	Ratio of inner to outer radius of annular or annular-sector tank, b/a
\hat{k}	-	Unit vector in z-direction
L_n	-	Pendulum length
M	-	Fixed mass
M_n	-	Magnitude of moment after n cycles
M_o	-	Magnitude of initial moment
M_{q_i}	-	Moment about q_i -axis
$M(s)$	-	Laplace transform of the moment M
$M_B(s)$	-	Laplace transform of the moment M on the baffle
m	-	Mode of vibration in the ϕ -direction or y-direction
m_L	-	Liquid mass

NOTATION (continued)

m_n	-	n^{th} slosh mass
n	-	Normal direction Mode of vibration in the r-direction or x-direction Number of baffles
P_{q_i}	-	Pressure in the q_i -direction
P_o	-	Gauge pressure
q_i	-	Generalized coordinate
R	-	Radius of circular cylindrical tank
r	-	Cylindrical coordinate, (r, ϕ, z)
r_1	-	Aspect ratio in xz-plane for rectangular tank, h/a
r_2	-	Aspect ratio in yz-plane for rectangular tank, h/b
r_3	-	Aspect ratio in xy-plane for rectangular tank, a/b
S, s	-	Laplace transform variable
T	-	Period of oscillation
t	-	Time
U	-	Potential function
U_m	-	Timewise maximum fluid velocity
\vec{u}	-	Rotation vector for vorticity, $\xi \hat{i} + \eta \hat{j} + \zeta \hat{k}$
u	-	Velocity component in x-direction
\vec{V}	-	Velocity vector, $u \hat{i} + v \hat{j} + w \hat{k}$
\vec{V}_n	-	Velocity component normal to tank wall
\vec{V}_1	-	Velocity of container
v	-	Velocity component in y-direction
W, w	-	Baffle width measured normal to tank wall
w	-	Velocity component in z-direction
x	-	Rectangular coordinate, (x, y, z) Displacement in x-direction

NOTATION (continued)

- x_n - Translational displacement of n^{th} slosh mass
- X_o, x_o - Amplitude of displacement function, $x = x_o e^{i\omega t}$ or $x = x_o \sin\omega t$
- $x(s)$ - Laplace transformed rectangular coordinate
- $Y_\nu(\beta)$ - Bessel function of the 2^{nd} kind of order ν and argument β
- $Y'_\nu(\beta)$ - First derivative of $Y_\nu(\beta)$ with respect to argument β
- y - Rectangular coordinate, (x,y,z)
Translational displacement in y -direction
- y_o - Amplitude of displacement function, $y = y_o e^{i\omega t}$
- z - Rectangular coordinate, (x,y,z)
Cylindrical coordinate, (r,ϕ,z)

Note: The notation given in articles 5.1.5.2 and 5.1.7.3 is applicable to these articles only.

GREEK LETTERS

α	-	Ratio of apex angle to 2π , $\alpha/2\pi$ Baffle width parameter in Miles' equation, $2a/W$
$\bar{\alpha}$	-	Apex angle of sector tank or similar configuration Effective baffle area for a baffle located below the undisturbed free surface
$\bar{\alpha}^*$	-	Effective baffle area for a baffle located above the undisturbed free surface
β_{mn}	-	Angular displacement of m^{th} slosh mass
Γ_n	-	Generalized coordinate, $\lambda_n - \theta$
ϵ_ν, ξ_ν	-	Roots of an eigenfunction where $\nu = mn, n$ or $(2m-1, n)$
γ, γ_s, δ	-	Damping factor or damping ratio
ζ, ζ_w, ζ_1	-	Surface displacement of liquid generally measured at tank wall
η_ν	-	Ratio of natural angular frequency to forcing frequency, ω_ν/ω , where $\nu = mn, n$, or $(2m-1, n)$
θ	-	Angular displacement of tank for pitching about y-axis
θ_0	-	Amplitude of displacement function, $\theta = \theta_0 e^{i\omega t}$ or $\theta = \theta_0 \sin\omega t$
$\theta(s)$	-	Laplace transform of the displacement θ
λ_n	-	Angular displacement of n^{th} pendulum
μ	-	Viscosity of liquid
ρ	-	Mass density of liquid
ϕ	-	Total velocity potential, $\phi_1 + \phi_2$
ϕ_1	-	Velocity potential of container
ϕ_2	-	Velocity potential of liquid
ϕ	-	Cylindrical coordinate, (r, ϕ, z) Angular displacement for roll about z-axis
ϕ_0	-	Amplitude of displacement function, $\phi = \phi_0 e^{i\omega t}$ or $\phi = \phi_0 \sin\omega t$

GREEK LETTERS (continued)

- χ - Angular displacement for pitching about x-axis
- χ_0 - Amplitude of displacement function, $\chi = \chi_0 e^{i\omega t}$
- ψ - Angular displacement of disc relative to tank
- ω - Forcing frequency
- ω_ν - Natural angular frequency for free liquid oscillations
where $\nu = mn, n,$ or $(2m-1, n)$
- $\Gamma(\nu)$ - Gamma function of argument ν

SPECIAL DEFINITIONS

$$\gamma_v = (\epsilon_v \text{ or } \xi_v) g / a \omega^2$$

$$\kappa_v = (\epsilon_v \text{ or } \xi_v) \frac{h}{a}$$

$$\rho_v = (\epsilon_v \text{ or } \xi_v) \frac{r}{a}$$

$$\sigma_v = (\epsilon_v \text{ or } \xi_v) k$$

$$\zeta_v = (\epsilon_v \text{ or } \xi_v) \frac{z}{a}$$

where $v = mn, m, n, \text{ or } (2m-1, n)$

$$\bar{\phi}_m = \frac{m}{2\alpha} \phi,$$

$$\bar{\phi}_m = \frac{2m-1}{2\alpha} \phi$$

DEFINITION OF PARAMETERS

Sector Tank

$$\begin{pmatrix} \bar{A}_{mn} \\ \bar{C}_{mn} \end{pmatrix} = \frac{a \bar{b}_{mn}}{\epsilon_{mn} (\eta_{mn}^2 - 1) \cosh \kappa_{mn}} \begin{pmatrix} a_m \\ c_m \end{pmatrix} \left[2 \sinh \frac{\kappa_{mn}}{2} - \left(\gamma_{mn} + \frac{\kappa_{mn}}{2} \right) \cosh \frac{\kappa_{mn}}{2} \right]$$

$$\begin{pmatrix} \bar{B}_{mn} \\ \bar{D}_{mn} \end{pmatrix} = \frac{a \bar{b}_{mn}}{\epsilon_{mn} (\eta_{mn}^2 - 1) \cosh \kappa_{mn}} \begin{pmatrix} a_m \\ c_m \end{pmatrix} \left[\left(\gamma_{mn} - \frac{\kappa_{mn}}{2} \right) \sinh \frac{\kappa_{mn}}{2} - 2 \cosh \frac{\kappa_{mn}}{2} \right]$$

$$a_m = \frac{\sin \bar{\alpha}}{\bar{\alpha}}, \quad m = 0$$

$$a_m = \frac{2\bar{\alpha}(-1)^{m+1} \sin \bar{\alpha}}{m^2 \pi^2 - \bar{\alpha}^2}, \quad m = 1, 2, 3, \dots$$

$$\bar{b}_{mn} = \frac{2a \Gamma(m/4\alpha + 3/2)}{\epsilon_{mn} (1 - m^2/4\alpha^2 \epsilon_{mn}^2) \Gamma(m/4\alpha - 1/2) J_{m/2\alpha}^2(\epsilon_{mn})} \cdot \sum_{\mu=0}^{\infty} \frac{(m/2\alpha + 2\mu + 1) \Gamma(m/4\alpha + \mu - 1/2)}{\Gamma(m/4\alpha + \mu + 5/2)} J_{m/2\alpha + 2\mu + 1}(\epsilon_{mn})$$

$$c_m = \frac{1 - \cos \bar{\alpha}}{\bar{\alpha}}, \quad m = 0$$

$$c_m = \frac{2\bar{\alpha}(-1)^m \cos \bar{\alpha} - 1}{m^2 \pi^2 - \bar{\alpha}^2}, \quad m = 1, 2, 3, \dots$$

Sector Tank (Continued)

$$\bar{e}_{2m-1,n} = \frac{2 \left[(2m-1)/4\alpha \right] \left[(2m-1)/4\alpha + 1 \right] \left[(2m-1)/4\alpha - 1 \right] \epsilon_{2m-1,n}}{\left\{ \epsilon_{2m-1,n}^2 - \left[(2m-1)/2\alpha \right]^2 \right\} J_{(2m-1)/2\alpha}^2(\epsilon_{2m-1,n})} \cdot$$

$$\sum_{\mu=0}^{\infty} \frac{\left[(2m-1)/2\alpha + 2\mu + 1 \right] J_{(2m-1)/2\alpha + 2\mu + 1}(\epsilon_{2m-1,n})}{\left[(2m-1)/2\alpha + \mu \right] \left[(2m-1)/2\alpha + \mu + 1 \right] \left[(2m-1)/2\alpha + \mu + 2 \right] \left[(2m-1)/2\alpha + \mu - 1 \right]}$$

$$\bar{f}_{2m-1,n} = \frac{2 \left[(2m-1)/2\alpha \right]}{\left\{ \epsilon_{2m-1,n}^2 - \left[(2m-1)/2\alpha \right]^2 \right\} J_{(2m-1)/2\alpha}(\epsilon_{2m-1,n})}$$

$$L_0(\epsilon_{mn}) = \frac{2}{\epsilon_{mn}} \sum_{\mu=0}^{\infty} J_{m/2\alpha + 2\mu + 1}(\epsilon_{mn}) \quad \left(\text{Re } \frac{m}{2\alpha} > 1 \right)$$

$$L_0(\epsilon_{2m-1,n}) = \frac{2}{\epsilon_{2m-1,n}} \sum_{\mu=0}^{\infty} J_{(2m-1)/2\alpha + 2\mu + 1}(\epsilon_{2m-1,n}) \quad \left[\text{Re } (2m-1)/2\alpha > 1 \right]$$

$$L_1(\epsilon_{2m-1,n}) = \frac{2m-1}{4\alpha \epsilon_{2m-1,n}} \sum_{\mu=0}^{\infty} \frac{\left[(2m-1)/2\alpha + 2\mu + 1 \right]}{\left[(2m-1)/4\alpha + \mu \right] \left[(2m-1)/4\alpha + \mu + 1 \right]} \cdot$$

$$J_{(2m-1)/2\alpha + 2\mu + 1}(\epsilon_{2m-1,n})$$

$$L_2(\epsilon_{mn}) = \frac{\Gamma(m/2\alpha + 3/2)}{\epsilon_{mn} \Gamma(m/4\alpha - 1/2)} \sum_{\mu=0}^{\infty} \frac{(m/2\alpha + 2\mu + 1) \Gamma(m/2\alpha + \mu - 1/2)}{\Gamma(m/4\alpha + \mu + 5/2)} J_{m/2\alpha + 2\mu + 1}(\epsilon_{mn})$$

$$L_2(\epsilon_{2m-1,n}) = \frac{\Gamma \left[(2m-1)/2\alpha + 3/2 \right]}{\epsilon_{2m-1,n} \Gamma \left[(2m-1)/4\alpha - 1/2 \right]} \sum_{\mu=0}^{\infty} \frac{\left[(2m-1)/2\alpha + 2\mu + 1 \right] \Gamma \left[(2m-1)/4\alpha + \mu - 1/2 \right]}{\Gamma \left[(2m-1)/4\alpha + \mu + 5/2 \right]} \cdot$$

$$J_{2m-1/2\alpha + 2\mu + 1}(\epsilon_{2m-1,n})$$

Quarter-Sectored Tank

$$\bar{A}_{mn} = \frac{a \bar{a}_m \bar{b}_{mn}}{\epsilon_{mn} (n_{mn}^2 - 1) \cosh \kappa_{mn}} \left[2 \sinh \frac{\kappa_{mn}}{2} - \left(\frac{\kappa_{mn}}{2} + \gamma_{mn} \right) \cosh \frac{\kappa_{mn}}{2} \right]$$

$$\bar{a}_m = \frac{2}{\pi}, \quad m = 0$$

$$\bar{a}_m = \frac{(-1)^{m+1}}{\pi(m^2 - 1/4)}, \quad m = 1, 2, 3, \dots$$

$$\bar{B}_{mn} = \frac{a \bar{a}_m \bar{b}_{mn}}{\epsilon_{mn} (n_{mn}^2 - 1) \cosh \kappa_{mn}} \left[\left(\gamma_{mn} - \frac{\kappa_{mn}}{2} \right) \sinh \frac{\kappa_{mn}}{2} - 2 \cosh \frac{\kappa_{mn}}{2} \right]$$

$$\bar{b}_{mn} = \frac{16a(m^2 - 1/4) \epsilon_{mn}}{(\epsilon_{mn}^2 - 4m^2) J_2^2(\epsilon_{mn})} \sum_{\mu=0}^{\infty} \frac{J_{2m+2\mu+1}(\epsilon_{mn})}{(2m+2\mu+3)(2m+2\mu-1)}$$

$$e_n = \frac{4}{(\epsilon_n^2 - 4) J_2(\epsilon_n)}$$

$$e_{2m-1,n} = \frac{2m(2m-1)\epsilon_{2m-1,n}}{(m-1) \left[\epsilon_{2m-1,n}^2 - 4(2m-1)^2 \right] J_{4m-2}^2(\epsilon_{2m-1,n})} \sum_{\mu=0}^{\infty} \frac{(4m+2\mu-1) J_{4m+2\mu-1}(\epsilon_{2m-1,n})}{(2m+\mu)(2m+\mu+1)(2m+2\mu-1)(2m+2\mu-2)}$$

$$f_n = \frac{-8}{(\epsilon_n^2 - 4) J_2^2(\epsilon_n)} \sum_{\mu=0}^{\infty} \frac{J_{2\mu+4}(\epsilon_n)}{(\mu+1)(\mu+3)}$$

Quarter-Sectorred Tank (Continued)

$$f_{2m-1,n} = \frac{4(2m-1)}{\left[\epsilon_{2m-1,n}^2 - 4(2m-1)^2 \right] J_{4m-2}(\epsilon_{2m-1,n})}$$

$$L_0(\epsilon_n) = \frac{2}{\epsilon_n} \sum_{\mu=0}^{\infty} J_{3+2\mu}(\epsilon_n)$$

$$L_0(\epsilon_{mn}) = \frac{2}{\epsilon_{mn}} \sum_{\mu=0}^{\infty} J_{2m+2\mu+1}(\epsilon_{mn}) \quad (\text{Re } 2m > -1)$$

$$L_0(\epsilon_{2m-1,n}) = \frac{2}{\epsilon_{2m-1,n}} \sum_{\mu=0}^{\infty} J_{4m+2\mu-1}(\epsilon_{2m-1,n})$$

$$L_1(\epsilon_n) = \frac{1}{\epsilon_n} \sum_{\mu=0}^{\infty} \frac{2\mu+3}{(\mu+1)(\mu+2)} J_{2\mu+3}(\epsilon_n)$$

$$L_1(\epsilon_{2m-1,n}) = \frac{2m-1}{\epsilon_{2m-1,n}} \sum_{\mu=0}^{\infty} \frac{4m+2\mu-1}{(2m+\mu-1)(2m+\mu)} J_{4m+2\mu-1}(\epsilon_{2m-1,n})$$

$$L_2(\epsilon_n) = \frac{\Gamma(7/2)}{\epsilon_n \Gamma(3/2)} \sum_{\mu=0}^{\infty} \frac{(2\mu+3)\Gamma(\mu+1/2)}{\Gamma(\mu+7/2)} J_{2\mu+3}(\epsilon_n)$$

$$L_2(\epsilon_{mn}) = \frac{2(4m^2-1)}{\epsilon_{mn}} \sum_{\mu=0}^{\infty} \frac{J_{2m+2\mu+1}(\epsilon_{mn})}{(2m+2\mu+3)(2m+2\mu-1)}$$

$$L_2(\epsilon_{2m-1,n}) = \frac{2(4m-1)(4m-3)}{\epsilon_{2m-1,n}} \sum_{\mu=0}^{\infty} \frac{J_{4m+2\mu-1}(\epsilon_{2m-1,n})}{(4m+2\mu+1)(4m+2\mu-3)}$$

Eighth-Sectored Tank

$$\bar{\epsilon}_{mn} = \frac{4m(4m^2-1) \epsilon_{mn}}{(\epsilon_{mn}^2 - 16m^2) J_{4m}^2(\epsilon_{mn})} \sum_{\mu=0}^{\infty} \frac{(4m+2\mu+1) J_{4m+2\mu+1}(\epsilon_{mn})}{(2m+\mu)(2m+\mu+1)(2m+\mu-1)(2m+\mu+2)}$$

$$\bar{f}_{mn} = \frac{8m}{(\epsilon_{mn}^2 - 16m^2) J_{4m}(\epsilon_{mn})}$$

$$L_2(\epsilon_{mn}) = \frac{2m}{\epsilon_{mn}} \sum_{\mu=0}^{\infty} \frac{(4m+2\mu+1) J_{4m+2\mu+1}(\epsilon_{mn})}{(2m+\mu)(2m+\mu+1)}$$

Annular Tank

$$A_n = \frac{2[2/\pi \xi_n - k C_1(\sigma_n)]}{(4/\pi^2 \xi_n^2)(\xi_n^2 - 1) + C_1^2(\sigma_n)(1 - \sigma_n^2)} \quad C_1(\rho_n) = J_1(\xi_n \frac{r}{a}) Y_1'(\xi_n) - J_1'(\xi_n) Y_1(\xi_n \frac{r}{a})$$

$$C_1(\sigma_n) = J_1(\xi_n k) Y_1'(\xi_n) - J_1'(\xi_n) Y_1(\xi_n k)$$

$$C_{m/2\alpha}(\rho_{mn}) = J_{m/2\alpha}(\xi_{mn} \frac{r}{a}) Y_{m/2\alpha}'(\xi_{mn}) - J_{m/2\alpha}'(\xi_{mn}) Y_{m/2\alpha}(\xi_{mn} \frac{r}{a})$$

$$C_{m/2\alpha}(\sigma_{mn}) = J_{m/2\alpha}(\xi_{mn} k) Y_{m/2\alpha}'(\xi_{mn}) - J_{m/2\alpha}'(\xi_{mn}) Y_{m/2\alpha}(\xi_{mn} k)$$

$C_{(2m-1)/2\alpha}(\rho_{2m-1,n}) = C_{m/2\alpha}(\rho_{mn})$ given above if whenever m occurs, it is replaced by $(2m-1)$

Annular-Sector Tank

$$\begin{pmatrix} A \\ C_{mn} \end{pmatrix} = \frac{a b_{mn}}{\xi_{mn} (\eta_{mn}^2 - 1) \cosh \kappa_{mn}} \begin{pmatrix} a \\ c_m \end{pmatrix} \left[2 \sinh \frac{\kappa_{mn}}{2} - \left(\frac{\kappa_{mn}}{2} + \gamma_{mn} \right) \cosh \frac{\kappa_{mn}}{2} \right]$$

$$\begin{pmatrix} B \\ D_{mn} \end{pmatrix} = \frac{a b_{mn}}{\xi_{mn} (\eta_{mn}^2 - 1) \cosh \kappa_{mn}} \begin{pmatrix} a \\ c_m \end{pmatrix} \left[\left(\gamma_{mn} - \frac{\kappa_{mn}}{2} \right) \sinh \frac{\kappa_{mn}}{2} - 2 \cosh \frac{\kappa_{mn}}{2} \right]$$

$$a_m = \frac{\sin \alpha}{\bar{\alpha}}, \quad m = 0$$

$$a_m = \frac{2\bar{\alpha}(-1)^{m+1} \sin \bar{\alpha}}{m^2 \pi^2 - \bar{\alpha}^2}, \quad m = 1, 2, 3, \dots$$

Annular-Sector Tank (continued)

$$b_{mn} = \frac{2a N_2(\xi_{mn})}{\left[\frac{4}{\pi^2} \xi_{mn}^2 - k^2 C_{m/2\alpha}^2(\sigma_{mn}) \right] - (m^2/4\alpha^2 \xi_{mn}^2) \left[\frac{4}{\pi^2} \xi_{mn}^2 - C_{m/2\alpha}^2(\sigma_{mn}) \right]}$$

$$c_m = \frac{1 - \cos \bar{\alpha}}{\bar{\alpha}}, \quad m = 0$$

$$c_m = \frac{2\bar{\alpha} [(-1)^m \cos \bar{\alpha} - 1]}{m^2 \pi^2 - \bar{\alpha}^2}, \quad m = 1, 2, 3, \dots$$

$$g_{2m-1,n} = \frac{\int_{\sigma_{2m-1,n}}^{\xi_{2m-1,n}} \rho_{2m-1,n}^3 C_{(2m-1)/2\alpha}(\rho_{2m-1,n}) d\rho_{2m-1,n}}{\xi_{2m-1,n}^2 \int_{\sigma_{2m-1,n}}^{\xi_{2m-1,n}} \rho_{2m-1,n}^2 C_{(2m-1)/2\alpha}(\rho_{2m-1,n}) d\rho_{2m-1,n}}$$

$$h_{2m-1,n} = \frac{\int_{\sigma_{2m-1,n}}^{\xi_{2m-1,n}} \rho_{2m-1,n}^{1+(2m-1)/2\alpha} C_{(2m-1)/2\alpha}(\rho_{2m-1,n}) d\rho_{2m-1,n}}{\xi_{2m-1,n}^{(2m-1)/2\alpha} \int_{\sigma_{2m-1,n}}^{\xi_{2m-1,n}} \rho_{2m-1,n}^2 C_{(2m-1)/2\alpha}(\rho_{2m-1,n}) d\rho_{2m-1,n}}$$

$$q_{2m-1,n} = \frac{\xi_{2m-1,n}^{(2m-1)/2\alpha} \int_{\sigma_{2m-1,n}}^{\xi_{2m-1,n}} \rho_{2m-1,n}^{1-(2m-1)/2\alpha} C_{(2m-1)/2\alpha}(\rho_{2m-1,n}) d\rho_{2m-1,n}}{\int_{\sigma_{2m-1,n}}^{\xi_{2m-1,n}} \rho_{2m-1,n}^2 C_{(2m-1)/2\alpha}(\rho_{2m-1,n}) d\rho_{2m-1,n}}$$

Annular-Sector Tank (continued)

$$N_j(\xi_{mn}) = Y'_{m/2\alpha}(\xi_{mn}) \frac{\Gamma(m/4\alpha+1/2+j/2)}{\xi_{mn} \Gamma(m/4\alpha+1/2-j/2)} \sum_{\mu=0}^{\infty} \frac{(m/2\alpha+2\mu+1)\Gamma(m/4\alpha+\mu+1/2-j/2)}{\Gamma(m/4\alpha+\mu+3/2+j/2)} .$$

$$\begin{aligned} & \left[J_{m/2\alpha+2\mu-1}(\xi_{mn}) - k^j J_{m/2\alpha+2\mu+1}(k\xi_{mn}) \right] \\ & + J'_{m/2\alpha}(\xi_{mn}) \left\{ \frac{1}{\pi} \sum_{\mu=0}^{\left(\frac{m}{2}-1\right)} \frac{\xi_{mn}^{2\mu-m/2\alpha} (m/2\alpha-\mu-1)! (1-k)^{2\mu-m/2\alpha+1+j}}{(2\mu-m/2\alpha+1+j) 2^{2\mu-m/2\alpha}} \right. \\ & + \frac{2}{\pi} \sum_{\mu=0}^{\infty} \frac{(-1)^\mu (1-k)^{m/2\alpha+2\mu-1+j} \xi_{mn}^{m/2\alpha+2\mu}}{\mu! (m/2\alpha+\mu)! (m/2\alpha+2\mu+1+j) 2^{m/2\alpha+\mu}} \\ & \left. + \frac{2k^{j+1}}{\pi} \sum_{\mu=0}^{\infty} \frac{(-1)^\mu (k\xi_{mn})^{m/2\alpha+2\mu}}{\mu! (m/2\alpha+\mu)! (m/2\alpha+2\mu+1+j) 2^{m/2\alpha+2\mu}} \right. . \end{aligned}$$

$$\begin{aligned} & \left[\ln\left(\frac{k\xi_{mn}}{2}\right) - \frac{1}{2} \psi(\mu+1) - \frac{1}{2} \psi\left(\frac{m}{2\alpha} + \mu+1\right) \right] \\ & - \frac{2}{\pi} \sum_{\mu=0}^{\infty} \frac{(-1)^\mu \xi_{mn}^{m/2\alpha+2\mu}}{\mu! (m/2\alpha+\mu)! (m/2\alpha+2\mu+1+j) 2^{m/2\alpha+2\mu}} . \end{aligned}$$

$$\left[\ln\left(\frac{\xi_{mn}}{2}\right) - \frac{1}{2} \psi(\mu+1) - \frac{1}{2} \psi(m/2\alpha+\mu+1) \right] \left. \right\} , \quad j = 0, 1, 2, \dots$$

where $\psi(z) = \frac{d \ln \Gamma(z)}{dz} = -\gamma + (z-1) \sum_{\lambda=0}^{\infty} \frac{1}{(\lambda+1)(\lambda+z)}$

z is the argument, $(\mu+1)$ and $(m/2\alpha+\mu+1)$ is the above equation.

$\gamma = 0.5772157$ is Euler's constant.

$N_j(\xi_{2m-1,n}) = N_j(\xi_{mn})$ if in the above equation for $N_j(\xi_{mn})$, m is

replaced by $(2m-1)$.

I. Introduction

Fuel sloshing is defined as any periodic motion of a contained liquid propellant and results from the missile's oscillatory motion about its flight trajectory. The most likely causes of such disturbances are gust loads, control modes, and structural modes. If any of these excitations have frequencies in the vicinity of the resonant frequency of a contained liquid, violent sloshing will occur. Since fuel and oxidizer amount to an extremely high percentage of the gross vehicle weight, the magnitudes of the liquid force and moment resultants are significant and cannot be neglected. A thorough knowledge of the magnitude and location of the external forces and moments acting on a space vehicle is required for making stability and structural investigations. Consequently, the effects of liquid propellants on their containers while undergoing forced vibrations have been investigated both analytically and experimentally. The results of such studies are found in Chapter IV.

The stability of a missile can be increased by reducing the force and moment resultants caused by the oscillating propellant and increasing the sloshing frequency. Increasing the eigen frequencies of the liquid decreases the depth below the surface to which the disturbances extend. The above fact can be accomplished by utilizing longitudinal partitions which effectively reduce the sloshing liquid mass and increase the frequencies of liquid oscillations. Also various types of baffles and floats can be used to help damp liquid motion. To evaluate the effectiveness of such anti-slosh devices, its damping factor and effect on the eigen frequencies of the fluid need to be known. Consequently, there has been a considerable amount of analytical and experimental work done in this area. The results of such investigations are found in Chapter V.

The exact formulation and solution to the problem of oscillations of a contained liquid with a free surface are extremely complex. To simplify the matter, it is convenient to assume that the fluid is nonviscous and the flow is irrotational, thereby permitting the use of potential theory. The problem then reduces to obtaining the velocity potential from Laplace's equation solved with the appropriate boundary conditions.

The overall problem of missile stability can be investigated more easily if the liquid is replaced with a dynamically equivalent mechanical model. The equations of motion for a model are derivable from either Lagrange's equations or simple equilibrium theory and from these equations, the force and moment resultants can be obtained. The characteristics of the model are then determined so that the force and moment resultants, frequencies of oscillation, and mass and inertial characteristics are identically equal to those of the liquid. Also by using equivalent mechanical models, the nonlinear nature of forced damped liquid oscillations can be approximated by equivalent linear damping. This makes it possible to obtain finite results near the resonant frequencies of the liquid, which was not possible in the fluid analysis, since the liquid was assumed to be inviscid.

II. Fluid Theory (9)

2.1 Assumptions

The difficulty in formulating and obtaining the exact solution to the problem of oscillations of a contained liquid is simplified by making several assumptions concerning the nature of the fluid and the type of flow encountered. These assumptions are: (1) the fluid is both incompressible ($\rho = \text{constant}$) and frictionless ($\mu = 0$), (2) the flow is irrotational ($\vec{u} = 0$), and (3) there are no sources or sinks; that is, the container is neither draining nor filling.

2.2 Basic Equations

Irrotationality is a necessary and sufficient condition that the velocity \vec{V} can be expressed as the gradient of a velocity potential ϕ , that is,

$$\nabla\phi = \vec{V} \quad (2-1)$$

Because of incompressibility and the nonexistence of sources and sinks, the equation of continuity reduces to Laplace's equation,

$$\nabla^2\phi = 0 \quad (2-2)$$

For an incompressible and frictionless fluid, irrotational flow, and conservative body forces, those forces derivable from a potential function, Bernoulli's energy equation is

$$\frac{p}{\rho} + \frac{\vec{V}^2}{2} + U + \frac{\partial\phi}{\partial t} = F(t)$$

where U is a potential function. Since gravity is the only important body force, then $U = gz$, and since the velocity is assumed to be small, the term containing \vec{v}^2 is neglected. Also since any arbitrary function of time can be added to the velocity potential without changing the flow it represents, the function $F(t)$ can be conveniently absorbed by ϕ . Consequently, the equation of motion reduces to

$$\frac{F}{\rho} + gz + \frac{\partial \phi}{\partial t} = 0 \quad (2-3)$$

From this expression, the pressure p is found to be

$$p = -\rho \left[\frac{\partial \phi}{\partial t} + gz \right] \quad (2-4)$$

For zero or uniform surface gauge pressure ($p = 0$ or $p = p_0 = \text{const.}$) the surface displacements can be found as follows:

$$z_{\text{surface}} = z = \zeta = -\frac{1}{g} \frac{\partial \phi}{\partial t} \quad (2-5)$$

where, in the case of uniform surface gauge pressure, the constant $\frac{p_0}{\rho}$ is absorbed by ϕ . The resultant liquid force acting on a container is then given by

$$F_{q_i} = \int_A p_{q_i} dA \quad (2-6)$$

where q_i is a generalized coordinate and F_{q_i} and p_{q_i} are components of the force and pressure distributions in the q_i -direction. Taking the z -axis to be the longitudinal axis of the container, the resultant liquid moment about a line perpendicular to the xz -plane and passing through the point $(0,0,\bar{z})$ is given by

$$M_{z=\bar{z}} = \int_{A_{\text{SIDE}}} p_{q_i} (z + \bar{z}) dA + \int_{A_{\text{BOTTOM}}} p_{q_i} x dA \quad (2-7)$$

2.3 Boundary Conditions

2.3.1 Velocity Potential. The total velocity potential ϕ is composed of two parts: ϕ_1 , the velocity potential of the container which is assumed to be small and ϕ_2 , the velocity potential of the liquid. These potentials must satisfy Laplace's equation in the following manner:

$$\nabla^2 \phi = \nabla^2(\phi_1 + \phi_2) = 0 \quad (2-8)$$

Since for a particular excitation the container velocity is known, the velocity potential of the container can easily be determined from equation (2-1)

$$\nabla \phi_1 = \vec{V}_1 \quad (2-9)$$

where the resulting constant of integration can be absorbed by ϕ_2 .

2.3.2 Free Oscillations. Consideration of free oscillations is necessary in order to determine the natural frequencies of liquids in variously shaped containers. For the occurrence of free liquid oscillations, the container must be at rest ($\vec{V}_1 = 0$), thus $\phi_1 = \text{constant}$. Consequently, $\phi = \phi_2$ since the constant can be absorbed by ϕ_2 . In order to avoid separation over the wetted surface, the velocity of the fluid normal to the container wall must be identical to that of the container itself, that is,

$$\frac{\partial \phi_2}{\partial n} = \vec{V}_n = 0 \quad (2-10)$$

Also, the pressure variation over the free surface must be equal to zero. Accordingly, the linearized free surface condition is

$$\frac{\partial^2 \phi_2}{\partial t^2} + g \frac{\partial \phi_2}{\partial z} = 0 \quad (2-11)$$

2.3.2 Forced Oscillations. When the container is subjected to harmonic excitation, the total velocity potential, $\phi = \phi_1 + \phi_2$, must be considered. Since over the wetted surface the normal velocity of the fluid must be the same as that of the container, it follows that

$$\frac{\partial \phi}{\partial n} = \vec{V}_n \quad (2-12)$$

The linearized free surface condition corresponding to zero pressure variation at the free surface is

$$\frac{\partial^2 \phi}{\partial t^2} + g \frac{\partial \phi}{\partial z} = 0 \quad (2-13)$$

The free surface boundary condition is actually composed of both a zero-pressure variation condition and a kinematic condition. In the kinematic condition, second and higher order terms were neglected thereby linearizing the free surface boundary condition. When the amplitude of the fluid is large relative to the tank dimensions, the effect of nonlinearity can become important, i.e., the magnitude of the higher order effects might not be negligible. Therefore, in order that the slope of the free surface be small, the resulting frequency of fluid oscillation must not be in the immediate neighborhood of a natural free surface frequency. Even so, relatively large amplitudes are possible when the container is also large. Also, it should be noted that the free surface condition given here and in Article 2.3.2 above is valid only in the case of a constant gravitational field. Consequently, the information presented in this handbook is applicable only for ground test applications.

The expression for the natural frequencies for free liquid oscillations is as follows:

$$\omega_{mn}^2 = \frac{g}{a} \epsilon_{mn} \tanh \left(\frac{h}{a} \epsilon_{mn} \right) \quad (2-14)$$

where

g = the acceleration due to gravity

a = the radius of the tank

h = the depth of liquid in the tank

ϵ_{mn} = the roots of an eigen function

It is observed that the eigen frequencies are proportional to the square root of g . However, when the vehicle experiences a large acceleration normal to the mean free surface of the fluid, g becomes the effective longitudinal acceleration of the missile. Therefore, the natural frequencies of the liquid remain a constant while the vehicle is at rest but vary when the missile is in flight. It is also seen that the frequencies are inversely proportional to the square root of a and thereby decrease with an increase in the cross-sectional area of the container. The influence of tank geometry upon the frequencies of the liquid is also exhibited by the value of ϵ_{mn} . The liquid height has relatively no effect on the frequencies for $h > a$. As h decreases below a , the frequencies tend to zero.

2.4 Initial Conditions

Assume the harmonic forcing function is equal to zero for all time t equal to and less than zero ($t \leq 0$).

III. Equivalent Mechanical Model Theory

An equivalent mechanical model is an assemblage of springs, dashpots, masses, and massless rods arranged in such a manner as to represent the dynamic behavior of a complex mechanical or non-mechanical system. Consideration is given here to those models which are dynamically equivalent to a liquid oscillating within its container. Dynamic equivalence is taken to mean the equivalence of force and moment resultants, frequencies of oscillation, and mass and inertial characteristics.

There are two reasons for using equivalent mechanical models to represent the sloshing behavior of a contained liquid. Since the problem of forced damped liquid oscillations is actually nonlinear in nature, an exact solution is practically impossible. However, through the use of an equivalent mechanical model, a good approximation can be made by introducing equivalent linear damping in the form of dashpots, thereby making it possible to obtain finite results near the resonant frequencies of the liquid. This was not possible in the fluid analysis, since the liquid was assumed to be inviscid. Secondly, the overall problem of missile stability is simplified in that the vehicle's equations of motion are not so complex.

When a container partially filled with fluid is excited, the liquid in the bottom of the tank is little disturbed, whereas the liquid near the free surface oscillates. Analogously, the model is composed of a fixed mass in the bottom of the container to represent the essentially rigid or non-sloshing part of the liquid and a movable mass near the top of the container to represent the sloshing part of the liquid. The sum of the fixed and movable masses of the model are taken equal to the total mass of the liquid and the ratio of the movable mass to the total mass of the liquid increases

as the depth of the liquid in the container decreases. Also, the fixed mass and the movable mass (when the fluid is not oscillating) are located along the longitudinal axis of the container at such distances from the tank bottom as to yield the same inertial characteristics for rotation about any axis perpendicular to and passing through the longitudinal axis. Therefore, the fixed mass is located near the center of gravity of the undisturbed fluid and the location of the movable mass shifts towards the center of gravity of the fluid as the liquid level decreases.

The kind of movable mass to be used and its restraints are dependent on the type of excitation encountered, namely: harmonic translation, harmonic pitching, or harmonic roll. For a particular model, harmonic translation and harmonic pitching have the following relationship: (a) translation refers to an excitation in a direction perpendicular to the longitudinal axis of the container while (b) pitching implies an excitation about an axis perpendicular to the direction of translation and the container's longitudinal axis. For translational and pitching excitations, two possibilities exist to represent a movable mass and its constraints; either a spring-mass system whose motion is restrained by springs and dashpots aligned in the direction of translation or a pendulum-mass system having its massless lever arm attached to the longitudinal axis of the container. Because "small oscillation theory" has been assumed, the amplitude of the pendulum motion must be small, thereby maintaining the pendulum mass at a relatively constant distance from the container bottom. Therefore the inertial characteristics of the pendulum mass are essentially the same as those of the spring mass.

For roll excitation, which is always taken to be about the longitudinal

axis of the container, two possibilities exist for representing a movable mass and its constraints; (a) a torsional pendulum whose shaft coincides with the container's longitudinal axis or (b) a torsional spring-mass system attached to the longitudinal axis of the container.

Because of the defined arrangement of the constraints of movable masses with respect to the direction of excitation, the model becomes a single degree of freedom system, i.e., only one generalized coordinate is necessary to specify the position of the movable mass at any particular time. Note, however, that when a container partially filled with fluid is excited, the liquid can oscillate in various modes of vibration depending on the frequency and amplitude of the forcing function. Thus, for a circular cylindrical tank, or some other similar configuration, it is possible to have modes of vibration in both the radial and tangential direction. In other words, an oscillating liquid can exhibit several degrees of freedom. In order for a model to simulate these various modes of vibration, it is necessary to add additional movable masses to the model. Each new mass increases the model's degree of freedom by one and thereby makes it possible to represent an additional liquid mode of oscillation. For this reason the subscript mn is used on various parameters in order to clarify which mode of vibration is of interest. m is to represent the m th mode of vibration in the tangential direction and n is to represent the n th mode in the radial direction for circular cylindrical tanks or similar configurations. In many cases, the only m th mode to be excited is $m=1$. Thus, when only the subscript n is used, it is to be understood that $m=1$.

In order for a particular movable mass to oscillate at the same

frequency as the liquid mode it represents, the following definitions have to be made: (1) the spring constant is defined as the slosh mass times the square of the natural angular frequency of the fluid, (2) the length of the pendulum axis is defined as the acceleration due to gravity over the square of the natural angular frequency of the fluid, and (3) the damping coefficient is defined as the slosh mass times the damping factor times the natural angular frequency of the fluid. Also, for the torsional pendulum, the torsional stiffness of the shaft is defined as the mass moment of inertia of the disc times the natural angular frequency and the damping coefficient of the disc is defined as the mass moment of inertia times the damping factor times the square of the natural angular frequency. The damping factor must be determined either analytically or experimentally (see Chapter V).

Component values of the model are determined so that the forces and moments exerted by the model are identically equal to those exerted by the liquid. This is done by making a term-wise comparison of the force and moment equations derived from hydrodynamic aspects with those derived from the model. In order to put the fluid and model equations into similar form for comparison, it is many times necessary to expand certain terms of these equations into series. Even though the model equations contain damping terms and the fluid equations do not, the comparison of equations is still valid because the modes of vibration change little as long as the amount of damping remains small.

IV. Rigid Tanks

4.1 Introduction

The following sections present results of analytical studies of liquid oscillations in containers of various shapes when subjected to different types of excitation. Each section is concerned with a particular container shape, either circular cylindrical, sector, quarter-sectored, eighth-sectored, annular, annular-sector, or rectangular and is preceded by a table of contents, a diagram showing the container and its coordinate system, and other information pertinent to the material that follows. The containers are assumed to have exhibited rigid-body behavior. The boundary conditions and resulting fluid velocity potentials, natural frequencies and liquid force and moment resultants are given along with equivalent mechanical models. The elements of these models are defined both analytically and graphically.

The orthogonal coordinate systems to which the force and moment resultants are referenced are identical to those shown in the figures, the coordinate origins always being located at the center of gravity of the undisturbed fluid. However, in the fluid analysis, it is frequently convenient to translate the coordinate origin along the z -axis to the free surface of the undisturbed liquid, thereby referencing the velocity potential to such a system. This fact presents no difficulty since equation (2-7), used for calculating the resultant moment, gives the moment referenced to any point $(0,0,\bar{z})$. Therefore, it is necessary to take $\bar{z} = -h/2$ when the velocity potential is referenced to the fluid surface and $\bar{z} = 0$ when the velocity potential is referenced to the center of gravity of the undisturbed fluid.

The orthogonal coordinate system to which a particular velocity

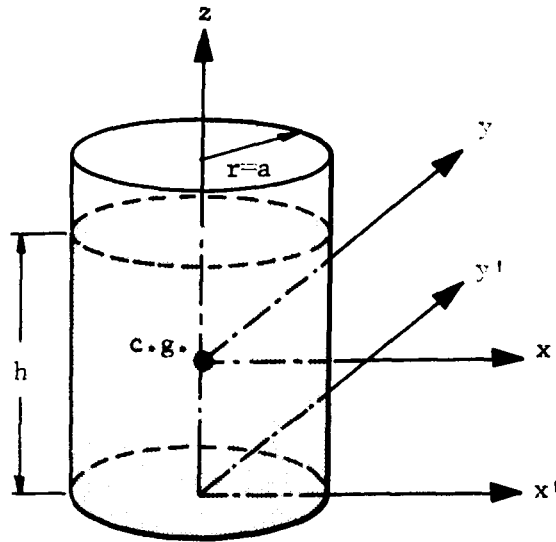
potential is referenced is determined in the following manner. The z-axis is always identical to that shown in the appropriate figure. The location of the coordinate origin along the z-axis will be either at the center of gravity of the undisturbed fluid or at the undisturbed free liquid surface. Upon examination of the z-coordinate at which the corresponding free surface boundary condition is evaluated, the location of the coordinate origin is obvious.

Also, it should be mentioned that, for a particular container, superposition of force and moment resultants resulting from several types of excitations is possible because of the linearized theory used herein.

4.2 Circular Cylindrical Tank

Table of Contents

General.....	4-4
Excitation: Harmonic Translation and/or Pitching	
Boundary Conditions, Velocity Potential, and Natural Frequency.....	4-5
Liquid Force and Moment Resultants.....	4-7
Spring-Mass Model	
Analysis.....	4-8
Diagram.....	4-10
Force and Moment Resultants.....	4-11
Elements.....	4-12
Graphs.....	4-13
Pendulum Model	
Analysis.....	4-25
Diagram.....	4-27
Force and Moment Resultants.....	4-28
Elements.....	4-29
Graphs.....	4-30
Excitation: Arbitrary Translation and/or Pitching	
Pendulum Model	
Analysis.....	4-33
Diagram.....	4-34
Force and Moment Resultants.....	4-35
Elements.....	4-36



Container: The tank is a right circular cylinder of radius a and is filled with a liquid to a depth h .

Coordinate System: The origin of the xyz -system is located at the center of gravity of the undisturbed fluid and the origin of the $x'y'z'$ system is located at the geometric center of the tank base.

References: (4,44,and 52)

Comments: The terms \bar{I} and \bar{c} , occurring in the model elements, must be experimentally determined, generally from torsion spring experiments of a sealed container of fluid. Their values are dependent upon container shape and the type of liquid.

Table 4-1. Boundary Conditions, Velocity Potential, and Natural Frequency

Circular Cylindrical Tank	Excitation: Harmonic Translation
Translation in the x-direction, $x = x_0 e^{i\omega t}$.	

1. Boundary conditions:

$$(a) \left(\frac{\partial \phi}{\partial r} \right)_{r=a} = i\omega x_0 e^{i\omega t} \cos \phi \quad (b) \left(\frac{\partial \phi}{\partial z} \right)_{z=-h} = 0 \quad (c) \left(\frac{\partial^2 \phi}{\partial t^2} + g \frac{\partial \phi}{\partial z} \right)_{z=0} = 0$$

2. Velocity Potential:

$$\phi = i\omega x_0 e^{i\omega t} \cos \phi \left[\frac{r}{a} + \sum_{n=0}^{\infty} \frac{2 J_1(\rho_n) \cosh(\kappa_n + \zeta_n)}{(\epsilon_n^2 - 1)(\eta_n^2 - 1) J_1(\epsilon_n) \cosh \kappa_n} \right]$$

3. Natural angular frequency:

$$\omega_n^2 = \frac{g}{a} \epsilon_n \tanh \kappa_n$$

where ϵ_n are roots of $J_1'(\epsilon_n) = 0$. (see Table A-3)

Table 4-1. Boundary Conditions, Velocity Potential, and Natural Frequency (continued)

Circular Cylindrical Tank	Excitation: Harmonic Pitching
---------------------------	-------------------------------

Pitching about the y-axis, $\theta = \theta_0 e^{i\omega t}$.

1. Boundary conditions:

$$(a) \left(\frac{\partial \phi}{\partial r} \right)_{r=a} = -i\omega z \theta_0 e^{i\omega t} \cos \phi \quad (b) \left(\frac{\partial \phi}{\partial z} \right)_{z=-h/2} = i\omega r \theta_0 e^{i\omega t} \cos \phi \quad (c) \left(\frac{\partial^2 \phi}{\partial t^2} + g \frac{\partial \phi}{\partial z} \right)_{z=th/2} = 0$$

2. Velocity potential:

$$\phi = -i\omega a^2 \theta_0 e^{i\omega t} \cos \phi \left\{ \frac{r}{a} z + \sum_{n=0}^{\infty} \frac{2 J_1(\rho_n)}{n^2 \epsilon_n (\epsilon_n^2 - 1)(\eta_n^2 - 1) J_1(\epsilon_n) \cosh \kappa_n} \right. \\ \left. \left[\left(\gamma_n + \frac{\kappa_n}{2} \right) \cosh \left(\frac{\kappa_n}{2} + \zeta_n \right) - 4 \gamma_n \sinh \frac{\kappa_n}{2} \sinh \zeta_n - 2 \sinh \left(\frac{\kappa_n}{2} - \zeta_n \right) \right] \right\}$$

3. Natural angular frequency:

$$\omega_n^2 = \frac{g}{a} \epsilon_n \tanh \kappa_n$$

where ϵ_n are roots of $J_1'(\epsilon_n) = 0$. (see Table A-3)

Table 4-2. Liquid Force and Moment Resultants

Circular Cylindrical Tank	Excitation: Harmonic Translation or Pitching
---------------------------	--

Translation in the x-direction, $x = x_0 e^{i\omega t}$.

$$1. F_x = m_L \omega^2 x_0 e^{i\omega t} \left[1 + 2 \sum_{n=0}^{\infty} \frac{\tanh \kappa_n}{\kappa_n (\epsilon_n^2 - 1)(\eta_n^2 - 1)} \right]$$

$$2. M_y = m_L a \omega^2 x_0 e^{i\omega t} \left[\frac{1}{4(h/a)} + 2 \sum_{n=0}^{\infty} \frac{(1/\kappa_n) (2/\cosh \kappa_n - 1) + (1/2) \tanh \kappa_n}{\epsilon_n (\epsilon_n^2 - 1)(\eta_n^2 - 1)} \right]$$

Pitching about the y-axis, $\theta = \theta_0 e^{i\omega t}$.

$$1. F_x = -m_L g \theta_0 e^{i\omega t} - 2 m_L a \omega^2 \theta_0 e^{i\omega t} \sum_{n=0}^{\infty} \frac{(2/\kappa_n) (1/\cosh \kappa_n - 1) + (\gamma_n/\kappa_n + 1/2) \tanh \kappa_n}{\epsilon_n (\epsilon_n^2 - 1)(\eta_n^2 - 1)}$$

$$2. M_y = -\frac{m_L g a \theta_0 e^{i\omega t}}{4(h/a)} - m_L^2 a^2 \omega^2 \theta_0 e^{i\omega t} \left\{ \frac{1}{12} \left(\frac{h}{a}\right)^2 - \frac{1}{8} + 2 \sum_{n=0}^{\infty} \frac{1}{\epsilon_n (\epsilon_n^2 - 1)(\eta_n^2 - 1)} \right\}$$

$$\left[\left(1 - \frac{2\gamma_n}{\kappa_n}\right) \frac{2}{\epsilon_n \cosh \kappa_n} + \frac{1}{\epsilon_n} \left(\frac{5\gamma_n}{\kappa_n} + \frac{1}{2}\right) + \frac{1}{\epsilon_n} \left(\frac{\kappa_n}{4} - \frac{3\gamma_n}{2} - \frac{4}{\kappa_n}\right) \tanh \kappa_n \right] \right\}$$

Table 4-3. Model Analysis

Circular Cylindrical Tank	Spring-Mass Model
Excitation: Harmonic Translation and/or Pitching	

Figure 4-1 shows a diagram of the spring-mass model used in representing the dynamic response of a liquid in a circular cylindrical tank when subjected to harmonic translation in the x-direction and/or pitching about the y-axis.

Coordinate System:

The origin is located at the center of gravity of the undisturbed liquid.

Model Description:

The components of the system are as follows:

1. A fixed mass M having a moment of inertia I is rigidly connected to the tank and is located on the z-axis at a distance H below the coordinate origin.
2. A set of movable masses m_n is distributed along the z-axis when the tank is at rest at distances h_n above the origin. These modal masses are constrained by spring-dashpot systems, having spring stiffness coefficients k_n and viscous damping coefficients c_n , to remain in the xy-plane and to move only in a direction parallel to the x-axis. Translational displacements of these masses with respect to the container are denoted by x_n .
3. A massless disc having a moment of inertia I_d is located at the coordinate origin. Its motion is confined to rotation about the y-axis and is cushioned by a dashpot having a viscous damping coefficient c_d . The angular displacement of the disc relative to the tank is defined by ψ .

Equations of Motion:

The equations, obtained through Lagrange's equations, are as follows:

1. Force Equation:

$$F_x = -M(\ddot{x} + H\ddot{\theta}) - \sum_{n=1}^{\infty} m_n(\ddot{x} + \ddot{x}_n + h_n\ddot{\theta})$$

2. Moment Equation:

$$M_y = -(I + MH^2)\ddot{\theta} - I_d(\ddot{\theta} + \ddot{\psi}) + g \sum_{n=1}^{\infty} m_n x_n - \sum_{n=1}^{\infty} m_n h_n (\ddot{x}_n + h_n \ddot{\theta})$$

Table 4.3 Model Analysis (continued)

Circular Cylindrical Tank	Spring-Mass Model
Excitation: Harmonic Translation and/or Pitching	

Equations of Motion (continued):

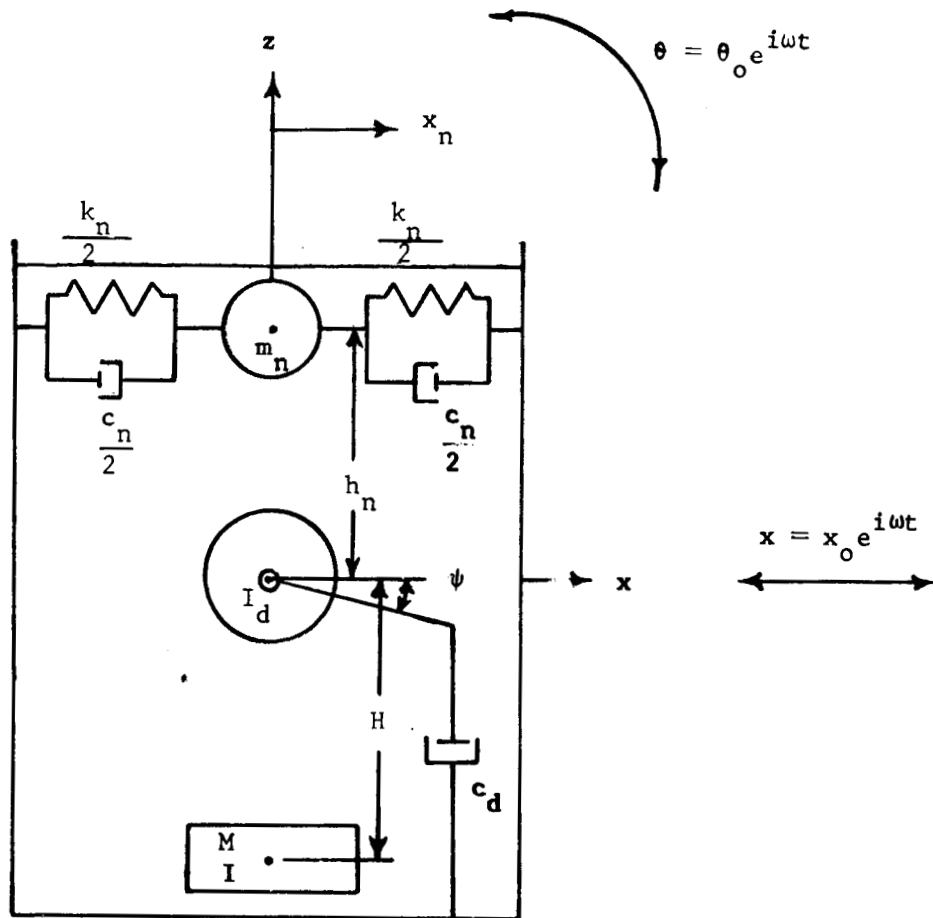
3. Disc Equation:

$$I_d (\ddot{\theta} + \ddot{\psi}) + c_d \dot{\psi} = 0$$

4. Slosh-Mass Equation:

$$m_n (\ddot{x} + \ddot{x}_n + h_n \ddot{\theta}) + m_n \bar{g}_n \omega_n \dot{x}_n + k_n x_n - m_n g \theta = 0$$

From these equations, the model force in the x-direction and the moment about the y-axis can be found (see Table 4-4).



Circular Cylindrical Tank

Spring-Mass Model

Excitation: Harmonic Translation and/or Pitching

Figure 4-1. Equivalent Mechanical Model

Table 4-4. Model Force and Moment Resultants

Circular Cylindrical Tank	Spring-Mass Model
Excitation: Harmonic Translation and/or Pitching	

Translation in the x-direction, $x = x_0 e^{i\omega t}$.

$$1. F_x = m_L \omega^2 x_0 e^{i\omega t} \left[1 + \sum_{n=0}^{\infty} \left(\frac{m_n}{m_L} \right) \left(\frac{1}{\eta_n^2 - 1 + i\bar{g}_n \eta_n} \right) \right]$$

$$2. M_y = m_L h \omega^2 x_0 e^{i\omega t} \sum_{n=0}^{\infty} \left(\frac{m_n}{m_L} \right) \left(\frac{h}{h} + \frac{g}{h\omega} \right) \left(\frac{1}{\eta_n^2 - 1 + i\bar{g}_n \eta_n} \right)$$

Pitching about the y-axis, $\theta = \theta_0 e^{i\omega t}$.

$$1. F_x = -m_L h \omega^2 \theta_0 e^{i\omega t} \sum_{n=0}^{\infty} \left(\frac{m_n}{m_L} \right) \left(\frac{h}{h} + \frac{g}{h\omega} \right) \left(\frac{1}{\eta_n^2 - 1 + i\bar{g}_n \eta_n} \right)$$

$$2. M_y = -m_L h^2 \omega^2 \theta_0 e^{i\omega t} \left[\frac{I}{m_L h^2} + \frac{Mh^2}{m_L h^2} + \frac{I_d}{m_L h^2} \left(1 - \frac{\omega^2 I_d^2}{c_d^2 + \omega^2 I_d^2} \right) \right] + \sum_{n=0}^{\infty} \frac{m_n h^2}{m_L h^2}$$

$$+ \sum_{n=0}^{\infty} \left(\frac{m_n}{m_L} \right) \left(\frac{h}{h} + \frac{g}{h\omega} \right)^2 \left(\frac{1}{\eta_n^2 - 1 + i\bar{g}_n \eta_n} \right) \left. \right] + i\omega \theta_0 e^{i\omega t} \left(\frac{c_d \omega^2 I_d^2}{c_d^2 + \omega^2 I_d^2} \right)$$

Table 4-5. Model Elements

Circular Cylindrical Tank	Spring-Mass Model
Excitation: Harmonic Translation and/or Pitching	
Natural Frequency	$\omega_n^2 = \frac{g}{a} \epsilon_n \tanh \kappa_n$ (fig. 4-2,4-3)
Spring Constant	$k_n = m_n \omega_n^2$ (fig. 4-4,4-5)
Damping Coefficient of Slosh Mass	$c_n = m_n \bar{g}_n \omega_n$
Damping Coefficient of Disc	$c_d = \bar{c} \left[1 + \frac{\bar{c}^2}{\omega^2 (I_s - \bar{I})^2} \right]$ (fig. 4-6, 4-7)
Ratio of Slosh Mass to Fluid Mass	$\frac{m_n}{m_L} = \frac{2 \tanh(\kappa_n)}{(\epsilon_n^2 - 1) \kappa_n}$ (fig. 4-8)
Ratio of Fixed Mass to Fluid Mass	$\frac{M}{m_L} = 1 - \sum_{n=0}^{\infty} \frac{m_n}{m_L}$ (fig. 4-9, 4-10)
Ratio of Slosh Mass Coordinate to Fluid Depth	$\left \frac{h_n}{h} \right = \frac{1}{2} \left[1 - \frac{4}{\kappa_n} \tanh \frac{\kappa_n}{2} \right]$ (fig. 4-11)
Ratio of Fixed Mass Coordinate to Fluid Depth	$\left \frac{H}{h} \right = \frac{m_L}{M} \sum_{n=0}^{\infty} \left(\frac{m_n}{m_L} \right) \left(\frac{h_n}{h} \right)$
Moment of Inertia of Solidified Fluid	$\frac{I_s}{m_L h^2} = \left(\frac{a}{h} \right)^2 \left[\frac{1}{12} \left(\frac{h}{a} \right)^2 + \frac{1}{4} \right]$ (fig. 4-12)
Moment of Inertia of Disc ($c_d = 0$)	$\frac{I_d}{m_L h^2} = 8 \left(\frac{a}{h} \right)^2 \sum_{n=0}^{\infty} \frac{[1 - (2/\kappa_n) \tanh(\kappa_n/2)]}{(\epsilon_n^2 - 1) \epsilon_n}$
Moment of Inertia of Disc ($c_d \neq 0$)	$\frac{I_d}{m_L h^2} = \frac{I_s - \bar{I}}{m_L h^2} \left[1 + \frac{\bar{c}^2}{\omega^2 (I_s - \bar{I})^2} \right]$ (fig. 4-13)
Moment of Inertia of Fixed Mass	$\frac{I}{m_L h^2} = \frac{I_s}{m_L h^2} - \frac{I_d}{m_L h^2} - \frac{M}{m_L} \left(\frac{H}{h} \right)^2 - \sum_{n=0}^{\infty} \frac{m_n}{m_L} \left(\frac{h_n}{h} \right)^2$

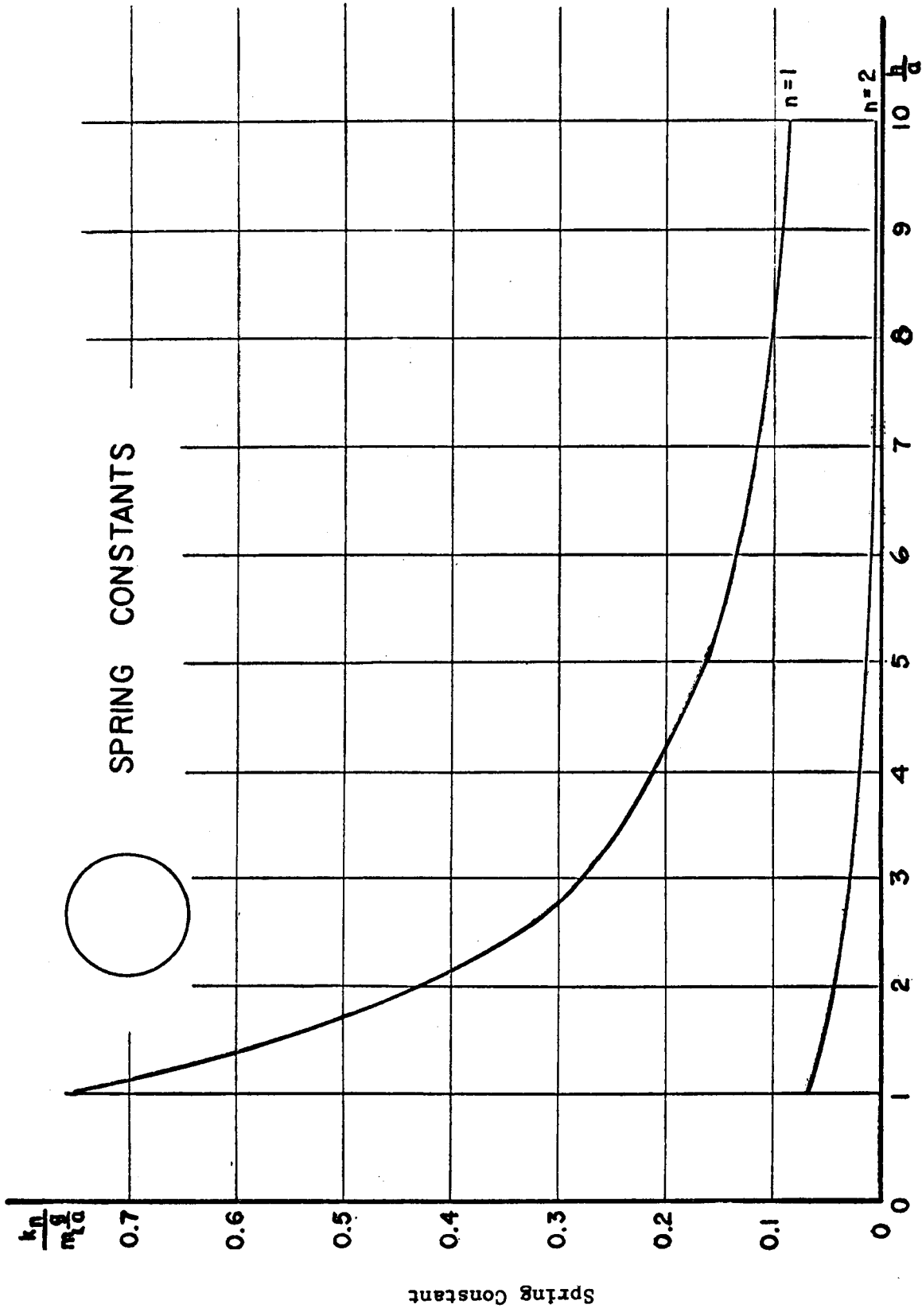


Figure 4-2. Model Element Graph

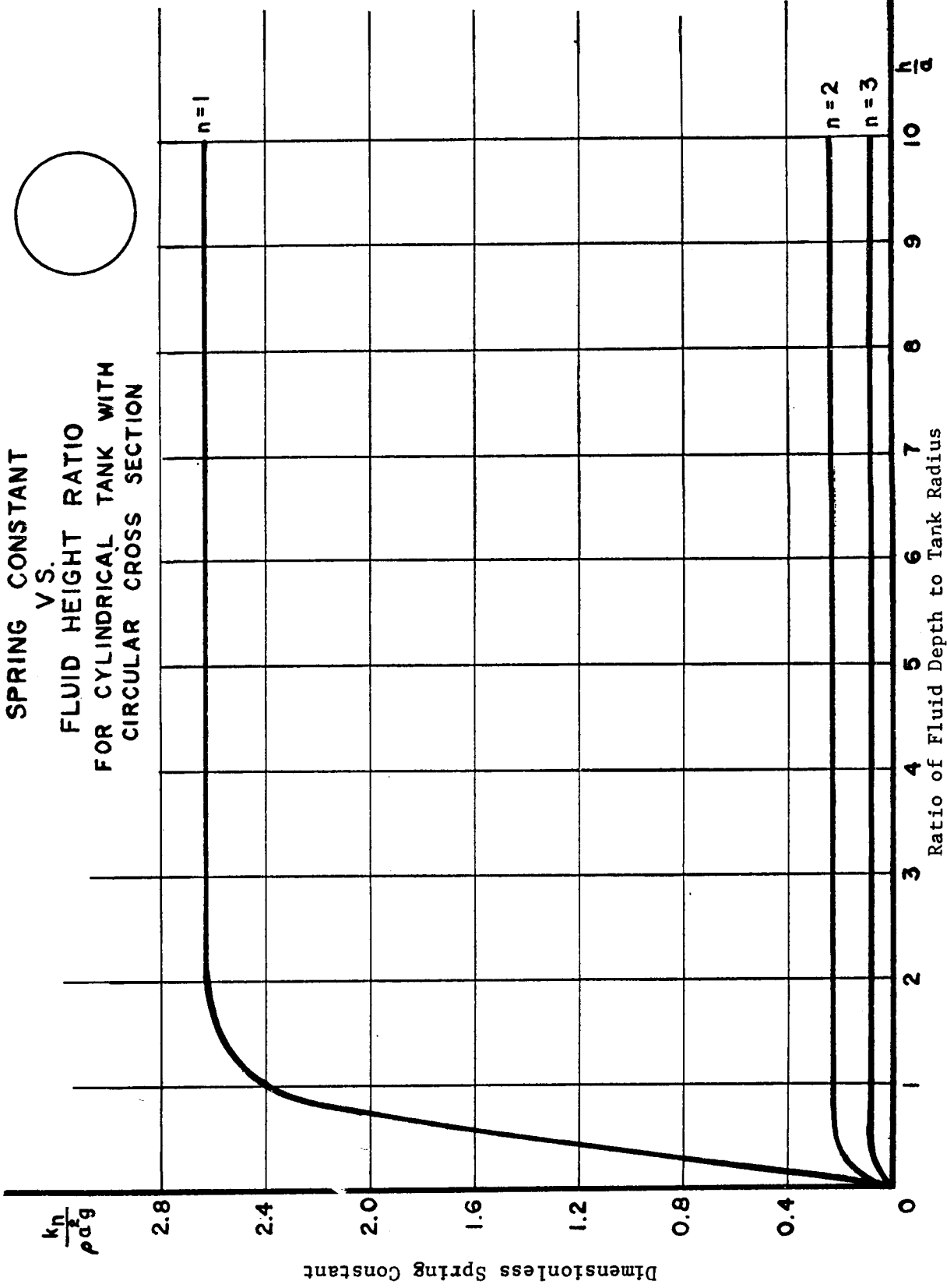


Figure 4-3 Model Element Graph

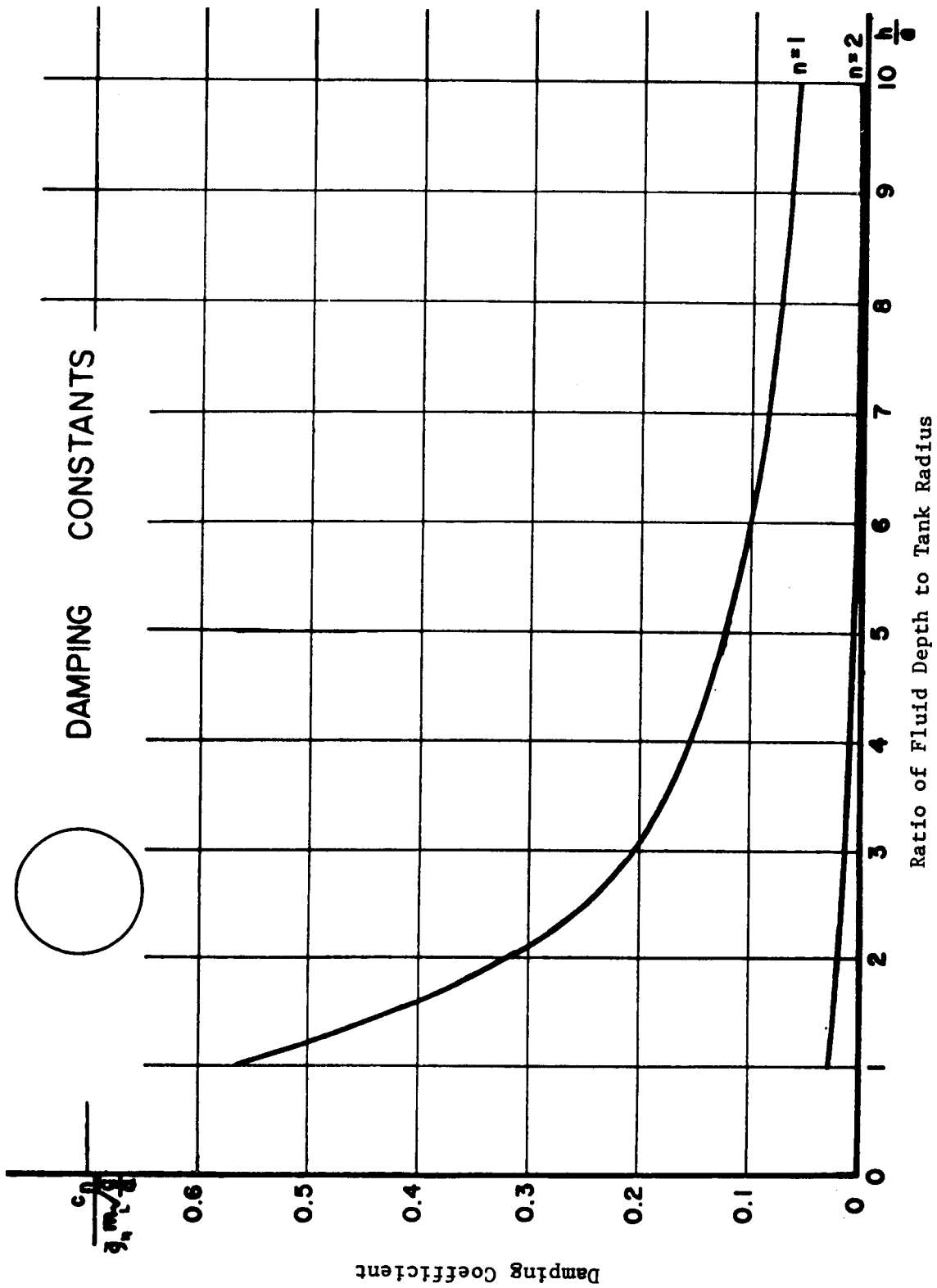


Figure 4-4. Model Element Graph

DAMPING CONSTANT
 VS.
 FLUID HEIGHT RATIO
 FOR CYLINDRICAL TANK WITH
 CIRCULAR CROSS SECTION

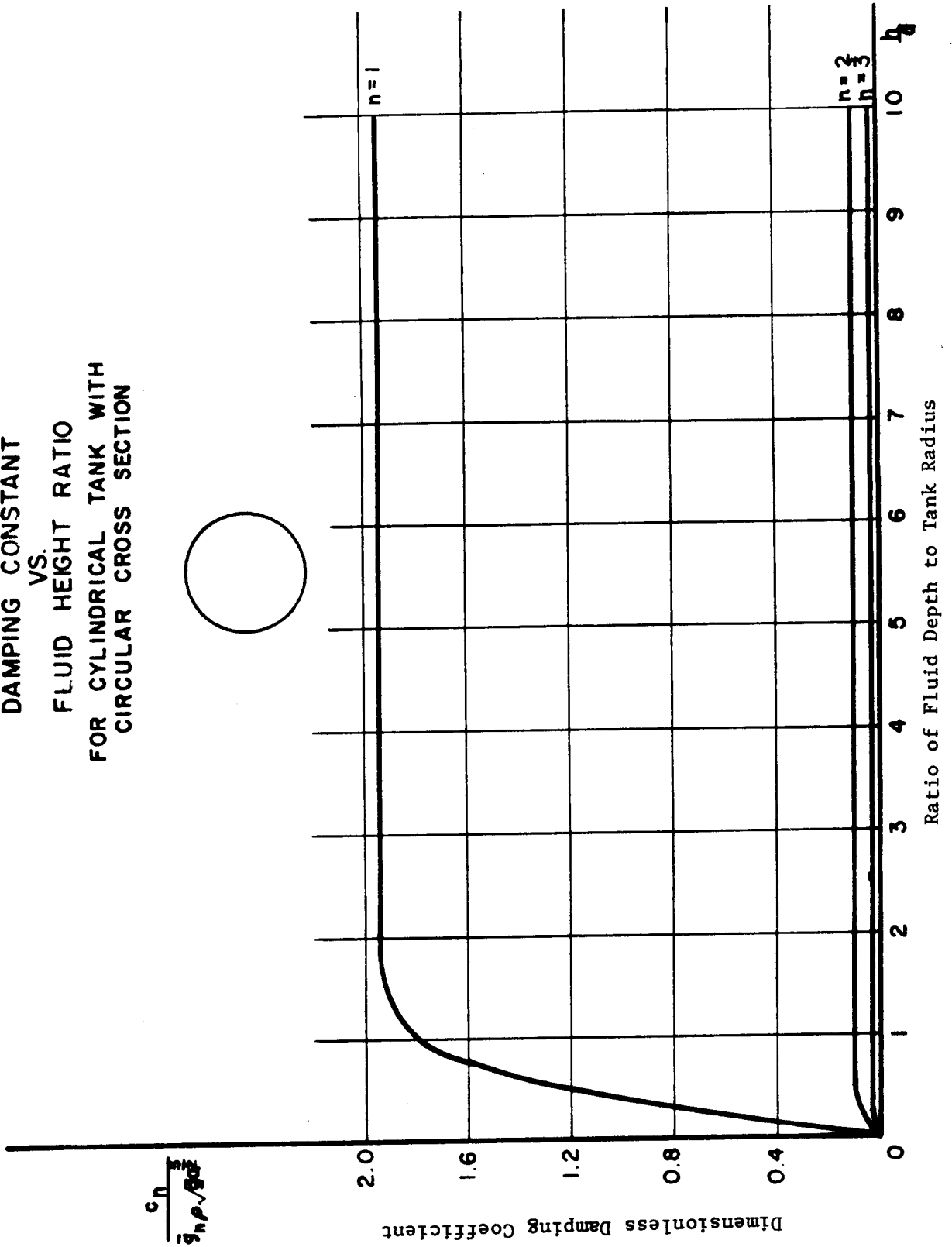
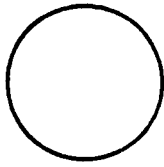


Figure 4-5. Model Element Graph

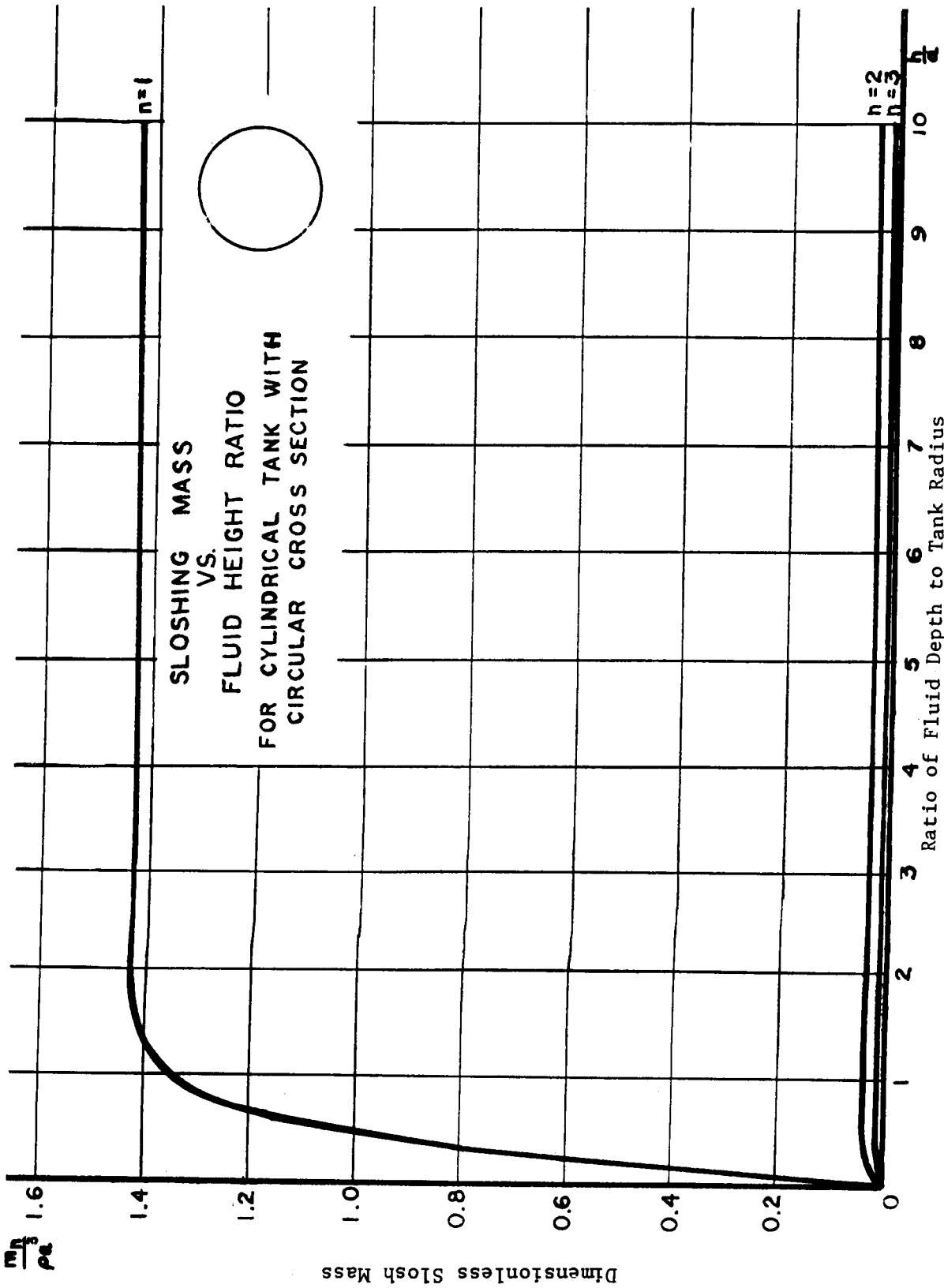
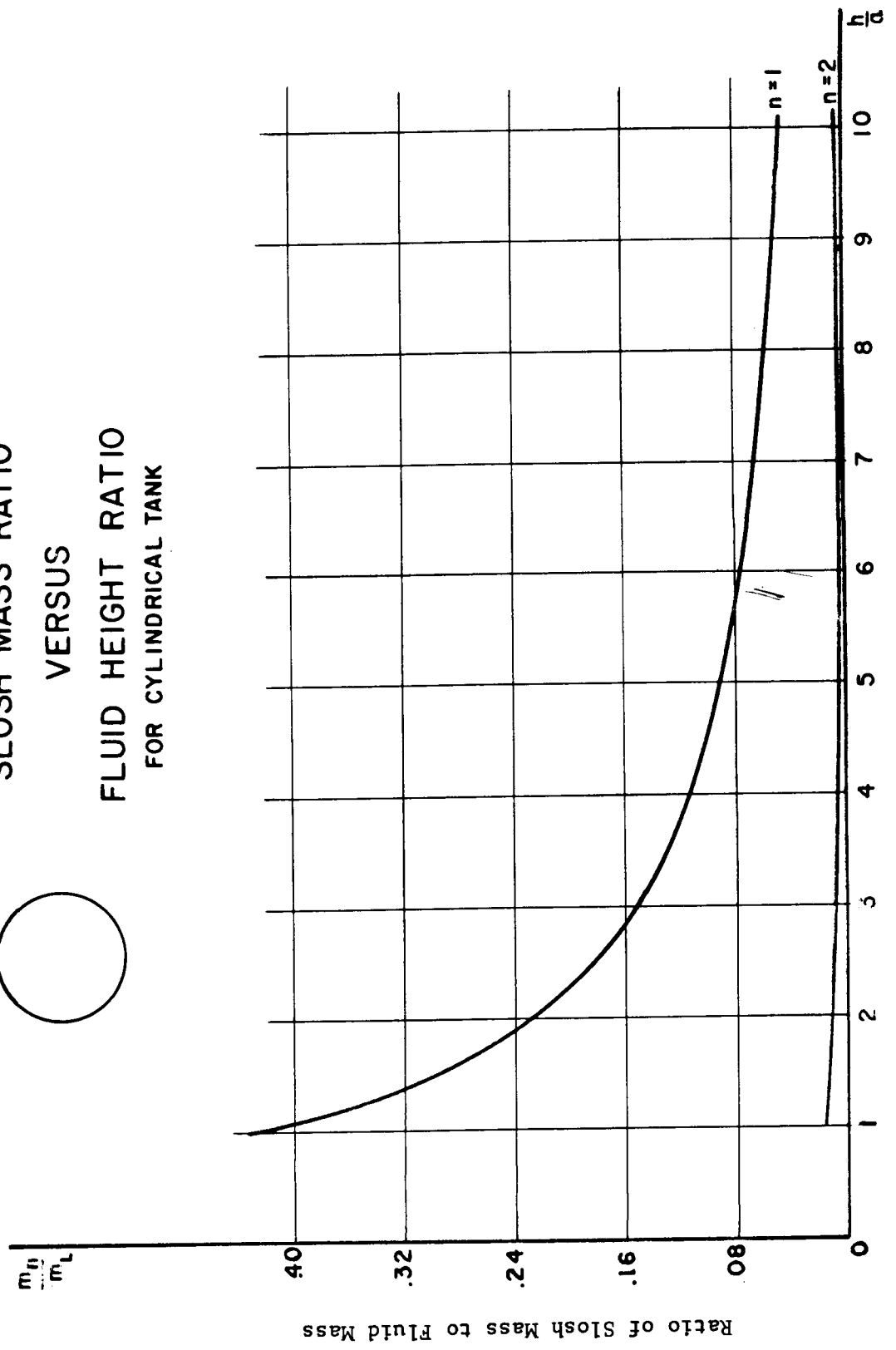
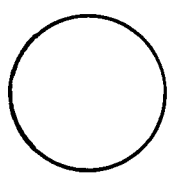


Figure 4-6. Model Element Graph

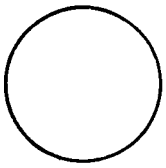
SLOSH MASS RATIO
VERSUS
FLUID HEIGHT RATIO
FOR CYLINDRICAL TANK



Ratio of Fluid Depth to Tank Radius

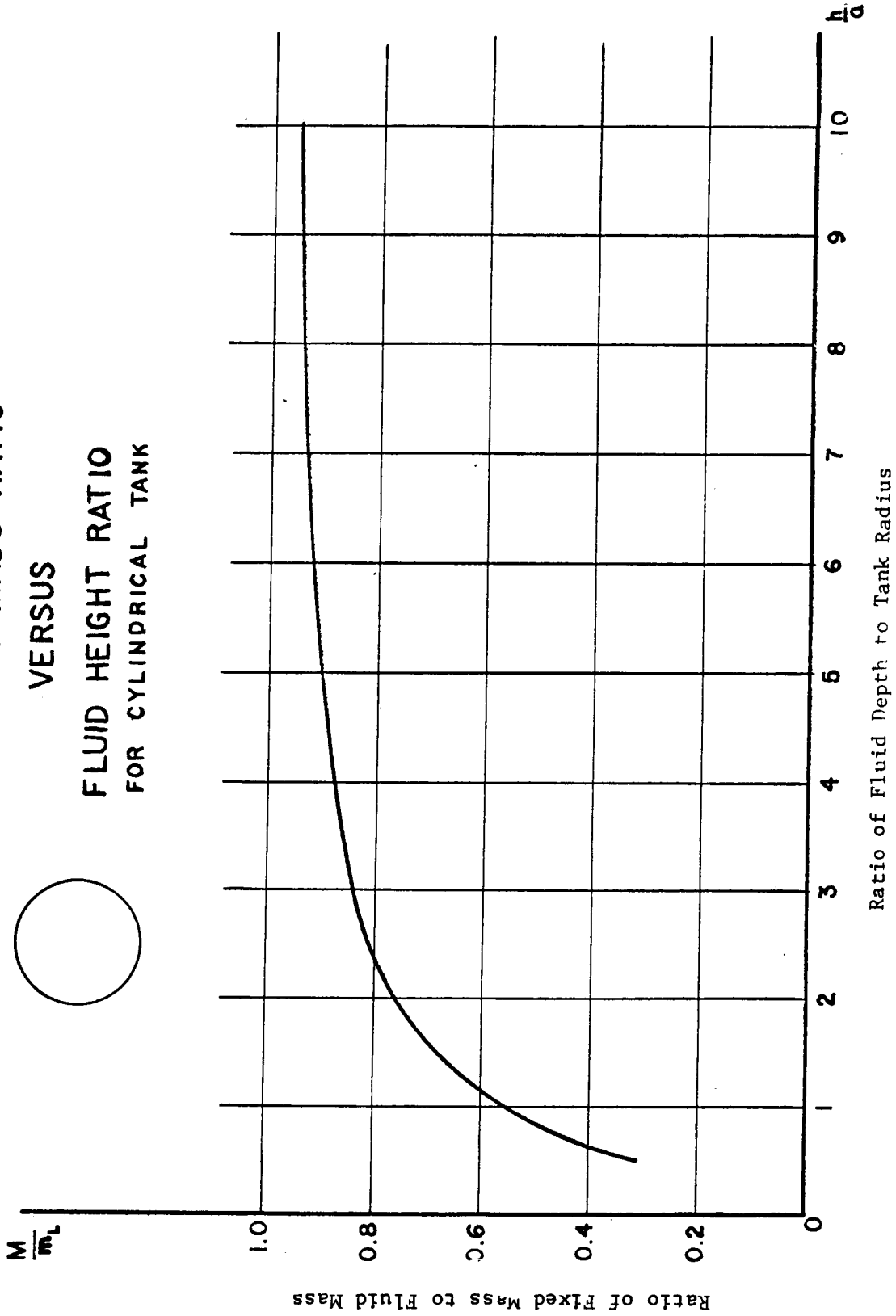
Figure 4-7. Model Element Graph

NONSLOSING MASS RATIO



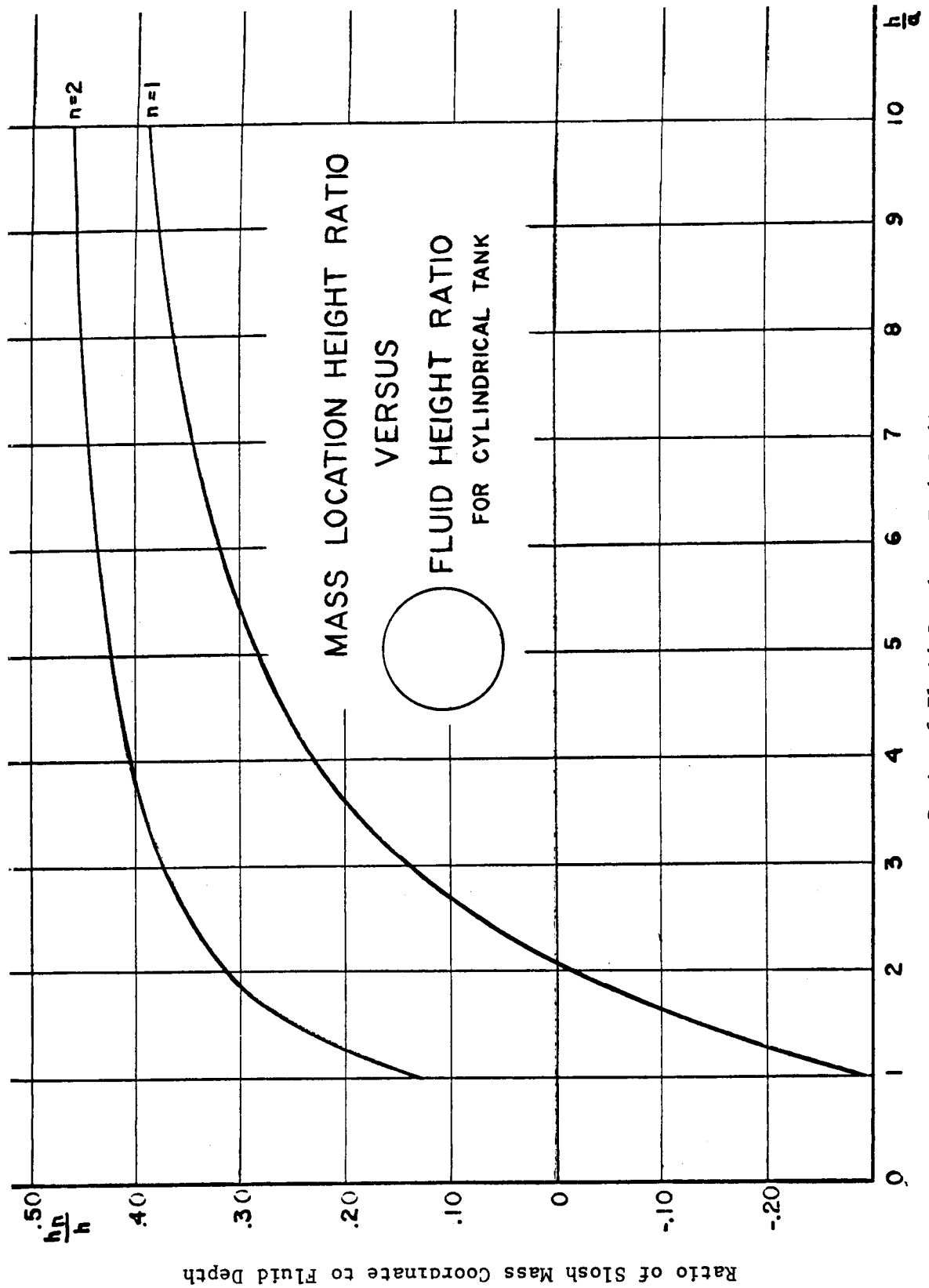
VERSUS

FLUID HEIGHT RATIO
FOR CYLINDRICAL TANK



Ratio of Fluid Depth to Tank Radius

Figure 4-8. Model Element Graph



Ratio of Fluid Depth to Tank Radius

Figure 4-9. Model Element Graph

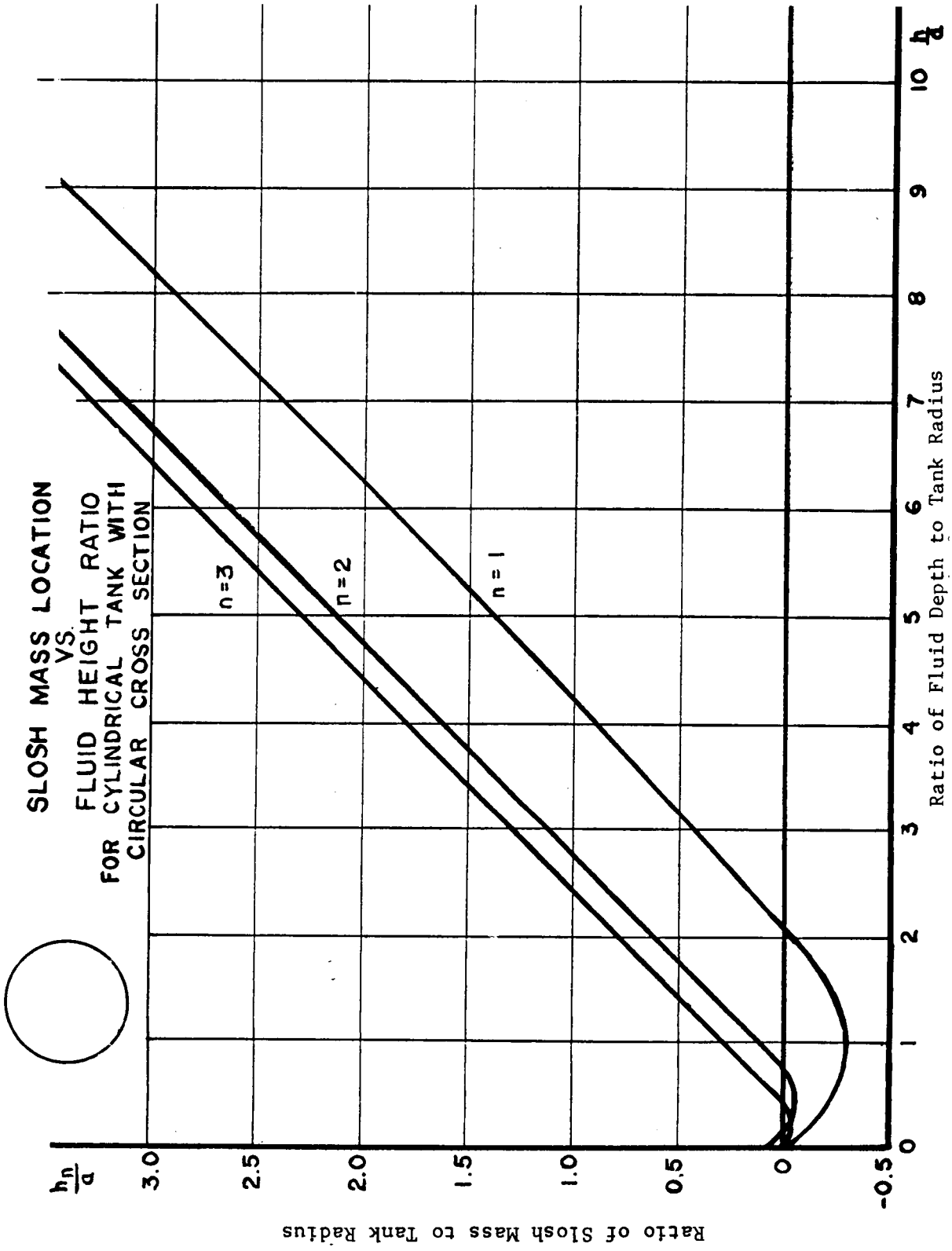


Figure 4-10. Model Element Graph

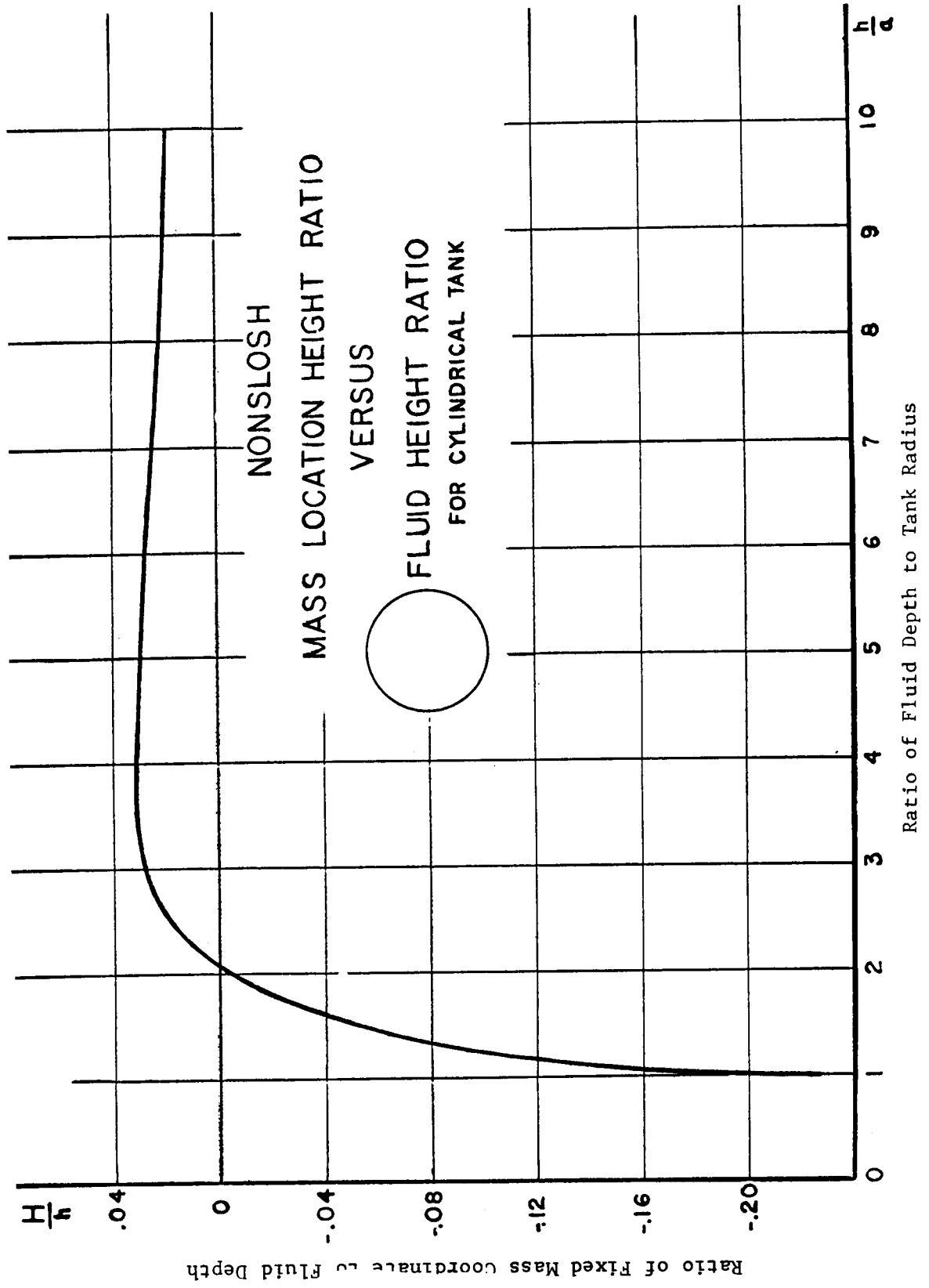


Figure 4-11. Model Element Graph

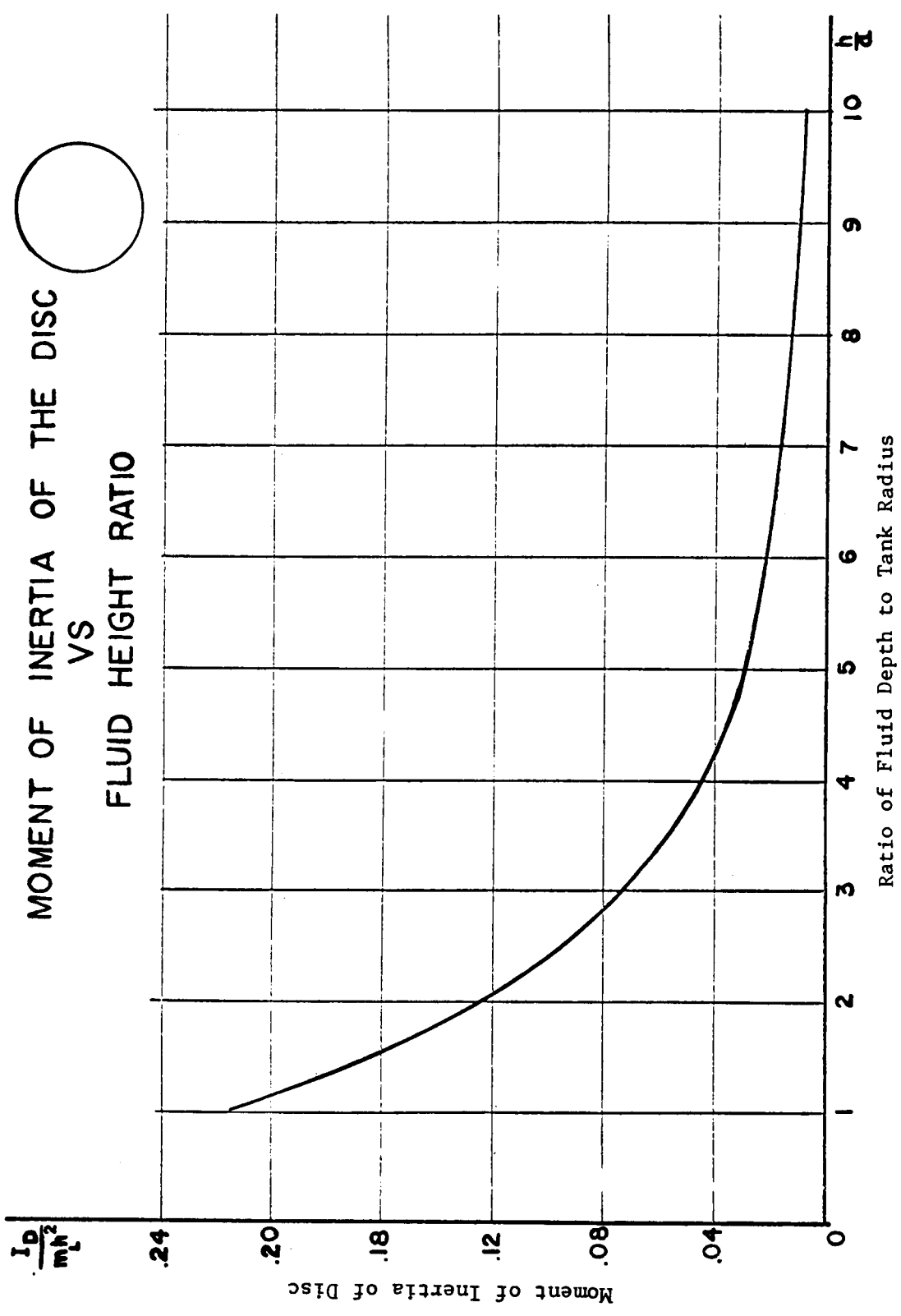


Figure 4-12. Model Element Graph

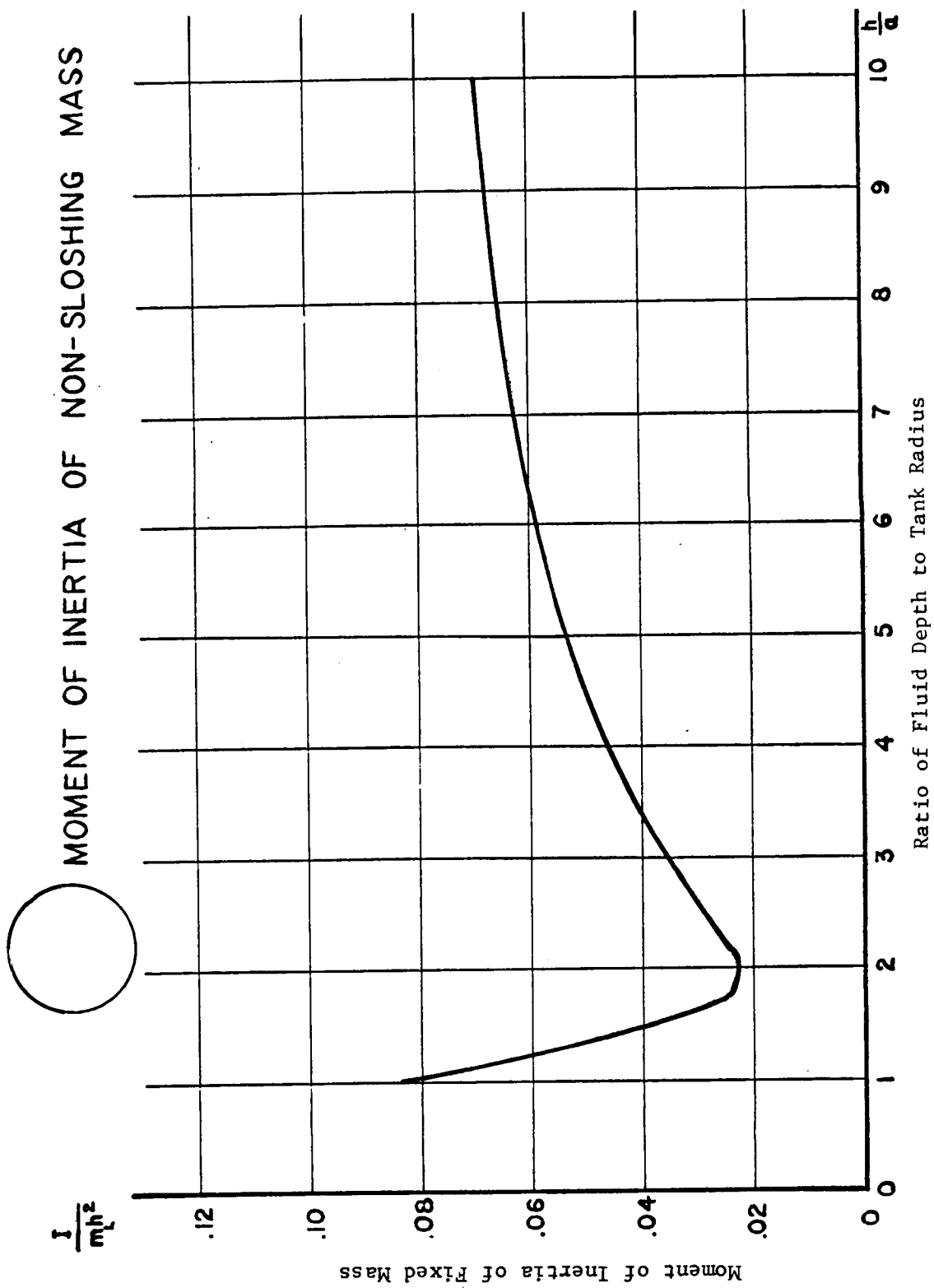


Figure 4-13. Model Element Graph

Table 4-6. Model Analysis

Circular Cylindrical Tank	Pendulum Model
Excitation: Harmonic Translation and/or Pitching	

Figure 4-14 shows a diagram of the pendulum model used in representing the dynamic response of a liquid in a circular cylindrical tank when subjected to harmonic translation in the x-direction and/or pitching about the y-axis.

Coordinate System:

The origin is located at the center of gravity of the undisturbed liquid.

Model Description:

The components of the system are as follows:

1. A fixed mass M having a moment of inertia I is rigidly connected to the tank and is located on the z -axis at a distance H below the coordinate origin.
2. A set of movable masses m_n is distributed along the z -axis when the tank is at rest. These modal masses are pendulums having massless lever arms of length L_n attached to the z -axis at distances H_n above the origin. They are constrained by dashpots having viscous damping coefficients c_n to remain approximately in the xy -plane and to move approximately parallel to the x -axis. Angular displacements of the pendulum with respect to the tank (z -axis) are denoted by λ_n .
3. A massless disc having a moment of inertia I_d is located at the coordinate origin. Its motion is confined to rotation about the y -axis and is cushioned by a dashpot having a viscous damping coefficient c_d . The angular displacement of the disc relative to the tank is defined by ψ .

Equations of Motion:

The equations, obtained through Lagrange's equations, are as follows:

1. Force Equation:

$$F_x = -M(\ddot{x} + H\ddot{\theta}) - \sum_{n=1}^{\infty} m_n \left[\ddot{x} + L_n \ddot{\lambda}_n + (H_n - L_n) \ddot{\theta} \right]$$

2. Moment Equation:

$$M_y = - (I + MH^2) \ddot{\theta} - I_d (\ddot{\theta} + \ddot{\psi}) + g \sum_{n=1}^{\infty} m_n L_n \lambda_n - \sum_{n=1}^{\infty} m_n (H_n - L_n) \cdot \left[L_n \ddot{\lambda}_n + (H_n - L_n) \ddot{\theta} \right]$$

Figure 4-6. Model Analysis (continued)

Circular Cylindrical Tank	Pendulum Model
Excitation: Harmonic Translation and/or Pitching	

Equations of Motion (continued):

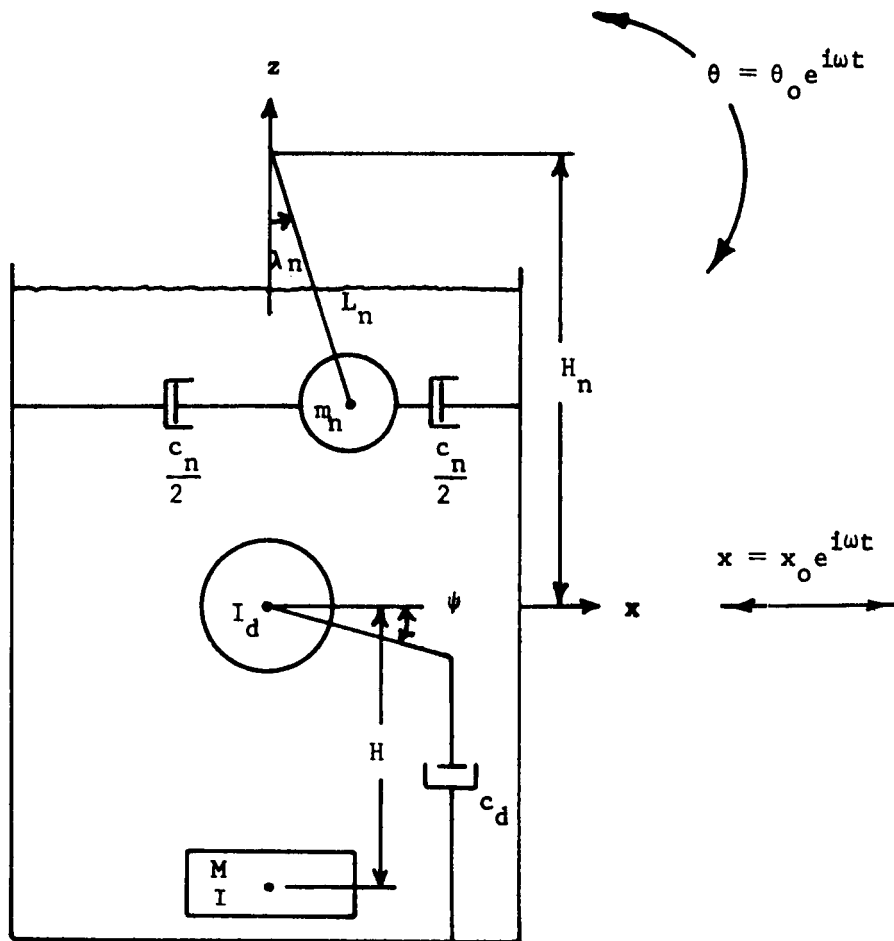
3. Disc Equation:

$$I_d (\ddot{\theta} + \ddot{\psi}) + c_d \dot{\psi} = 0$$

4. Slosh-Mass Equation:

$$m_n \left[\ddot{x} + L_n \ddot{\lambda}_n + (H_n - L_n) \ddot{\theta} \right] + m_n \bar{g}_n \omega_n L_n \dot{\lambda}_n - m_n g \theta = 0$$

From these equations, the model force in the x-direction and the moment about the y-axis can be found (see Table 4-7).



Circular Cylindrical Tank

Pendulum Model

Excitation: Harmonic Translation and/or Pitching

Figure 4-14. Equivalent Mechanical Model

Table 4-7. Model Force and Moment Resultants

Circular Cylindrical Tank	Pendulum Model
Excitation: Harmonic Translation and/or Pitching	

Translation in the x-direction, $x = x_0 e^{i\omega t}$.

$$1. F_x = m_L \omega^2 x_0 e^{i\omega t} \left[1 + \sum_{n=0}^{\infty} \left(\frac{m_n}{m_L} \right) \left(\frac{1}{\eta_n^2 - 1 + i\bar{g}_n \eta_n} \right) \right]$$

$$2. M_y = m_L h \omega^2 x_0 e^{i\omega t} \sum_{n=0}^{\infty} \left(\frac{m_n}{m_L} \right) \left(\frac{H_n - L_n}{h} + \frac{g}{h\omega^2} \right) \left(\frac{1}{\eta_n^2 - 1 + i\bar{g}_n \eta_n} \right)$$

Pitching about the y-axis, $\theta = \theta_0 e^{i\omega t}$.

$$1. F_x = -m_L h \omega^2 \theta_0 e^{i\omega t} \sum_{n=0}^{\infty} \left(\frac{m_n}{m_L} \right) \left(\frac{H_n - L_n}{h} + \frac{g}{h\omega^2} \right) \left(\frac{1}{\eta_n^2 - 1 + i\bar{g}_n \eta_n} \right)$$

$$2. M_y = -m_L h^2 \omega^2 \theta_0 e^{i\omega t} \left[\frac{I}{m_L h^2} + \frac{Mh^2}{m_L h^2} + \frac{I_d}{m_L h^2} \left(1 - \frac{\omega^2 I_d}{c_d^2 + \omega^2 I_d^2} \right) + \sum_{n=0}^{\infty} \frac{m_n (H_n - L_n)^2}{m_L h^2} \right. \\ \left. + \sum_{n=0}^{\infty} \left(\frac{m_n}{m_L} \right) \left(\frac{H_n - L_n}{h} + \frac{g}{h\omega^2} \right)^2 \left(\frac{1}{\eta_n^2 - 1 + i\bar{g}_n \eta_n} \right) \right] + i\omega \theta_0 e^{i\omega t} \left(\frac{c_d \omega^2 I_d^2}{c_d^2 + \omega^2 I_d^2} \right)$$

Table 4-8. Model Elements

Circular Cylindrical Tank	Pendulum Model
Excitation: Harmonic Translation and/or Pitching	
Natural Frequency	$\omega_n^2 = \frac{g}{a} \epsilon_n \tanh \kappa_n \quad (\text{fig. 4-15})$
Pendulum Length	$L_n = g/\omega_n^2$
Damping Coefficient of Slosh Mass	$c_n = m_n \bar{g}_n \omega_n$
Damping Coefficient of Disc	$c_d = \bar{c} \left[1 + \frac{\bar{c}^2}{\omega^2 (I_s - \bar{I})^2} \right]$
Ratio of Slosh Mass to Fluid Mass	$\frac{m_n}{m_L} = \frac{2 \tanh(\kappa_n)}{(\epsilon_n^2 - 1) \kappa_n}$
Ratio of Fixed Mass to Fluid Mass	$\frac{M}{m_L} = 1 - \sum_{n=0}^{\infty} \frac{m_n}{m_L} \quad (\text{fig. 4-16, 4-17})$
Ratio of Pendulum Mass Coordinate to Fluid Depth	$\left \frac{H_n - L_n}{h} \right = \frac{1}{2} \left[1 - \frac{4}{\kappa_n} \tanh \frac{\kappa_n}{2} \right]$
Ratio of Fixed Mass Coordinate to Fluid Depth	$\left \frac{H}{h} \right = \frac{m_L}{M} \sum_{n=0}^{\infty} \left(\frac{m_n}{m_L} \right) \left(\frac{H_n - L_n}{h} \right)$
Moment of Inertia of Solidified Fluid	$\frac{I_s}{m_L h^2} = \left(\frac{a}{h} \right)^2 \left[\frac{1}{12} \frac{h^2}{a^2} + \frac{1}{4} \right]$
Moment of Inertia of Disc ($c_d = 0$)	$\frac{I_d}{m_L h^2} = 8 \left(\frac{a}{h} \right)^2 \sum_{n=0}^{\infty} \frac{[1 - (2/\kappa_n) \tanh(\kappa_n/2)]}{(\epsilon_n^2 - 1) \epsilon_n}$
Moment of Inertia of Disc ($c_d \neq 0$)	$\frac{I_d}{m_L h^2} = \frac{I_s - \bar{I}}{m_L h^2} \left[1 + \frac{\bar{c}^2}{\omega^2 (I_s - \bar{I})^2} \right]$
Moment of Inertia of Fixed Mass	$\frac{I}{m_L h^2} = \frac{I_s}{m_L h^2} - \frac{I_d}{m_L h^2} - \frac{M}{m_L} \left(\frac{H}{h} \right)^2 - \sum_{n=0}^{\infty} \frac{m_n}{m_L} \left[\frac{H_n - L_n}{h} \right]^2$

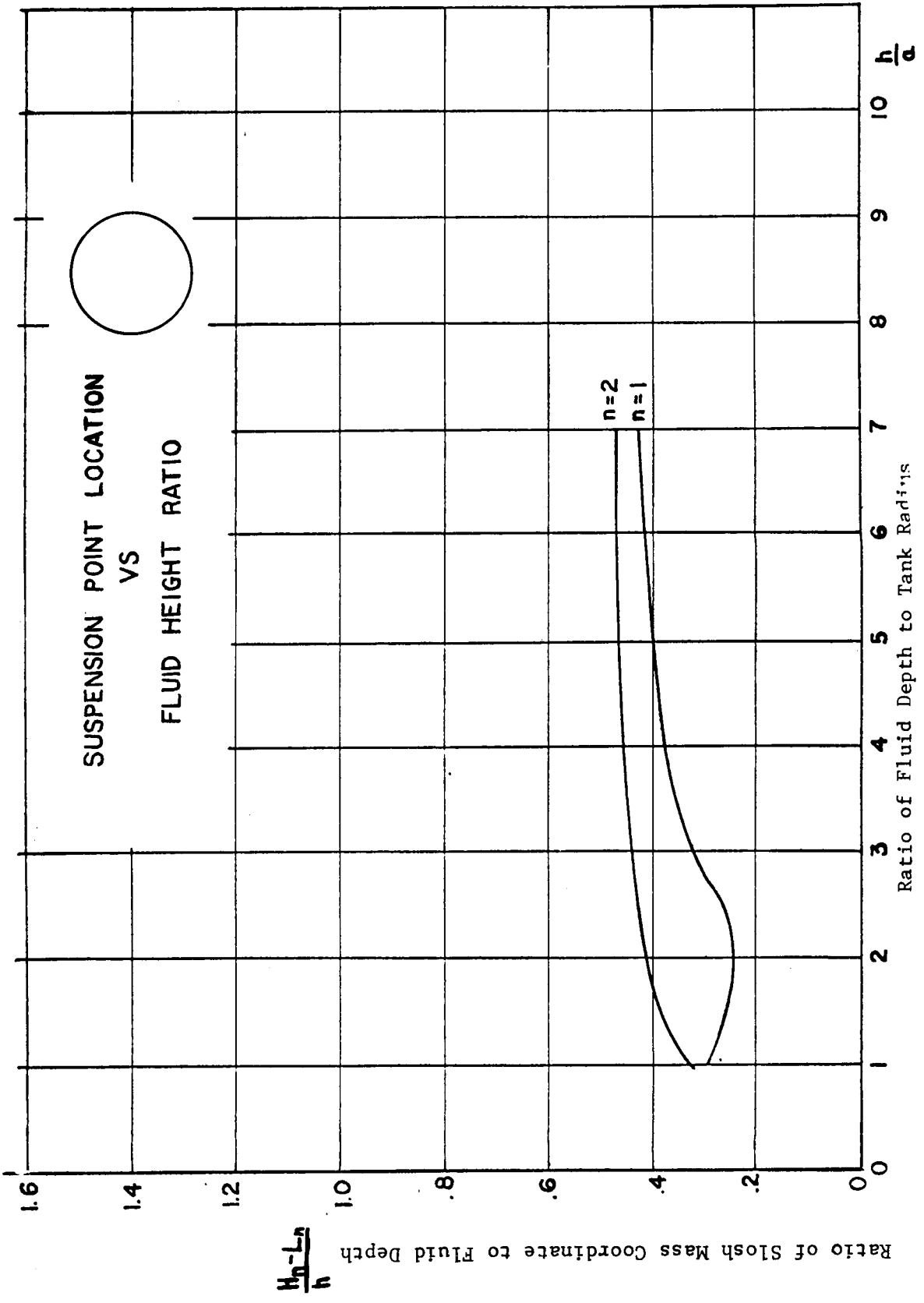


Figure 4-15. Model Element Graph

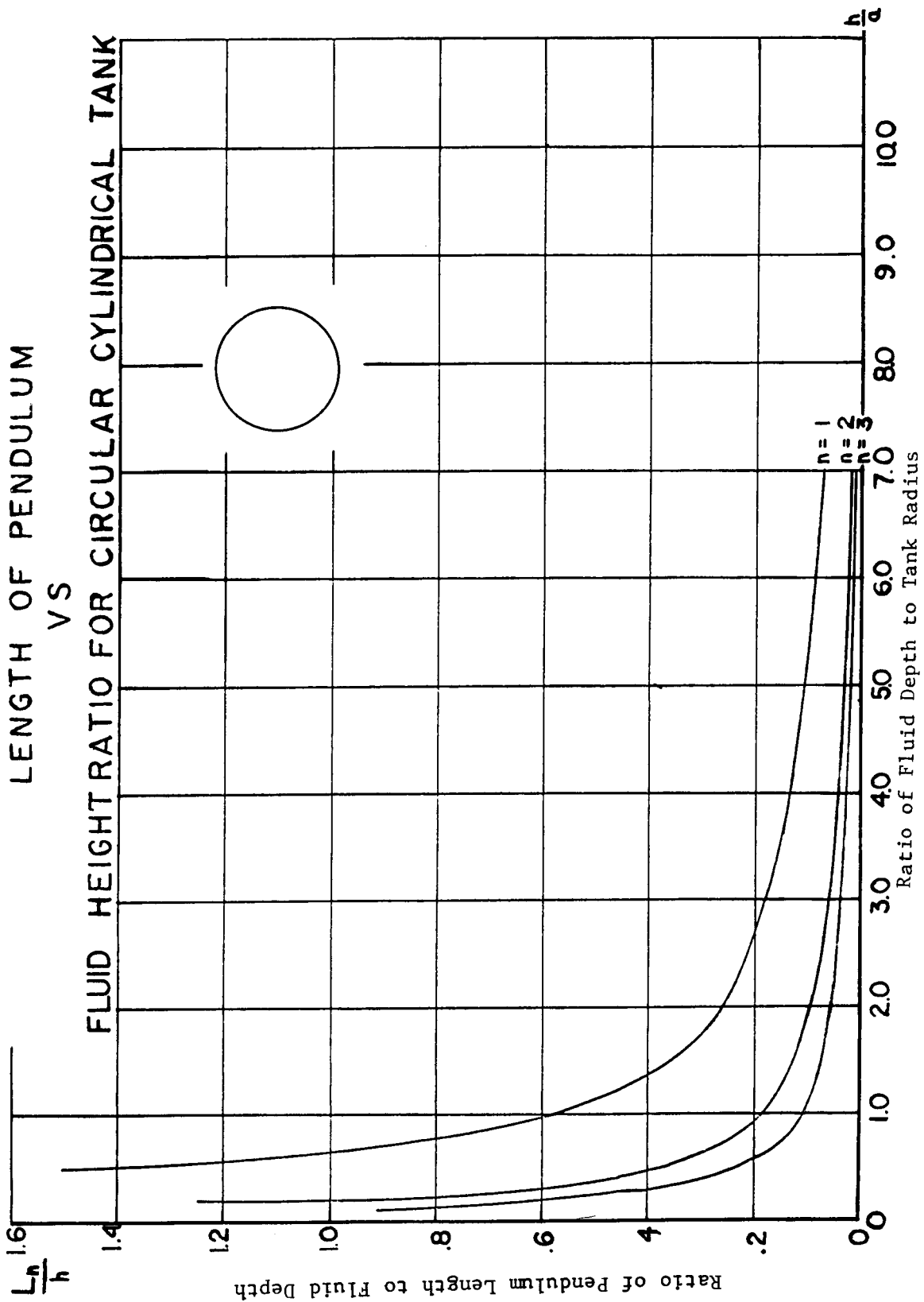


Figure 4-16. Model Element Graph

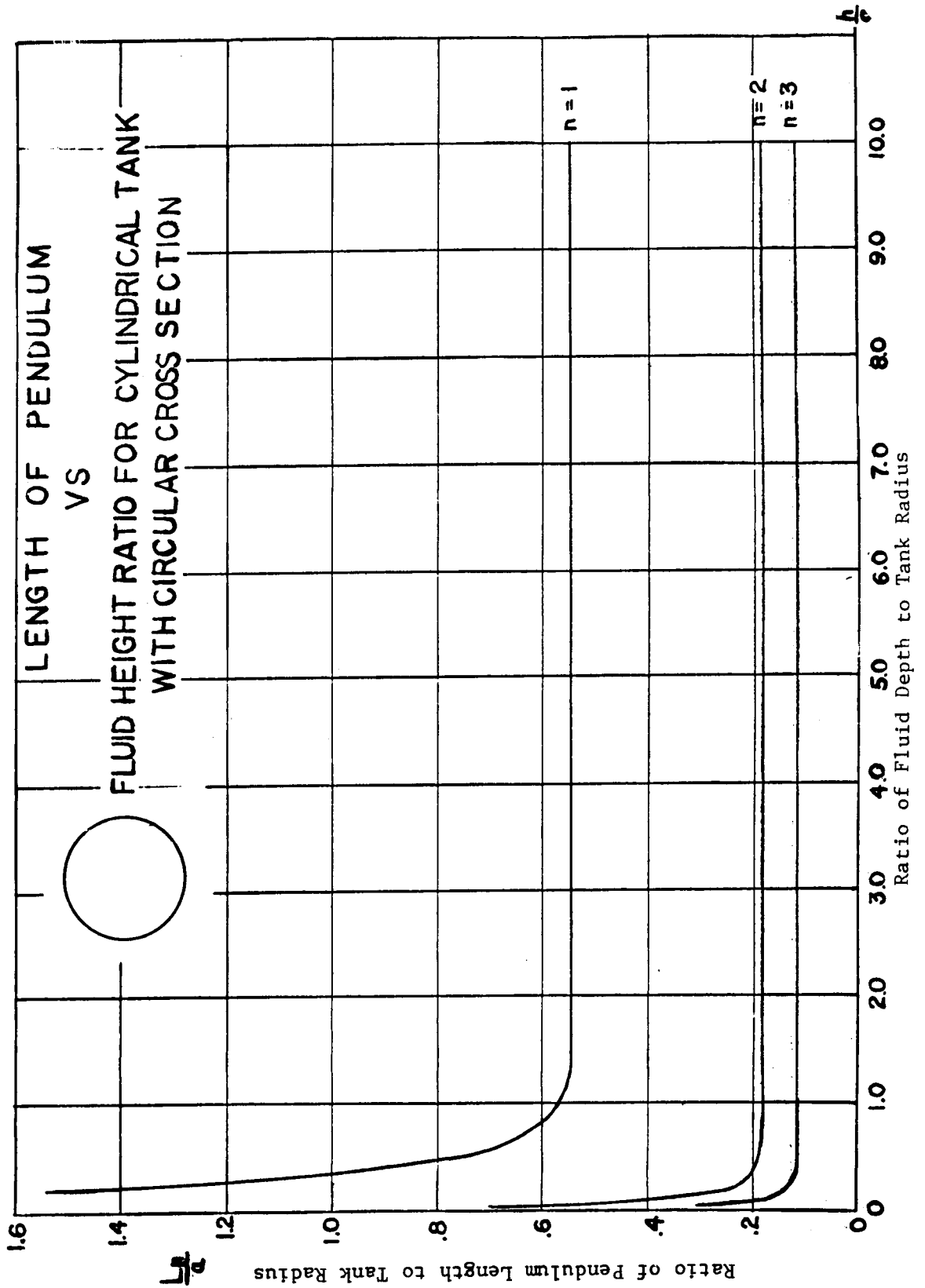


Figure 4-17. Model Element Graph

Table 4-9. Model Analysis

Circular Cylindrical Tank	Pendulum Model
Excitation: Arbitrary Translation and/or Pitching	

Figure 4-18 shows a diagram of the pendulum model used in representing the dynamic response of a liquid in a circular cylindrical tank when subjected to an arbitrary translation in the x-direction and/or pitching about the y-axis.

Coordinate System:

The origin is located at the geometric center of the tank bottom.

Model Description:

The components of the system are as follows:

1. A fixed mass M having a moment of inertia I is rigidly connected to the tank and is located on the z-axis at a distance H above the coordinate origin.
2. A set of movable masses m_n is distributed along the z-axis when the tank is at rest. The modal masses are pendulums having massless lever arms of length L_n attached to the z-axis at distances H_n above the origin. Angular displacements of the pendulums with respect to the tank (z-axis) is denoted by λ_n and θ is a space fixed coordinate defining the pitching angle of the container. Angular displacements of the pendulums are therefore defined by a generalized space fixed coordinate, $\Gamma_n = \lambda_n - \theta$.

Equations of Motion:

The equations, obtained through Lagrange's equations, are as follows:

1. Force Equation:

$$F = - (M + m_n) \ddot{x} - [MH + m_n(H_n - L_n)] \ddot{\theta} - m_n L_n \ddot{\lambda}_n$$

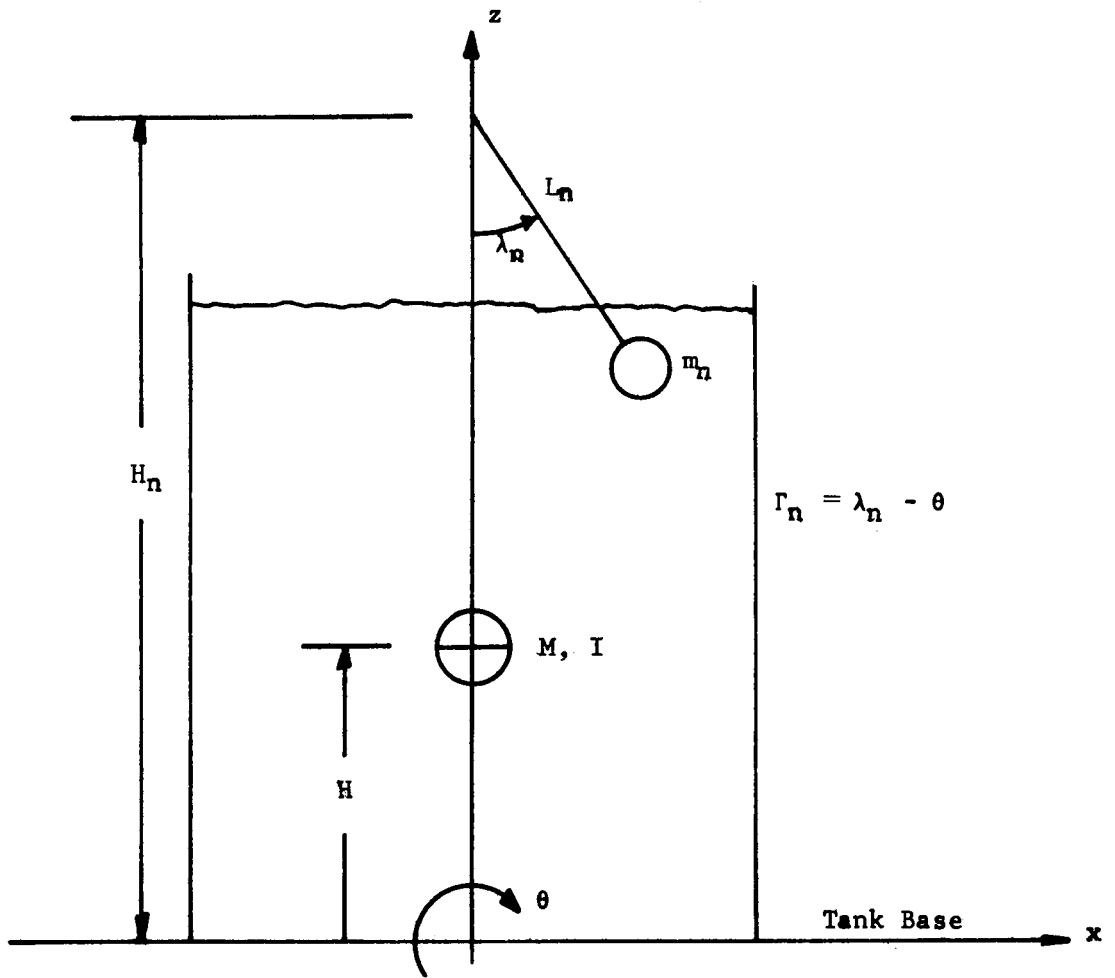
2. Moment Equation:

$$M = - [MH + m_n(H_n - L_n)] \ddot{x} - [MH^2 + m_n(H_n - L_n)^2 + I] \ddot{\theta} + [MH + m_n(H_n - L_n)] \theta - m_n L_n (H_n - L_n) \ddot{\lambda}_n + m_n g L_n \lambda_n$$

3. Slosh Mass Equation:

$$\ddot{\lambda}_n + \omega_n^2 \lambda_n = - \frac{1}{L_n} \left[\ddot{x} + (H_n - L_n) \ddot{\theta} - g\theta \right]$$

Using the method of Laplace transforms, the force and moment have been represented as transformed variables, which thereby become a function of the Laplace-transform operator s (see Table 4-10).



Circular Cylindrical Tank	Pendulum Model
Excitation: Arbitrary Translation and/or Pitching	

Figure 4-18. Equivalent Mechanical Model

Table 4-10. Model Force and Moment Resultants

Circular Cylindrical Tank	Pendulum Model
Excitation: Arbitrary Translation and/or Pitching	

Arbitrary translation in the x'-direction and/or pitching about the y'-axis.

$$1. F(s) = - Mx(s)s^2 - MH\theta(s)s^2 - gs^2 \sum_{n=0}^{\infty} m_n \left(\sum_{n=0}^{\infty} \frac{x(s) + H_n \theta(s)}{L_n (s^2 + \omega^2)} \right)$$

$$2. M(s) = - MHx(s)s^2 - (I + MH^2)\theta(s)s^2 + g \sum_{n=0}^{\infty} \left[(MH + m_n H_n)\theta(s) - m_n H_n \sum_{n=0}^{\infty} \frac{[x(s) + H_n \theta(s)]s^2}{L_n (s^2 + \omega^2)} \right]$$

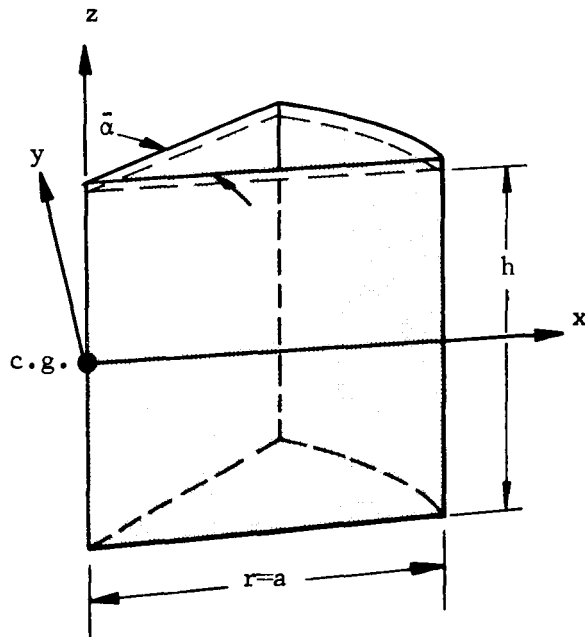
Table 4-11. Model Elements

Circular Cylindrical Tank	Pendulum Model
Excitation: Arbitrary Translation and/or Pitching	
Natural Frequency	$\omega_n^2 = \frac{g}{a} \epsilon_n \tanh \kappa_n$
Pendulum Length	$L_n = \frac{g}{\omega_n^2}$
Slosh Mass	$m_n = m_L \left[\frac{2 \tanh \kappa_n}{\kappa_n (\epsilon_n^2 - 1)} \right]$
Fixed Mass	$M = m_L - \sum_{n=1}^{\infty} m_n$
Slosh Mass Coordinate	$ H_n - L_n = h \left[1 - \frac{2 - \cosh \kappa_n}{\kappa_n \sinh \kappa_n} \right]$
Fixed Mass Coordinate	$ H = \frac{m_L h}{m_L - m_n} \left[\frac{1}{2} + \frac{a^2}{4h^2} - \frac{2(2 + \kappa_n \sinh \kappa_n - \cosh \kappa_n)}{\kappa_n^2 (\epsilon_n^2 - 1) \cosh \kappa_n} \right]$
Moment of Inertia of Fixed Mass	$I = m_L h^2 \left[\frac{1}{3} - \frac{8\kappa_n + (2\kappa_n^2 - 8) \sinh \kappa_n - 2\kappa_n \cosh \kappa_n}{\kappa_n^3 (\epsilon_n^2 - 1) \cosh \kappa_n} \right] - M H^2$

4.3 Sector Tank

Table of Contents

General.....	4-38
Excitation: Harmonic Translation	
Boundary Conditions, Velocity Potential, and Natural Frequency.....	4-39
Liquid Force and Moment Resultants.....	4-41
Excitation: Harmonic Pitching	
Boundary Conditions, Velocity Potential, and Natural Frequency.....	4-42
Liquid Force and Moment Resultants.....	4-44
Excitation: Harmonic Roll	
Boundary Conditions, Velocity Potential, and Natural Frequency.....	4-46
Liquid Force and Moment Resultants.....	4-47



Container: The tank is a sector of a right circular cylinder of radius a and filled with a liquid to a depth h . The vertex angle is denoted by $\bar{\alpha}$.

Coordinate System: The origin is located at the center of gravity of the undisturbed fluid which would be contained in a right circular cylinder generated by revolving the sector tank about the z -axis. The x -axis must lie in the sector wall.

References: (4)

Comments: The results given in this section are not valid for $\bar{\alpha} = \frac{\pi}{2}, \frac{3\pi}{2}$.

Table 4-12. Boundary Conditions, Velocity Potential, and Natural Frequency

Sector Tank	Excitation: Harmonic Translation
-------------	----------------------------------

Translation in the x-direction, $x = x_0 e^{i\omega t}$.

1. Boundary conditions:

$$(a) \left(\frac{\partial \phi}{\partial r} \right)_{r=a} = i\omega x_0 e^{i\omega t} \cos \phi \quad (b) \left(\frac{\partial \phi}{\partial z} \right)_{z=-h} = 0$$

$$(c) \left(\frac{1}{r} \frac{\partial \phi}{\partial \phi} \right)_{\phi=0} = 0 \quad (d) \left(\frac{1}{r} \frac{\partial \phi}{\partial \phi} \right)_{\phi=\bar{\alpha}} = -i\omega x_0 e^{i\omega t} \sin \bar{\alpha} \quad (e) \left(\frac{\partial^2 \phi}{\partial t^2} + g \frac{\partial \phi}{\partial z} \right)_{z=0} = 0$$

2. Velocity potential:

$$\phi = i\omega x_0 e^{i\omega t} \left[r \cos \phi + \sum_{m=0}^{\infty} \sum_{n=0}^{\infty} \frac{a_m \bar{b}_n J_{m/2\alpha}(\rho_{mn}) \cos \bar{\phi}_m \cosh(\kappa_{mn} + \zeta_{mn})}{(\eta_{mn}^2 - 1)} \right]$$

3. Natural angular frequency:

$$\omega_{mn}^2 = \frac{g}{a} \epsilon_{mn} \tanh \kappa_{mn}$$

where ϵ_{mn} are roots of $J'_{m/2\alpha}(\epsilon_{mn}) = 0$.

Table 4-12. Boundary Conditions, Velocity Potential, and Natural Frequency (continued)

Sector Tank	Excitation: Harmonic Translation
-------------	----------------------------------

Translation in the y-direction, $y = y_0 e^{i\omega t}$.

1. Boundary conditions:

$$(a) \left(\frac{\partial \phi}{\partial r} \right)_{r=a} = i\omega y_0 e^{i\omega t} \sin \phi \quad (b) \left(\frac{\partial \phi}{\partial z} \right)_{z=-h} = 0$$

$$(c) \left(\frac{1}{r} \frac{\partial \phi}{\partial \phi} \right)_{\phi=0} = i\omega y_0 e^{i\omega t} \quad (d) \left(\frac{1}{r} \frac{\partial \phi}{\partial \phi} \right)_{\phi=\bar{\alpha}} = i\omega y_0 e^{i\omega t} \cos \bar{\alpha} \quad (e) \left(\frac{\partial^2 \phi}{\partial t^2} + g \frac{\partial \phi}{\partial z} \right)_{z=0} = 0$$

2. Velocity potential:

$$\phi = i\omega y_0 e^{i\omega t} \left[r \sin \phi + \sum_{m=0}^{\infty} \sum_{n=0}^{\infty} \frac{c_m b_m J_m(\rho_{mn}) \cos \bar{\phi}_m \cosh(\kappa_{mn} + \zeta_{mn})}{(\eta_{mn}^2 - 1)} \right]$$

3. Natural angular frequency:

$$\omega_{mn}^2 = \frac{g}{a} \epsilon_{mn} \tanh \kappa_{mn}$$

where ϵ_{mn} are roots of $J_m'(\epsilon_{mn}) = 0$.

Table 4-13. Liquid Force and Moment Resultants

Sector Tank	Excitation: Harmonic Translation
Translation in the x-direction, $x = x_0 e^{i\omega t}$ and translation in the y-direction, $y = y_0 e^{i\omega t}$.	

$$1. F_x = m_L \omega^2 \begin{pmatrix} x_0 \\ y_0 \end{pmatrix} e^{i\omega t} \left[\begin{pmatrix} 1 \\ 0 \end{pmatrix} + \sum_{m=0}^{\infty} \sum_{n=0}^{\infty} 2(-1)^{m+1} \begin{pmatrix} a_m \\ c_m \end{pmatrix} \left(\frac{\bar{b}_m \sin \bar{\alpha} \tanh \kappa_{mn}}{\bar{\alpha} a (\eta_{mn}^2 - 1) \kappa_{mn}} \right) \left(\frac{\bar{\alpha}^2 J_{m/2\alpha}(\epsilon_{mn})}{\pi^2 2^2 - \bar{\alpha}^2} + L_0(\epsilon_{mn}) \right) \right]$$

$$2. F_y = m_L \omega^2 \begin{pmatrix} x_0 \\ y_0 \end{pmatrix} e^{i\omega t} \left[\begin{pmatrix} 0 \\ 1 \end{pmatrix} - \sum_{m=0}^{\infty} \sum_{n=0}^{\infty} 2 \begin{pmatrix} a_m \\ c_m \end{pmatrix} \left(\frac{\bar{b}_m [1 - (-1)^m \cos \bar{\alpha}] \tanh \kappa_{mn}}{\bar{\alpha} a (\eta_{mn}^2 - 1) \kappa_{mn}} \right) \left(\frac{\bar{\alpha}^2 J_{m/2\alpha}(\epsilon_{mn})}{\pi^2 2^2 - \bar{\alpha}^2} + L_0(\epsilon_{mn}) \right) \right]$$

$$3. M_y = m_L a \omega^2 \begin{pmatrix} x_0 \\ y_0 \end{pmatrix} e^{i\omega t} \left[\frac{1}{4(h/a)} \left(1 + (\sin \bar{\alpha} \cos \bar{\alpha})/\bar{\alpha} \right) + \sum_{m=0}^{\infty} \sum_{n=0}^{\infty} (-1)^{m+1} \begin{pmatrix} a_m \\ c_m \end{pmatrix} \left(\frac{\bar{b}_m \sin \bar{\alpha}}{\bar{\alpha} a (\eta_{mn}^2 - 1) \epsilon_{mn}} \right) \right]$$

$$\left[\left[\frac{\bar{\alpha}^2 J_{m/2\alpha}(\epsilon_{mn})}{\pi^2 2^2 - \bar{\alpha}^2} + L_0(\epsilon_{mn}) \right] \left[\tanh \kappa_{mn} + \frac{2}{\kappa_{mn}} \left(\frac{1}{\cosh \kappa_{mn}} - 1 \right) \right] + \frac{2\bar{\alpha}^2 \epsilon_{mn} L_2(\epsilon_{mn})}{(\pi^2 2^2 - \bar{\alpha}^2) \kappa_{mn} \cosh \kappa_{mn}} \right] \left. \right\} + \frac{2mga \sin \bar{\alpha}}{3 \bar{\alpha}}$$

$$4. M_x = -m_L a \omega^2 \begin{pmatrix} x_0 \\ y_0 \end{pmatrix} e^{i\omega t} \left[\frac{1}{4(h/a)} \left((2 \sin^2 \bar{\alpha})/\bar{\alpha} \right) - \sum_{m=0}^{\infty} \sum_{n=0}^{\infty} \begin{pmatrix} a_m \\ c_m \end{pmatrix} \left(\frac{\bar{b}_m [1 - (-1)^m \cos \bar{\alpha}]}{\bar{\alpha} a (\eta_{mn}^2 - 1) \epsilon_{mn}} \right) \right]$$

$$\left[\left[\frac{\bar{\alpha}^2 J_{m/2\alpha}(\epsilon_{mn})}{\pi^2 2^2 - \bar{\alpha}^2} + L_0(\epsilon_{mn}) \right] \left[\tanh \kappa_{mn} + \frac{2}{\kappa_{mn}} \left(\frac{1}{\cosh \kappa_{mn}} - 1 \right) \right] + \frac{2\bar{\alpha}^2 \epsilon_{mn} L_2(\epsilon_{mn})}{(\pi^2 2^2 - \bar{\alpha}^2) \kappa_{mn} \cosh \kappa_{mn}} \right] \left. \right\} - \frac{2mga(1 - \cos \bar{\alpha})}{3 \bar{\alpha}}$$

Table 4-14. Boundary Conditions, Velocity Potential, and Natural Frequency

Sector Tank	Excitation: Harmonic Pitching
-------------	-------------------------------

Pitching about the x-axis, $\chi = \chi_0 e^{i\omega t}$.

1. Boundary Conditions:

$$(a) \left(\frac{\partial \phi}{\partial r} \right)_{r=a} = -i\omega \chi_0 e^{i\omega t} \sin \phi$$

$$(b) \left(\frac{\partial \phi}{\partial z} \right)_{z=-h/2} = i\omega \chi_0 e^{i\omega t} \sin \phi$$

$$(c) \left(\frac{\partial^2 \phi}{\partial t^2} + g \frac{\partial \phi}{\partial z} \right)_{z=+h/2} = 0$$

$$(d) \left(\frac{1}{r} \frac{\partial \phi}{\partial \phi} \right)_{\phi=0} = -i\omega \chi_0 e^{i\omega t}$$

$$(e) \left(\frac{1}{r} \frac{\partial \phi}{\partial \phi} \right)_{\phi=\alpha} = -i\omega \chi_0 e^{i\omega t} \cos \alpha$$

4-142

2. Velocity potential:

$$\phi = -i\omega \chi_0 e^{i\omega t} \left[rz \sin \phi - \sum_{m=0}^{\infty} \sum_{n=0}^{\infty} J_{m/2\alpha}(\rho_{mn}) \cos \bar{\phi}_m (C_{mn} \cosh \zeta_{mn} + D_{mn} \sinh \zeta_{mn}) \right]$$

3. Natural angular frequency:

$$\omega_{mn}^2 = \frac{g}{a} \epsilon_{mn} \tanh \kappa_{mn}$$

where ϵ_{mn} are zeros of $J'_{m/2\alpha}(\epsilon_{mn}) = 0$.

Table 4-14. Boundary Conditions, Velocity Potential, and Natural Frequency (continued)

Sector Tank	Excitation: Harmonic Pitching
-------------	-------------------------------

Pitching about the y-axis, $\theta = \theta_0 e^{i\omega t}$.

1. Boundary conditions:

$$(a) \left(\frac{\partial \phi}{\partial r} \right)_{r=a} = -i\omega z \theta_0 e^{i\omega t} \cos \phi \quad (b) \left(\frac{\partial \phi}{\partial z} \right)_{z=-h/2} = i\omega r \theta_0 e^{i\omega t} \cos \phi$$

$$(c) \left(\frac{\partial^2 \phi}{\partial t^2} + g \frac{\partial \phi}{\partial z} \right)_{z=+h/2} = 0 \quad (d) \left(\frac{1}{r} \frac{\partial \phi}{\partial \phi} \right)_{\phi=0} = 0$$

$$(e) \left(\frac{1}{r} \frac{\partial \phi}{\partial \phi} \right)_{\phi=\alpha} = i\omega z \theta_0 e^{i\omega t} \sin \alpha$$

2. Velocity potential:

$$\phi = -i\omega \theta_0 e^{i\omega t} \left[rz \cos \phi - \sum_{m=0}^{\infty} \sum_{n=0}^{\infty} J_{m/2\alpha}(\rho_{mn}) \cos \bar{\phi}_m (A_{mn} \cosh \zeta_{mn} + B_{mn} \sinh \zeta_{mn}) \right]$$

3. Natural angular frequency:

$$\omega_{mn}^2 = \frac{g}{a} \epsilon_{mn} \tanh \kappa_{mn}$$

where ϵ_{mn} are zeros of $J'_{m/2\alpha}(\epsilon_{mn}) = 0$.

Table 4-15. Liquid Force and Moment Resultants

Sector Tank	Excitation: Harmonic Pitching
-------------	-------------------------------

Pitching about the y-axis, $\theta = \theta_0 e^{i\omega t}$ and pitching about the x-axis, $\chi = \chi_0 e^{i\omega t}$.

$$1. F_x = -m_L g \begin{pmatrix} \theta_0 \\ 0 \end{pmatrix} e^{i\omega t} + m_L \omega^2 \begin{pmatrix} \theta_0 \\ \chi_0 \end{pmatrix} e^{i\omega t} \sum_{m=0}^{\infty} \sum_{n=0}^{\infty} 4(-1)^{m+n} \left(\frac{A_{mn}}{C_{mn}} \right) \frac{\sin \bar{\alpha} \sinh(\kappa_{mn}/2)}{\bar{\alpha} a \kappa_{mn}} \left[\frac{\bar{\alpha}^2 J_m/2\alpha(\epsilon_{mn})}{\pi^2 2^{-2} - \bar{\alpha}^2} + L_0(\epsilon_{mn}) \right]$$

$$2. F_y = -m_L g \begin{pmatrix} 0 \\ \chi_0 \end{pmatrix} e^{i\omega t} - m_L \omega^2 \begin{pmatrix} \theta_0 \\ \chi_0 \end{pmatrix} e^{i\omega t} \sum_{m=0}^{\infty} \sum_{n=0}^{\infty} 4 \left(\frac{A_{mn}}{C_{mn}} \right) \frac{[1 - (-1)^m \cos \bar{\alpha}] \sinh(\kappa_{mn}/2)}{\bar{\alpha} a \kappa_{mn}} \left[\frac{\bar{\alpha}^2 J_m/2\alpha(\epsilon_{mn})}{\pi^2 2^{-2} - \bar{\alpha}^2} + L_0(\epsilon_{mn}) \right]$$

$$3. M_y = -m_L g a \begin{pmatrix} \theta_0 \\ \chi_0 \end{pmatrix} e^{i\omega t} \left(\frac{1}{4(h/a)} \right) \left(1 + \frac{\sin \bar{\alpha} \cos \bar{\alpha}}{\sin^2 \bar{\alpha}} \right) + m_L a^2 \omega^2 \begin{pmatrix} \theta_0 \\ \chi_0 \end{pmatrix} e^{i\omega t} \left\{ \frac{1}{8} \left((1 + \sin \bar{\alpha} \cos \bar{\alpha}) - 2(h/a)^2/3 \right) \frac{\bar{\alpha}^2}{\sin^2 \bar{\alpha}} \right\}$$

$$+ \sum_{m=0}^{\infty} \sum_{n=0}^{\infty} \frac{2(-1)^{m+n} \sin \bar{\alpha}}{\bar{\alpha}^2 \epsilon_{mn}} \left[\begin{pmatrix} B_{mn} \\ D_{mn} \end{pmatrix} \left[\cosh \left(\frac{\kappa_{mn}}{2} \right) - \frac{2}{\kappa_{mn}} \sinh \left(\frac{\kappa_{mn}}{2} \right) \right] \left[\frac{\bar{\alpha}^2 J_m/2\alpha(\epsilon_{mn})}{\pi^2 2^{-2} - \bar{\alpha}^2} + L_0(\epsilon_{mn}) \right] \right]$$

$$+ \frac{\bar{\alpha}^2 L_2(\epsilon_{mn})}{(\pi^2 2^{-2} - \bar{\alpha}^2) \kappa_{mn}} \left[\left(\frac{A_{mn}}{C_{mn}} \right) \cosh \left(\frac{\kappa_{mn}}{2} \right) - \left(\frac{B_{mn}}{D_{mn}} \right) \sinh \left(\frac{\kappa_{mn}}{2} \right) \right] + \frac{2mga \sin \bar{\alpha}}{3 \bar{\alpha}}$$

Table 4-15. Liquid Force and Moment Resultants (continued)

Sector Tank	Excitation: Harmonic Pitching
-------------	-------------------------------

$$\begin{aligned}
 4. M_x = m_L g a \begin{pmatrix} \theta_0 \\ \chi_0 \end{pmatrix} e^{i\omega t} & \left(\frac{1}{4(h/a)} \right) \left(\frac{\sin^2 \bar{\alpha}}{1 - \sin \bar{\alpha} \cos \bar{\alpha}} \right) - m_L a^2 \omega^2 \begin{pmatrix} \theta_0 \\ \chi_0 \end{pmatrix} e^{i\omega t} \left\{ \frac{1}{8} \left(\frac{\sin^2 \bar{\alpha}}{1 - \sin \bar{\alpha} \cos \bar{\alpha}} \right) \right. \\
 & - \sum_{m=0}^{\infty} \sum_{n=0}^{\infty} \frac{2 \left[1 - (-1)^m \cos \bar{\alpha} \right]}{\bar{\alpha}^2 a^2 \epsilon_{mn}} \left[\left(\frac{B_{mn}}{D_{mn}} \right) \left[\cosh \left(\frac{\kappa_{mn}}{2} \right) - \frac{2}{\kappa_{mn}} \sinh \left(\frac{\kappa_{mn}}{2} \right) \right] \left[\frac{\alpha^2 J_{m/2n}(\epsilon_{mn})}{\pi^2 m^2 - \alpha^2} + L_0(\epsilon_{mn}) \right] \right. \\
 & \left. \left. + \frac{\alpha^2 \epsilon_{mn} L_2(\epsilon_{mn})}{(\pi^2 m^2 - \alpha^2) \kappa_{mn}} \left[\left(\frac{A_{mn}}{C_{mn}} \right) \cosh \left(\frac{\kappa_{mn}}{2} \right) - \left(\frac{B_{mn}}{D_{mn}} \right) \sinh \left(\frac{\kappa_{mn}}{2} \right) \right] \right] \right\} - \frac{2mga(1 - \cos \bar{\alpha})}{3\bar{\alpha}}
 \end{aligned}$$

Table 4-16. Boundary Conditions, Velocity Potential, and Natural Frequency

Sector Tank	Excitation: Harmonic Roll
-------------	---------------------------

Roll about the z-axis, $\phi = \phi_0 e^{i\omega t}$.

1. Boundary condition:

$$(a) \left(\frac{\partial \phi}{\partial r} \right)_{r=a} = 0$$

$$(b) \left(\frac{\partial \phi}{\partial z} \right)_{z=-h} = 0$$

$$(c) \left(\frac{1}{r} \frac{\partial \phi}{\partial r} \right)_{\phi=0, \bar{\alpha}} = i\omega r \phi_0 e^{i\omega t}$$

$$(d) \left(\frac{\partial^2 \phi}{\partial t^2} + g \frac{\partial \phi}{\partial z} \right)_{z=0} = 0$$

2. Velocity potential:

$$\phi = i\omega a^2 \phi_0 e^{i\omega t} \left\{ \left(\frac{r}{a} \right)^2 \left(\phi - \frac{\bar{\alpha}}{2} \right) + \sum_{m=1}^{\infty} \frac{8\bar{\alpha}^2 \cos \bar{\alpha} \phi_m}{\pi (2m-1) [(2m-1)^2 \pi^2 - 4\bar{\alpha}^2]} \left[\left(\frac{r}{a} \right)^{2(2m-1)/2\alpha} - \left(\frac{r}{a} \right)^2 \frac{4\alpha}{2m-1} \right] \right. \\ \left. + \sum_{m=1}^{\infty} \sum_{n=0}^{\infty} \frac{4\bar{\alpha} [4\alpha / (2m-1)] f_{2m-1,n} - e^{2m-1,n}}{[(2m-1)^2 \pi^2 - 4\bar{\alpha}^2] (n_{2m-1,n}^{-1}) \cosh \kappa_{2m-1,n}} \cos \bar{\alpha} \phi_m \cosh (\kappa_{2m-1,n} + \zeta_{2m-1,n}) \right\}$$

3. Natural angular frequency:

$$\omega_{2m-1,n}^2 = \frac{g}{a} e^{2m-1,n} \tanh \kappa_{2m-1,n}$$

where $\epsilon_{2m-1,n}$ are solutions of $J'_{4m-2}(\epsilon_{2m-1,n}) = 0$.

Table 4-17. Liquid Force and Moment Resultants

Sector Tank	Excitation: Harmonic Roll
Roll about the z-axis, $\phi = \phi_0 e^{i\omega t}$.	
1.	$\begin{aligned} \begin{pmatrix} F_x \\ F_y \end{pmatrix} &= m_L a \omega^2 \phi_0 e^{i\omega t} \left\{ 2 \left(\frac{\cos \bar{\alpha} - 1}{\sin \bar{\alpha}} \right) \frac{\bar{\alpha} + \sin \bar{\alpha}/3}{2 - (\cos \bar{\alpha} + 1)/3} + \frac{16 \bar{\alpha} \sin \bar{\alpha}}{\pi} \sum_{m=1}^{\infty} \left[\frac{2\alpha / (2m + 2\alpha - 1) - 4\alpha / 3(2m - 1)}{(2m - 1) [(2m - 1)^2 \pi^2 - 4 \bar{\alpha}^2]} \right. \right. \\ &+ \left. \frac{\bar{\alpha}^2}{(2m - 1)^2 [(2m - 1)^2 \pi^2 - \bar{\alpha}^2]} \right] + \sum_{m=1}^{\infty} \sum_{n=0}^{\infty} \left. \left[\frac{8 [(4\alpha / 2m - 1) f_{2m-1,n} - e_{2m-1,n}] \sin \bar{\alpha} \tanh \kappa_{2m-1,n} \left[\frac{\bar{\alpha}^2 J_{2m-1,n} / 2\alpha (\epsilon_{2m-1,n})}{(2m-1)^2 \pi^2 - \bar{\alpha}^2} + L_0 (\epsilon_{2m-1,n}) \right]}{(h/a) \epsilon_{2m-1,n} [(2m-1)^2 \pi^2 - 4 \bar{\alpha}^2]} (\eta_{2m-1,n} - 1) \right] \right\} \end{aligned}$
2.	$\begin{aligned} \begin{pmatrix} M_x \\ M_y \end{pmatrix} &= m_L a^2 \omega \phi_0 e^{i\omega t} \left\{ \left[\frac{1}{5(h/a)} \left(\frac{1 + \cos \bar{\alpha} - 2 \sin \bar{\alpha} / \bar{\alpha}}{\sin \bar{\alpha} + 2 \cos \bar{\alpha} - 2 / \bar{\alpha}} \right) + \frac{48 \bar{\alpha}^4 \sin \bar{\alpha}}{5\pi^2 (h/a)} \sum_{m=1}^{\infty} \right. \right. \\ &+ \left. \frac{2m-1 - 4\alpha}{(2m-1)^2 (2m-1 + 6\alpha) [(2m-1)^2 \pi^2 - 4\bar{\alpha}^2]} + \frac{4 \sin \bar{\alpha}}{a^2} \sum_{m=1}^{\infty} \sum_{n=0}^{\infty} \left[\frac{[4\alpha / (2m-1)] f_{2m-1,n} - e_{2m-1,n}}{\epsilon_{2m-1,n} [(2m-1)^2 \pi^2 - 4 \bar{\alpha}^2]} (\eta_{2m-1,n} - 1) \right] \left[\tanh \left[\frac{\kappa_{2m-1,n}}{2} \right] + \frac{2}{\kappa_{2m-1,n}} \left(\frac{1}{\cosh \kappa_{2m-1,n}} - 1 \right) \right] \right. \\ &\left. \left[\frac{\bar{\alpha}^2 J_{2m-1,n} / 2\alpha (\epsilon_{2m-1,n})}{(2m-1)^2 \pi^2 - \bar{\alpha}^2} + L_0 (\epsilon_{2m-1,n}) \right] + \frac{2\bar{\alpha}^2 \epsilon_{2m-1,n} L_2 (\epsilon_{2m-1,n})}{[(2m-1)^2 \pi^2 - \bar{\alpha}^2] \kappa_{2m-1,n} \cosh \kappa_{2m-1,n}} \right] \left. \right\} + \frac{2mga}{3\bar{\alpha}} \begin{pmatrix} \cos \bar{\alpha} \\ \sin \bar{\alpha} \end{pmatrix} \end{aligned}$

Table 4-17. Liquid Force and Moment Resultants (continued)

Sector Tank	Excitation: Harmonic Roll
-------------	---------------------------

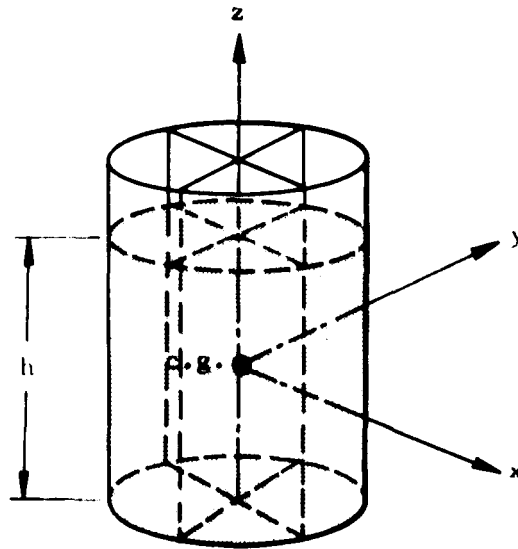
$$3. M_z = m_L a^2 \omega^2 \phi_0 e^{i\omega t} \left\{ \frac{1}{2} - \frac{16 \bar{\alpha}^2}{\pi^2} \sum_{m=1}^{\infty} \frac{1}{(2m-1)^2 [(2m-1)\pi + 2\bar{\alpha}]^2} \right.$$

$$\left. - 16 \sum_{m=1}^{\infty} \sum_{n=0}^{\infty} \frac{[(4\alpha/(2m-1)) f_{2m-1,n} - e_{2m-1,n}] L_1(\epsilon_{2m-1,n}) \tanh \kappa_{2m-1,n}}{[(2m-1)^2 \pi^2 - 4\bar{\alpha}^2] (n_{2m-1,n} - 1) \kappa_{2m-1,n}} \right\}$$

4.4 Quarter-Sectored Tank

Table of Contents

General.....	4-50
Excitation: Harmonic Translation and/or Pitching	
Boundary Conditions, Velocity Potential, and Natural Frequency.....	4-51
Liquid Force and Moment Resultants.....	4-53
Spring-Mass Model	
Analysis.....	4-54
Diagram.....	4-56
Force and Moment Resultants.....	4-57
Elements.....	4-58
Graphs.....	4-59
Pendulum Model	
Analysis.....	4-62
Diagram.....	4-64
Force and Moment Resultants.....	4-65
Elements.....	4-66
Excitation: Harmonic Roll	
Boundary Conditions, Velocity Potential, and Natural Frequency.....	4-67
Liquid Force and Moment Resultants.....	4-68
Torsional Pendulum Model	
Analysis.....	4-70
Diagram.....	4-71
Moment Resultant.....	4-72
Elements.....	4-73
Graphs.....	4-74



Container: The tank is a right circular cylinder of radius a divided by longitudinal partitions intersecting at right angles, $\bar{\alpha} = \pi/2$, and is filled with liquid to a depth h .

Coordinate System: The origin is located at the center of gravity of the undisturbed fluid and the x -axis must lie in a sector wall.

References: (4, 60)

Comments: The results given in this section are applicable to only one sector, i.e., the boundary conditions and resulting velocity potential, natural frequency, and force and moment resultants are responses due to liquid oscillations in only one sector (except for the material concern-equivalent mechanical models which applies to the complete tank of four sectors).

Table 4-18. Boundary Conditions, Velocity Potential, and Natural Frequency

Quarter-Sectorred Tank	Excitation: Harmonic Translation
Translation in the x-direction, $x = x_0 e^{i\omega t}$.	

1. Boundary condition:

$$(a) \left(\frac{\partial \phi}{\partial r} \right)_{r=a} = i\omega x_0 e^{i\omega t} \cos \phi$$

$$(b) \left(\frac{\partial \phi}{\partial z} \right)_{z=-h} = 0$$

$$(c) \left(\frac{\partial^2 \phi}{\partial t^2} + g \frac{\partial \phi}{\partial z} \right)_{z=0} = 0$$

$$(d) \left(\frac{1}{r} \frac{\partial \phi}{\partial \phi} \right)_{\phi=0} = 0$$

$$(e) \left(\frac{1}{r} \frac{\partial \phi}{\partial \phi} \right)_{\phi=\alpha} = -i\omega x_0 e^{i\omega t} \sin \alpha$$

4-51

2. Velocity potential:

$$\phi = i\omega x_0 e^{i\omega t} \left[r \cos \phi + \sum_{m=0}^{\infty} \sum_{n=0}^{\infty} \frac{\bar{a}_m \bar{b}_n J_{2m}(\rho_{mn}) \cos 2m\phi \cosh(\kappa_{mn} + \tau_{mn})}{(n_{mn}^2 - 1) \cosh \kappa_{mn}} \right]$$

3. Natural angular frequency:

$$\omega_{mn}^2 = \frac{g}{a} \epsilon_{mn} \tanh \kappa_{mn}$$

where ϵ_{mn} are roots of $J'_{2m}(\epsilon_{mn}) = 0$. (see Table A-4).

Table 4-18. Boundary Conditions, Velocity Potential, and Natural Frequency (continued)

Quarter-Sectorized Tank	Excitation: Harmonic Pitching
-------------------------	-------------------------------

Pitching about the y-axis $\theta = \theta_0 e^{i\omega t}$.

1. Boundary conditions:

$$(a) \left(\frac{\partial \phi}{\partial r} \right)_{r=a} = -i\omega z \theta_0 e^{i\omega t} \cos \phi$$

$$(b) \left(\frac{\partial \phi}{\partial z} \right)_{z=-h/2} = i\omega r \theta_0 e^{i\omega t} \cos \phi$$

$$(c) \left(\frac{\partial^2 \phi}{\partial t^2} + g \frac{\partial \phi}{\partial z} \right)_{z=h/2} = 0$$

$$(d) \left(\frac{1}{r} \frac{\partial \phi}{\partial \phi} \right)_{\phi=0} = 0$$

$$(e) \left(\frac{1}{r} \frac{\partial \phi}{\partial \phi} \right)_{\phi=\bar{\alpha}} = i\omega z \theta_0 e^{i\omega t} \sin \bar{\alpha}$$

2. Velocity potential:

$$\phi = -i\omega \theta_0 e^{i\omega t} \left[rz \cos \phi - \sum_{m=0}^{\infty} \sum_{n=0}^{\infty} (\bar{A}_{mn} \cosh \zeta_{mn} + \bar{B}_{mn} \sinh \zeta_{mn}) J_{2m}(\rho_{mn}) \cos 2m\phi \right]$$

3. Natural angular frequency:

$$\omega_{mn}^2 = \frac{g}{a} \epsilon_{mn} \tanh \kappa_{mn}$$

where ϵ_{mn} are roots of $J_{2m}'(\epsilon_{mn}) = 0$. (see Table A-4).

Table 4-19. Liquid Force and Moment Resultants

Quarter-Sector Tank	Harmonic Translation and/or Pitching
---------------------	--------------------------------------

Translation in the x-direction, $x = x_0 e^{i\omega t}$.

$$\begin{aligned}
 1. \begin{pmatrix} F_x \\ F_y \end{pmatrix} &= m_L \omega^2 x_0 e^{i\omega t} \begin{pmatrix} 1 \\ 0 \end{pmatrix} + \sum_{m=0}^{\infty} \sum_{n=0}^{\infty} \begin{pmatrix} (-1)^{m+1} \\ 1 \end{pmatrix} \frac{4 \bar{a}_m \bar{b}_{mn} \tanh \kappa_{mn}}{\pi a_{mn} (\eta_{mn}^2 - 1) \kappa_{mn}} \left(\frac{J_{2m}(\epsilon_{mn})}{4 m^2 - 1} + L_0(\epsilon_{mn}) \right) \\
 2. \begin{pmatrix} M_x \\ M_y \end{pmatrix} &= \mp m_L a \omega^2 x_0 e^{i\omega t} \left[\left(\frac{1/\pi}{1/4} \right) \sum_{m=0}^{\infty} \sum_{n=0}^{\infty} \begin{pmatrix} 1 \\ (-1)^{m+1} \end{pmatrix} \frac{2 \bar{a}_m \bar{b}_{mn}}{\pi a_{mn} (\eta_{mn}^2 - 1) \epsilon_{mn}} \left\{ \left[\frac{J_{2m}(\epsilon_{mn})}{4 m^2 - 1} + L_0(\epsilon_{mn}) \right] \right. \right. \right. \\
 &\quad \left. \left. \left. + \frac{2 \epsilon_{mn}^2 L_2(\epsilon_{mn})}{(4m^2 - 1) \kappa_{mn} \cosh \kappa_{mn}} \right\} \right] + \frac{4mga}{3\pi}
 \end{aligned}$$

Pitching about the y-axis, $\theta = \theta_0 e^{i\omega t}$.

$$\begin{aligned}
 1. \begin{pmatrix} F_x \\ F_y \end{pmatrix} &= -m_L g \theta_0 e^{i\omega t} + \frac{8 m_L a \omega^2}{\pi} \theta_0 e^{i\omega t} \sum_{m=0}^{\infty} \sum_{n=0}^{\infty} \left[\begin{pmatrix} (-1)^{m+1} \\ 1 \end{pmatrix} \frac{\bar{A}_{mn} \sinh(\kappa_{mn}/2)}{\kappa_{mn}} \right] \left[\frac{J_{2m}(\epsilon_{mn})}{4 m^2 - 1} + L_0(\epsilon_{mn}) \right] \\
 2. \begin{pmatrix} M_x \\ M_y \end{pmatrix} &= -\frac{m_L g a \theta_0 e^{i\omega t}}{2(h/a)} \begin{pmatrix} 1/\pi \\ 1/2 \end{pmatrix} + m_L a^2 \omega^2 \theta_0 e^{i\omega t} \left\{ \left(1/8 - (h/a)^2/12 \right) + \sum_{m=0}^{\infty} \sum_{n=0}^{\infty} \frac{4}{\pi \epsilon_{mn}} \begin{pmatrix} 1 \\ (-1)^{m+1} \end{pmatrix} \right\} \left[\bar{B}_{mn} \left(\cosh \frac{\kappa_{mn}}{2} \right. \right. \right. \\
 &\quad \left. \left. \left. - \frac{2}{\kappa_{mn}} \sinh \frac{\kappa_{mn}}{2} \right) \right] \left(\frac{J_{2m}(\epsilon_{mn})}{4m^2 - 1} + L_0(\epsilon_{mn}) \right) + \frac{L_2(\epsilon_{mn}) \epsilon_{mn}^2}{(4m^2 - 1) \kappa_{mn}} \left(\bar{A}_{mn} \cosh \frac{\kappa_{mn}}{2} - \bar{B}_{mn} \sinh \frac{\kappa_{mn}}{2} \right) \right\} + \frac{4mga}{3\pi}
 \end{aligned}$$

Table 4-20. Model Analysis

Quarter-Sector Tank	Spring-Mass Model
Excitation: Harmonic Translation and/or Pitching	

Figure 4-19 shows a diagram of the spring-mass model used in representing the dynamic response of a liquid in a quarter-sector tank when subjected to harmonic translation in the x-direction and/or pitching about the y-axis.

Coordinate System:

The origin is located at the center of gravity of the undisturbed liquid.

Model Description:

The components of the system are as follows:

1. A fixed mass M having a moment of inertia I is rigidly connected to the tank and is located on the z -axis at a distance H below the coordinate origin.
2. A set of movable masses m_{mn} is distributed along the z -axis when the tank is at rest at distances h_{mn} above the origin. These modal masses are constrained by spring-dashpot systems, having spring stiffness coefficients k_{mn} and viscous damping coefficients c_{mn} , to remain in the xy -plane and to move only in a direction parallel to the x -axis. Translational displacements of these masses with respect to the container are denoted by x_{mn} .
3. A massless disc having a moment of inertia I_d is located at the coordinate origin. Its motion is confined to rotation about the y -axis and is cushioned by a dashpot having a viscous damping coefficient c_d . The angular displacement of the disc relative to the tank is defined by ψ .

Equations of Motion:

The equations, obtained through Lagrange's equations, are as follows:

1. Force Equation:

$$F_x = -M(\ddot{x} + H\ddot{\theta}) - \sum_{m=1}^{\infty} \sum_{n=1}^{\infty} m_{mn} (\ddot{x} + \ddot{x}_{mn} + h_{mn} \ddot{\theta})$$

2. Moment Equation:

$$M_y = - (I + MH^2)\ddot{\theta} - I_d (\ddot{\theta} + \ddot{\psi}) + g \sum_{m=1}^{\infty} \sum_{n=1}^{\infty} m_{mn} x_{mn} - \sum_{m=1}^{\infty} \sum_{n=1}^{\infty} m_{mn} h_{mn} (\ddot{x}_{mn} + h_{mn} \ddot{\theta})$$

Table 4-20. Model Analysis (continued)

Quarter-Sector Tank	Spring-Mass Model
Excitation: Harmonic Translation and/or Pitching	

Equations of Motion (continued):

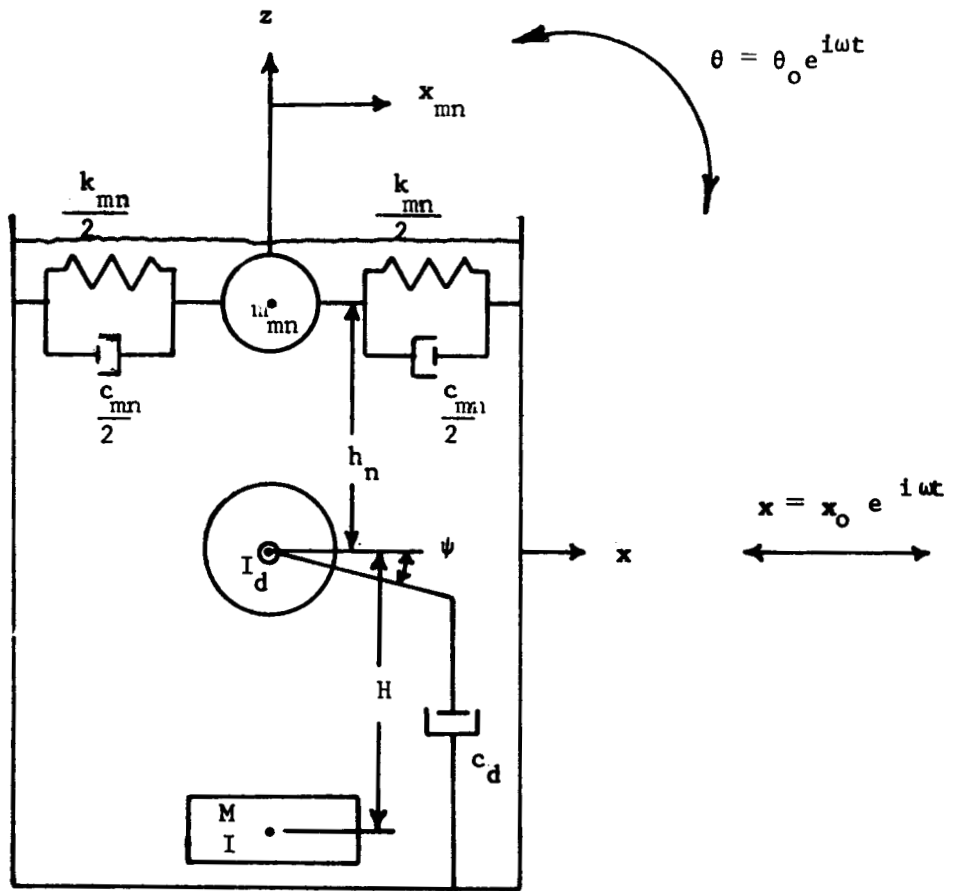
3. Disc Equation:

$$I_d (\ddot{\theta} + \ddot{\psi}) + c_d \dot{\psi} = 0$$

4. Slosh-Mass Equation:

$$m_{mn} (\ddot{x} + \ddot{x}_{mn} + h_{mn} \ddot{\theta}) + m_{mn} \bar{g}_{mn} \omega_{mn} \dot{x}_{mn} + k_{mn} x_{mn} - m_{mn} g \theta = 0$$

From these equations, the model force in the x-direction and the moment about the y-axis can be found (see Table 4-21).



Quarter-Sectored Tank	Spring-Mass Model
Excitation: Harmonic Translation and/or Pitching	

Figure 4-19. Equivalent Mechanical Model

Table 4-21. Model Force and Moment Resultants

Quarter-Sectored Tank	Spring-Mass Model
Excitation: Harmonic Translation and/or Pitching	

Translation in the x-direction, $x = x_0 e^{i\omega t}$.

$$1. F_x = m_L \omega^2 x_0 e^{i\omega t} \left[1 + \sum_{m=0}^{\infty} \sum_{n=0}^{\infty} \left(\frac{m_{mn}}{m_L} \right) \left(\frac{1}{\eta_{mn}^2 - 1 + i\bar{g}_{mn} \eta_{mn}} \right) \right]$$

$$2. M_y = m_L h \omega^2 x_0 e^{i\omega t} \sum_{m=0}^{\infty} \sum_{n=0}^{\infty} \left(\frac{m_{mn}}{m_L} \right) \left(\frac{h_{mn}}{h} + \frac{g}{h\omega^2} \right) \left(\frac{1}{\eta_{mn}^2 - 1 + i\bar{g}_{mn} \eta_{mn}} \right)$$

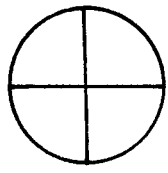
Pitching about the y-axis, $\theta = \theta_0 e^{i\omega t}$.

$$1. F_x = -m_L h \omega^2 \theta_0 e^{i\omega t} \sum_{m=0}^{\infty} \sum_{n=0}^{\infty} \left(\frac{m_{mn}}{m_L} \right) \left(\frac{h_{mn}}{h} + \frac{g}{h\omega^2} \right) \left(\frac{1}{\eta_{mn}^2 - 1 + i\bar{g}_{mn} \eta_{mn}} \right)$$

$$2. M_y = -m_L h \omega^2 \theta_0 e^{i\omega t} \left[\frac{I}{m_L h^2} + \frac{Mh^2}{m_L h^2} + \frac{I_d}{m_L h^2} \left(1 - \frac{\omega^2 I_d^2}{c_d^2 + \omega^2 I_d^2} \right) + \sum_{m=0}^{\infty} \sum_{n=0}^{\infty} \frac{m_{mn} h^2}{m_L h^2} \right. \\ \left. + \sum_{m=0}^{\infty} \sum_{n=0}^{\infty} \left(\frac{m_{mn}}{m_L} \right) \left(\frac{h_{mn}}{h} + \frac{g}{h\omega^2} \right)^2 \left(\frac{1}{\eta_{mn}^2 - 1 + i\bar{g}_{mn} \eta_{mn}} \right) \right] + i\omega \theta_0 e^{i\omega t} \left(\frac{c_d \omega^2 I_d^2}{c_d^2 + \omega^2 I_d^2} \right)$$

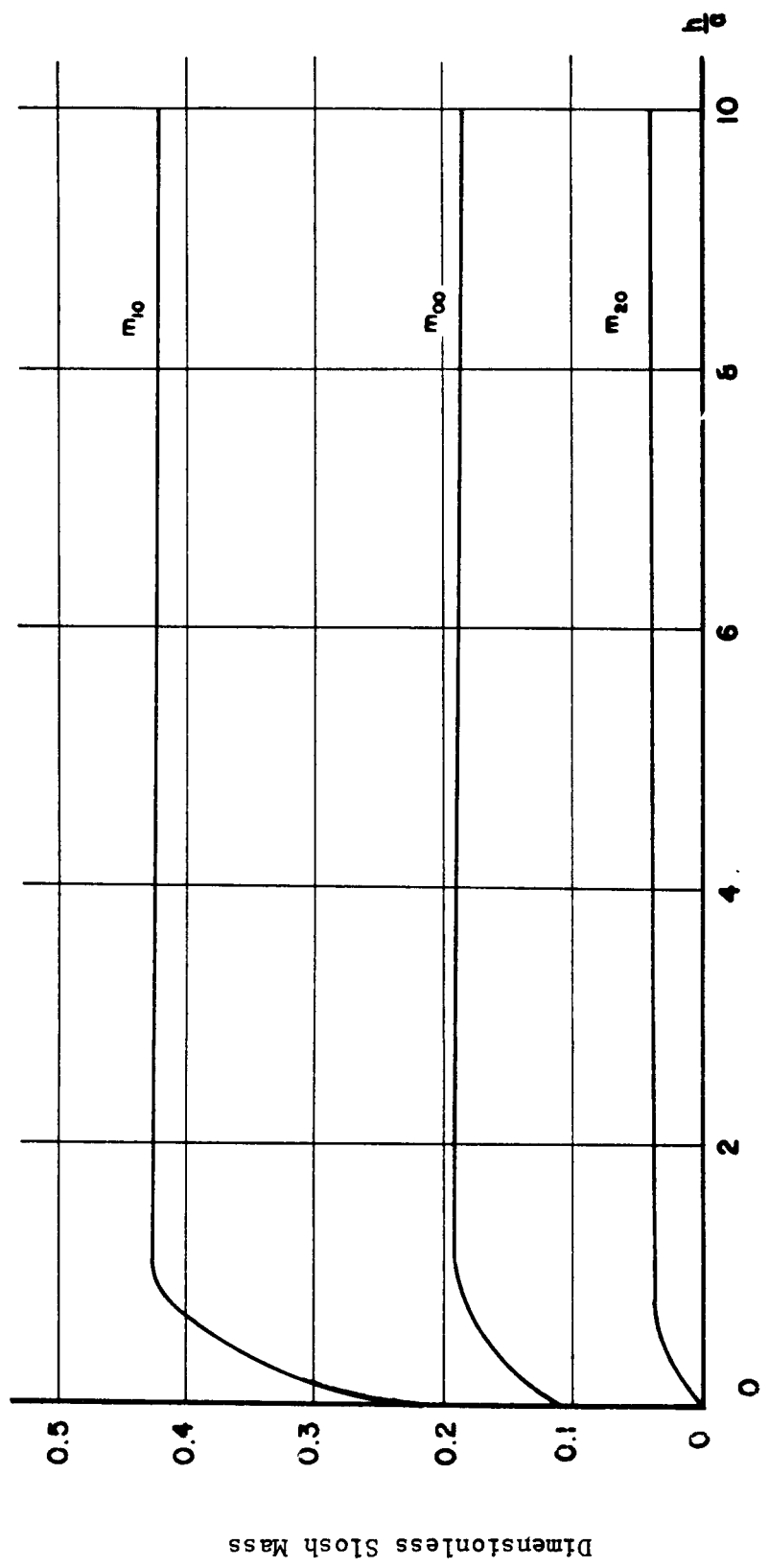
Table 4-22. Model Elements

Quartered-Sectored Tank	Spring-Mass Model
Excitation: Harmonic Translation or Pitching	
Natural Frequency	$\omega_{mn}^2 = \frac{g}{a} \epsilon_{mn} \tanh \kappa_{mn}$
Spring Constant	$k_{mn} = m_{mn} \omega_{mn}^2$
Damping Coefficient of Slosh Mass	$c_{mn} = m_{mn} \bar{g}_{mn} \omega_{mn}$
Ratio of Slosh Mass to Fluid Mass	$\frac{m_{mn}}{m_L} = \frac{64 \tanh \kappa_{mn}}{\pi^2 \kappa_{mn} (\epsilon_{mn}^2 - 4m^2) J_{2m}^2(\epsilon_{mn})} \left[\frac{\epsilon_{mn} J_{2m}(\epsilon_{mn})}{(4m^2 - 1)} \right. \quad (\text{fig. 4-20, 4-21})$ $\left. + 2 \sum_{\mu=0}^{\infty} J_{2m+2\mu+1}(\epsilon_{mn}) \right] \sum_{\mu=0}^{\infty} \frac{J_{2m+2\mu+1}(\epsilon_{mn})}{(2m+2\mu+3)(2m+2\mu-1)}$
Ratio of Fixed Mass to Fluid Mass	$\frac{M}{m_L} = 1 - \sum_{n=0}^{\infty} \sum_{m=0}^{\infty} \frac{m_{mn}}{m_L}$
Ratio of Slosh Mass Coordinate to Fluid Depth	$\left \frac{h_{mn}}{h} \right = \frac{1}{2} \left[1 - \frac{4}{\kappa_{mn}} \tanh \frac{\kappa_{mn}}{2} \right] \quad (\text{fig. 4-22})$
Ratio of Fixed Mass Coordinate to Fluid Depth	$\left \frac{H}{h} \right = \frac{m_L}{M} \sum_{m=0}^{\infty} \sum_{n=0}^{\infty} \left(\frac{m_{mn}}{m_L} \right) \left(\frac{h_{mn}}{h} \right)$
Moment of Inertia of Solidified Fluid	$\frac{I_s}{m_L h^2} = \left(\frac{a}{h} \right)^2 \left[\frac{1}{12} \left(\frac{h}{a} \right)^2 + \frac{1}{4} \right]$
Moment of Inertia of Disc ($c_d = 0$)	$\frac{I_d}{m_L h^2} = \left(\frac{a}{h} \right)^2 \left\{ \frac{1}{2} + 8 \sum_{m=0}^{\infty} \sum_{n=0}^{\infty} \frac{(-1)^{m+n} a^m b^n}{\pi a \epsilon_{mn}^2} \left[\left(1 - \frac{2}{\kappa_{mn}} \tanh \frac{\kappa_{mn}}{2} \right) \cdot \right. \right.$ $\left. \left(\frac{J_{2m}(\epsilon_{mn})}{4m^2 - 1} + L_0(\epsilon_{mn}) \right) - \frac{2\epsilon_{mn}^2 L_2(\epsilon_{mn}) \tanh \kappa_{mn}}{(4m^2 - 1) \kappa_{mn}} \right] \right\}$
Moment of Inertia of Fixed Mass	$\frac{I}{m_L h^2} = \frac{I_s}{m_L h^2} - \frac{I_d}{m_L h^2} - \frac{M}{m_L} \left(\frac{H}{h} \right)^2 - \sum_{m=0}^{\infty} \sum_{n=0}^{\infty} \frac{m_{mn}}{m_L} \left(\frac{h_{mn}}{h} \right)^2$



SLOSHING MASS
VS.
FLUID HEIGHT RATIO

$$\frac{m_{slosh}}{\rho_0 V}$$



Ratio of Fluid Depth to Tank Radius

Figure 4-20. Model Element Graph

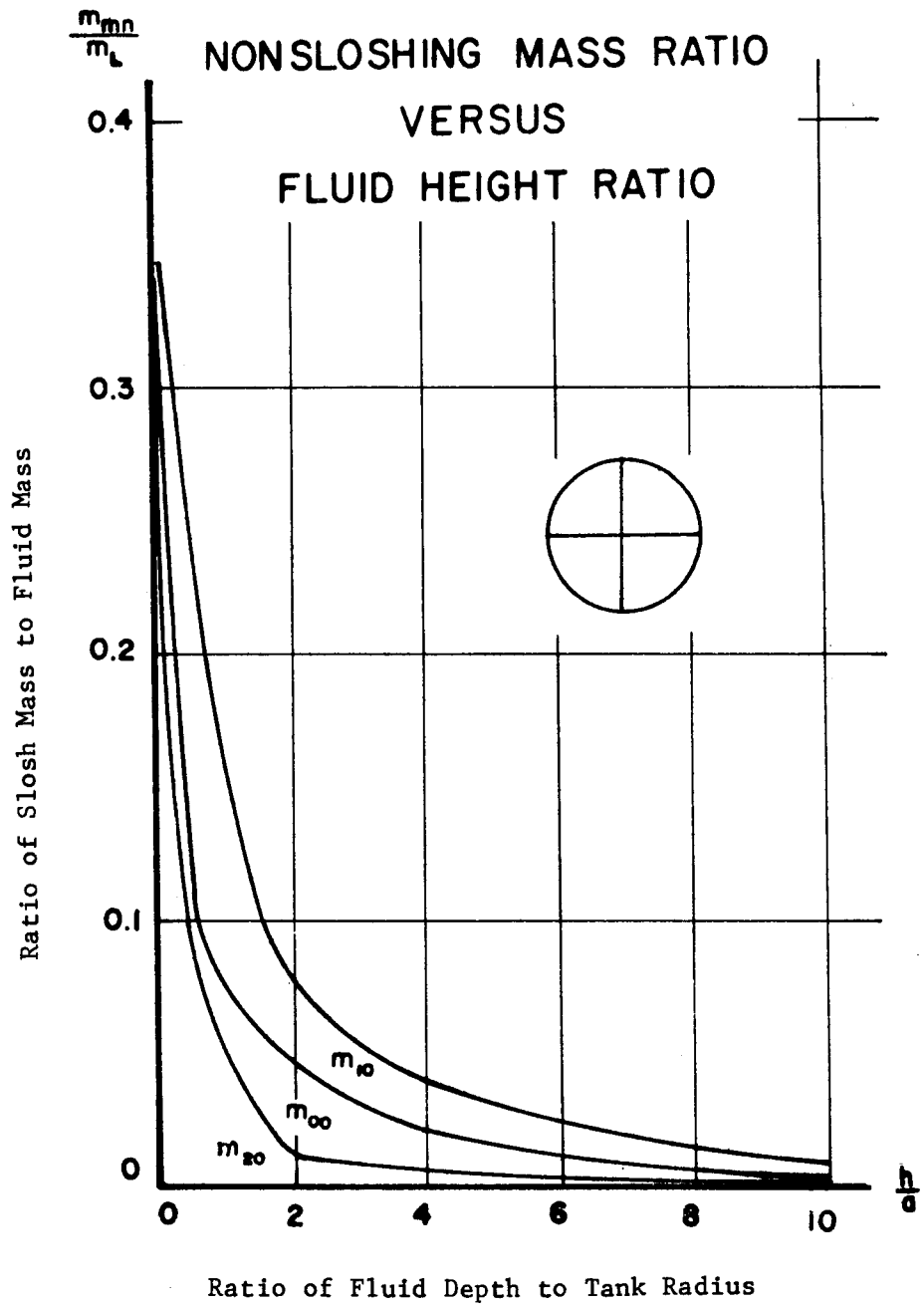


Figure 4-21. Model Element Graph

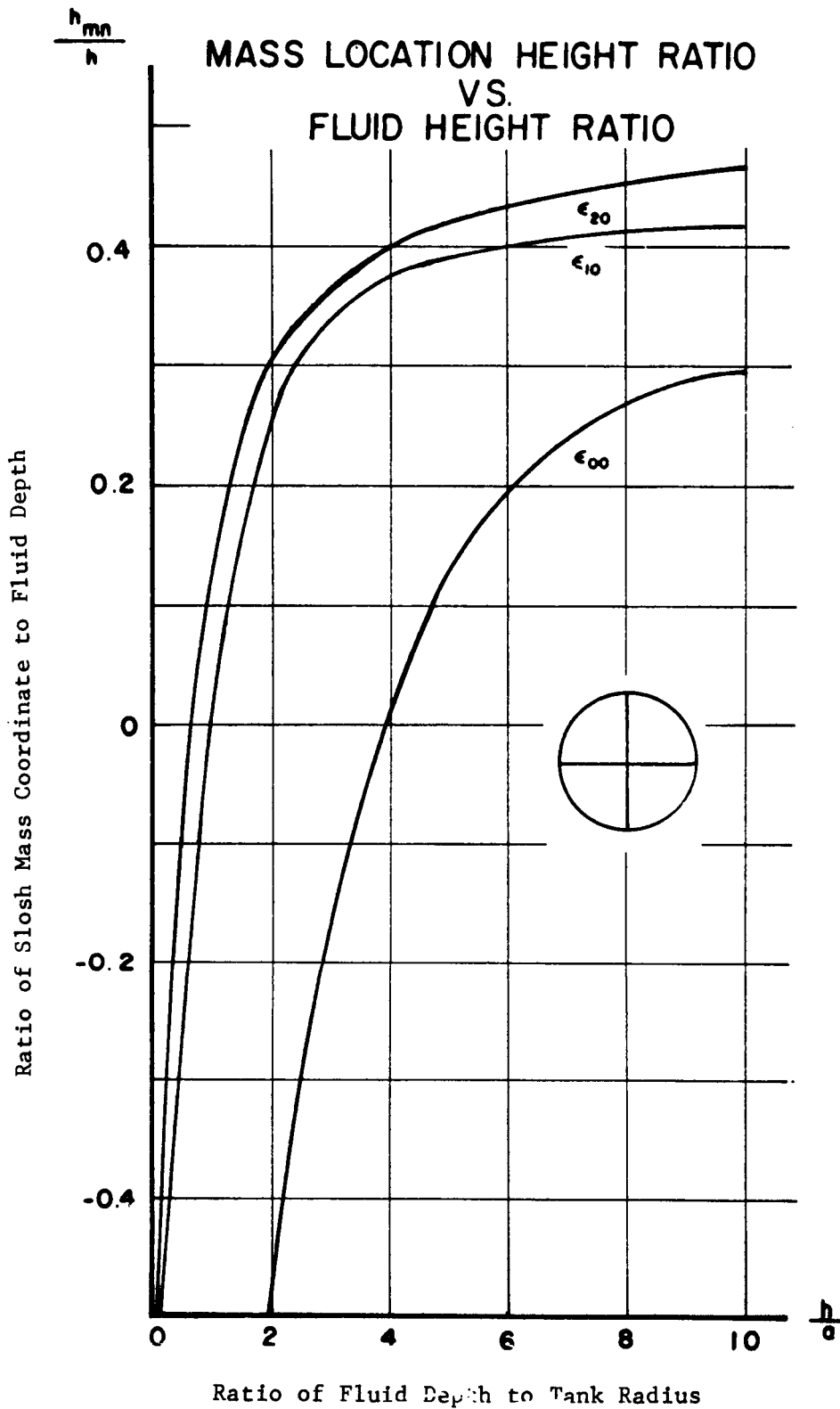


Figure 4-22. Model Element Graph

Table 4-23. Model Analysis

Quarter-Sector Tank	Pendulum Model
Excitation: Harmonic Translation and/or Pitching	

Figure 4-23 shows a diagram of the pendulum model used in representing the dynamic response of a liquid in a quarter-sector tank when subjected to harmonic translation in the x-direction and/or pitching about the y-axis.

Coordinate System:

The origin is located at the center of gravity of the undisturbed liquid.

Model Description:

The components of the system are as follows:

1. A fixed mass M having a moment of inertia I is rigidly connected to the tank and is located on the z-axis at a distance H below the coordinate origin.
2. A set of movable masses m_{mn} is distributed along the z-axis when the tank is at rest. These modal masses are pendulums having massless lever arms of length L_{mn} attached to the z-axis at distances H_{mn} above the origin. They are constrained by dashpots having viscous damping coefficients c_{mn} to remain approximately in the xy-plane and to move approximately parallel to the x-axis. Angular displacements of the pendulum with respect to the tank (z-axis) are denoted by λ_{mn} .
3. A massless disc having a moment of inertia I_d is located at the coordinate origin. Its motion is confined to rotation about the y-axis and is cushioned by a dashpot having a viscous damping coefficient c_d . The angular displacement of the disc relative to the tank is defined by ψ .

Equations of Motion:

The equations, obtained through Lagrange's equations, are as follows:

1. Force Equation:

$$F_x = -M(\ddot{x} + H\ddot{\theta}) - \sum_{m=1}^{\infty} \sum_{n=1}^{\infty} m_{mn} \left[\ddot{x} + L_{mn} \ddot{\lambda}_{mn} + (H_{mn} - L_{mn}) \ddot{\theta} \right]$$

2. Moment Equation:

$$M_y = - (I + MH^2) \ddot{\theta} - I_d (\ddot{\theta} + \ddot{\psi}) + g \sum_{m=1}^{\infty} \sum_{n=1}^{\infty} m_{mn} L_{mn} \lambda_{mn} - \sum_{m=1}^{\infty} \sum_{n=1}^{\infty} m_{mn} (H_{mn} - L_{mn}) \left[L_{mn} \ddot{\lambda}_{mn} + (H_{mn} - L_{mn}) \ddot{\theta} \right]$$

Table 4-23. Model Analysis (continued)

Quarter-Sectored Tank	Pendulum Model
Excitation: Harmonic Translation and/or Pitching	

Equations of Motion (continued):

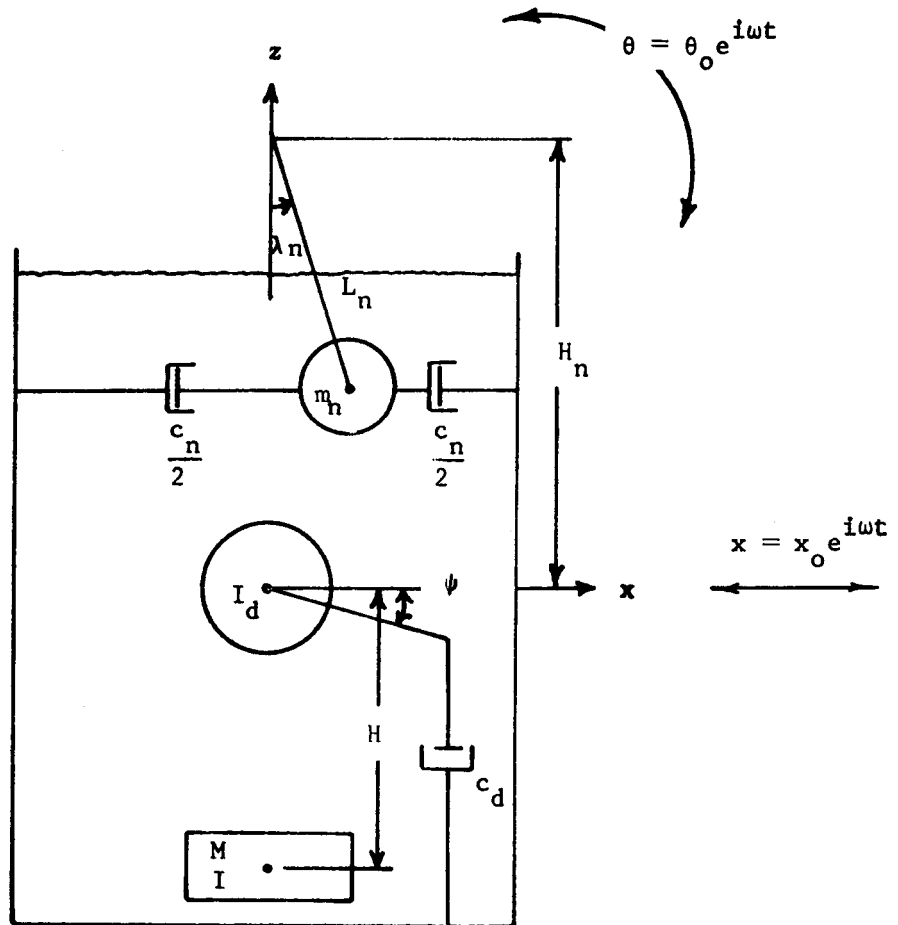
3. Disc Equation:

$$I_d (\ddot{\theta} + \ddot{\psi}) + c_d \dot{\psi} = 0$$

4. Slosh-Mass Equation:

$$m_{mn} \left[\ddot{x} + L_{mn} \ddot{\lambda}_{mn} + (H_{mn} - L_{mn}) \ddot{\theta} \right] + m_{mn} \bar{g}_{mn} \omega_{mn} L_{mn} \dot{\lambda}_{mn} - m_{mn} g \theta = 0$$

From these equations, the model force in the x-direction and the moment about the y-axis can be found (see Table 4-24).



Quarter-Sectored Tank	Pendulum Model
Excitation: Harmonic Translation and/or Pitching	

Figure 4-23. Equivalent Mechanical Model

Table 4-24. Model Force and Moment Resultants

Quarter-Sectored Tank	Pendulum Model
Excitation: Harmonic Translation and/or Pitching	

Translation in the x-direction, $x = x_0 e^{i\omega t}$.

$$1. F_x = m_L \omega^2 x_0 e^{i\omega t} \left[1 + \sum_{m=0}^{\infty} \sum_{n=0}^{\infty} \left(\frac{m_{mn}}{m_L} \right) \left(\frac{1}{\eta_{mn}^2 - 1 + i\bar{g}_{mn} \eta_{mn}} \right) \right]$$

$$2. M_y = m_L h \omega^2 x_0 e^{i\omega t} \sum_{m=0}^{\infty} \sum_{n=0}^{\infty} \left(\frac{m_{mn}}{m_L} \right) \left(\frac{H_{mn} - L_{mn} + \frac{g}{h}}{h\omega^2} \right) \left(\frac{1}{\eta_{mn}^2 - 1 + i\bar{g}_{mn} \eta_{mn}} \right)$$

Pitching about the y-axis, $\theta = \theta_0 e^{i\omega t}$.

$$1. F_x = -m_L h \omega^2 \theta_0 e^{i\omega t} \sum_{m=0}^{\infty} \sum_{n=0}^{\infty} \left(\frac{m_{mn}}{m_L} \right) \left(\frac{H_{mn} - L_{mn}}{h} + \frac{g}{h\omega^2} \right) \left(\frac{1}{\eta_{mn}^2 - 1 + i\bar{g}_{mn} \eta_{mn}} \right)$$

$$2. M_y = -m_L h \omega^2 \theta_0 e^{i\omega t} \left[\frac{I}{m_L h^2} + \frac{MH^2}{m_L h^2} + \frac{I_d}{m_L h^2} \left(1 - \frac{\omega^2 I_d}{c_d^2 + \omega^2 I_d} \right) + \sum_{m=0}^{\infty} \sum_{n=0}^{\infty} \frac{m_{mn} (H_{mn} - L_{mn})^2}{m_L h^2} \right. \\ \left. + \sum_{m=0}^{\infty} \sum_{n=0}^{\infty} \left(\frac{m_{mn}}{m_L} \right) \left(\frac{H_{mn} - L_{mn}}{h} + \frac{g}{h\omega^2} \right)^2 \left(\frac{1}{\eta_{mn}^2 - 1 + i\bar{g}_{mn} \eta_{mn}} \right) \right] + i\omega \theta_0 e^{i\omega t} \left(\frac{c_d \omega^2 I_d}{c_d^2 + \omega^2 I_d} \right)$$

Table 4-25. Model Elements.

Quarter-Sector Tank	Pendulum Model
Excitation: Harmonic Translation and/or Pitching	
Natural Frequency	$\omega_{mn}^2 = \frac{g}{a} \epsilon_{mn} \tanh \kappa_{mn}$
Pendulum Length	$L_{mn} = \frac{g}{\omega_{mn}^2}$
Damping Coefficient of Slosh Mass	$c_{mn} = m_{mn} \bar{g}_{mn} \omega_{mn}$
Ratio of Slosh Mass to Fluid Mass	$\frac{m_{mn}}{m_L} = \frac{64 \tanh \kappa_{mn}}{\pi^2 \kappa_{mn}^2 (\epsilon_{mn}^2 - 4m^2) J_{2m}^2(\epsilon_{mn})} \left[\frac{\epsilon_{mn} J_{2m}(\epsilon_{mn})}{(4m^2 - 1)} \right.$ $\left. + 2 \sum_{\mu=0}^{\infty} J_{2m+2\mu+1}(\epsilon_{mn}) \right] \sum_{\mu=0}^{\infty} \frac{J_{2m+2\mu+1}(\epsilon_{mn})}{(2m+2\mu+3)(2m+2\mu-1)}$
Ratio of Fixed Mass to Fluid Mass	$\frac{M}{m_L} = 1 - \sum_{n=0}^{\infty} \sum_{m=0}^{\infty} \frac{m_{mn}}{m_L}$
Ratio of Pendulum Mass Coordinate to Fluid Depth	$\left \frac{H_{mn} - L_{mn}}{h} \right = \frac{1}{2} \left[1 - \frac{4}{\kappa_{mn}} \tanh \left(\frac{\kappa_{mn}}{2} \right) \right]$
Ratio of Fixed Mass Coordinate to Fluid Depth	$\left \frac{H}{h} \right = \frac{m_L}{M} \sum_{m=0}^{\infty} \sum_{n=0}^{\infty} \left(\frac{m_{mn}}{m_L} \right) \left(\frac{H_{mn} - L_{mn}}{h} \right)$
Moment of Inertia of Solidified Fluid	$\frac{I_s}{m_L h^2} = \left(\frac{a}{h} \right)^2 \left[\frac{1}{12} \left(\frac{h}{a} \right)^2 + \frac{1}{4} \right]$
Moment of Inertia of Disc ($c_d = 0$)	$\frac{I_d}{m_L h^2} = \left(\frac{a}{h} \right)^2 \left\{ \frac{1}{2} + 8 \sum_{m=0}^{\infty} \sum_{n=0}^{\infty} \frac{(-1)^{m+n} a^m b^n}{\pi a \epsilon_{mn}^2} \left[\left(1 - \frac{2}{\kappa_{mn}} \tanh \frac{\kappa_{mn}}{2} \right) \cdot \right. \right.$ $\left. \left(\frac{J_{2m}(\epsilon_{mn})}{4m^2 - 1} + L_0(\epsilon_{mn}) \right) - \frac{2\epsilon_{mn}^2 L_2(\epsilon_{mn}) \tanh \kappa_{mn}}{(4m^2 - 1) \kappa_{mn}} \right] \right\}$
Moment of Inertia of Fixed Mass	$\frac{I}{m_L h^2} = \frac{I_s}{m_L h^2} - \frac{I_d}{m_L h^2} - \frac{m}{m_L} \left(\frac{H}{h} \right)^2 - \sum_{m=0}^{\infty} \sum_{n=0}^{\infty} \frac{m_{mn}}{m_L} \left[\frac{H_{mn} - L_{mn}}{h} \right]^2$

Table 4-26. Boundary Conditions, Velocity Potential, and Natural Frequency

Quarter-Sector Tank	Excitation: Harmonic Roll
---------------------	---------------------------

Roll about the z-axis, $\phi = \phi_0 e^{i\omega t}$.

1. Boundary conditions:

(a) $\left(\frac{\partial \phi}{\partial r} \right)_{r=a} = 0$

(b) $\left(\frac{\partial \phi}{\partial z} \right)_{z=-h} = 0$

(c) $\left(\frac{1}{r} \frac{\partial \phi}{\partial \phi} \right)_{\phi=0, \bar{\alpha}} = i\omega r \phi_0 e^{i\omega t}$

(d) $\left(\frac{\partial^2 \phi}{\partial t^2} + g \frac{\partial \phi}{\partial z} \right)_{z=0} = 0$

2. Velocity potential:

$$\begin{aligned} \phi = & i\omega \phi_0 e^{i\omega t} \left\{ r^2 \left(\phi - \frac{\pi}{4} \right) + \sum_{m=1}^{\infty} \frac{2a^2 \cos(4m-2)\phi}{\pi(2m-1) \left[(2m-1)^2 - 1 \right]} \left[\left(\frac{r}{a} \right)^{4m-2} - \frac{(r/a)^2}{(2m-1)} \right] + \frac{2a^2}{\pi} \left(\frac{r}{a} \right)^2 \left[\ln \left(\frac{r}{a} \right) + \frac{1}{2} \right] \cos 2\phi \right. \\ & + \sum_{m=1}^{\infty} \sum_{n=0}^{\infty} \frac{2a^2}{\pi} \left[\frac{[f_{2m-1,n} - e_{2m-1,n} (2m-1)] J_{4m-2}(\rho_{2m-1,n})}{(2m-1) \left[(2m-1)^2 - 1 \right] (\eta_{2m-1,n}^2 - 1) \cosh \kappa_{2m-1,n}} \right] \cosh(\kappa_{2m-1,n} + \zeta_{2m-1,n}) \cos(4m-2)\phi \\ & \left. + \sum_{n=0}^{\infty} \frac{a^2}{\pi} \left[\frac{(2f_n - e_n) J_2(\rho_n) \cos 2\phi \cosh(\kappa_n + \zeta_n)}{(\eta_n^2 - 1) \cosh \kappa_n} \right] \right\} \end{aligned}$$

3. Natural angular frequency:

$$\omega_{2m-1,n}^2 = \frac{g}{a} \epsilon_{2m-1,n} \tanh \kappa_{2m-1,n} \quad \text{and} \quad \omega_n^2 = \frac{g}{a} \epsilon_n \tanh \kappa_n$$

where $\epsilon_{2m-1,n}$ are solutions of $J'_{4m-2}(\epsilon_{2m-1,n}) = 0$
and ϵ_n are roots of $J'_2(\epsilon_n) = 0$.

Table 4-27. Liquid Force and Moment Resultants

Quarter-Sectored Tank	Excitation: Harmonic Roll
-----------------------	---------------------------

Roll about the z-axis, $\phi = \phi_0 e^{i\omega t}$.

$$1. F_x = -F_y = m_L \omega^2 a \phi_0 e^{i\omega t} \left[\frac{2}{3} - \frac{4}{\pi} + \frac{16}{9\pi^2} + \sum_{m=1}^{\infty} \left[\frac{8 \left[\frac{1}{\pi^2 (2m-1)^2 (4m-1) - (1/3)(2m-1)} \right]}{\pi^2 (2m-1)^2 [(2m-1)^2 - 1/4]} + \frac{1}{8m(2m-1)^2 [(2m-1)^2 - 1/4]} \right] \right. \\ \left. + \sum_{m=1}^{\infty} \sum_{n=0}^{\infty} \left\{ \frac{4(2f_n - e_n) \tanh \kappa_n}{\pi^2 (\eta_n^2 - 1) \kappa_n} \left[\frac{1}{3} J_2(\epsilon_n) + L_0(\epsilon_n) \right] + \frac{8 \left[f_{2m-1,n} \sqrt{2m-1} - e_{2m-1,n} \right] \tanh \kappa_{2m-1,n}}{\pi^2 (h/a) (\eta_{2m-1,n}^2 - 1) [(2m-1)^2 - 1]} \right\} \epsilon_{2m-1,n} \right]$$

$$\left[\frac{J_{4m-2}(\epsilon_{2m-1,n})}{4 [(2m-1)^2 - 1/4]} + L_0(\epsilon_{2m-1,n}) \right]$$

$$2. M_x = M_y = m_L \omega^2 a \phi_0 e^{i\omega t} \left[\frac{1}{5(h/a)} \left(1 - \frac{4}{\pi} \right) + \frac{4}{25 \pi^2 (h/a)} + \sum_{m=1}^{\infty} \frac{6(m-1)}{5 \pi^2 (h/a) [(2m-1)^2 - 1/4]} \right] [(2m-1)^2 - 1] [2m+1/2] [2m-1]^2$$

$$+ \sum_{n=0}^{\infty} \left\{ \frac{2(2f_n - e_n)}{2(\eta_n^2 - 1) \epsilon_n^2} \left[\tanh \kappa_n + \frac{2}{\kappa_n} \left(\frac{1}{\cosh \kappa_n} - 1 \right) \right] \left[L_0(\epsilon_n) + \frac{1}{3} J_2(\epsilon_n) \right] + \frac{2\epsilon_n^2 L_2(\epsilon_n)}{3 \kappa_n \cosh \kappa_n} \right\}$$

$$+ \sum_{m=1}^{\infty} \sum_{n=0}^{\infty} \frac{4 \left[f_{2m-1,n} \sqrt{2m-1} - e_{2m-1,n} \right]}{\pi^2 [(2m-1)^2 - 1] \epsilon_{2m-1,n} (\eta_{2m-1,n}^2 - 1)} \left\{ \tanh \kappa_{2m-1,n} + \frac{2}{\kappa_{2m-1,n}} \left(\frac{1}{\cosh \kappa_{2m-1,n}} - 1 \right) \right\}$$

$$\left[\frac{J_{4m-2}(\epsilon_{2m-1,n})}{4 [(2m-1)^2 - 1/4]} + L_0(\epsilon_{2m-1,n}) \right] + \frac{\epsilon_{2m-1,n}^2 L_2(\epsilon_{2m-1,n})}{2 [(2m-1)^2 - 1/4] \kappa_{2m-1,n} \cosh \kappa_{2m-1,n}} \left. \right] + \frac{4mga}{3\pi}$$

Table 4-27. Liquid Force and Moment Resultants (continued)

Quarter-Sectored Tank	Excitation: Harmonic Roll
-----------------------	---------------------------

$$\begin{aligned}
 3. \quad M_z = & m_L \omega^2 a^2 \phi_0 e^{i\omega t} \left\{ \frac{1}{2} - \frac{1}{2\pi} \sum_{m=1}^{\infty} \left[\frac{1}{2^2 \pi^m (2m-1)^2} + \frac{8(2f_n - e_n) L_1(\epsilon_n) \tanh \kappa_n}{\pi^2 (\eta_n^2 - 1) \kappa_n} \right] \right. \\
 & \left. + \frac{16 \left[\frac{f_{2m-1,n}}{(2m-1)^2 - 1} - e_{2m-1,n} \right] L_1(\epsilon_{2m-1,n}) \tanh \kappa_{2m-1,n}}{\pi^2 \left[(2m-1)^2 - 1 \right] (\eta_{2m-1,n}^2 - 1) \kappa_{2m-1,n}} \right\}
 \end{aligned}$$

Table 4-28. Model Analysis

Quarter-Sectored Tank	Torsional Pendulum Model
Excitation: Harmonic Roll	

Figure 4-24 shows a diagram of the torsional pendulum model used in representing the dynamic response of a liquid in a quarter-sectored tank when subjected to harmonic roll about the z-axis.

Coordinate System:

The origin is located at the center of gravity of the undisturbed liquid.

Model Description:

1. A fixed mass having a mass moment of inertia J is rigidly connected to the tank and is located on the z-axis at the base of the tank.
2. A disc having a mass moment of inertia J_{mn} is connected to a shaft having a torsional stiffness K_{mn} which is in turn rigidly attached to the tank. Viscous damping is introduced along the periphery of the disc, the damping coefficient of which is c_{mn} . Angular displacement of the disc relative to the tank is denoted by β_{mn} .

Equations of Motion:

The equations, obtained through Lagrange's equations, are as follows:

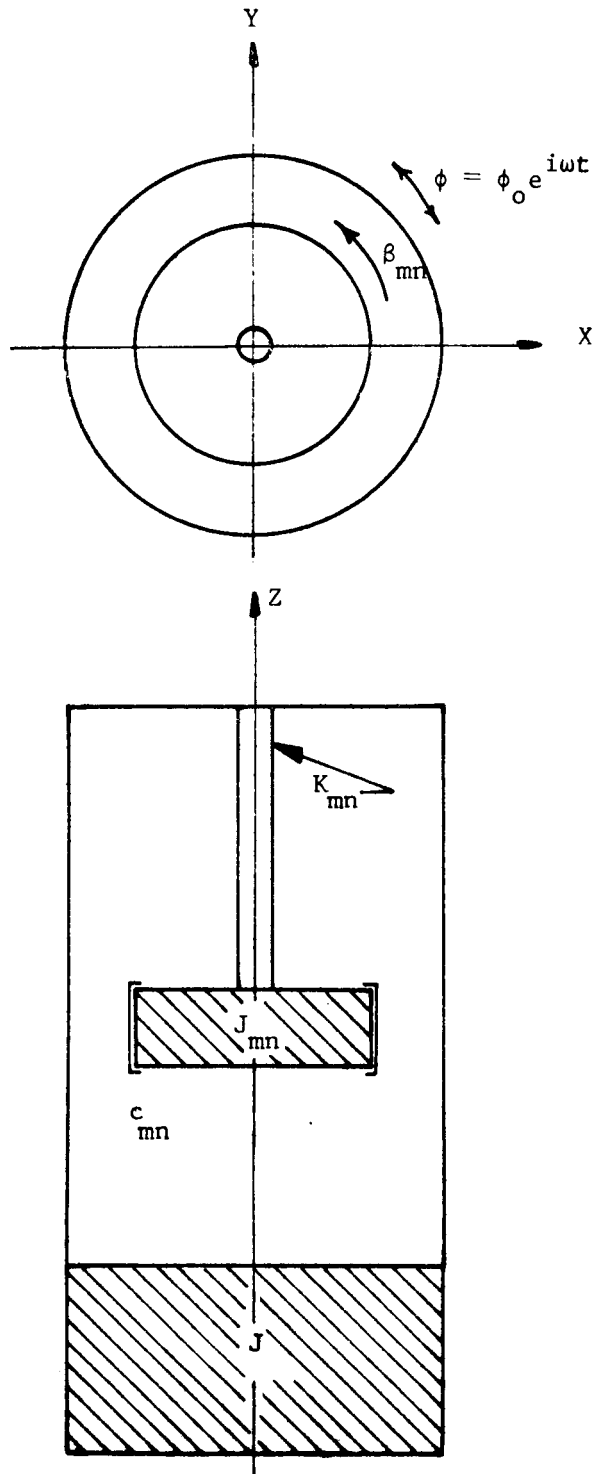
1. Moment Equation:

$$M_z = -J\ddot{\beta}_{mn} + \sum_{m=1,3,5,\dots}^{\infty} \sum_{n=0}^{\infty} J_{mn} (\ddot{\phi} + \ddot{\beta}_{mn})$$

2. Slosh Mass Equation:

$$\sum_{m=1,3,5,\dots}^{\infty} \sum_{n=0}^{\infty} J_{mn} (\ddot{\phi} + \ddot{\beta}_{mn}) + \sum_{m=1,3,5,\dots}^{\infty} \sum_{n=0}^{\infty} c_{mn} \dot{\beta}_{mn} + \sum_{m=1,3,5,\dots}^{\infty} \sum_{n=0}^{\infty} K_{mn} \beta_{mn} = 0$$

From these equations, the model moment about the z-axis can be found (see Table 4-29).



Quarter-Sectored Tank

Torsional Pendulum Model

Excitation: Harmonic Roll

Figure 4-24. Equivalent Mechanical Model

Table 4-29. Moment Resultants

Quarter-Sectored Tank	Torsional Pendulum Model
Excitation: Harmonic Roll	

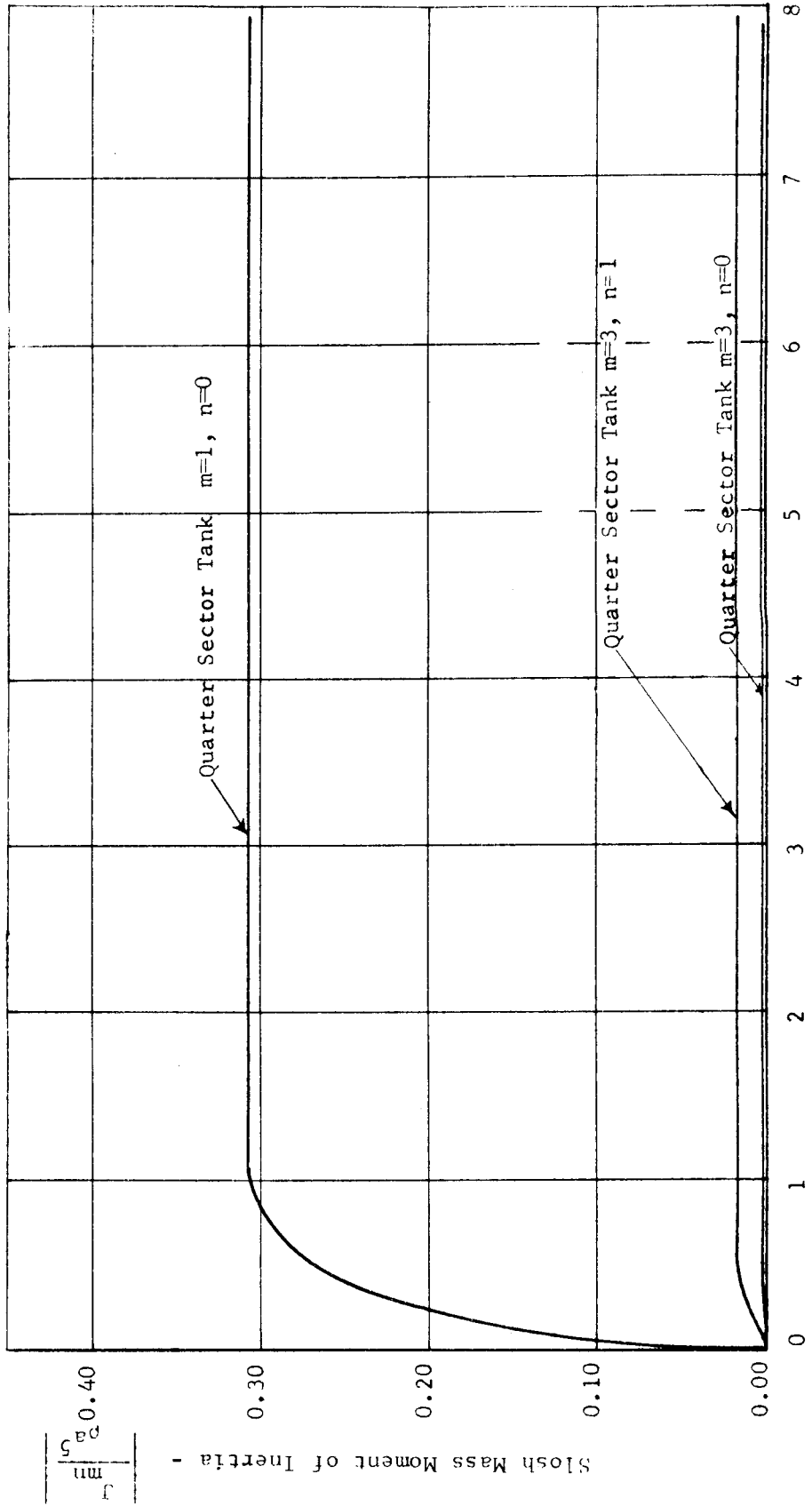
Roll about the z-axis, $\phi = \phi_0 e^{i\omega t}$.

$$M_z = J\omega^2 \theta_0 e^{i\omega t} \left[1 + \sum_{m=1,3,5,\dots}^{\infty} \sum_{n=0}^{\infty} \frac{J_{mn}}{J(\eta_{mn}^2 - 1 + i\delta_{mn} \eta_{mn})} \right]$$

Table 4-30. Model Elements

Quartered-Sectored Tank	Torsional Pendulum Model
Excitation: Harmonic Roll	
Natural Frequency	$\omega_{mn}^2 = \frac{g}{2} \epsilon_{mn} \tanh \kappa_{mn}$
Torsional Stiffness of Shaft	$K_{mn} = J_{mn} \omega_{mn}^2$
Damping Coefficient of Slosh Disc	$c_{mn} = J_{mn} \bar{g}_{mn} \omega_{mn}$
Moment of Inertia of Slosh Disc ($c_{mn} = 0$)	$J_{mn} = \frac{8m_L a^2}{\pi^2} \left[- \frac{(2f_n - e_n) L_1(\epsilon_n) \tanh \kappa_n}{\kappa_n} + \right. \\ \left. - \frac{2(f_{mn} - me_{mn}) L_1(\epsilon_{mn}) \tanh \kappa_{mn}}{m(m^2 - 1) \kappa_{mn}} \right]$
Moment of Inertia of Slosh Disc ($c_{mn} \neq 0$)	$J_{mn} = \frac{8m_L a^2 (\eta_{mn}^2 + i\bar{g}_{mn} \eta_{mn} - 1)}{\pi^2} \left[- \frac{(2f_n - e_n) L_1(\epsilon_n) \tanh \kappa_n}{(\eta_n^2 - 1) \kappa_n} \right. \\ \left. - \frac{2(f_{mn} - me_{mn}) L_1(\epsilon_{mn}) \tanh \kappa_{mn}}{m^2 (m^2 - 1) (\eta_{mn}^2 - 1) \kappa_{mn}} \right]$
Moment of Inertia of Solidified Fluid	$J_s = \frac{1}{2} m_L a^2$
Effective Moment of Inertia of Fluid	$\bar{J} = J_s \left[1 - \frac{8}{\pi^2} \sum_{m=1,3,5,\dots}^{\infty} \frac{1}{m^2(m+1)^2} \right]$
Moment of Inertia of Fixed Mass	$J = \bar{J} - \sum_{m=1,3,5,\dots}^{\infty} \sum_{n=0}^{\infty} J_{mn}$

Slosh Mass Moment of Inertia
vs Fluid Height Ratio for a Quarter
Sector Tank When Subjected
to Harmonic Roll



Fluid Height Ratio - h/a

Figure 4-25. Model Element Graph

Ratio of Slosh Mass Moment of Inertia
to Fluid Mass Moment of Inertia for
a Quarter Sector Tank When
Subjected to Harmonic Roll

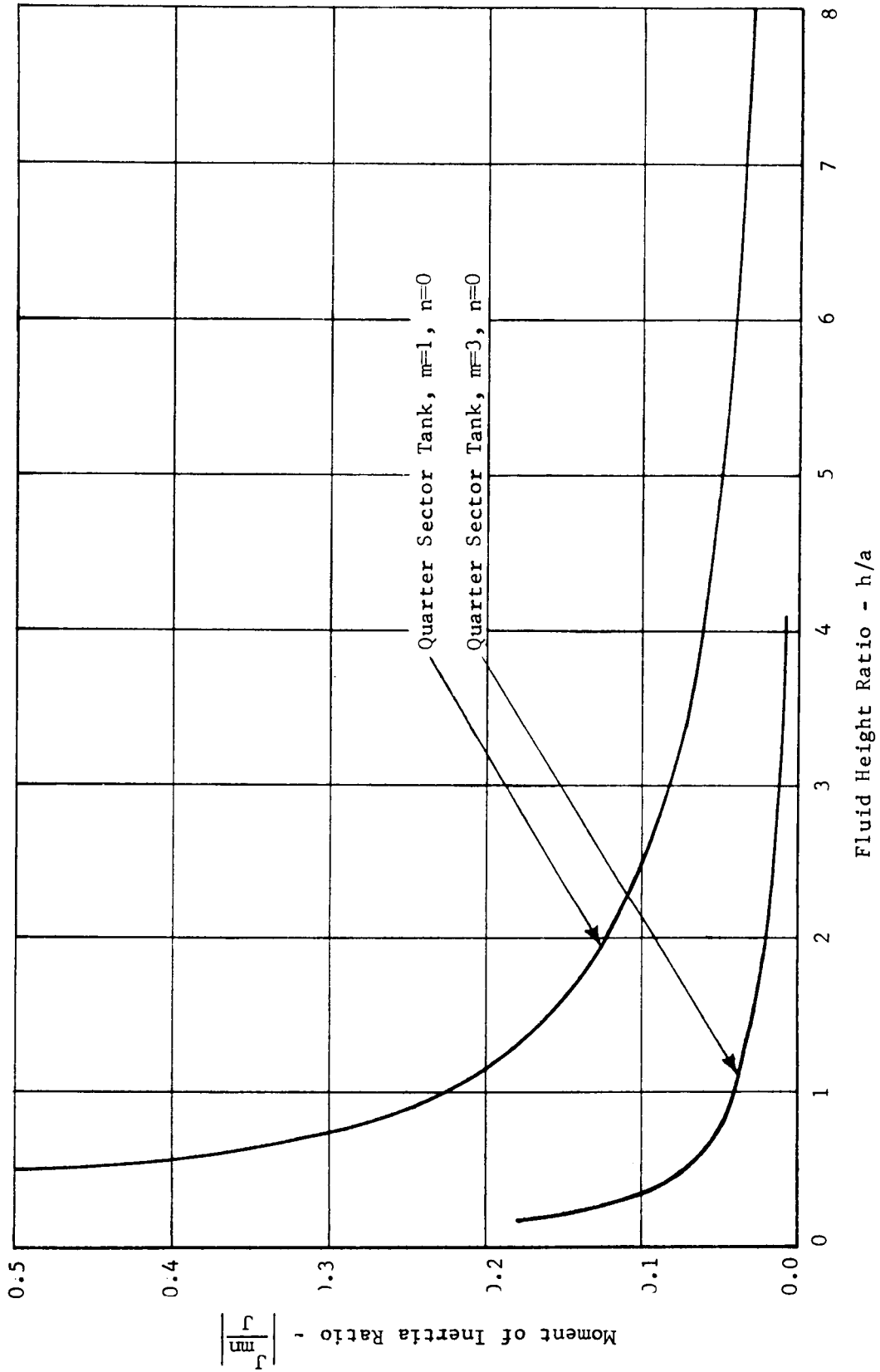
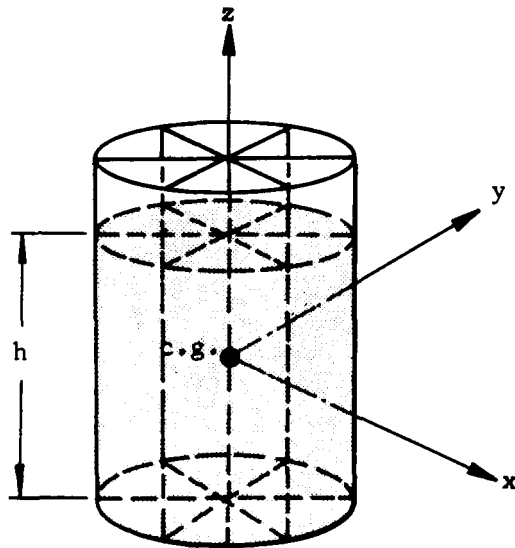


Figure 4-26. Model Element Graph

4.5 Eighth-Sector Tank

Table of Contents

General.....	4-77
Excitation: Harmonic Roll	
Boundary Conditions, Velocity Potential, and Natural Frequency.....	4-78
Liquid Moment Resultant.....	4-79
Torsional Pendulum Model	
Analysis.....	4-80
Diagram.....	4-81
Moment Resultant.....	4-82
Elements.....	4-83
Graphs.....	4-84



Container: The tank is a right circular cylinder of radius a divided by longitudinal partitions intersecting at equal angles, $\bar{\alpha} = \pi/4$, and is filled with liquid to a depth h .

Coordinate System: The origin is located at the center of gravity of the undisturbed fluid and the x -axis must lie in a sector wall.

References: (60)

Comments: The results given in this section are applicable to only one sector, i.e., the boundary conditions and resulting velocity potential, natural frequency, and force and moment results are responses due to liquid oscillations in only one sector (except for the material concerning equivalent mechanical models which applies to the complete tank of eight sectors).

Table 4-31. Boundary Conditions, Velocity Potential, and Natural Frequency

Eighth-Sector Tank	Excitation: Harmonic Roll
--------------------	---------------------------

Roll about the z-axis, $\phi = \phi_0 e^{i\omega t}$.

1. Boundary conditions:

$$(a) \left(\frac{\partial \phi}{\partial r} \right)_{r=a} = 0$$

$$(b) \left(\frac{\partial \phi}{\partial z} \right)_{z=-h} = 0$$

$$(c) \left(\frac{1}{r} \frac{\partial \phi}{\partial r} \right)_{\phi=0, \bar{\alpha}} = i\omega r \phi_0 e^{i\omega t}$$

$$(d) \left(\frac{\partial^2 \phi}{\partial t^2} + g \frac{\partial \phi}{\partial z} \right)_{z=0} = 0$$

2. Velocity potential:

$$\phi = i\omega \phi_0 a^2 e^{i\omega t} \left\{ \left(\frac{r}{a} \right)^2 \left(\phi - \frac{\pi}{8} \right) + \frac{2}{\pi} \sum_{m=1,3,5,\dots}^{\infty} \frac{\cos 4m\phi}{2 - 1} \left[\left(\frac{r}{a} \right)^{4m} - \frac{1}{2m} \left(\frac{r}{a} \right)^2 \right] \right. \\ \left. + \frac{2}{\pi} \sum_{m=1,3,5,\dots}^{\infty} \sum_{n=0}^{\infty} \frac{(\bar{f}_{mn} - 2m \bar{e}_{mn}) J_{4m}(\rho_{mn}) \cos 4m\phi \cosh(\kappa_{mn} + \zeta_{mn})}{m(4m^2 - 1)(n^2 - 1) \cosh \kappa_{mn}} \right\}$$

3. Natural angular frequency:

$$\omega_{mn}^2 = \frac{g}{a} \epsilon_{mn} \tanh \rho_{mn}$$

where ϵ_{mn} are roots of $J'_{4m}(\epsilon_{mn}) = 0$. (see table A-5)

Table 4-32. Liquid Moment Resultant

Eighth-Sector Tank	Excitation: Harmonic Roll
--------------------	---------------------------

Roll about the z-axis, $\phi = \phi_0 e^{i\omega t}$.

$$M_z = m_L a^2 \omega^2 \phi_0 e^{i\omega t} \left[\frac{1}{2} - \frac{4}{\pi^2} \sum_{m=1,3,5,\dots}^{\infty} \frac{1}{m^2 (2m+1)^2} - \frac{32}{\pi^2} \sum_{m=1,3,5,\dots}^{\infty} \frac{(\bar{f}_{mn} - 2m \bar{e}_{mn}) L_2(\epsilon_{mn}) \tanh \kappa_{mn}}{m(4m^2 - 1)(\eta_{mn}^2 - 1) \kappa_{mn}} \right]$$

Table 4-33. Model Analysis

Eighth-Sectored Tank	Torsional Pendulum Model
Excitation: Harmonic Roll	

Figure 4-7 shows a diagram of the torsional pendulum model used in representing the dynamic response of a liquid in an eighth-sectored tank when subjected to harmonic roll about the z-axis.

Coordinate System:

The origin is located at the center of gravity of the undisturbed liquid.

Model Description:

1. A fixed mass having a mass moment of inertia J is rigidly connected to the tank and is located on the z-axis at the base of the tank.
2. A disc having a mass moment of inertia J_{mn} is connected to a shaft having a torsional stiffness K_{mn} which is in turn rigidly attached to the tank. Viscous damping is introduced along the periphery of the disc, the damping coefficient of which is c_{mn} . Angular displacement of the disc relative to the tank is denoted by β_{mn} .

Equations of Motion:

The equations, obtained through Lagrange's equation, are as follows:

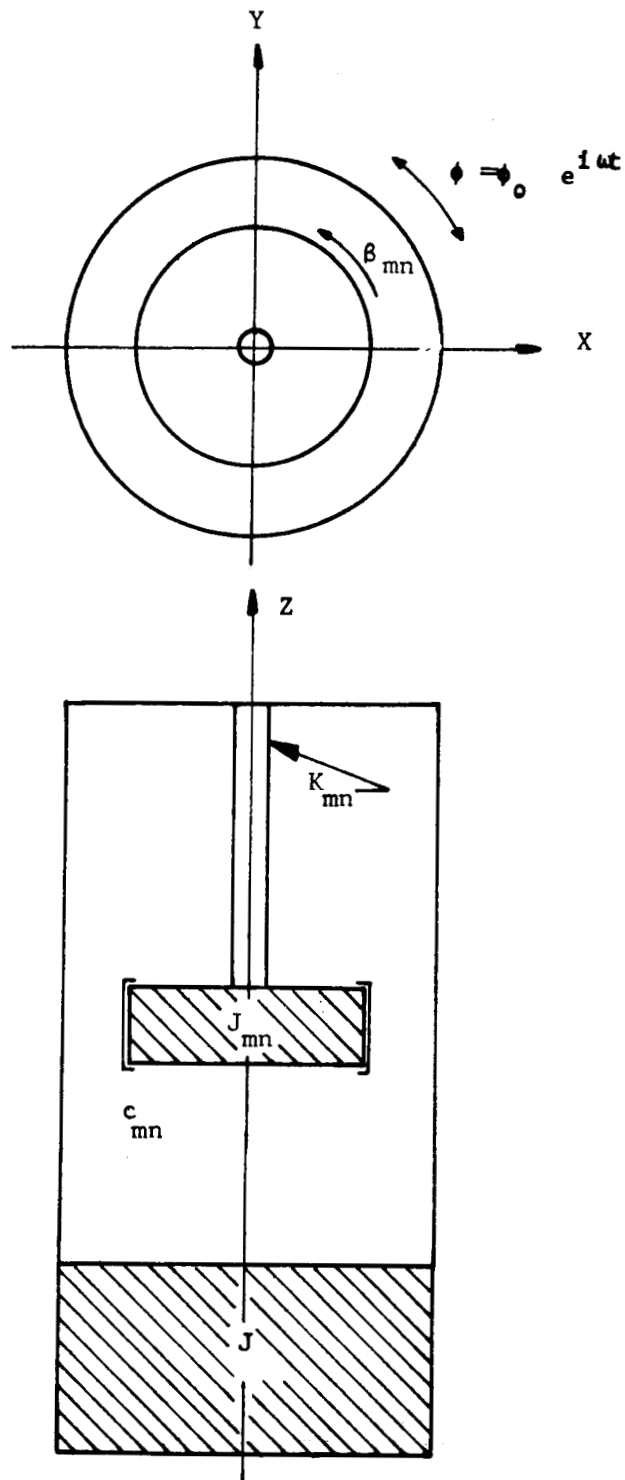
1. Moment Equation:

$$M_z = -J\ddot{\beta}_{mn} + \sum_{m=1,3,5,\dots}^{\infty} \sum_{n=0}^{\infty} J_{mn} (\ddot{\phi} + \ddot{\beta}_{mn})$$

2. Slosh Mass Equation:

$$\sum_{m=1,3,5,\dots}^{\infty} \sum_{n=0}^{\infty} J_{mn} (\ddot{\phi} + \ddot{\beta}_{mn}) + \sum_{m=1,3,5,\dots}^{\infty} \sum_{n=0}^{\infty} c_{mn} \dot{\beta}_{mn} + \sum_{m=1,3,5,\dots}^{\infty} \sum_{n=0}^{\infty} K_{mn} \beta_{mn} = 0$$

From these equations, the model moment about the z-axis can be found (see Table 4-34).



Eighth-Sectored Tank

Torsional Pendulum Model

Excitation: Harmonic Roll

Figure 4-27. Equivalent Mechanical Model

Table 4-34. Model Moment Resultant

Eighth-Sectored Tank	Torsional Pendulum Model
Excitation: Harmonic Roll	

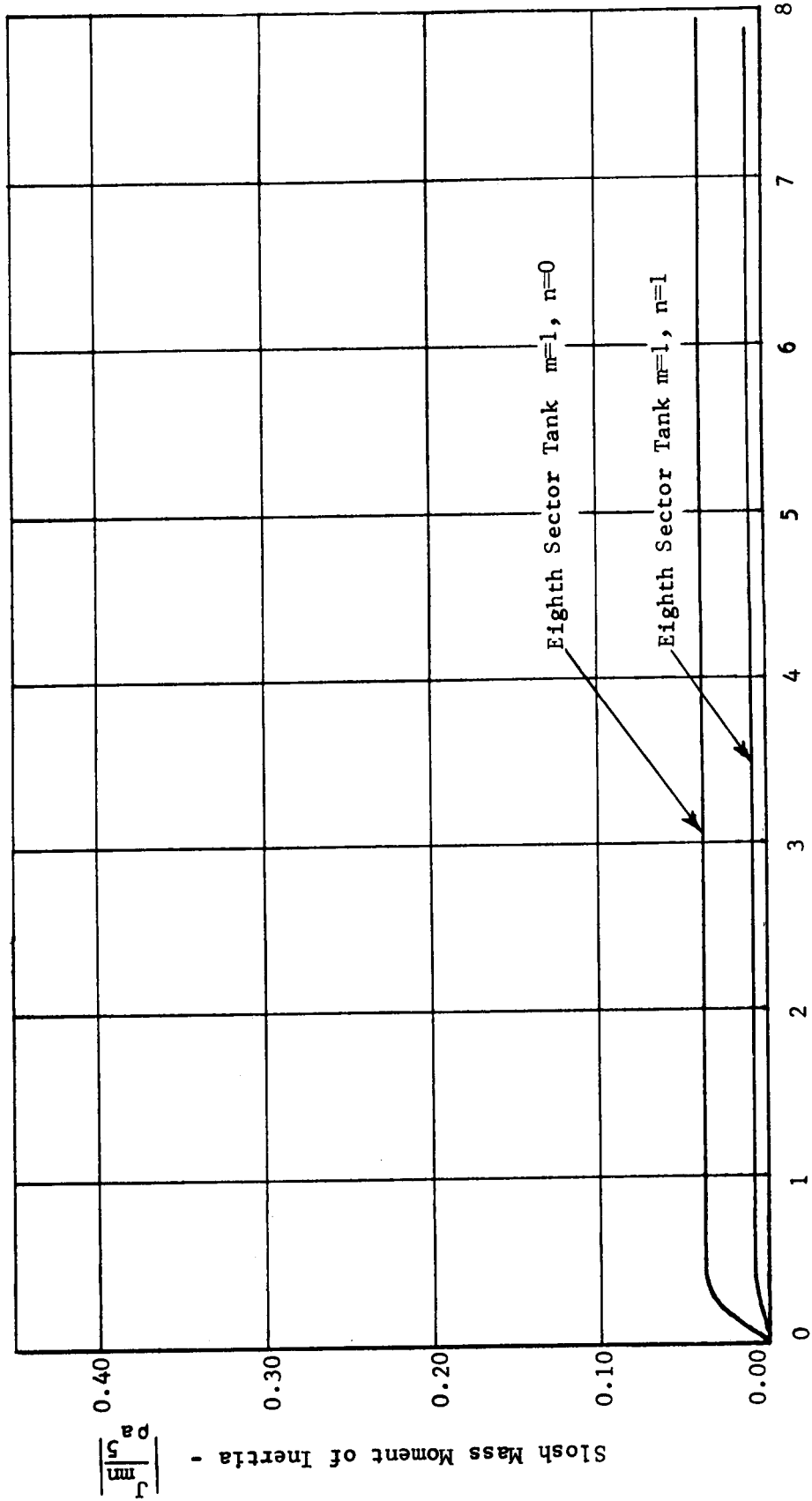
Roll about the z-axis, $\phi = \phi_0 e^{i\omega t}$.

$$M_z = J\omega^2 \phi_0 e^{i\omega t} \left[1 + \sum_{m=1,3,5,\dots}^{\infty} \sum_{n=0}^{\infty} \frac{J_{mn}}{J(\eta_{mn}^2 - 1 + i\bar{g}_{mn} \eta_{mn})} \right]$$

Table 4-35. Model Elements

Eighth-Sectored Tank	Torsional Pendulum Model
Excitation: Harmonic Roll	
Natural Frequency	$\omega_{mn}^2 = \frac{g}{a} \epsilon_{mn} \tanh \kappa_{mn}$
Torsional Stiffness of Shaft	$K_{mn} = J_{mn} \omega_{mn}^2$
Damping Coefficient of Slosh Disc	$c_{mn} = J_{mn} \bar{g}_{mn} \omega_{mn}$
Moment of Inertia of Slosh Disc ($c_{mn} = 0$)	$J_{mn} = \frac{32m_L a^2}{\pi^2} \left[\frac{-(\bar{f}_{mn} - 2m\bar{e}_{mn}) L_2(\epsilon_{mn}) \tanh \kappa_{mn}}{m(4m^2 - 1) \kappa_{mn}} \right]$ (fig. 4-28, 4-29)
Moment of Inertia of Slosh Disc ($c_{mn} \neq 0$)	$J_{mn} = \frac{-32m_L a^2 (\eta_{mn}^2 + i\bar{g}_{mn} \eta_{mn} - 1)}{\pi^2 (\eta_{mn}^2 - 1)} \cdot \frac{(\bar{f}_{mn} - 2m\bar{e}_{mn}) L_2(\epsilon_{mn}) \tanh \kappa_{mn}}{m(4m^2 - 1) \kappa_{mn}}$
Moment of Inertia of Solidified Fluid	$J_s = \frac{1}{2} m_L a^2$
Effective Moment of Inertia of Fluid	$\bar{J} = J_s \left[1 - \frac{8}{\pi^2} \sum_{m=1,3,5,\dots}^{\infty} \frac{1}{m^2(m+1)^2} \right]$
Moment of Inertia of Fixed Mass	$J = \bar{J} - \sum_{m=1,3,5,\dots}^{\infty} \sum_{n=0}^{\infty} J_{mn}$

Slosh Mass Moment of Inertia
vs Fluid Height Ratio for an Eighth
Sector Tank When Subjected to
Harmonic Roll



48-4

Figure 4-28. Model Element Graph

Ratio of Slosh Mass Moment of Inertia
to Fluid Mass Moment of Inertia for
an Eighth Sector Tank When Subjected
to Harmonic Roll

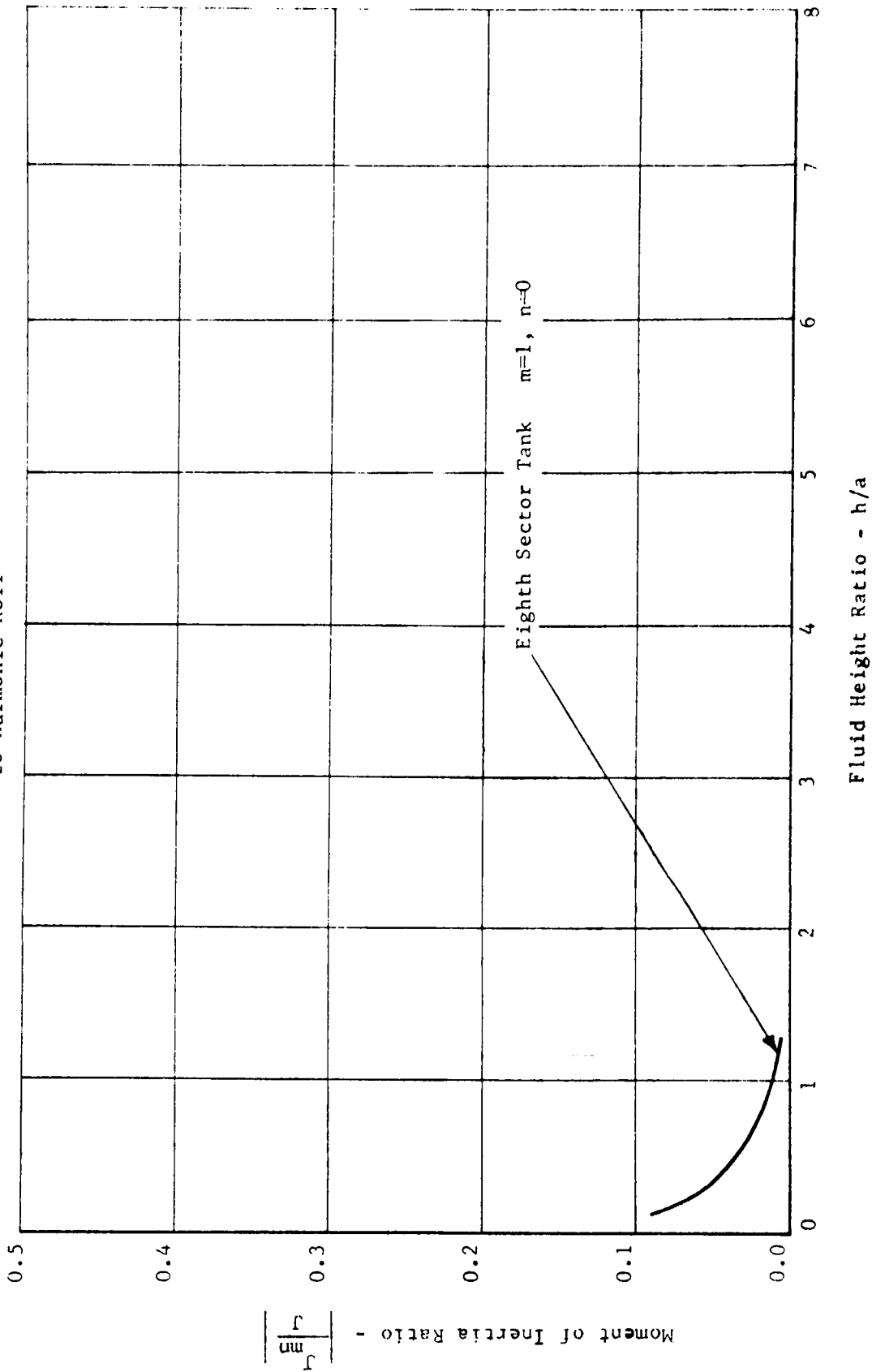
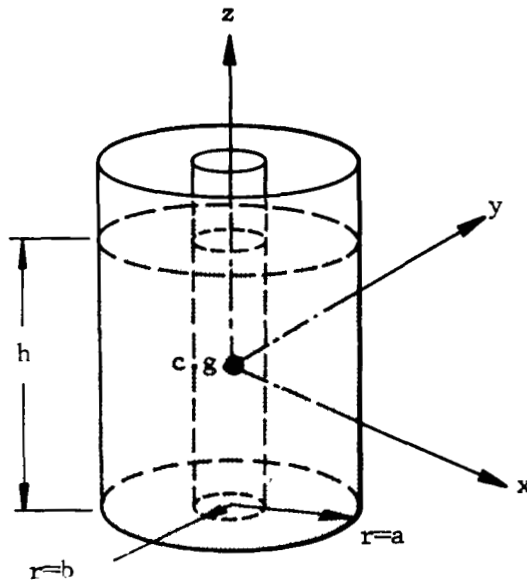


Figure 4-29. Model Element Graph

4.6 Annular Tank

Table of Contents

General.....	4-87
Excitation: Harmonic Translation and/or Pitching	
Boundary Conditions, Velocity Potential, and Natural Frequency.....	4-88
Liquid Force and Moment Resultants.....	4-90
Spring-Mass Model	
Analysis.....	4-91
Diagram.....	4-93
Force and Moment Resultants.....	4-94
Elements.....	4-95
Graphs.....	4-96
Pendulum Model	
Analysis.....	4-105
Diagram.....	4-107
Force and Moment Resultants.....	4-108
Elements.....	4-109
Graphs.....	4-110



Container: The tank consists of two concentric right circular cylinders having an inner radius $r = b$ and an outer radius $r = a$. The space between the concentric walls is filled with liquid to a depth h .

Coordinate System: The origin is located at the center of gravity of the undisturbed fluid.

References: (52 and 63)

Comments: The terms \bar{I} and \bar{c} , occurring in the model elements, must be experimentally determined, generally from torsion spring experiments of a sealed container of fluid. Their values are dependent upon container shape and the type of liquid. The model element graphs are given for $k = b/a = 0.5$. These graphs are, within ± 10 per cent, applicable for values $0.3 \leq k \leq 0.7$.

Table 4-36. Boundary Conditions, Velocity Potential, and Natural Frequency

Annular Tank	Excitation: Harmonic Translation
--------------	----------------------------------

Translation in the x-direction, $x = x_0 e^{i\omega t}$.

1. Boundary conditions:

$$(a) \left(\frac{\partial \phi}{\partial r} \right)_{r=a,b} = i\omega x_0 e^{i\omega t} \cos \phi \qquad (b) \left(\frac{\partial \phi}{\partial z} \right)_{z=-h} = 0$$

$$(c) \left(\frac{\partial^2 \phi}{\partial t^2} + g \frac{\partial \phi}{\partial z} \right)_{z=0} = 0$$

2. Velocity potential:

$$\phi = i\omega x_0 e^{i\omega t} \cos \phi \left[\frac{r}{a} + \sum_{n=0}^{\infty} \frac{A_n C_1(\rho_n) \cosh(\kappa_n + \zeta_n)}{(n_n^2 - 1) \cosh \kappa_n} \right]$$

3. Natural angular frequency:

$$\omega_n^2 = \frac{g}{a} \xi_n \tanh \kappa_n$$

where ξ_n are roots of $\Delta_1(\xi_n) = J_1'(\xi_n) Y_1'(k\xi_n) - J_1'(k\xi_n) Y_1'(\xi_n) = 0$. (see Table A-6)

Table 4-36. Boundary Conditions, Velocity Potential, and Natural Frequency (continued)

	Annular Tank	Excitation: Harmonic Pitching
Pitching about the y-axis, $y = y_0 e^{i\omega t}$.		
1. Boundary conditions:	$(a) \left(\frac{\partial \phi}{\partial r} \right)_{r=a,b} = -i\omega \theta_0 e^{i\omega t} z \cos \phi$ $(c) \left(\frac{\partial^2 \phi}{\partial t^2} + g \frac{\partial \phi}{\partial z} \right)_{z=+h/2} = 0$	$(b) \left(\frac{\partial \phi}{\partial z} \right)_{z=-h/2} = i\omega \theta_0 e^{i\omega t} r \cos \phi$
2. Velocity potential:	$\phi = i\omega a^2 \theta_0 e^{i\omega t} \cos \phi \left\{ \frac{rz}{a^2} + \sum_{n=0}^{\infty} \frac{A_n C_1(\rho_n)}{(\eta_n^2 - 1) \cosh \kappa_n} \left[\left(\frac{Y_n}{\xi_n} + \frac{h}{2a} \right) \cosh \left(\frac{\kappa_n}{2} + \zeta_n \right) - \frac{4Y_n}{\xi_n} \sinh \zeta_n \sinh \frac{\kappa_n}{2} - \frac{2}{\xi_n} \sinh \left(\frac{\kappa_n}{2} - \zeta_n \right) \right] \right\}$	
3. Natural angular frequency:	$\omega_n^2 = \frac{g}{a} \xi_n \tanh \kappa_n$	<p>where ξ_n are roots of $\Delta_1(\xi_n) = J_1'(\xi_n) Y_1'(k\xi_n) - J_1'(k\xi_n) Y_1'(\xi_n) = 0$. (see Table A-6)</p>

Table 4-37. Liquid Force and Moment Resultants

Annular Tank	Excitation: Harmonic Translation
--------------	----------------------------------

Translation in the x-direction, $x = x_0 e^{i\omega t}$.

$$1. F_x = m_L \omega^2 x_0 e^{i\omega t} \left[1 + \sum_{n=0}^{\infty} \frac{A_n [2/\pi \xi_n - k C_1(\sigma_n)] \tanh \kappa_n}{(1-k^2)(\eta_n^2 - 1) \kappa_n} \right]$$

$$2. M_y = m_L a \omega^2 x_0 e^{i\omega t} \left\{ \frac{1+k^2}{4(h/a)} + \sum_{n=0}^{\infty} \frac{A_n [2/\pi \xi_n - k C_1(\sigma_n)]}{2(1-k^2)(\eta_n^2 - 1)} \left[\tanh \kappa_n + \frac{2}{\kappa_n} \left(\frac{2}{\cosh \kappa_n} - 1 \right) \right] \right\}$$

Pitching about the y-axis, $\theta = \theta_0 e^{i\omega t}$.

$$1. F_x = -m_L g \theta_0 e^{i\omega t} - m_L a \omega^2 \theta_0 e^{i\omega t} \sum_{n=0}^{\infty} \frac{A_n [2/\pi \xi_n - k C_1(\sigma_n)]}{(1-k^2)(\eta_n^2 - 1) \xi_n} \left[\left(\frac{\gamma_n}{\kappa_n} + \frac{1}{2} \right) \tanh \kappa_n + \frac{2}{\kappa_n} \left(\frac{1}{\cosh \kappa_n} - 1 \right) \right]$$

$$2. M_y = -m_L g a \theta_0 e^{i\omega t} \frac{(1+k^2)}{4(h/a)} - m_L a^2 \omega^2 \theta_0 e^{i\omega t} \left\{ \frac{1}{12} \left(\frac{h}{a} \right)^2 - \frac{1}{8} (1+k^2) + \sum_{n=0}^{\infty} \frac{A_n [2/\pi \xi_n - k C_1(\sigma_n)]}{(1-k^2)(\eta_n^2 - 1) \xi_n} \right\}$$

$$\left[\left(\frac{h}{4a} - \frac{3\gamma_n}{2\xi_n} - \frac{4}{\kappa_n \xi_n} \tanh \kappa_n + \left(2 - \frac{4\gamma_n}{\kappa_n} \right) \frac{1}{\xi_n \cosh \kappa_n} + \left(\frac{5\gamma_n}{\kappa_n \xi_n} + \frac{1}{2\xi_n} \right) \right) \right]$$

Table 4-38. Model Analysis

Annular Tank	Spring-Mass Model
Excitation: Harmonic Translation and/or Pitching	

Figure 4-30 shows a diagram of the spring-mass model used in representing the dynamic response of a liquid in an annular tank when subjected to harmonic translation in the x-direction and/or pitching about the y-axis.

Coordinate System:

The origin is located at the center of gravity of the undisturbed liquid.

Model Description:

The components of the system are as follows:

1. A fixed mass M having a moment of inertia I is rigidly connected to the tank and is located on the z-axis at the distance H below the coordinate origin.
2. A set of movable masses m_n is distributed along the z-axis when the tank is at rest at distances h_n above the origin. These modal masses are constrained by spring-dashpot systems, having spring stiffness coefficients k_n and viscous damping coefficients c_n , to remain in the xy-plane and to move only in a direction parallel to the x-axis. Translational displacements of these masses with respect to the container are denoted by x_n .
3. A massless disc having a moment of inertia I_d is located at the coordinate origin. Its motion is confined to rotation about the y-axis and is cushioned by a dashpot having a viscous damping coefficient c_d . The angular displacement of the disc relative to the tank is defined by ψ .

Equations of Motion:

The equations, obtained through Lagrange's equations, are as follows:

1. Force Equation:

$$F_x = -M(\ddot{x} + H\ddot{\theta}) - \sum_{n=1}^{\infty} m_n(\ddot{x} + \ddot{x}_n + h_n\ddot{\theta})$$

2. Moment Equation:

$$M_y = -(I + MH^2)\ddot{\theta} - I_d(\ddot{\theta} + \ddot{\psi}) + g \sum_{n=1}^{\infty} m_n x_n - \sum_{n=1}^{\infty} m_n h_n (\ddot{x}_n + h_n \ddot{\theta})$$

Table 4-38. Model Analysis (continued)

Annular Tank	Spring-Mass Model
Excitation: Harmonic Translation and/or Pitching	

Equations of Motion (continued):

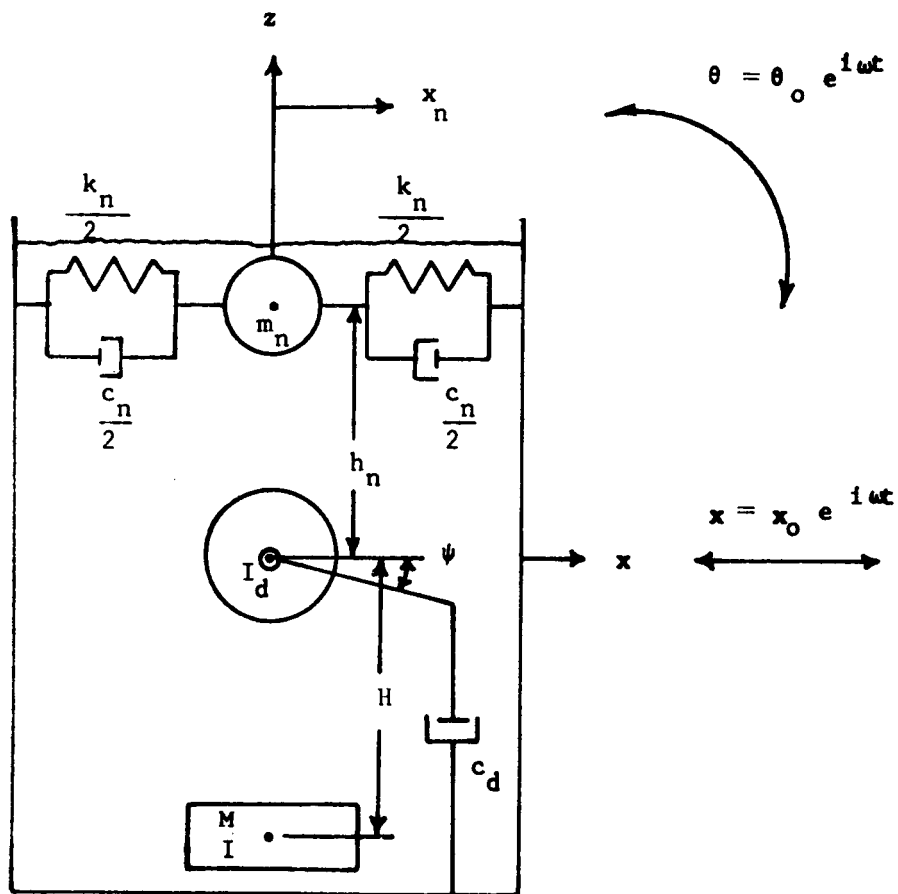
3. Disc Equation:

$$I_d (\ddot{\theta} + \ddot{\psi}) + c_d \dot{\psi} = 0$$

4. Slosh-Mass Equation:

$$\dot{m}_n (\ddot{x} + \ddot{x}_n + h_n \ddot{\theta}) + m_n \bar{g}_n \omega_n \dot{x}_n + k_n x_n - m_n g \theta = 0$$

From these equations, the model force in the x-direction and the moment about the y-axis can be found (see Table 4-39).



Annular Tank	Spring-Mass Model
Excitation: Harmonic Translation and/or Pitching	

Figure 4-30. Equivalent Mechanical Model

Table 4-39. Model Force and Moment Resultants

Annular Tank	Spring-Mass Model
Excitation: Harmonic Translation and/or Pitching	

Translation in the x-direction, $x = x_0 e^{i\omega t}$.

$$1. F_x = m_L \omega^2 x_0 e^{i\omega t} \left[1 + \sum_{n=0}^{\infty} \left(\frac{m_n}{m_L} \right) \left(\frac{1}{\eta_n^2 - 1 + i\bar{g}_n \eta_n} \right) \right]$$

$$2. M_y = m_L h \omega^2 x_0 e^{i\omega t} \sum_{n=0}^{\infty} \left(\frac{m_n}{m_L} \right) \left(\frac{h}{h} \eta_n + \frac{g}{h \omega^2} \right) \left(\frac{1}{\eta_n^2 - 1 + i\bar{g}_n \eta_n} \right)$$

Pitching about the y-axis, $\theta = \theta_0 e^{i\omega t}$.

$$1. F_x = -m_L h \omega^2 \theta_0 e^{i\omega t} \sum_{n=0}^{\infty} \left(\frac{m_n}{m_L} \right) \left(\frac{h}{h} \eta_n + \frac{g}{h \omega^2} \right) \left(\frac{1}{\eta_n^2 - 1 + i\bar{g}_n \eta_n} \right)$$

$$2. M_y = -m_L h^2 \omega^2 \theta_0 e^{i\omega t} \left[\frac{I}{m_L h^2} + \frac{M H^2}{m_L h^2} + \frac{I_d}{m_L h^2} \left(1 - \frac{\omega^2 I_d}{2 + \omega^2 I_d} \right) + \sum_{n=0}^{\infty} \frac{m_n h^2}{m_L h^2} \right. \\ \left. + \sum_{n=0}^{\infty} \left(\frac{m_n}{m_L} \right) \left(\frac{h}{h} \eta_n + \frac{g}{h \omega^2} \right)^2 \left(\frac{1}{\eta_n^2 - 1 + i\bar{g}_n \eta_n} \right) \right] + i\omega \theta_0 e^{i\omega t} \frac{c_d \omega I_d^2}{c_d^2 + \omega^2 I_d^2}$$

Table 4-40. Model Elements

Annular Tank	Spring-Mass Model
Excitation: Harmonic Translation or Pitching	
Natural Frequency	$\omega_n^2 = \frac{g}{a} \xi_n \tanh \kappa_n$
Spring Constant	$k_n = m_n \omega_n^2$ (fig. 4-31)
Damping Coefficient of Slosh Mass	$c_n = m_n \bar{g}_n \omega_n$ (fig. 4-32)
Damping Coefficient of Disc	$c_d = \bar{c} \left[1 + \frac{\bar{c}^2}{\omega^2 (I_s - \bar{I})^2} \right]$
Ratio of Slosh Mass to Fluid Mass	$\frac{m_n}{m_L} = \frac{A_n \left[2/\pi \xi_n - kC_1(\sigma_n) \right] \tanh \kappa_n}{(1-k^2) \kappa_n}$ (fig. 4-33) (fig. 4-34)
Ratio of Fixed Mass to Fluid Mass	$\frac{M}{m_L} = 1 - \sum_{n=0}^{\infty} \frac{m_n}{m_L}$ (fig. 4-35)
Ratio of Slosh Mass Coordinate to Fluid Depth	$\left \frac{h_n}{h} \right = \frac{1}{2} \left[1 - \frac{4}{\kappa_n} \tanh \frac{\kappa_n}{2} \right]$ (fig. 4-36)
Ratio of Fixed Mass Coordinate to Fluid Depth	$\left \frac{H}{h} \right = \frac{m_L}{M} \sum_{n=0}^{\infty} \left(\frac{m_n}{m_L} \right) \left(\frac{h_n}{h} \right)$ (fig. 4-37)
Moment of Inertia of Solidified Fluid	$\frac{I_s}{m_L h^2} = \left(\frac{a}{h} \right)^2 \left[\frac{1}{12} \left(\frac{h}{a} \right)^2 + \frac{1}{4} \right]$
Moment of Inertia of Disc ($c_d = 0$)	$\frac{I_d}{m_L h^2} = 4 \left(\frac{a}{h} \right)^2 \sum_{n=0}^{\infty} \frac{A_n \left[2/\pi \xi_n - kC_1(\sigma_n) \right] \left[1 - 2/\kappa_n \tanh(\kappa_n/2) \right]}{(1-k^2) \xi_n}$ (fig. 4-38)
Moment of Inertia of Disc ($c_d \neq 0$)	$\frac{I_d}{m_L h^2} = \frac{I_s - \bar{I}}{m_L h^2} \left[1 + \frac{\bar{c}^2}{\omega^2 (I_s - \bar{I})^2} \right]$
Moment of Inertia of Fixed Mass	$\frac{I}{m_L h^2} = \frac{I_s}{m_L h^2} - \frac{I_d}{m_L h^2} - \frac{M}{m_L} \left(\frac{H}{h} \right) - \sum_{n=0}^{\infty} \frac{m_n}{m_L} \left(\frac{h_n}{h} \right)^2$ (fig. 4-39)

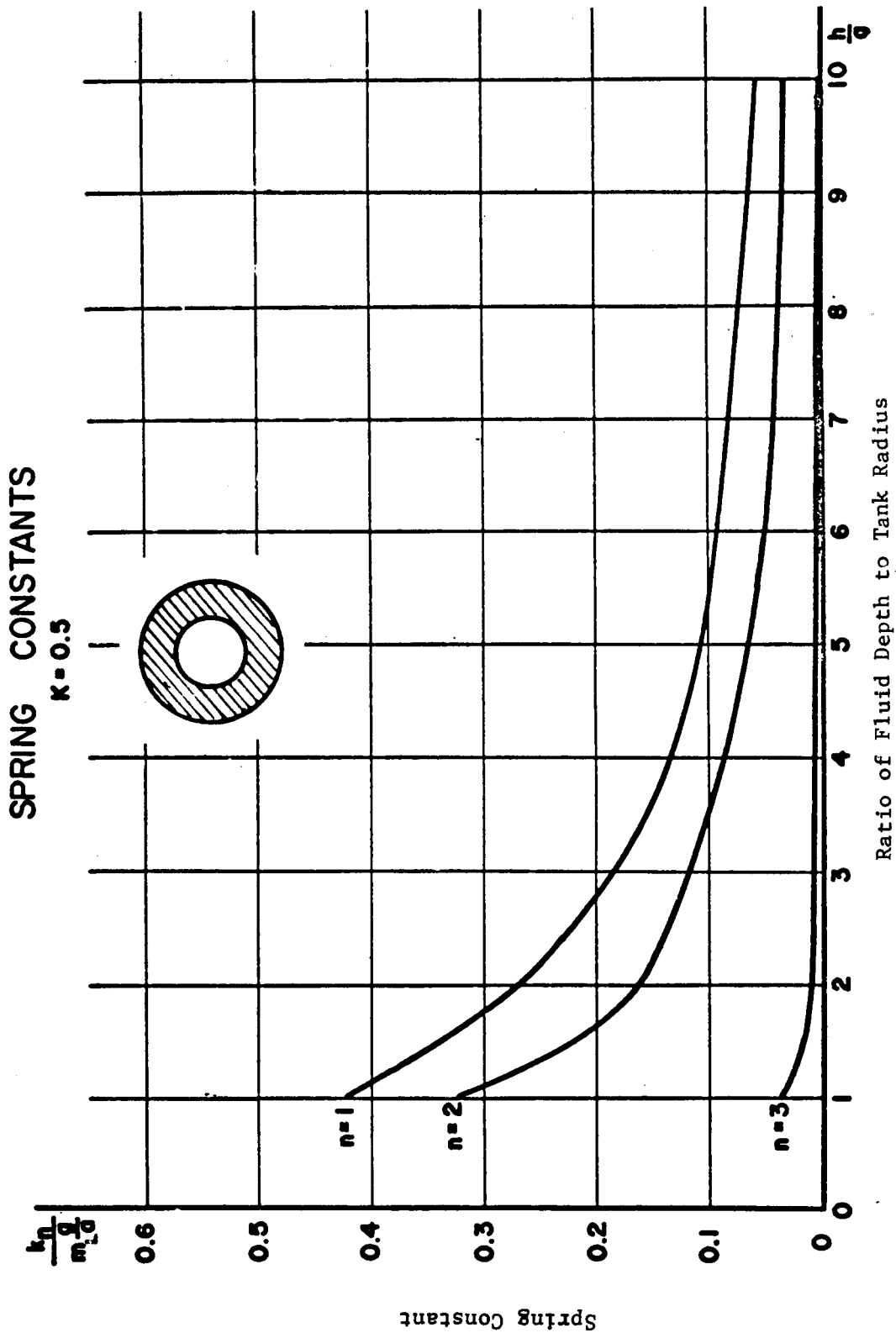


Figure 4-31. Model Element Graph

DAMPING CONSTANTS

$K = 0.5$

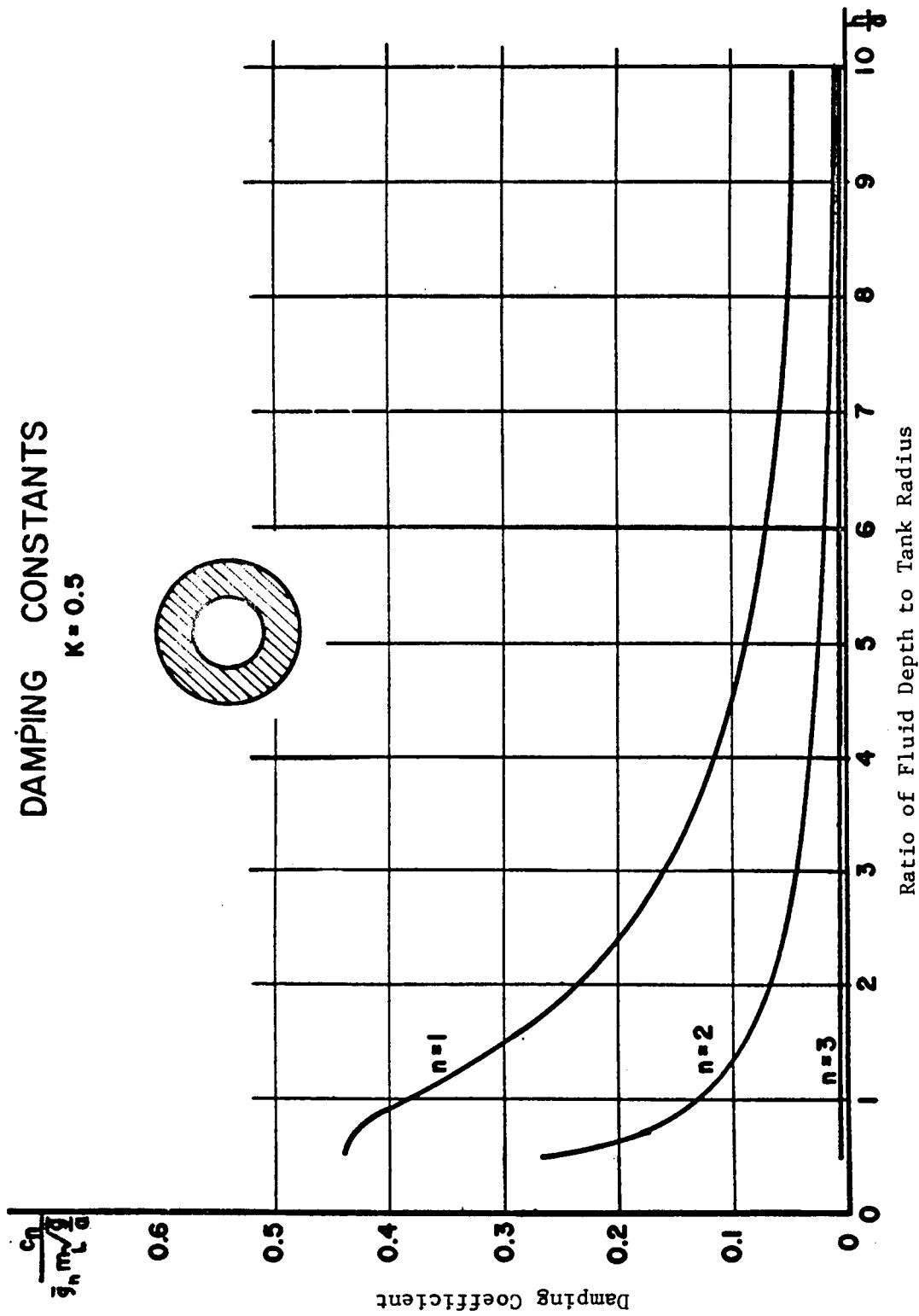


Figure 4-32. Model Element Graph

SLOSHING MASS
VS.
FLUID HEIGHT RATIO
FOR CYLINDRICAL TANK WITH
ANNULAR CROSS SECTION
 $\kappa = 0.5$

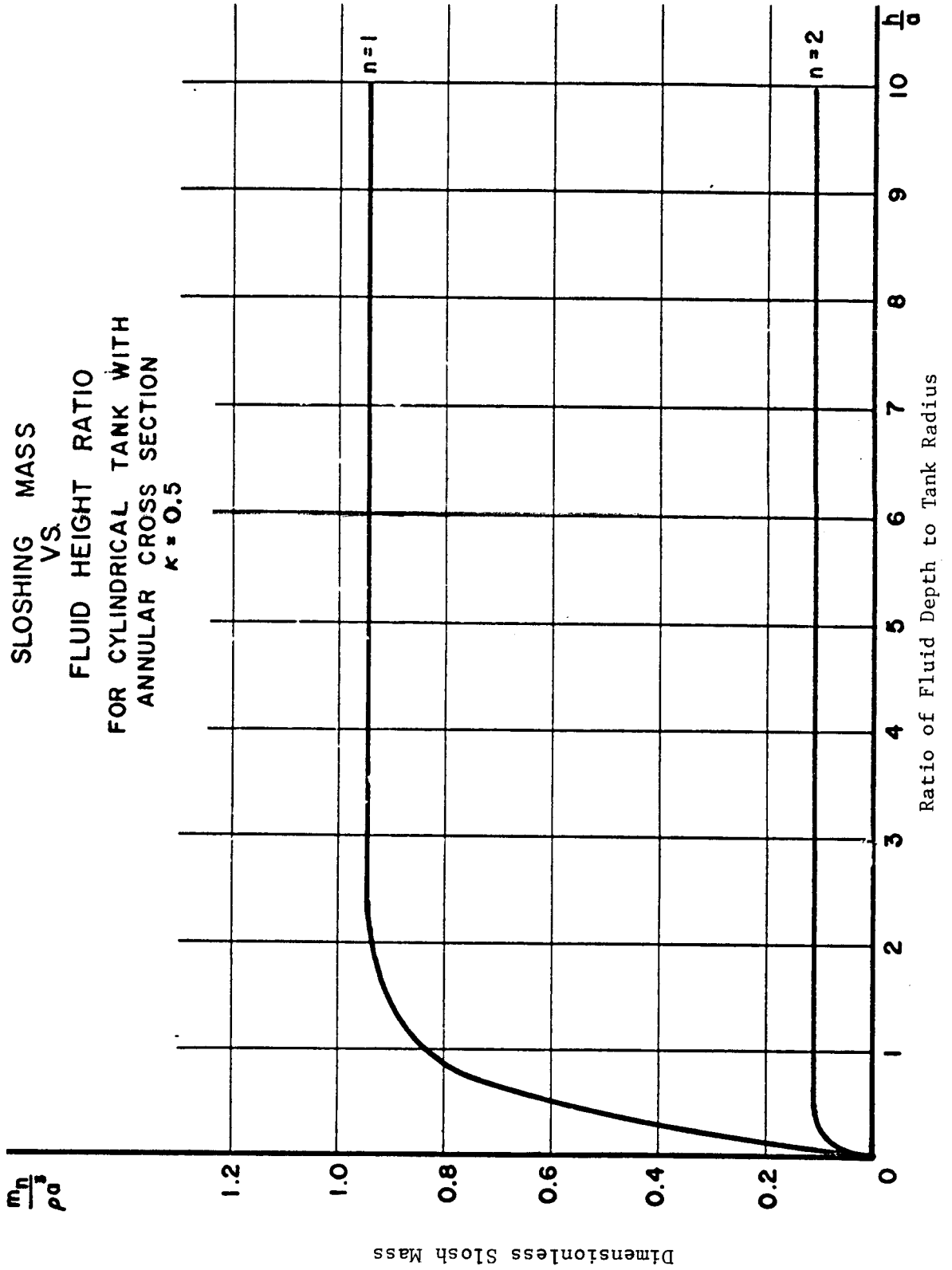


Figure 4-33. Model Element Graph

SLOSH MASS RATIO
VS.
FLUID HEIGHT RATIO
K=0.5

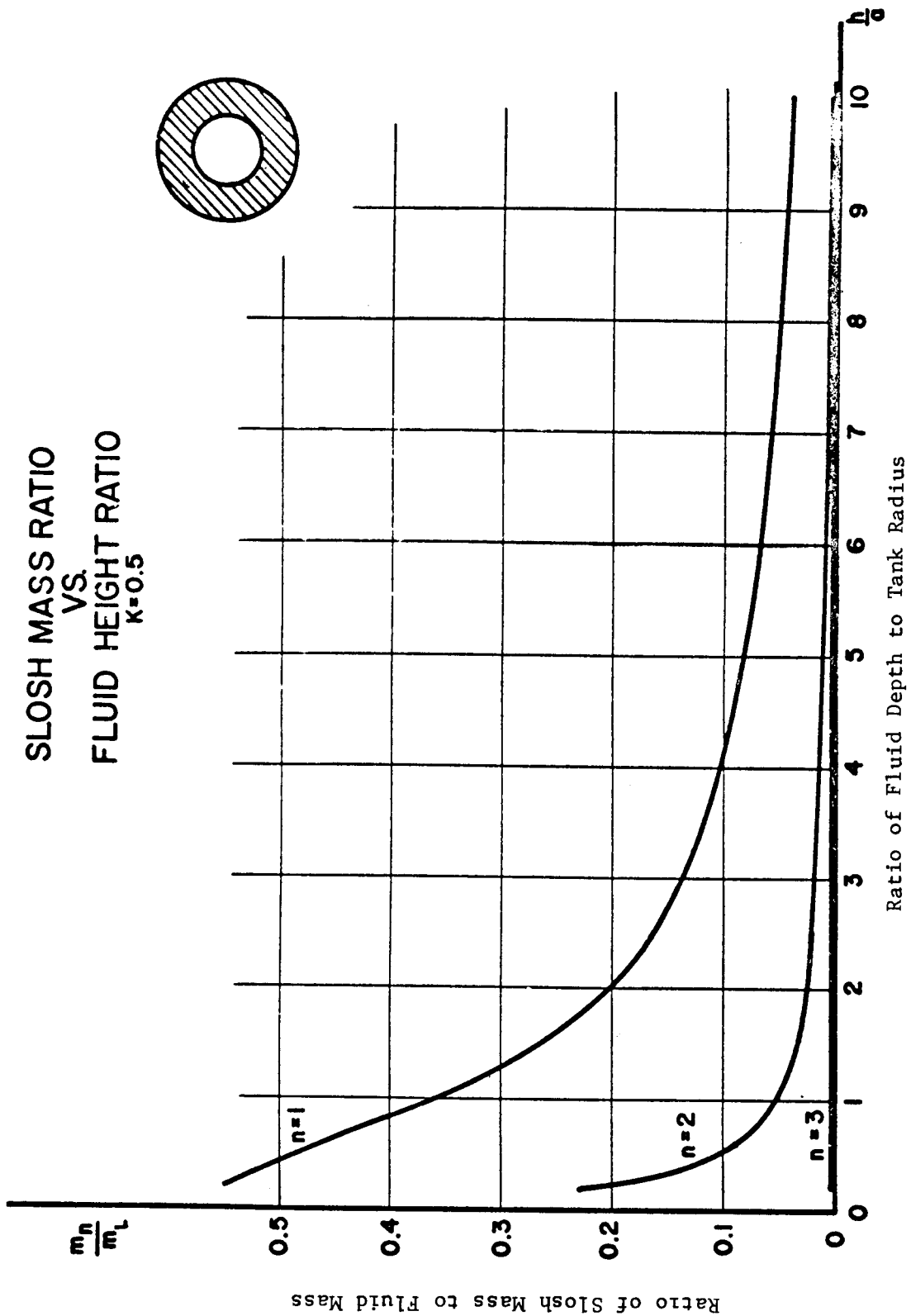


Figure 4-34. Model Element Graph

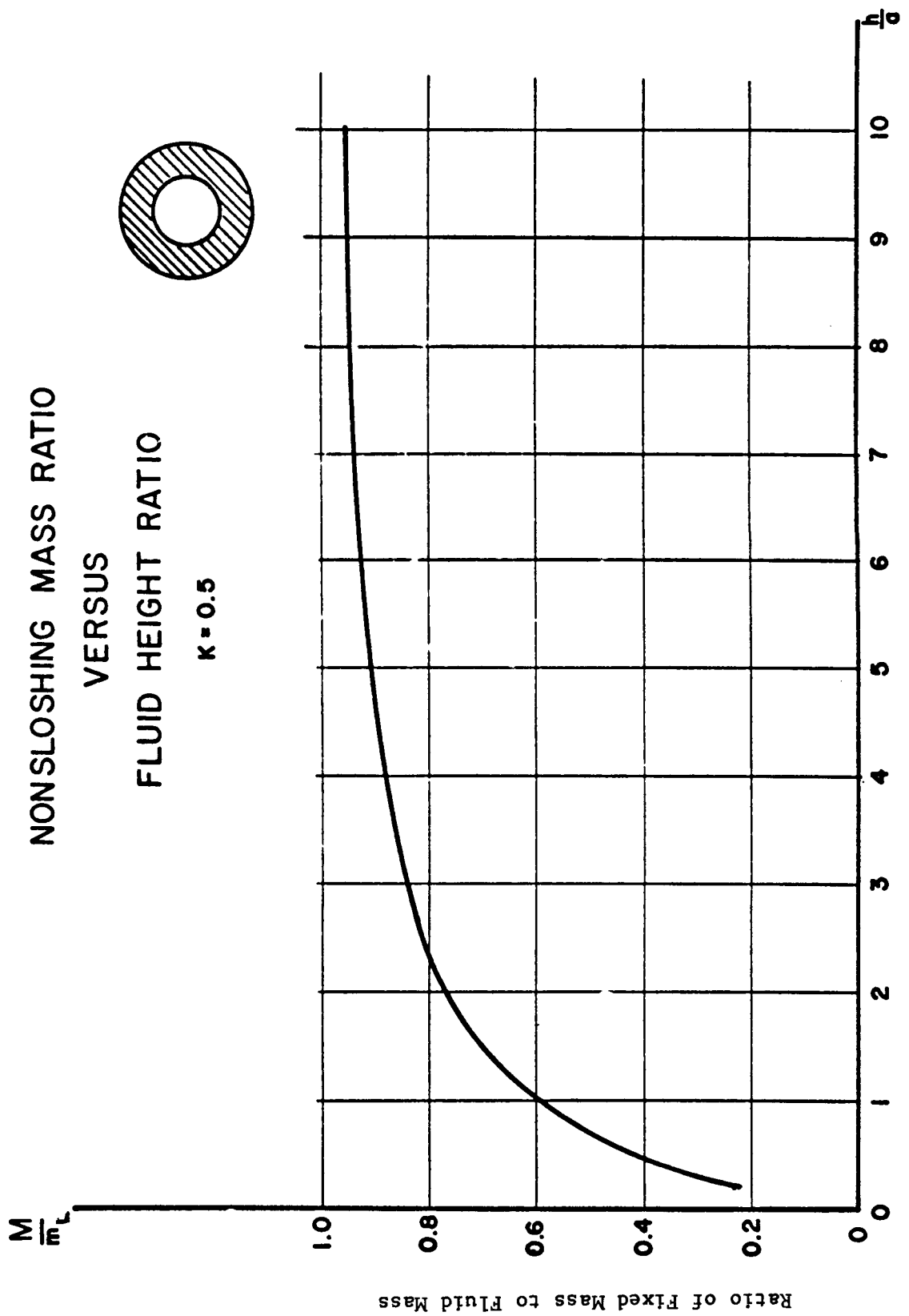


Figure 4-35. Model Element Graph

MASS LOCATION HEIGHT RATIO
VS.
FLUID HEIGHT RATIO
K=0.5

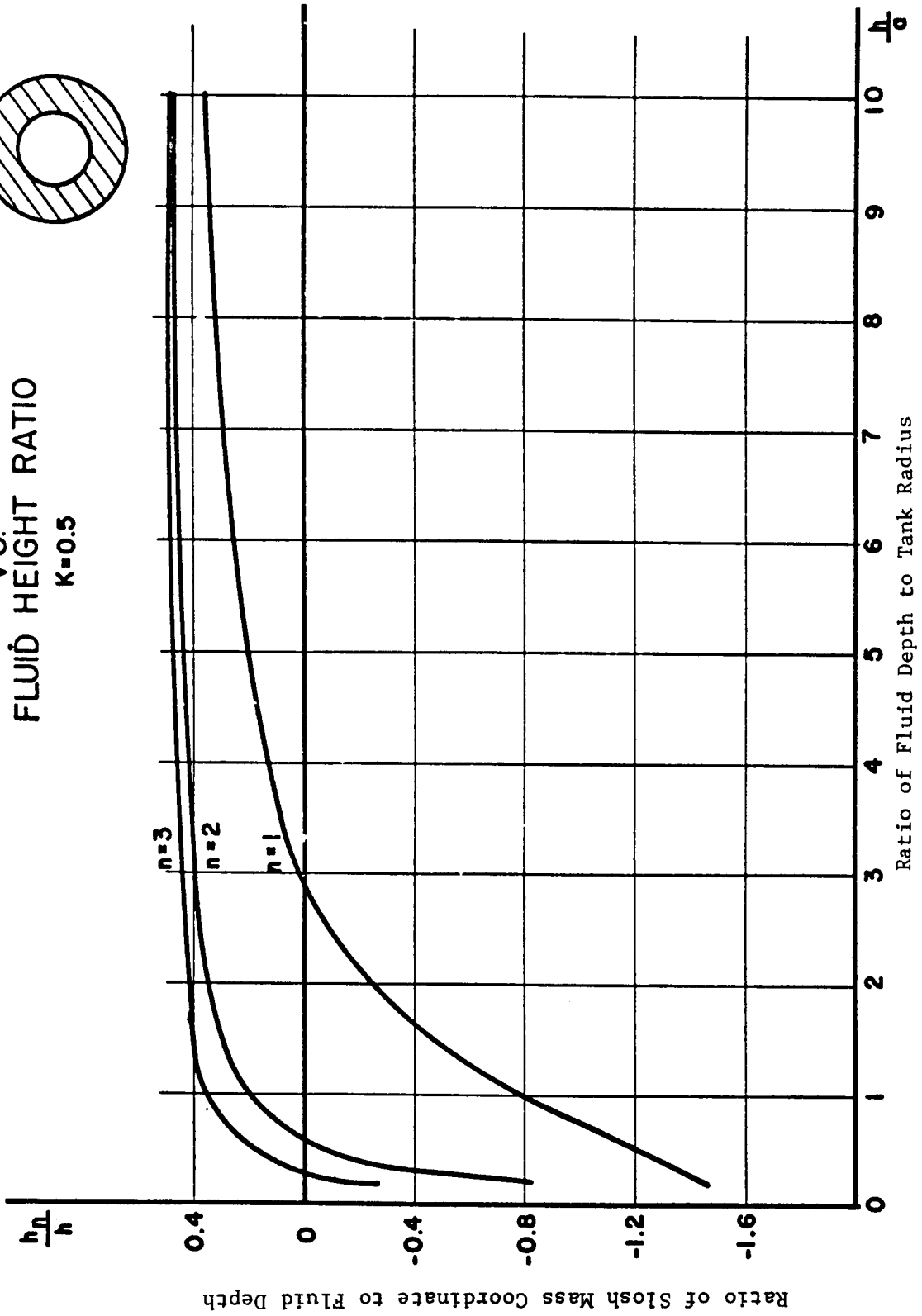
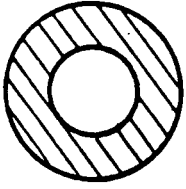


Figure 4-36. Model Element Graph

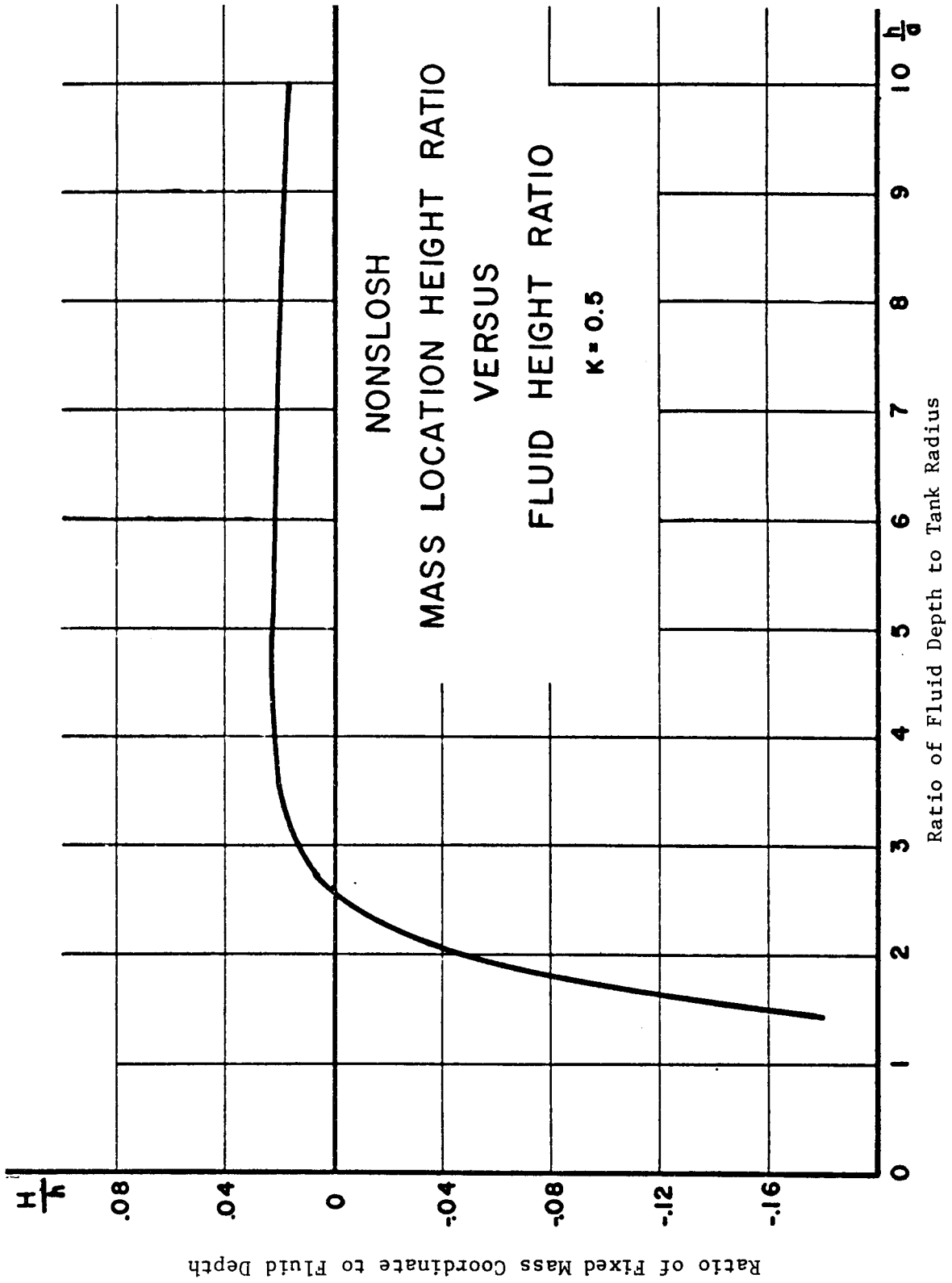


Figure 4-37. Model Element Graph

MOMENT OF INERTIA RATIO OF THE DISC
 VS
 FLUID HEIGHT RATIO

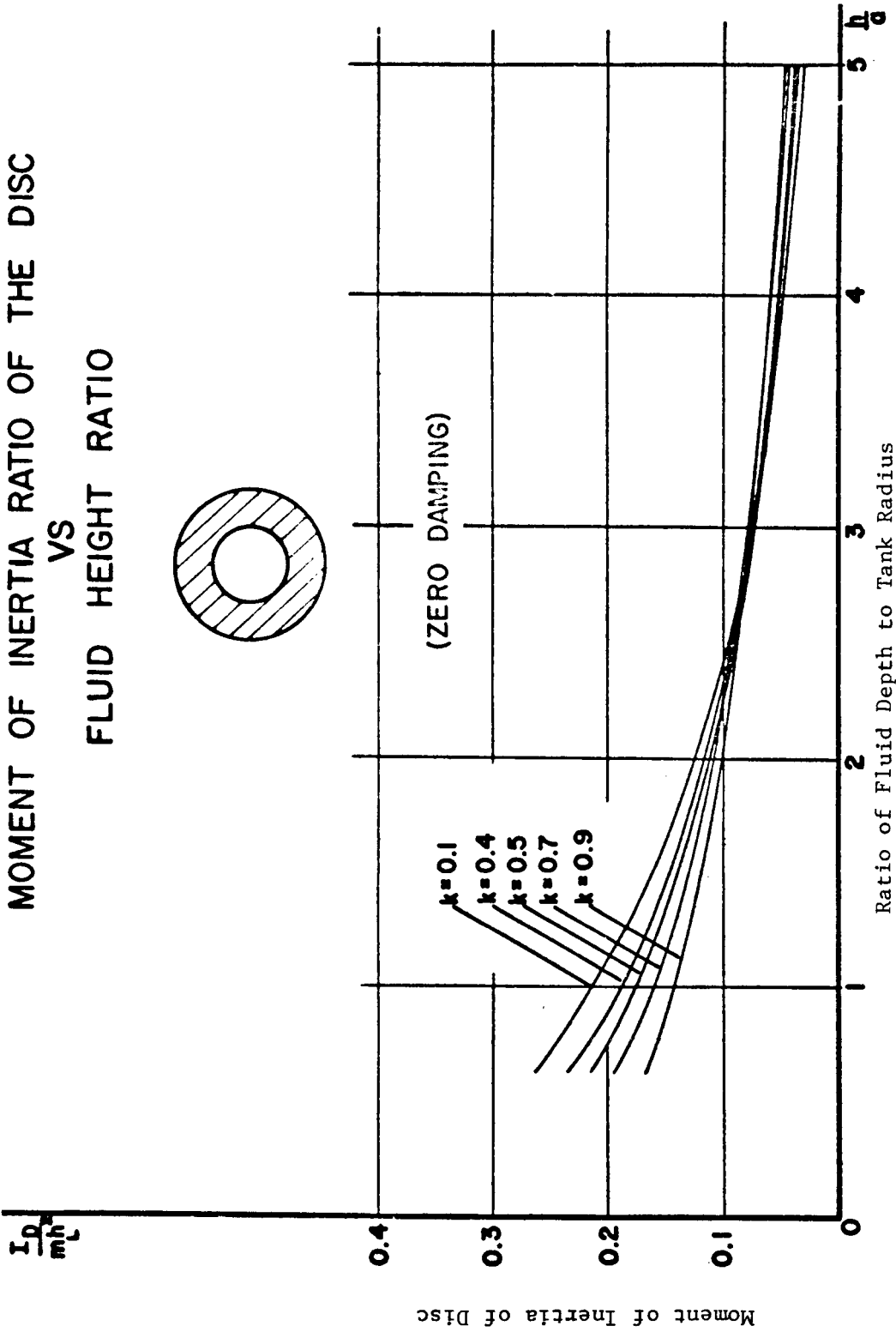
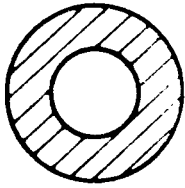


Figure 4-38. Model Element Graph

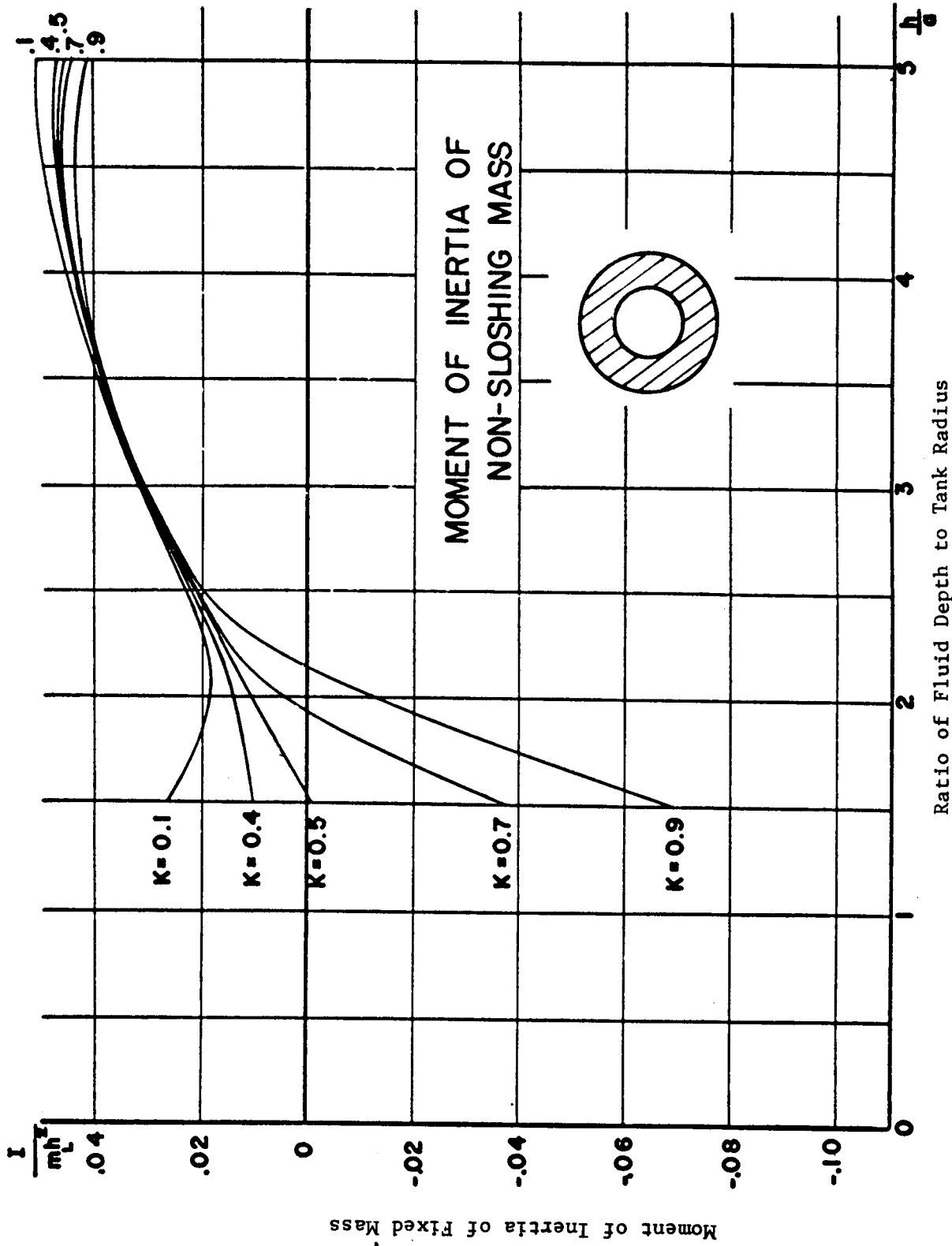


Figure 4-39. Model Element Graph

Table 4-41. Model Analysis

Annular Tank	Pendulum Model
Excitation: Harmonic Translation and/or Pitching	

Figure 4-40 shows a diagram of the pendulum model used in representing the dynamic response of a liquid in an annular tank when subjected to harmonic translation in the x-direction and/or pitching about the y-axis.

Coordinate System:

The origin is located at the center of gravity of the undisturbed liquid

Model Description:

The components of the system are as follows:

1. A fixed mass M having a moment of inertia I is rigidly connected to the tank and is located on the z-axis at a distance H below the coordinate origin.
2. A set of movable masses m_n is distributed along the z-axis when the tank is at rest. These modal masses are pendulums having massless lever arms of length L_n attached to the z-axis at distances H_n above the origin. They are constrained by dashpots having viscous damping coefficients c_n to remain approximately in the xy-plane and to move approximately parallel to the x-axis. Angular displacements of the pendulum with respect to the tank (z-axis) are denoted by λ_n .
3. A massless disc having a moment of inertia I_d is located at the coordinate origin. Its motion is confined to rotation about the y-axis and is cushioned by a dashpot having a viscous damping coefficient c_d . The angular displacement of the disc relative to the tank is defined by ψ .

Equations of Motion:

The equations, obtained through Lagrange's equations, are as follows:

1. Force Equation:

$$F_x = -M(\ddot{x} + H\ddot{\theta}) - \sum_{n=1}^{\infty} m_n \left[\ddot{x} + L_n \ddot{\lambda}_n + (H_n - L_n)\ddot{\theta} \right]$$

2. Moment Equation:

$$M_y = - (I + MH^2)\ddot{\theta} - I_d(\ddot{\theta} + \ddot{\psi}) + g \sum_{n=1}^{\infty} m_n L_n \lambda_n - \sum_{n=1}^{\infty} m_n (H_n - L_n) \cdot \left[L_n \ddot{\lambda}_n + (H_n - L_n)\ddot{\theta} \right]$$

Table 4-41. Model Analysis (continued)

Annular Tank	Pendulum Model
Excitation: Harmonic Translation and/or Pitching	

Equations of Motion (continued):

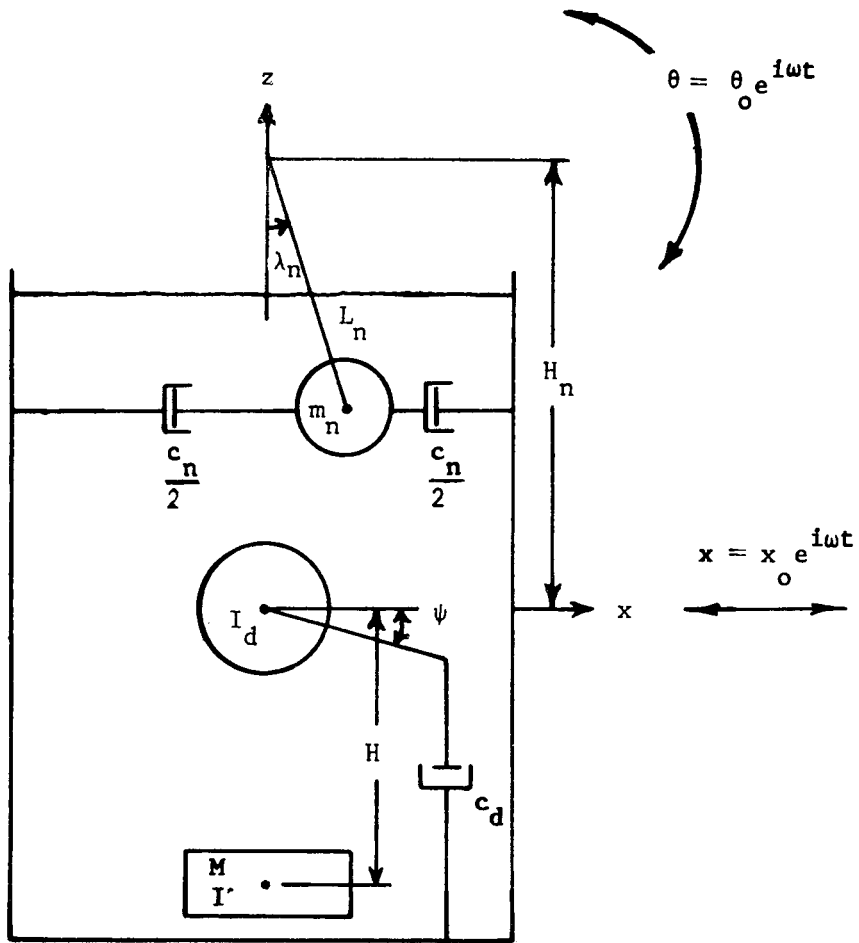
3. Disc Equation:

$$I_d (\ddot{\theta} + \ddot{\psi}) + c_d \dot{\psi} = 0$$

4. Slosh-Mass Equation:

$$m_n \left[\ddot{x} + L_n \ddot{\lambda}_n + (H_n - L_n) \ddot{\theta} \right] + m_n \bar{g}_n \omega_n L_n \dot{\lambda}_n - m_n g \theta = 0$$

From these equations, the model force in the x-direction and the moment about the y-axis can be found (see Table 4-42).



Annular Tank

Pendulum Model

Excitation: Harmonic Translation and/or Pitching

Figure 4-40. Equivalent Mechanical Model

Table 4-42. Model Force and Moment Resultants

Annular Tank	Pendulum Model
Excitation: Harmonic Translation and/or Pitching	

Translation in the x-direction, $x = x_0 e^{i\omega t}$.

$$1. F_x = m_L \omega^2 x_0 e^{i\omega t} \left[1 + \sum_{n=0}^{\infty} \left(\frac{m_n}{m_L} \right) \left(\frac{1}{\eta_n^2 - 1 + i\bar{g}_n \eta_n} \right) \right]$$

$$2. M_y = m_L h \omega^2 x_0 e^{i\omega t} \sum_{n=0}^{\infty} \left(\frac{m_n}{m_L} \right) \left(\frac{H_n - L_n}{h} + \frac{g}{2} \right) \left(\frac{1}{\eta_n^2 - 1 + i\bar{g}_n \eta_n} \right)$$

Pitching about the y-axis, $\theta = \theta_0 e^{i\omega t}$.

$$1. F_x = -m_L h \omega^2 \theta_0 e^{i\omega t} \sum_{n=0}^{\infty} \left(\frac{m_n}{m_L} \right) \left(\frac{H_n - L_n}{h} + \frac{g}{2} \right) \left(\frac{1}{\eta_n^2 - 1 + i\bar{g}_n \eta_n} \right)$$

$$2. M_y = -m_L h^2 \omega^2 \theta_0 e^{i\omega t} \left[\frac{I}{m_L h^2} + \frac{Mh^2}{m_L h^2} + \frac{I_d}{m_L h^2} \left(1 - \frac{\omega^2 I_d^2}{c_d^2 + \omega^2 I_d^2} \right) + \sum_{n=0}^{\infty} \frac{m_n (H_n - L_n)^2}{m_L h^2} \right] + 1\omega \theta_0 e^{i\omega t} \left(\frac{c_d \omega I_d^2}{c_d^2 + \omega^2 I_d^2} \right)$$

Table 4-43. Model Elements

Annular Tank	Pendulum Model
Excitation: Harmonic Translation and/or Pitching	
Natural Frequency	$\omega_n^2 = \frac{g}{a} \xi_n \tanh \kappa_n$
Pendulum Length	$L_n = \frac{g}{\omega_n^2}$ (fig. 4-41)
Damping Coefficient of Slosh Mass	$c_n = m_n \bar{g}_n \omega_n$
Damping Coefficient	$c_d = \bar{c} \left[1 + \frac{\bar{c}^2}{\omega^2 (I_s - \bar{I})^2} \right]$
Ratio of Slosh Mass to Fluid Mass	$\frac{m_n}{m_L} = \frac{A_n [2/\pi \xi_n - kC_1(\sigma_n)] \tanh \kappa_n}{(1-k^2) \kappa_n}$
Ratio of Fixed Mass to Fluid Mass	$\frac{M}{m_L} = 1 - \sum_{n=0}^{\infty} \frac{m_n}{m_L}$
Ratio of Pendulum Mass Coordinate to Fluid Depth	$\frac{ H_n - L_n }{h} = \frac{1}{2} \left[1 - \frac{4}{\kappa_n} \tanh \left(\frac{\kappa_n}{2} \right) \right]$ (fig. 4-42)
Ratio of Fixed Mass Coordinate to Fluid Depth	$\frac{ H }{h} = \frac{m_L}{M} \sum_{n=0}^{\infty} \left(\frac{m_n}{m_L} \right) \left(\frac{H_n - L_n}{h} \right)$
Moment of Inertia of Solidified Fluid	$\frac{I_s}{m_L h^2} = \left(\frac{a}{h} \right)^2 \left[\frac{1}{12} \left(\frac{h}{a} \right)^2 + \frac{1}{4} \right]$
Moment of Inertia of Disc ($c_d = 0$)	$\frac{I_d}{m_L h^2} = 4 \left(\frac{a}{h} \right)^2 \sum_{n=0}^{\infty} \frac{A_n [2/\pi \xi_n - kC_1(\sigma_n)] [1 - (2/\kappa_n) \tanh(\kappa_n/2)]}{(1-k^2) \xi_n}$
Moment of Inertia of Disc ($c_d \neq 0$)	$\frac{I_d}{m_L h^2} = \frac{I_s - \bar{I}}{m_L h^2} \left[1 + \frac{\bar{c}^2}{\omega^2 (I_s - \bar{I})^2} \right]$
Moment of Inertia of Fixed Mass	$\frac{I}{m_L h^2} = \frac{I_s}{m_L h^2} - \frac{I_d}{m_L h^2} - \frac{M}{m_L} \left(\frac{H}{h} \right) - \sum_{n=0}^{\infty} \frac{m_n}{m_L} \left[\frac{H_n - L_n}{h} \right]^2$

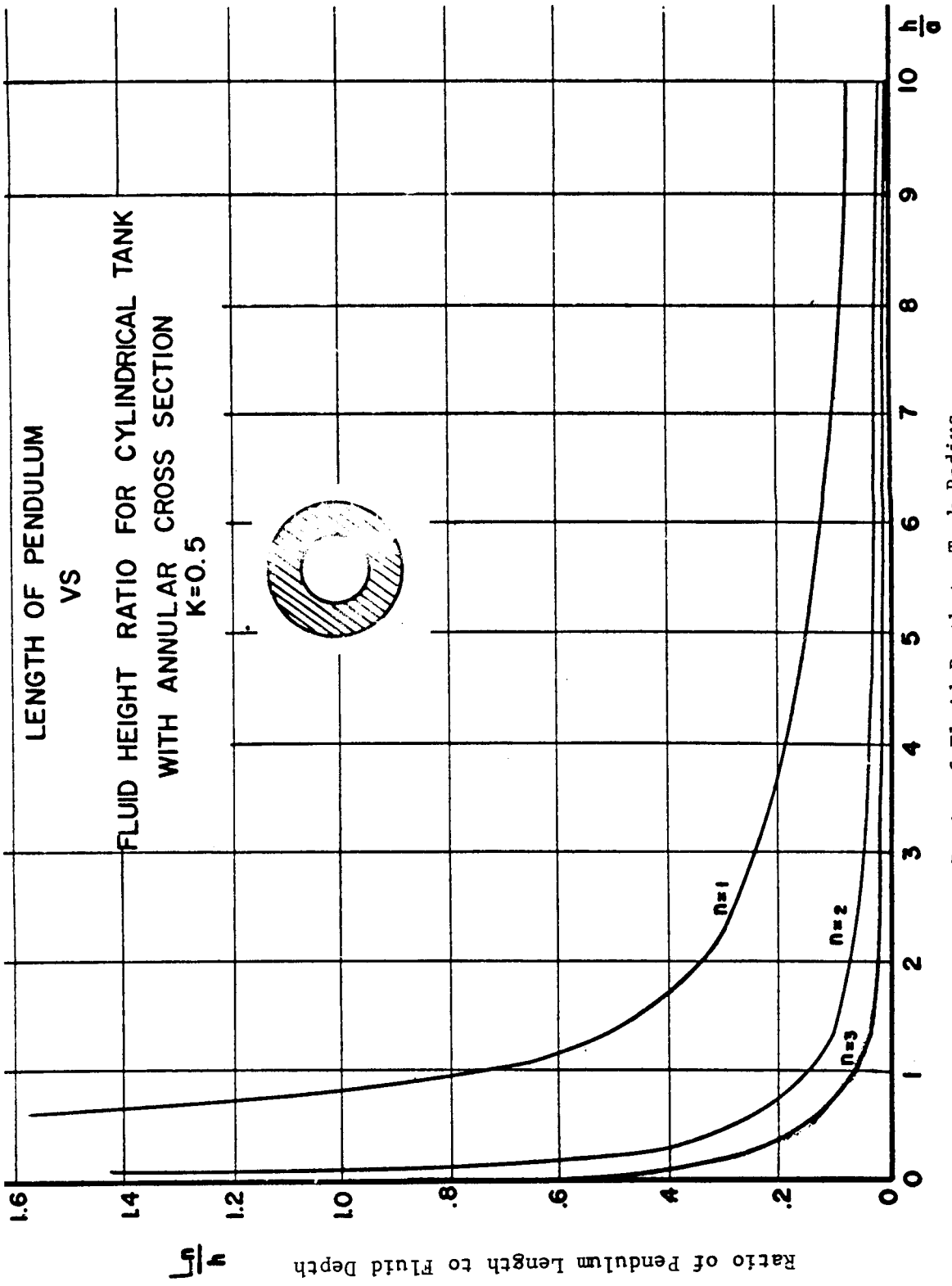


Figure 4-41. Model Element Graph

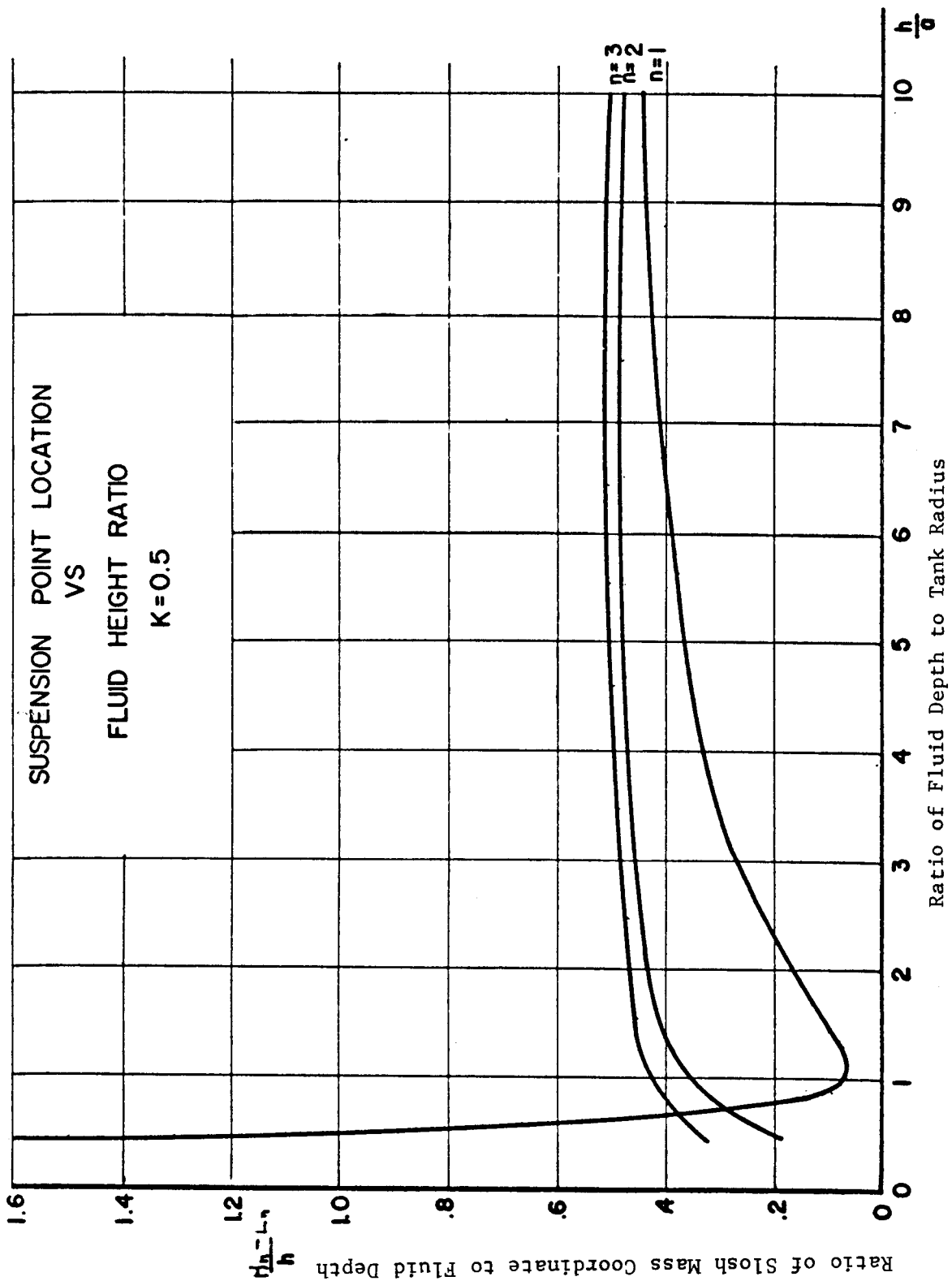
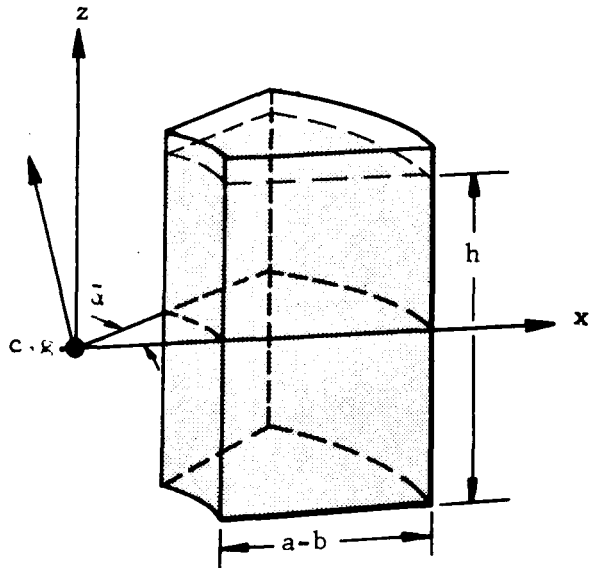


Figure 4-42. Model Element Graph

Table of Contents

General.....	4-113
Excitation: Harmonic Translation	
Boundary Conditions, Velocity Potential, and Natural Frequency.....	4-114
Liquid Force and Moment Resultants.....	4-116
Excitation: Harmonic Pitching	
Boundary Conditions, Velocity Potential, and Natural Frequency.....	4-118
Liquid Force and Moment Resultants.....	4-120
Excitation: Harmonic Roll	
Boundary Conditions, Velocity Potential, and Natural Frequency.....	4-122
Liquid Force and Moment Resultants.....	4-124



Container: The tank is a sector of an annular tank having an inner radius $r=b$ and an outer radius $r=a$ and is filled with a liquid to a depth h .

Coordinate System: The origin is located at the center of gravity of the undisturbed fluid which would be contained in an annular tank generated by revolving the annular-sector tank about the z -axis. The x -axis must lie in the sector wall.

Reference: (4)

Comments: The results given in this section are not valid for $\bar{\alpha} = \frac{\pi}{2}, \frac{3\pi}{2}$.

Table 4-44. Boundary Conditions, Velocity Potential, and Natural Frequency

Annular-Sector Tank	Excitation: Harmonic Translation
---------------------	----------------------------------

Translation in the x-direction, $x = x_0 e^{i\omega t}$.

1. Boundary conditions:

$$(a) \left(\frac{\partial \phi}{\partial r} \right)_{r=a,b} = i\omega x_0 e^{i\omega t} \cos \phi \quad (b) \left(\frac{\partial \phi}{\partial z} \right)_{z=-h} = 0$$

$$(c) \left(\frac{\partial^2 \phi}{\partial t^2} + g \frac{\partial \phi}{\partial z} \right)_{z=0} = 0 \quad (d) \left(\frac{1}{r} \frac{\partial \phi}{\partial \phi} \right)_{\phi=0} = 0$$

$$(e) \left(\frac{1}{r} \frac{\partial \phi}{\partial \phi} \right)_{\phi=\bar{\alpha}} = -i\omega x_0 e^{i\omega t} \sin \bar{\alpha}$$

2. Velocity potential:

$$\phi = i\omega x_0 e^{i\omega t} \left[r \cos \phi + \sum_{m=0}^{\infty} \sum_{n=0}^{\infty} \frac{a_m b_n C_{mn} / 2\alpha (\rho_{mn}) \cos \phi_m \cosh (\kappa_{mn} + \zeta_{mn})}{(\eta_{mn}^2 - 1) \cosh \kappa_{mn}} \right]$$

3. Natural angular frequency:

$$\omega_{mn}^2 = \frac{g}{a} \xi_{mn} \tanh \kappa_{mn}$$

where ξ_{mn} are roots of $\Delta_{m/2\alpha}(\xi_{mn}) = J'_{m/2\alpha}(\xi_{mn}) Y'_{m/2\alpha}(k\xi_{mn}) - J'_{m/2\alpha}(k\xi_{mn}) Y'_{m/2\alpha}(\xi_{mn}) = 0$.

Table 4-44. Boundary Conditions, Velocity Potential, and Natural Frequency (continued)

Annular-Sector Tank	Excitation: Harmonic Translation
Translation in the y-direction, $y = y_0 e^{i\omega t}$.	

1. Boundary conditions:

$$(a) \left(\frac{\partial \phi}{\partial r} \right)_{r=a,b} = i\omega y_0 e^{i\omega t} \sin \phi$$

$$(b) \left(\frac{\partial \phi}{\partial z} \right)_{z=-h} = 0$$

$$(c) \left(\frac{\partial^2 \phi}{\partial t^2} + g \frac{\partial \phi}{\partial z} \right)_{z=0} = 0$$

$$(d) \left(\frac{1}{r} \frac{\partial \phi}{\partial \phi} \right)_{\phi=0} = i\omega y_0 e^{i\omega t}$$

$$(e) \left(\frac{1}{r} \frac{\partial \phi}{\partial \phi} \right)_{\phi=\bar{\alpha}} = i\omega y_0 e^{i\omega t} \cos \bar{\alpha}$$

2. Velocity potential:

$$\phi = i\omega y_0 e^{i\omega t} \left[r \sin \phi + \sum_{m=0}^{\infty} \sum_{n=0}^{\infty} \frac{c_{mn}^b C_{m/2\alpha}(\rho_{mn}) \cos \bar{\phi}_m \cosh(\kappa_{mn} + \zeta_{mn})}{(\eta_{mn}^2 - 1) \cosh \kappa_{mn}} \right]$$

3. Natural angular frequency:

$$\omega_{mn}^2 = \frac{g}{a} \xi_{mn} \tanh \kappa_{mn}$$

where ξ_{mn} are roots of $\Delta_{m/2\alpha}(\xi_{mn}) = J'_{m/2\alpha}(\xi_{mn}) Y'_{m/2\alpha}(k\xi_{mn}) - J'_{m/2\alpha}(k\xi_{mn}) Y'_{m/2\alpha}(\xi_{mn}) = 0$.

Table 4-45. Liquid Force and Moment Resultants

Annular-Sector Tank	Excitation: Harmonic Translation
---------------------	----------------------------------

Translation in the x-direction, $x = x_0 e^{i\omega t}$.

$$1. \begin{pmatrix} F_x \\ F_y \end{pmatrix} = \frac{m_L \omega^2 x_0 e^{i\omega t}}{\alpha} \sum_{m=0}^{\infty} \sum_{n=0}^{\infty} \left\{ \begin{pmatrix} 1+ \\ 0 \end{pmatrix} \frac{2 a b_{mn} \tanh \kappa_{mn}}{\alpha a (1-k^2) (\eta_{mn}^2 - 1) \kappa_{mn}} \begin{pmatrix} (-1)^{m+1} \sin \bar{\alpha} \\ 1 - (-1)^m \cos \bar{\alpha} \end{pmatrix} \left[N_0(\xi_{mn}) + \right. \right.$$

$$\left. \left. \frac{\bar{\alpha}^2}{\pi^2 m^2 - \bar{\alpha}^2} \left(\frac{2}{\pi \xi_{mn}} - k G_{m/2\alpha}(\sigma_{mn}) \right) \right\} \right\}$$

$$2. \begin{pmatrix} M_x \\ M_y \end{pmatrix} = \frac{m_L a \omega^2 x_0 e^{i\omega t}}{\alpha} \sum_{m=0}^{\infty} \sum_{n=0}^{\infty} \left\{ \left\{ \frac{(1+k^2)}{4(h/a)} \left(\frac{\sin^2 \bar{\alpha}/\alpha}{1 + \sin \bar{\alpha} \cos \bar{\alpha}/\alpha} \right) \right. \right. \cdot$$

$$\left. \left. \left(\frac{1 - (-1)^m \cos \bar{\alpha}}{(-1)^{m+1} \sin \bar{\alpha}} \right) \left[\tanh \kappa_{mn} + \frac{2}{\kappa_{mn}} \left(\frac{1}{\cosh \kappa_{mn}} - 1 \right) \right] \left[N_0(\xi_{mn}) + \frac{\bar{\alpha}^2}{\pi^2 m^2 - \bar{\alpha}^2} \left(\frac{2}{\pi \xi_{mn}} - k G_{m/2\alpha}(\sigma_{mn}) \right) \right] \right. \right.$$

$$\left. \left. + \frac{2\bar{\alpha}^2 \xi_{mn}^2 N_2(\xi_{mn})}{(\pi^2 m^2 - \bar{\alpha}^2) \kappa_{mn} \cosh \kappa_{mn}} \right\} \right\} + \frac{2m_L g a (1-k^3)}{3\bar{\alpha} (1-k^2)} \begin{pmatrix} 1 - \cos \bar{\alpha} \\ \sin \bar{\alpha} \end{pmatrix}$$

Table 4-45. Liquid Force and Moment Resultants (continued)

Annular-Sector Tank

Excitation: Harmonic Translation

Translation in the y-direction, $y = y_0 e^{i\omega t}$.

$$1. \begin{pmatrix} F_x \\ F_y \end{pmatrix} = m_L \omega^2 y_0 e^{i\omega t} \sum_{m=0}^{\infty} \sum_{n=0}^{\infty} \begin{pmatrix} 0 \\ 1 \end{pmatrix} \frac{2c_{m,n}^b \tanh \kappa_{mn}}{\bar{\alpha} \alpha (1-k^2) (\eta_{mn}^2 - 1) \kappa_{mn}} \begin{pmatrix} (-1)^{m+1} \sin \bar{\alpha} \\ 1 - (-1)^m \cos \bar{\alpha} \end{pmatrix} \left[\frac{2}{\pi \xi_{mn}^2 - \bar{\alpha}^2} - \frac{2}{\pi \xi_{mn}} \right]$$

$$kC_{m/2\alpha}(\sigma_{mn}) + N_0(\xi_{mn})$$

$$2. \begin{pmatrix} M_x \\ M_y \end{pmatrix} = \mp m_L a \omega^2 y_0 e^{i\omega t} \sum_{m=0}^{\infty} \sum_{n=0}^{\infty} \left\{ \left\{ \frac{(1+k^2)}{4(h/a)} \right\} \left(\frac{1 + \sin \bar{\alpha} \cos \bar{\alpha} / 2}{\sin^2 \bar{\alpha} / \alpha} \right) \mp \frac{c_{m,n}^b}{\bar{\alpha} \alpha (1-k^2) (\eta_{mn}^2 - 1) \xi_{mn}} \right\} \begin{pmatrix} 1 - (-1)^m \cos \bar{\alpha} \\ (-1)^{m+1} \sin \bar{\alpha} \end{pmatrix}$$

$$\left\{ \left[\tanh \kappa_{mn} + \frac{2}{\kappa_{mn}} \left(\frac{1}{\cosh \kappa_{mn}} - 1 \right) \right] \left[\frac{\bar{\alpha}^2}{\pi \xi_{mn}^2 - \bar{\alpha}^2} - \frac{2}{\pi \xi_{mn}} - kC_{m/2\alpha}(\eta_{mn}) + N_0(\xi_{mn}) \right] \right. \\ \left. + \frac{2}{(\pi^2 m^2 - \bar{\alpha}^2) \xi_{mn}^2} \frac{N_2(\xi_{mn})}{\kappa_{mn} \cosh \kappa_{mn}} \right\} \mp \frac{2m_L g \alpha (1-k^3)}{3\bar{\alpha} (1-k^2)} \begin{pmatrix} 1 - \cos \bar{\alpha} \\ \sin \bar{\alpha} \end{pmatrix}$$

Table 4-46. Boundary Conditions, Velocity Potential, and Natural Frequency

Annular-Sector Tank	Excitation: Harmonic Pitching
---------------------	-------------------------------

Pitching about the x-axis, $X = X_0 e^{i\omega t}$.

1. Boundary conditions:

$$(a) \left(\frac{\partial \phi}{\partial r} \right)_{r=a,b} = -i\omega z X_0 e^{i\omega t} \sin \phi$$

$$(b) \left(\frac{\partial \phi}{\partial z} \right)_{z=h/2} = i\omega r X_0 e^{i\omega t} \sin \phi$$

$$(c) \left(\frac{\partial^2 \phi}{\partial t^2} + g \frac{\partial \phi}{\partial z} \right)_{z=h/2} = 0$$

$$(d) \left(\frac{1}{r} \frac{\partial \phi}{\partial \phi} \right)_{\phi=0} = -i\omega z X_0 e^{i\omega t}$$

$$(e) \left(\frac{1}{r} \frac{\partial \phi}{\partial \phi} \right)_{\phi=\bar{\alpha}} = -i\omega X_0 e^{i\omega t} \cos \bar{\alpha}$$

2. Velocity potential:

$$\phi = -i\omega X_0 e^{i\omega t} \left[rz \sin \phi - \sum_{m=0}^{\infty} \sum_{n=0}^{\infty} C_{m/2\alpha}(\rho_{mn}) \cos \bar{\phi}_m (C_{mn} \cosh \zeta_{mn} + D_{mn} \sinh \zeta_{mn}) \right]$$

3. Natural angular frequency:

$$\omega_{mn}^2 = \frac{g}{a} \xi_{mn} \tanh \kappa_{mn}$$

where ξ_{mn} are roots of $\Delta_{m/2\alpha}(\xi_{mn}) = J_{m/2\alpha}'(\xi_{mn}) Y_{m/2\alpha}'(k\xi_{mn}) - J_{m/2\alpha}'(k\xi_{mn}) Y_{m/2\alpha}'(\xi_{mn}) = 0$.

Table 4-46. Boundary Conditions, Velocity Potential, and Natural Frequency (continued)

Annular-Sector Tank	Excitation: Harmonic Pitching
---------------------	-------------------------------

Pitching about the y-axis, $\theta = \theta_0 e^{i\omega t}$.

1. Boundary conditions:

$$(a) \left(\frac{\partial \phi}{\partial r} \right)_{r=a,b} = -i\omega z \theta_0 e^{i\omega t} \cos \phi \quad (b) \left(\frac{\partial \phi}{\partial z} \right)_{z=-h/2} = i\omega r \theta_0 e^{i\omega t} \cos \phi$$

$$(c) \left(\frac{\partial^2 \phi}{\partial t^2} + g \frac{\partial \phi}{\partial z} \right)_{z=+h/2} = 0 \quad (d) \left(\frac{1}{r} \frac{\partial \phi}{\partial \phi} \right)_{\phi=0} = 0$$

$$(e) \left(\frac{1}{r} \frac{\partial \phi}{\partial \phi} \right)_{\phi=\bar{\alpha}} = i\omega z \theta_0 e^{i\omega t} \sin \bar{\alpha}$$

2. Velocity potential:

$$\phi = -i\omega \theta_0 e^{i\omega t} \left[rz \cos \phi - \sum_{m=0}^{\infty} \sum_{n=0}^{\infty} C_{m/2\alpha}(\rho_{mn}) \cos \bar{\phi}_m (A_{mn} \cosh \zeta_{mn} + B_{mn} \sinh \zeta_{mn}) \right]$$

3. Natural angular frequency:

$$\omega_{mn}^2 = \frac{g}{a} \xi_{mn} \tanh \kappa_{mn}$$

where ξ_{mn} are roots of $\Delta_{m/2\alpha}(\xi_{mn}) = J'_{m/2\alpha}(\xi_{mn}) Y'_{m/2\alpha}(k\xi_{mn}) - J'_{m/2\alpha}(k\xi_{mn}) Y'_{m/2\alpha}(\xi_{mn}) = 0$.

Table 4-47. Liquid Force and Moment Resultants

Annular-Sector Tank	Excitation: Harmonic Pitching
---------------------	-------------------------------

Pitching about the y-axis, $\theta = \theta_0 e^{i\omega t}$ and pitching about the x-axis, $\chi = \chi_0 e^{i\omega t}$.

$$1. F_y = -m_L g \begin{pmatrix} 0 \\ \chi_0 \end{pmatrix} e^{i\omega t} - 4m_L \omega^2 \begin{pmatrix} \theta_0 \\ \chi_0 \end{pmatrix} e^{i\omega t} + \sum_{m=0}^{\infty} \sum_{n=0}^{\infty} \left(\frac{A_{mn}}{C_{mn}} \right) \frac{[1 - (-1)^m \cos \bar{\alpha}] \sinh(\kappa_{mn}/2)}{\bar{\alpha} a (1 - k^2) \kappa_{mn}} \left[N_0(\xi_{mn}) + \right.$$

$$\left. \frac{\bar{\alpha}^2}{(\pi^2 m^2 - \bar{\alpha}^2)} \left(\frac{2}{\pi \xi_{mn}} - k C_{m/2\alpha_{mn}}(\sigma) \right) \right]$$

$$2. M_x = m_L g a \begin{pmatrix} \theta_0 \\ \chi_0 \end{pmatrix} e^{i\omega t} \left[\frac{1+k^2}{4(h/a)} \right] \left(\frac{\sin^2 \bar{\alpha}/\bar{\alpha}}{1 - \sin \bar{\alpha} \cos \bar{\alpha}/\bar{\alpha}} \right) - m_L a \omega^2 \begin{pmatrix} \theta_0 \\ \chi_0 \end{pmatrix} e^{i\omega t} \sum_{m=0}^{\infty} \sum_{n=0}^{\infty} \left[\left(\frac{1+k^2}{(1+k^2)(1 - \sin \bar{\alpha} \cos \bar{\alpha}/\bar{\alpha})} \right) \frac{\sin^2 \bar{\alpha}/8\bar{\alpha}}{8(h/a)^2/12} \right]$$

$$- \frac{2[1 - (-1)^m \cos \bar{\alpha}]}{\bar{\alpha} a^2 (1 + k^2) \xi_{mn}} \left\{ \left(\frac{B_{mn}}{D_{mn}} \right) \left[\cosh \frac{\kappa_{mn}}{2} - \frac{2}{\kappa_{mn}} \sinh \frac{\kappa_{mn}}{2} \right] \left[\frac{\alpha^2}{\pi^2 m^2 - \alpha^2} \right. \right.$$

$$\left. \left. \left(\frac{2}{\pi \xi_{mn}} - k C_{m/2\alpha_{mn}}(\sigma) \right) + N_0(\xi_{mn}) \right] + \frac{\bar{\alpha}^2 \xi^2 N_0(\xi_{mn})}{(\pi^2 m^2 - \bar{\alpha}^2) \kappa_{mn}} \left[\left(\frac{A_{mn}}{C_{mn}} \right) \cosh \frac{\kappa_{mn}}{2} - \left(\frac{B_{mn}}{D_{mn}} \right) \sinh \frac{\kappa_{mn}}{2} \right] \right\}$$

$$- \frac{2m_L g a (1 - k^3)(1 - \cos \bar{\alpha})}{3\bar{\alpha}(1 - k^2)}$$

Table 4-47. Liquid Force and Moment Resultants (continued)

Annular-Sector Tank	Excitation: Harmonic Pitching
---------------------	-------------------------------

$$\begin{aligned}
 3. \quad M_y = & -m_L g a \begin{pmatrix} 0 \\ x_o \end{pmatrix} e^{i\omega t} \left[\frac{1+k^2}{4(h/a)} \right] \left(\frac{1+\sin\bar{\alpha}\cos\bar{\alpha}/\bar{\alpha}}{\sin^2\bar{\alpha}/\bar{\alpha}} \right) + m_L a^2 \omega^2 \begin{pmatrix} 0 \\ x_o \end{pmatrix} e^{i\omega t} \sum_{n=0}^{\infty} \sum_{m=0}^{\infty} \cdot \\
 & \left[\left[\left((1+k^2) \left[1 + \frac{\sin\bar{\alpha}\cos\bar{\alpha}}{\bar{\alpha}} \right] / 8 - (h/a)^2 / 12 \right) + \frac{2(-1)^{m+1} \sin\bar{\alpha}}{\bar{\alpha} a^2 (1-k^2) \xi_{mn}} \left\{ \left(\frac{B_{mn}}{D_{mn}} \right) \left[\cosh \frac{\kappa_{mn}}{2} - \frac{2}{\kappa_{mn}} \sinh \frac{\kappa_{mn}}{2} \right] \right\} \right. \right. \\
 & \left. \left[\frac{\bar{\alpha}^2}{\pi^2 m^2 - \bar{\alpha}^2} \left(\frac{2}{\pi \xi_{mn}} - k C_{m/2\alpha}(\sigma_{mn}) \right) + N_o(\xi_{mn}) \right] + \frac{\bar{\alpha}^2 \xi_{mn}^2 N_2(\xi_{mn})}{(\pi^2 m^2 - \bar{\alpha}^2)^2} \kappa_{mn} \left[\left(\frac{A_{mn}}{C_{mn}} \right) \cosh \frac{\kappa_{mn}}{2} - \right. \right. \\
 & \left. \left. \left(\frac{B_{mn}}{D_{mn}} \right) \sinh \frac{\kappa_{mn}}{2} \right] \right] \left. \right] + \frac{2m_L g a (1-k^3) \sin\bar{\alpha}}{3\bar{\alpha}(1-k^2)}
 \end{aligned}$$

Table 4-48. Boundary Conditions, Velocity Potential, and Natural Frequency

Annular-Sector Tank	Excitation: Harmonic Roll
Roll about the z-axis, $\phi = \phi_0 e^{i\omega t}$.	
1. Boundary conditions:	
(a) $\left(\frac{\partial \phi}{\partial r}\right)_{r=a,b} = 0$	(b) $\left(\frac{\partial \phi}{\partial z}\right)_{z=h} = 0$
(c) $\left(\frac{1}{r} \frac{\partial \phi}{\partial \phi}\right)_{\phi=0, \bar{\alpha}} = i\omega r \phi_0 e^{i\omega t}$	(d) $\left(\frac{\partial^2 \phi}{\partial t^2} + g \frac{\partial \phi}{\partial z}\right)_{z=0} = 0$
2. Velocity potential:	
$\phi = i\omega a^2 \phi_0 e^{i\omega t} \left\{ \left(\frac{r}{a}\right)^2 \left(\phi - \frac{\bar{\alpha}}{2}\right) + \sum_{m=1}^{\infty} \frac{8\bar{\alpha} \cos \bar{\phi}_m}{\pi^2 (2m-1)^2 - 4\bar{\alpha}^2} \right\}$ $\left[\frac{(r/a)^{(2m-1)/2\alpha} (1-k)^{(2m-1)/2\alpha+2} - (a/r)^{(2m-1)/2\alpha} (k^2 - k^{(2m-1)/2\alpha})_k (2m-1)/2\alpha}{1 - k^{(2m-1)/2\alpha}} - \frac{2\bar{\alpha}}{\pi(2m-1)} \left(\frac{r}{a}\right)^2 \right]$ $+ \sum_{m=1}^{\infty} \frac{8\bar{\alpha}^2 C_{(2m-1)/2\alpha}^{(\rho)} \cos \bar{\phi}_m \cosh(\kappa_{2m-1,n} + \zeta_{2m-1,n})}{\pi^2 (2m-1)^2 - 4\bar{\alpha}^2} (\eta_{2m-1,n}^{-1}) \cosh \kappa_{2m-1,n}$ $\left[\frac{g_{2m-1,n} (1-k)^{(2m-1)/2\alpha+2} - q_{2m-1,n} (k^2 - k^{(2m-1)/2\alpha})_k (2m-1)/2\alpha}{1 - k^{(2m-1)/2\alpha}} - \frac{\pi(2m-1)}{2\bar{\alpha}} g_{2m-1,n} \right]$	
3. Natural angular frequency:	
$\omega_{2m-1,n}^2 = \frac{g}{a} \xi_{2m-1,n} \tanh \kappa_{2m-1,n}$ where $\xi_{2m-1,n}$ are roots of $C_{(2m-1)/2\alpha}^{(\xi)} (\xi_{2m-1,n} \frac{r}{a}) = J_{(2m-1)/2\alpha}^{(\rho)} (\rho_{2m-1,n})$. $Y_{(2m-1)/2\alpha}^{(\xi)} (\xi_{2m-1,n}) - J_{(2m-1)/2\alpha}^{(\xi)} (\xi_{2m-1,n}) Y_{(2m-1)/2\alpha}^{(\rho)} (\rho_{2m-1,n}) = 0$.	

Table 4-49. Liquid Force and Moment Resultants

Annular-Sector Tank	Excitation: Harmonic Roll
---------------------	---------------------------

Roll about the z-axis, $\phi = \phi_0 e^{i\omega t}$.

$$\begin{aligned}
 1. \quad \begin{pmatrix} F_x \\ F_y \end{pmatrix} &= m_L a \omega^2 \phi_0 e^{i\omega t} \left\{ \frac{2(1-k^3)}{1-k^2} \left(\frac{\sin \bar{\alpha} / 3 + (\cos \bar{\alpha} - 1) / \bar{\alpha}}{\sin \bar{\alpha} / \bar{\alpha} - (1 + \cos \bar{\alpha}) / 3} \right) + \frac{16\bar{\alpha}}{\pi} \left(\frac{\sin \bar{\alpha}}{1 + \cos \bar{\alpha}} \right) \sum_{m=1}^{\infty} \frac{1}{(2m-1)(1-k)^2 [\pi^2 (2m-1)^2 - 4\bar{\alpha}^2]} \right\} \\
 &\left\{ \frac{\bar{\alpha}^2}{\pi^2 (2m-1)^2 - \bar{\alpha}^2} \left[\frac{1 - 2k(2m-1)/2\alpha + 2 + k(2m-1)/2\alpha - 2k(2m-1)/2\alpha + 1 + k(2m-1)/\alpha + 3}{1 - k(2m-1)/\alpha} + \frac{2\bar{\alpha}(1-k^3)}{\pi(2m-1)} \right] \right. \\
 &+ \bar{\alpha}^2 \left[\frac{[(2m-1)/2\alpha - 1](1-k(2m-1)/2\alpha + 1)(1-k(2m-1)/2\alpha + 2)}{[\pi^2 (2m-1)^2 - \bar{\alpha}^2]} + \frac{[(2m-1)/2\alpha + 1](k(2m-1)/2\alpha - k)(k-k(2m-1)/2)}{[\pi^2 (2m-1)^2 - \bar{\alpha}^2]} \right] \\
 &- \frac{2\bar{\alpha}(1-k^3)}{3\pi(2m-1)} \left\{ + \frac{16\bar{\alpha}}{\pi} \left(\frac{\sin \bar{\alpha}}{1 + \cos \bar{\alpha}} \right) \sum_{m=1}^{\infty} \sum_{n=0}^{\infty} \cdot \right. \\
 &\left. \left[\left\{ \frac{[\bar{\alpha}^2 / (\pi^2 (2m-1)^2 - \bar{\alpha}^2)] [2/\pi \xi_{2m-1,n} - k C_{2m-1/2\alpha}(\sigma_{2m-1,n})] + N_0(\xi_{2m-1,n}) \right\} \tanh \kappa_{2m-1,n}}{(2m-1)(1-k)^2 (\eta_{2m-1,n}^2 - 1) [\pi^2 (2m-1)^2 - 4\bar{\alpha}^2]} \right\} \kappa_{2m-1,n} \right. \\
 &\left. \left[\frac{\ell_{2m-1,n} (1-k(2m-1)/2\alpha + 2) - q_{2m-1,n} (k-k(2m-1)/2\alpha)}{1-k(2m-1)/\alpha} \right] k_{(2m-1)/2\alpha} \right\} - g_{2m-1,n} \left(\frac{2m-1}{4\alpha} \right) \left. \right\}
 \end{aligned}$$

Table 4-49. Liquid Force and Moment Resultants (continued)

Annular-Sector Tank	Excitation: Harmonic Roll
---------------------	---------------------------

Roll about the z-axis, $\phi = \phi_0 e^{i\omega t}$ (continued).

$$\begin{aligned}
 2. \quad \begin{pmatrix} M_x \\ M_y \end{pmatrix} &= m_L a^2 \omega^2 \phi_0 e^{i\omega t} \left\{ \frac{1-k^5}{5(h/a)(1-k^2)} \begin{pmatrix} -[\sin \bar{\alpha} + 2(\cos \bar{\alpha} - 1)/\bar{\alpha}] \\ 2\sin \bar{\alpha} / \bar{\alpha} - (1 + \cos \bar{\alpha}) \end{pmatrix} + \frac{16\bar{\alpha}}{\pi(h/a)(1-k^2)} \begin{pmatrix} \sin \bar{\alpha} \\ 1 + \cos \bar{\alpha} \end{pmatrix} \sum_{n=1}^{\infty} \cdot \right. \\
 &\quad \frac{1}{(2m-1) [\pi^2 (2m-1)^2 - 4\alpha^2]} \left\{ \frac{\bar{\alpha}^2}{\pi^2 (2m-1)^2 - \alpha^2} \cdot \right. \\
 &\quad \left. \left[\frac{(2m-1)/2\alpha-3}{(2m-1)/2\alpha+2} (1-k)^{2m-1} / 2\alpha + 3 \right] + \left[\frac{(2m-1)/2\alpha+3}{(2m-1)/2\alpha} \right] (k)^{2m-1} / 2\alpha - k^3 (k^2 - k)^{2m-1} / 2\alpha \right\} \\
 &\quad - \frac{2\bar{\alpha}(1-k^5)}{5\pi(2m-1)} \left\{ + \frac{4\bar{\alpha}}{\pi} \begin{pmatrix} \sin \bar{\alpha} \\ 1 + \cos \bar{\alpha} \end{pmatrix} \sum_{n=1}^{\infty} \sum_{m=0}^{\infty} \frac{1}{(2m-1) [\pi^2 (2m-1)^2 - 4\bar{\alpha}^2]} (1-k)^{2m-1, n} - 1 \right\} \xi_{2m-1, n} \\
 &\quad \xi_{2m-1, n} (1-k)^{2m-1} / 2\alpha + 2 - q_{2m-1, n} (k-k)^{2m-1} / 2\alpha + k^{2m-1} / 4\alpha (1-k)^{2m-1} / \alpha \\
 &\quad \left. \left\{ \left[\tanh \kappa_{2m-1, n} + \frac{2}{\kappa_{2m-1, n}} \left(\frac{1}{\cosh \kappa_{2m-1, n}} - 1 \right) \right] \left[\frac{\bar{\alpha}^2}{\pi^2 (2m-1)^2 - \alpha^2} - k^2 \right] \right. \right. \\
 &\quad \left. \left. + N_0 (\xi_{2m-1, n}) \right] + \frac{2\bar{\alpha}^2 \xi_{2m-1, n} N_2 (\xi_{2m-1, n})}{\left[\pi^2 (2m-1)^2 - \alpha^2 \right] \kappa_{2m-1, n} \cosh \kappa_{2m-1, n}} \right\} + \frac{2m_L g a (1-k^3)}{3\bar{\alpha} (1-k^2)} \begin{pmatrix} \sin \bar{\alpha} \\ 1 - \cos \bar{\alpha} \end{pmatrix}
 \end{aligned}$$

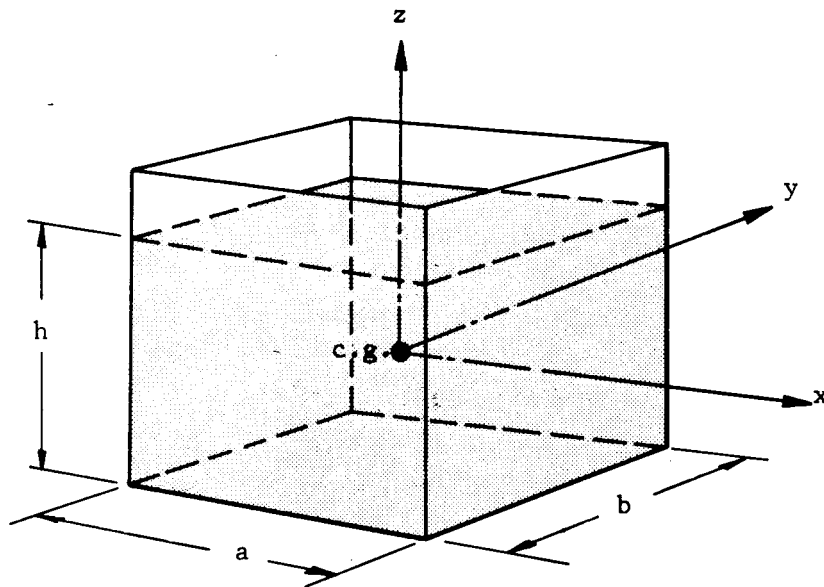
Table 4-49. Liquid Force and Moment Resultants (continued)

Annular-Sector Tank	Excitation: Harmonic Roll
$3. \quad M_z = m_L a^2 \omega^2 \phi_0 e^{i\omega t} \left\{ \frac{1+k^2}{2} + \frac{32\bar{\alpha}}{\pi} \sum_{m=1}^{\infty} \frac{1}{(2m-1)(1-k)^2 [\pi^2 (2m-1)^2 - 4\bar{\alpha}^2]} \right. \\ - \frac{[(2m-1)/2\alpha-2](1-k)^{2(2m-1)/2\alpha+2} - [(2m-1)/2\alpha+2](k-k)^2 (2m-1)/2\alpha^2}{[(2m-1)/2\alpha-2][(2m-1)/2\alpha+2](1-k)^{(2m-1)/\alpha}} \\ + \frac{32\bar{\alpha}}{\pi} \sum_{m=1}^{\infty} \sum_{n=0}^{\infty} \frac{N_1(\xi_{2m-1,n}) \tanh \kappa_{2m-1,n}}{(2m-1)[\pi^2 (2m-1)^2 - 4\bar{\alpha}^2] (\eta_{2m-1,n} - 1) \kappa_{2m-1,n}} \\ \left. \left[\frac{g_{2m-1,n} (1-k)^{(2m-1)/2\alpha+2}}{1-k} - \frac{q_{2m-1,n} (k^2 - k)^{2(2m-1)/2\alpha}}{1-k} \right] \right\} - g_{2m-1,n} \left(\frac{2m-1}{4\alpha} \right)$	

4.8 Rectangular Tank

Table of Contents

General.....	4-127
Excitation: Harmonic Translation and/or Pitching	
Boundary Conditions, Velocity Potential, and Natural Frequency.....	4-128
Liquid Force and Moment Resultants.....	4-130
Spring-Mass Model	
Analysis.....	4-131
Diagram.....	4-132
Force and Moment Resultants.....	4-133
Elements.....	4-134
Graphs.....	4-135
Excitation: Harmonic Roll	
Boundary Conditions, Velocity Potential, and Natural Frequency.....	4-139
Liquid Moment Resultant.....	4-140
Torsional Spring-Mass Model	
Analysis.....	4-141
Diagram.....	4-142
Moment Resultant.....	4-143
Elements.....	4-144
Graphs.....	4-145



Container: The tank is rectangular having base dimensions a and b in the x and y directions, respectively, and is filled with a liquid to a depth h .

Coordinate System: The origin is located at the center of gravity of the undisturbed fluid.

References: (76)

Table 4-50. Boundary Conditions, Velocity Potential, and Natural Frequency

Rectangular Tank	Excitation: Harmonic Translation
Translation in the x-direction, $x = x_0 \sin \omega t$.	

1. Boundary conditions:

$$(a) \left(\frac{\partial \phi}{\partial x} \right)_{x=a/2} = -\omega x_0 \cos \omega t$$

$$(b) \left(\frac{\partial \phi}{\partial z} \right)_{z=-h/2} = 0$$

$$(c) \left(\frac{\partial^2 \phi}{\partial t^2} + g \frac{\partial \phi}{\partial z} \right)_{z=h/2} = 0$$

2. Velocity potential:

$$\phi = -\omega x_0 \cos \omega t \left[x + \sum_{n=0}^{\infty} \frac{4a(-1)^n \sin[(2n+1)(\pi/a)x] \cosh[(2n+1)(\pi/a)(z+h/2)]}{\pi^2(2n+1)^2(\eta_n^2 - 1) \cosh[(2n+1)(\pi h)/a]} \right]$$

3. Natural angular frequency:

$$\omega_n^2 = g(2n+1)(\pi/a) \tanh \left[(2n+1) \frac{\pi h}{a} \right]$$

Table 4-50. Boundary Conditions, Velocity Potential, and Natural Frequency (continued)

Rectangular Tank	Excitation: Harmonic Pitching
------------------	-------------------------------

Pitching about the y-axis, $\theta = \theta_0 \sin \omega t$.

1. Boundary conditions:

$$(a) \left(\frac{\partial \phi}{\partial x} \right)_{x=-a/2} = -\omega z \theta_0 \cos \omega t$$

$$(b) \left(\frac{\partial \phi}{\partial z} \right)_{z=-h/2} = \omega x \theta_0 \cos \omega t$$

$$(c) \left(\frac{\partial^2 \phi}{\partial t^2} + g \frac{\partial \phi}{\partial z} \right)_{z=h/2} = 0$$

2. Velocity potential:

$$\begin{aligned} \phi = & -\omega \theta_0 \cos \omega t \left\{ \sum_{n=0}^{\infty} \frac{4(-1)^n}{\pi^3 (2n+1)^3} \left[\frac{h^2 \sin[(2n+1)(\pi/h)z] \sinh[(2n+1)(\pi/h)x]}{\cosh[(2n+1)(\pi a)/2h]} \right] \right. \\ & \left. + \frac{a^2 \sin[(2n+1)(\pi/a)x] \cosh[(2n+1)(\pi/a)(z-h/2)]}{\sinh[(2n+1)(\pi/a)h]} \right\} + \sum_{n=0}^{\infty} \frac{4a(-1)^n \sin[(2n+1)(\pi/a)x] \cosh[(2n+1)(\pi/a)(z+h/2)]}{\pi^2 (2n+1)^2 (\eta_n^2 - 1) \cosh[(2n+1)(\pi h)/a]} \\ & \left. \left[\frac{h}{2} - \frac{2a \tanh[(2n+1)(\pi h)/2a] + \frac{g}{\omega_n^2}}{\pi(2n+1)} \right] \right\} \end{aligned}$$

3. Natural angular frequency:

$$\omega_n^2 = g (2n+1)(\pi/a) \tanh \left[(2n+1) \frac{\pi h}{a} \right]$$

Table 4-51. Liquid Force and Moment Resultants

Rectangular Tank	Excitation: Harmonic Translation and/or Pitching
------------------	--

Translation in the x-direction, $x = x_0 \sin \omega t$.

1. $F_x = m_L \omega^2 x_0 \sin \omega t \left[1 + \sum_{n=0}^{\infty} \frac{8 \tanh[(2n+1)\pi r_1]}{3^3 r_1^3 (\eta_n^2 - 1)} \right]$
2. $M_y = m_L h \omega^2 x_0 \sin \omega t \left[\frac{1}{12 r_1^2} + \sum_{n=0}^{\infty} \frac{8 \tanh[(2n+1)\pi r_1]}{3^3 \pi^3 r_1^3 (\eta_n^2 - 1)} \left(\frac{1}{2} - \frac{\tanh[(2n+1)\pi r_1/2]}{(2n+1)\pi r_1/2} + \frac{g}{h \omega_n^2} \right) \right]$

Pitching about the y-axis, $\theta = \theta_0 \sin \omega t$.

1. $F_x = m_L h \omega^2 \theta_0 \sin \omega t \left[\frac{1}{12 r_1^2} + \sum_{n=0}^{\infty} \frac{8 \tanh[(2n+1)\pi r_1]}{3^3 \pi^3 r_1^3 (\eta_n^2 - 1)} \left(\frac{1}{2} - \frac{\tanh[(2n+1)\pi r_1/2]}{(2n+1)\pi r_1/2} + \frac{g}{h \omega_n^2} \right) \right]$
2. $M_y = m_L h^2 \omega^2 \theta_0 \sin \omega t \left[\frac{1}{m_L h^2} + 2 \sum_{n=0}^{\infty} \frac{8 g \tanh[(2n+1)\pi r_1]}{3^3 \pi^3 r_1^3 h \omega_n^2} \left(\frac{1}{2} - \frac{\tanh[(2n+1)\pi r_1/2]}{(2n+1)\pi r_1/2} + \frac{g}{2 h \omega_n^2} \right) + \sum_{n=0}^{\infty} \frac{8 \tanh[(2n+1)\pi r_1]}{3^3 \pi^3 r_1^3 (\eta_n^2 - 1)} \left(\frac{1}{2} - \frac{\tanh[(2n+1)\pi r_1/2]}{(2n+1)\pi r_1/2} + \frac{g}{h \omega_n^2} \right)^2 \right] + \frac{\theta_0 \sin \omega t}{12 r_1^2}$

Table 4-52. Model Analysis

Rectangular Tank	Spring-Mass Model
Excitation: Harmonic Translation and/or Pitching	

Figure 4-43 shows a diagram of the spring-mass model used in representing the dynamic response of a liquid in a rectangular tank when subjected to harmonic translation in the x-direction and/or pitching about the y-axis.

Coordinate System:

The origin is located at the center of gravity of the undisturbed liquid.

Model Description:

The components of the system are as follows:

1. A fixed mass M having a moment of inertia I is rigidly connected to the tank and is located on the z -axis at a distance H below the coordinate origin.
2. A set of movable masses m_n is distributed along the z -axis when the container is at rest at distances h_n above the origin. These modal masses are constrained by springs k_n having spring stiffness coefficients k_n to remain in the xy -plane and to move only in a direction parallel to the x -axis.

Equations of Motion:

The equations, obtained from either an equilibrium or energy formulation, are as follows:

1. Slosh Mass Equation for Translation:

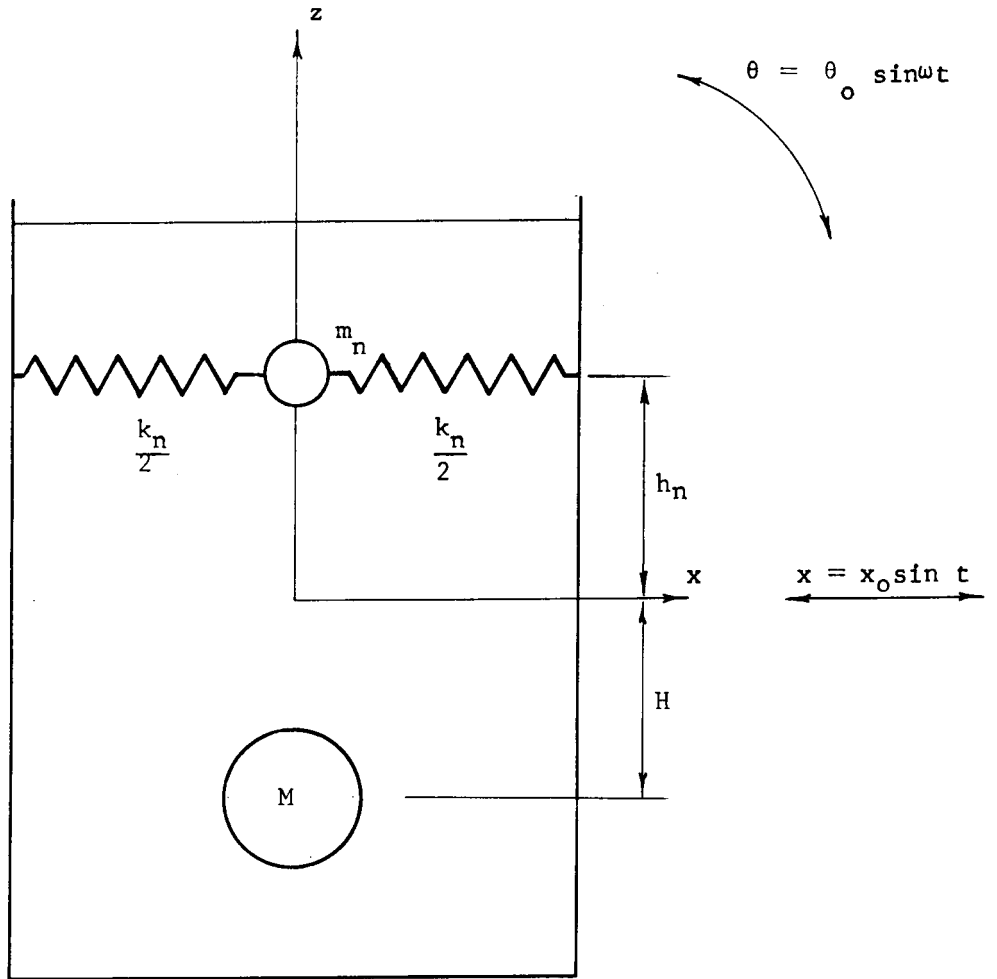
$$m_n \ddot{x} + k_n x = m_n x_o \omega^2 \sin \omega t$$

2. Slosh Mass Equation for Pitching:

$$m_n \ddot{x} + k_n x = (m_n g + h_n k_n) \theta_o \sin \omega t$$

From these equations, the model force in the x -direction and the moment about the y -axis can be found (see Table 4-53).

*



Rectangular Tank	Spring-Mass Model
Excitation: Harmonic Translation and/or Pitching	

Figure 4-43. Equivalent Mechanical Model

Table 4-53. Model Force and Moment Resultants

Rectangular Tank	Spring-Mass Model
Excitation: Harmonic Translation and/or Pitching	

1. Translation in the x-direction, $x = x_o \sin \omega t$.

$$(a) F_x = m_L \omega^2 x_o \sin \omega t \left[\frac{M}{m_L} + \sum_{n=0}^{\infty} \frac{m_n}{m_L} \left(\frac{\eta_n^2}{2\eta_n^2 - 1} \right) \right]$$

$$(b) M_y = m_L h \omega^2 x_o \sin \omega t \left[\frac{MH}{m_L h} + \sum_{n=0}^{\infty} \frac{m_n}{m_L} \left(\frac{h}{h} + \frac{g}{h \omega_n^2} \right) \left(\frac{\eta_n^2}{2\eta_n^2 - 1} \right) \right]$$

2. Pitching about the y-axis, $\theta = \theta_o \sin \omega t$.

$$(a) F_x = m_L h \omega^2 \theta_o \sin \omega t \left[\frac{MH}{m_L h} + \sum_{n=0}^{\infty} \frac{m_n}{m_L} \left(\frac{h}{h} + \frac{g}{h \omega_n^2} \right) \left(\frac{\eta_n^2}{2\eta_n^2 - 1} \right) \right]$$

$$(b) M_y = m_L h^2 \omega^2 \theta_o \sin \omega t \left[\frac{I}{m_L h^2} + \frac{M}{m_L} \left(\frac{H}{h} \right)^2 + \sum_{n=0}^{\infty} \frac{m_n}{m_L} \left(\frac{h}{h} + \frac{g}{h \omega_n^2} \right) \left(\frac{\eta_n^2}{2\eta_n^2 - 1} \right) \right] \\ + \theta_o \sin \omega t \left[\frac{MH}{m_L h} + \sum_{n=0}^{\infty} \frac{m_n}{m_L} \left(\frac{h}{h} + \frac{g}{h \omega_n^2} \right) \right]$$

Table 4-54. Model Elements

Rectangular Tank	Spring-Mass Model
Excitation: Harmonic Translation and/or Pitching	
Natural Frequency	$\omega_n^2 = \frac{g}{a} (2n+1)\pi \tanh[(2n+1)\pi r_1]$
Spring Constant	$k_n = m_n \omega_n^2$ (fig. 4-44)
Ratio or Spring Constant to Fluid Weight	$\frac{hk_n}{m_L g} = \frac{8 \tanh^2[(2n+1)\pi r_1]}{[(2n+1)\pi]^2}$
Ratio of Slosh Mass to Fluid Mass	$\frac{m_n}{m_L} = \frac{8 \tanh[(2n+1)\pi r_1]}{[(2n+1)\pi]^3 r_1}$ (fig. 4-46)
Ratio of Fixed Mass to Fluid Mass	$\frac{M}{m_L} = 1 - \sum_{n=0}^{\infty} \frac{m_n}{m_L}$ (fig. 4-46)
Ratio of Slosh Mass Coordinate to Fluid Depth	$\left \frac{h_n}{h} \right = \frac{1}{2} - \frac{\tanh[(2n+1)\pi r_1/2]}{(2n+1)\pi r_1/2}$ (fig. 4-45)
Ratio of Fixed Mass Coordinate to Fluid Depth	$\left \frac{H}{h} \right = - \frac{m_L}{M} \sum_{n=0}^{\infty} \left(\frac{m_n}{m_L} \right) \left(\frac{h_n}{h} \right)$ (fig. 4-45)
Moment of Inertia of Solidified Fluid	$\frac{I_s}{m_L h^2} = \frac{1}{12} \left[\left(\frac{a}{h} \right)^2 + 1 \right]$
Effective Moment of Inertia of Fluid	$\frac{\bar{I}}{m_L h^2} = \frac{I_s}{m_L h^2} \left[1 - \frac{4}{r_1^2 + 1} + \frac{768}{(r_1^2 + 1)\pi^5 r_1} \sum_{n=0}^{\infty} \frac{\tanh[(2n+1)\pi r_1/2]}{(2n+1)^5} \right]$ (fig. 4-47)
Moment of Inertia of Fixed Mass	$\frac{I}{m_L h^2} = \frac{\bar{I}}{m_L h^2} - \frac{M}{m_L} \left(\frac{H}{h} \right)^2 - \sum_{n=0}^{\infty} \frac{m_n}{m_L} \left(\frac{h_n}{h} \right)^2$ (fig. 4-47)

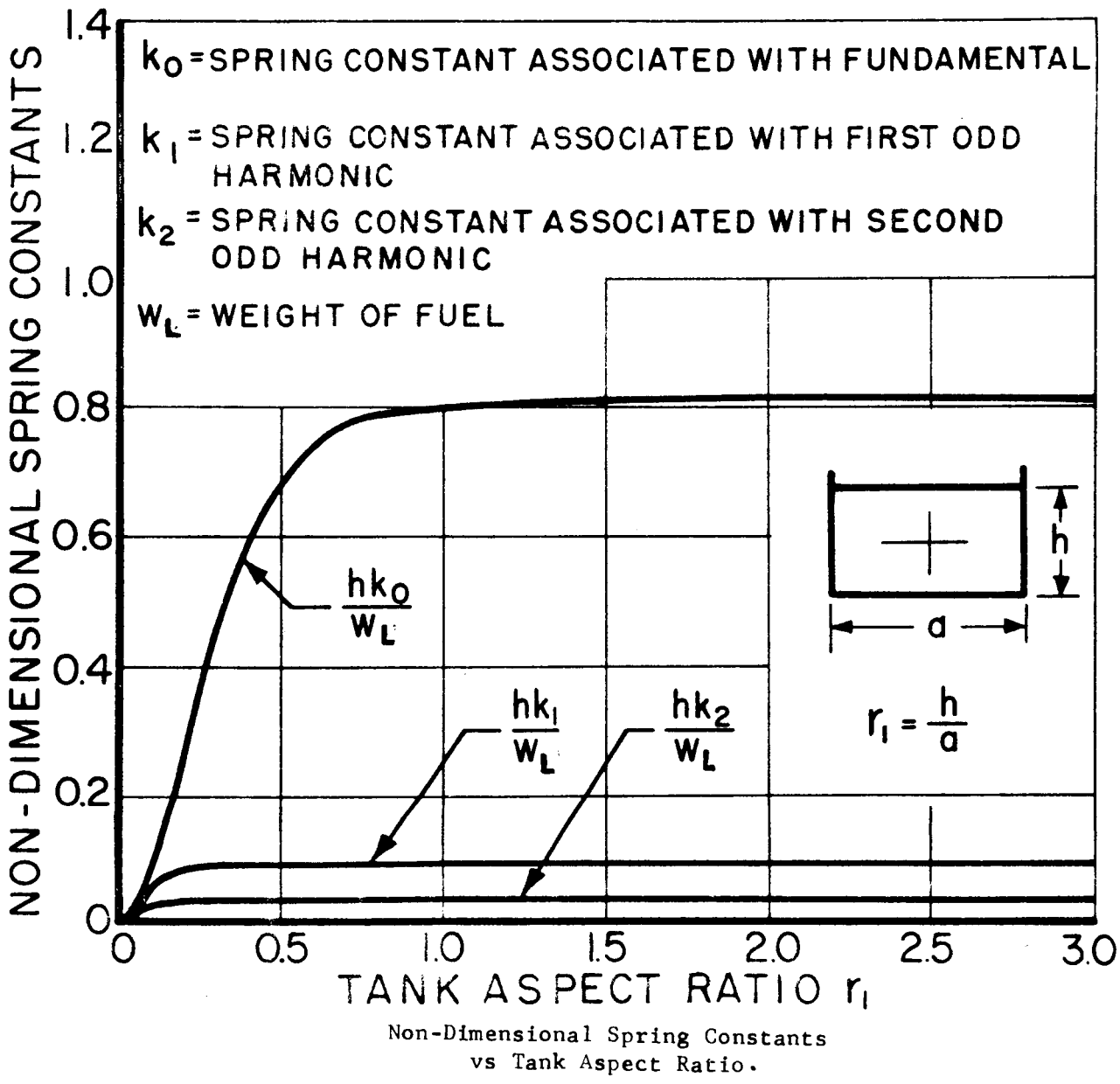
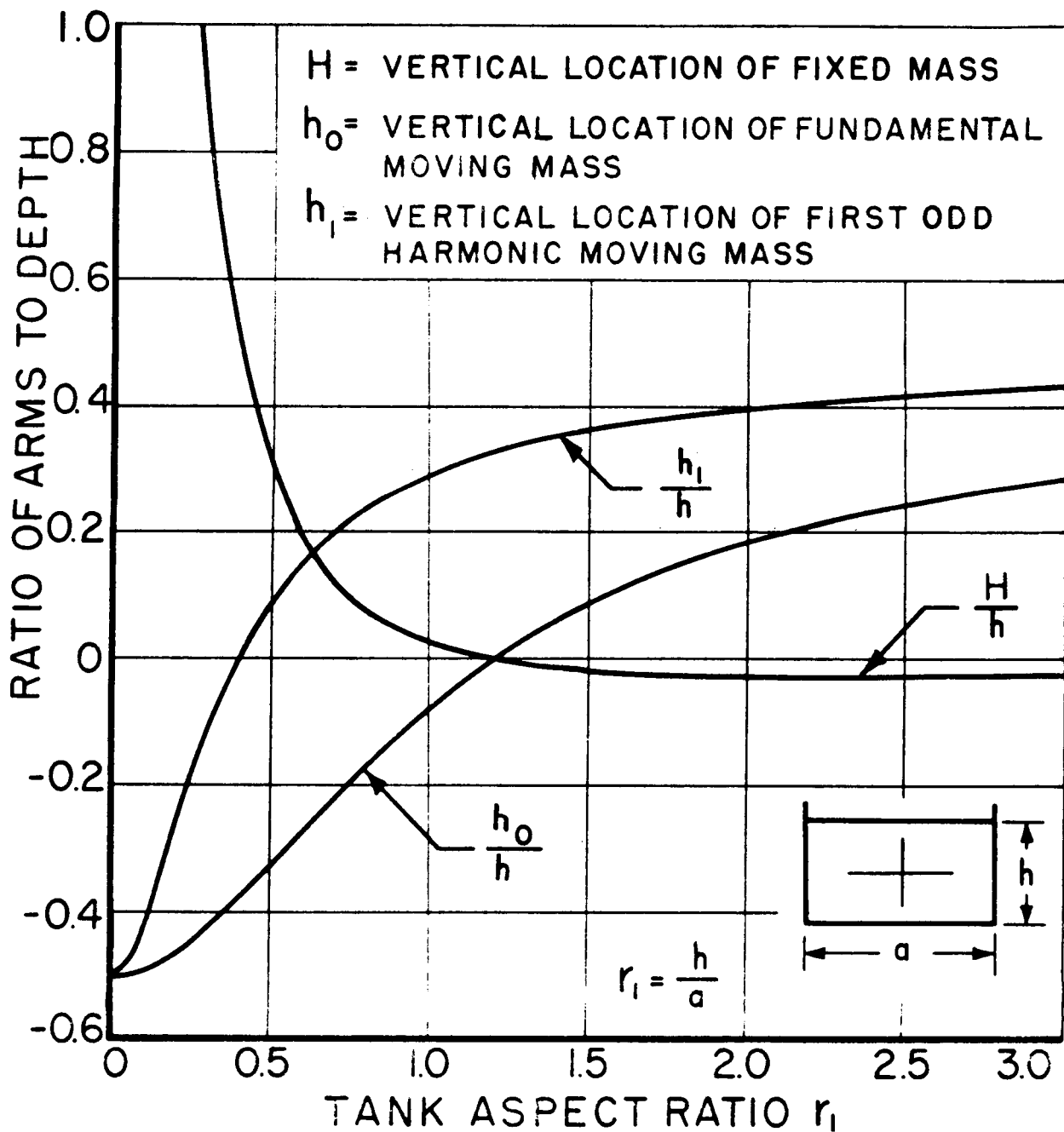
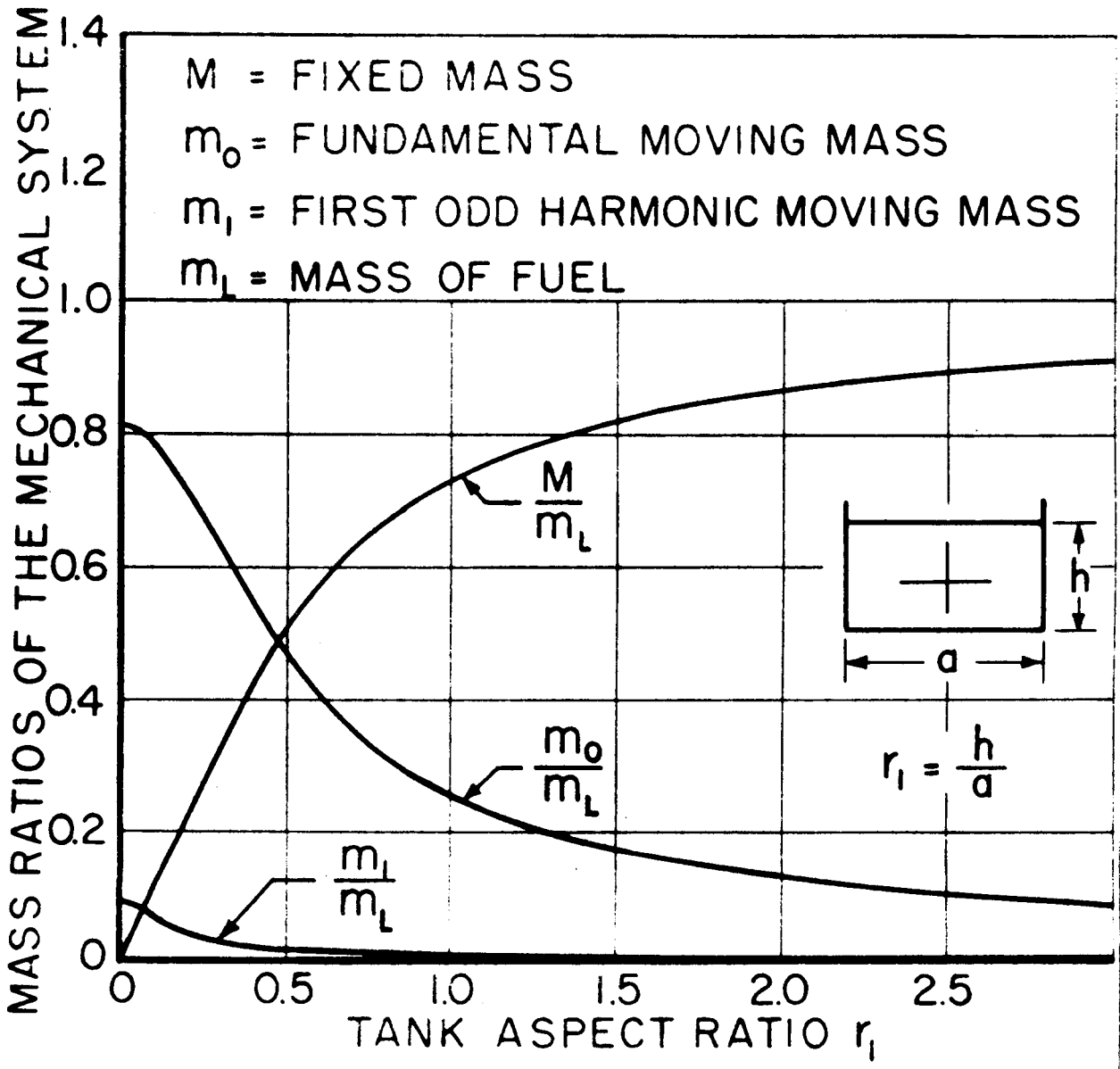


Figure 4-44. Model Element Graph



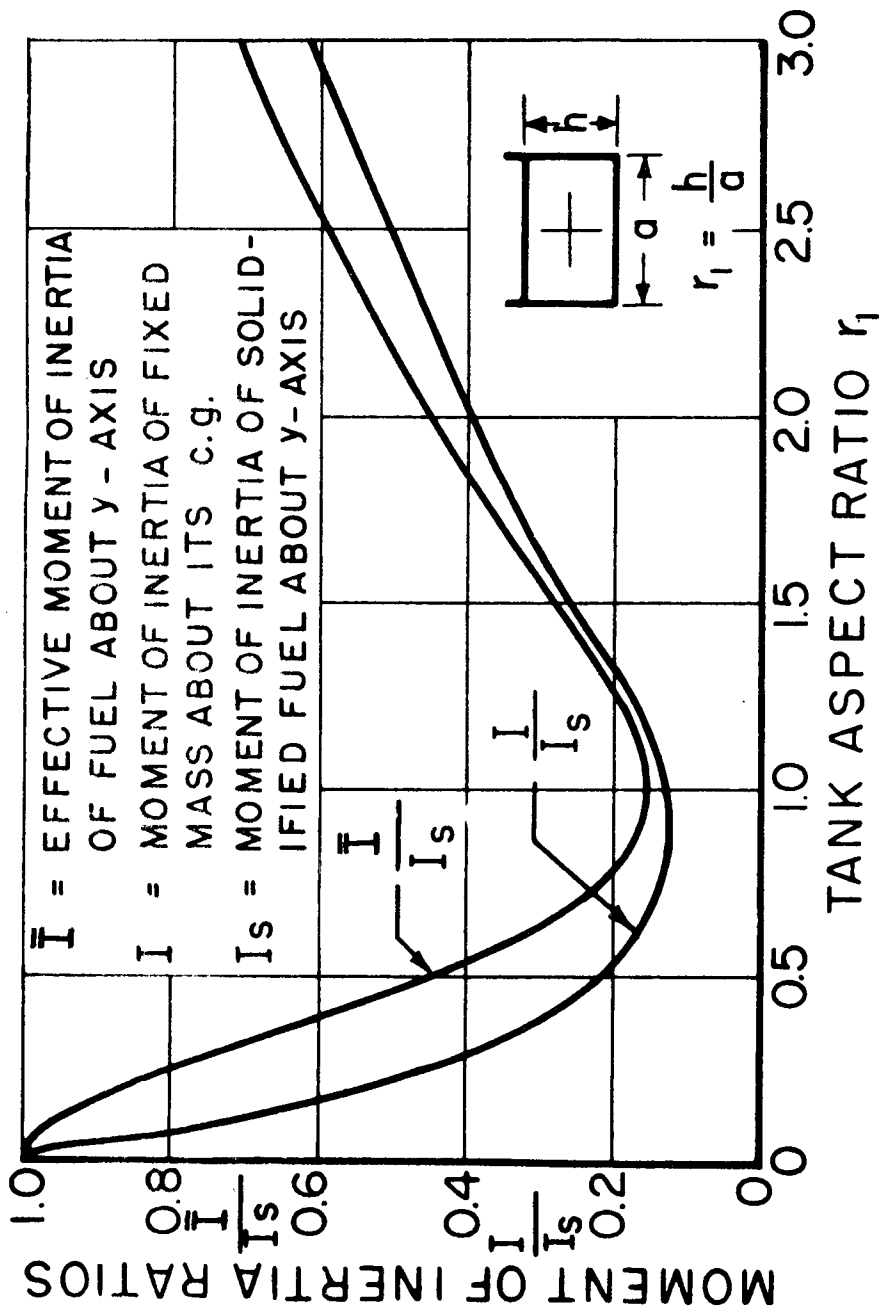
Ratios of the Vertical Locations or Arms
 of the Fixed Mass and First Two Slosh
 Masses to Fluid Depth vs Tank Aspect Ratio.

Figure 4-45. Model Element Graph



Ratio of Fixed Mass and First Two Slosh Masses to Fluid Mass vs Tank Aspect Ratio.

Figure 4-46. Model Element Graph



Ratios of Moments of Inertia of Fluid and Fixed Mass to the Moment of Inertia of the Solidified Fuel vs Tank Aspect Ratio.

Figure 4-47. Model Element Graph

Table 4-55. Boundary Conditions, Velocity Potential, and Natural Frequency

Rectangular Tank	Excitation: Harmonic Roll
Roll about the z-axis, $\phi = \phi_0 \sin \omega t$.	
1. Boundary conditions:	
(a) $\left(\frac{\partial \phi}{\partial x} \right)_{x=\pm a/2} = \omega y \phi_0 \cos \omega t$	(b) $\left(\frac{\partial \phi}{\partial y} \right)_{y=\pm b/2} = -\omega x \phi_0 \cos \omega t$
(c) $\left(\frac{\partial \phi}{\partial z} \right)_{z=-h/2} = 0$	(d) $\left(\frac{\partial^2 \phi}{\partial t^2} + g \frac{\partial \phi}{\partial z} \right)_{z=\pm h/2} = 0$
2. Velocity potential:	
$\phi = \omega \phi_0 \cos \omega t \left\{ \sum_{n=0}^{\infty} \frac{4(-1)^n}{3 \pi^3 (2n+1)^3} \left[\frac{b^2 \sin[(2n+1)(\pi/b)y] \sinh[(2n+1)(\pi/b)x]}{\cosh[(2n+1)(\pi a)/2b]} \right] \right.$ $- \frac{a^2 \sin[(2n+1)(\pi/a)x] \sinh[(2n+1)(\pi/a)y]}{\cosh[(2n+1)\pi b/2a]} + \sum_{m=0}^{\infty} \sum_{n=0}^{\infty} \frac{16ab(-1)^{m+n} [b^2(2n+1)^2 - a^2(2m+1)^2]}{\pi^4 (2m+1)^2 (2n+1)^2 [b^2(2n+1)^2 + a^2(2m+1)^2]} (r_{mn}^2 - 1)$ $\left. \sin[(2m+1) \frac{\pi}{b} y] \sin \left[(2n+1) \frac{\pi}{a} x \right] \operatorname{sech} \left[\frac{\pi h}{ab} \sqrt{b^2(2n+1)^2 + a^2(2m+1)^2} \right] \right\}$ $\cosh \left[\frac{\pi}{ab} \left(z + \frac{h}{2} \right) \sqrt{b^2(2n+1)^2 + a^2(2m+1)^2} \right]$	
3. Natural angular frequency:	
$\omega_{mn} = g \frac{\pi}{ab} \sqrt{b^2(2n+1)^2 + a^2(2m+1)^2} \quad \tanh \left[\frac{\pi h}{ab} \sqrt{b^2(2n+1)^2 + a^2(2m+1)^2} \right]$	

Table 4-56. Liquid Moment Resultant

Rectangular Tank	Excitation: Harmonic Roll
------------------	---------------------------

Roll about the z-axis, $\phi = \phi_0 \sin \omega t$.

$$M_z = I_{s1} \omega^2 \theta_0 \sin \omega t \left[\frac{\bar{I}}{I_s} + \sum_{m=0}^{\infty} \sum_{n=0}^{\infty} \frac{768 [r_3^2 (2m+1)^2 - (2n+1)^2]^2 \tanh[\pi r_1 \sqrt{r_3^2 (2m+1)^2 + (2n+1)^2}]}{\pi r_1 (1+r_3^2)(2m+1)^4 (2n+1)^4 [r_3^2 (2m+1)^2 + (2n+1)^2]^{3/2} (\eta_{mn} - 1)} \right]$$

Table 4-57. Model Analysis

Rectangular Tank	Torsional Spring-Mass Model
Excitation: Harmonic Roll	

Figure 4-48 shows a diagram of the torsional spring-mass model used in representing the dynamic response of a liquid in a rectangular tank when subjected to harmonic roll about the z-axis.

Coordinate System:

The origin is located at the center of gravity of the undisturbed liquid.

Model Description:

The components of the system are as follows:

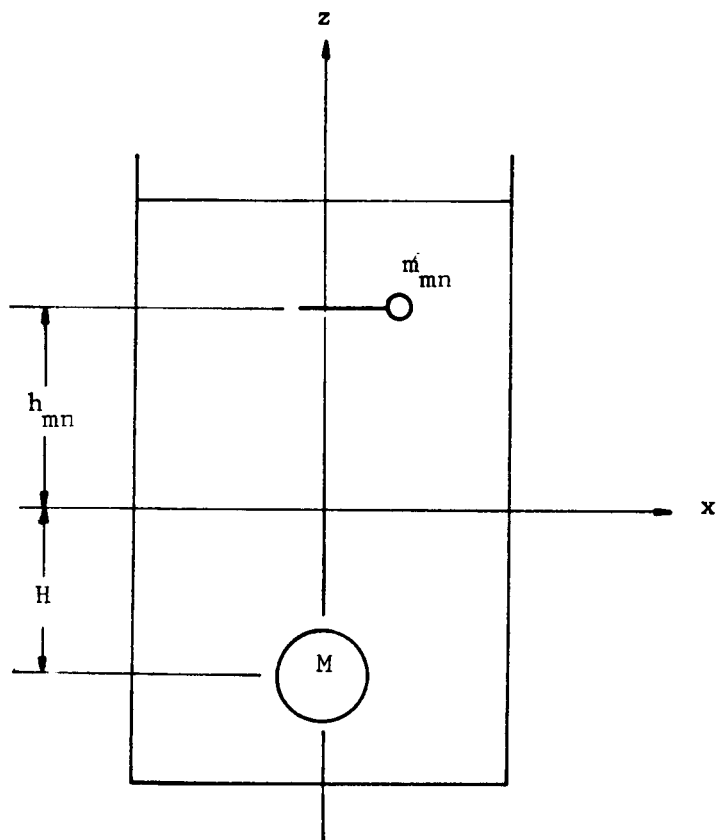
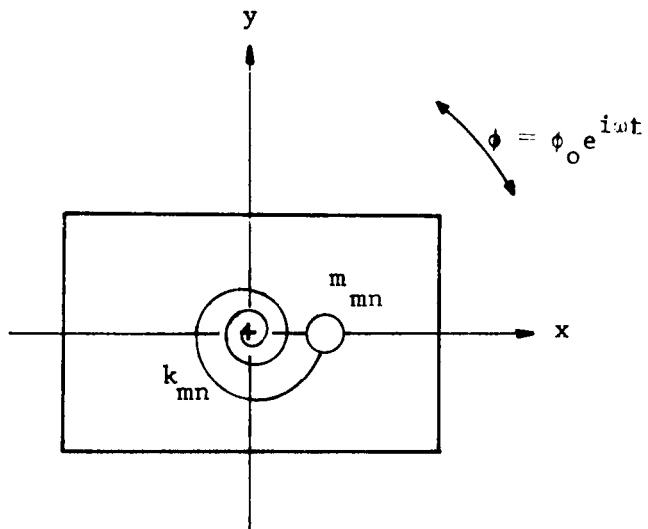
1. A fixed mass M having a moment of inertia I is rigidly connected to the tank and is located on the z-axis at a distance H below the coordinate origin.
2. A set of movable masses m_{mn} is constrained by torsional springs having stiffness coefficients k_{mn} to remain in planes parallel to the xy-plane and at distances h_{mn} above it.

Equation of Motion:

The equation, obtained from either an equilibrium or energy formulation, is as follows:

$$I_{mn} \ddot{\phi} + k_{mn} \phi = k_{mn} \phi_o \sin \omega t$$

From this equation, the moment about the z-axis can be found (see Table 4-58).



Rectangular Tank	Torsional Spring-Mass Model
Excitation: Harmonic Roll	

Figure 4-48. Equivalent Mechanical Model

Table 4-58. Model Moment Resultant

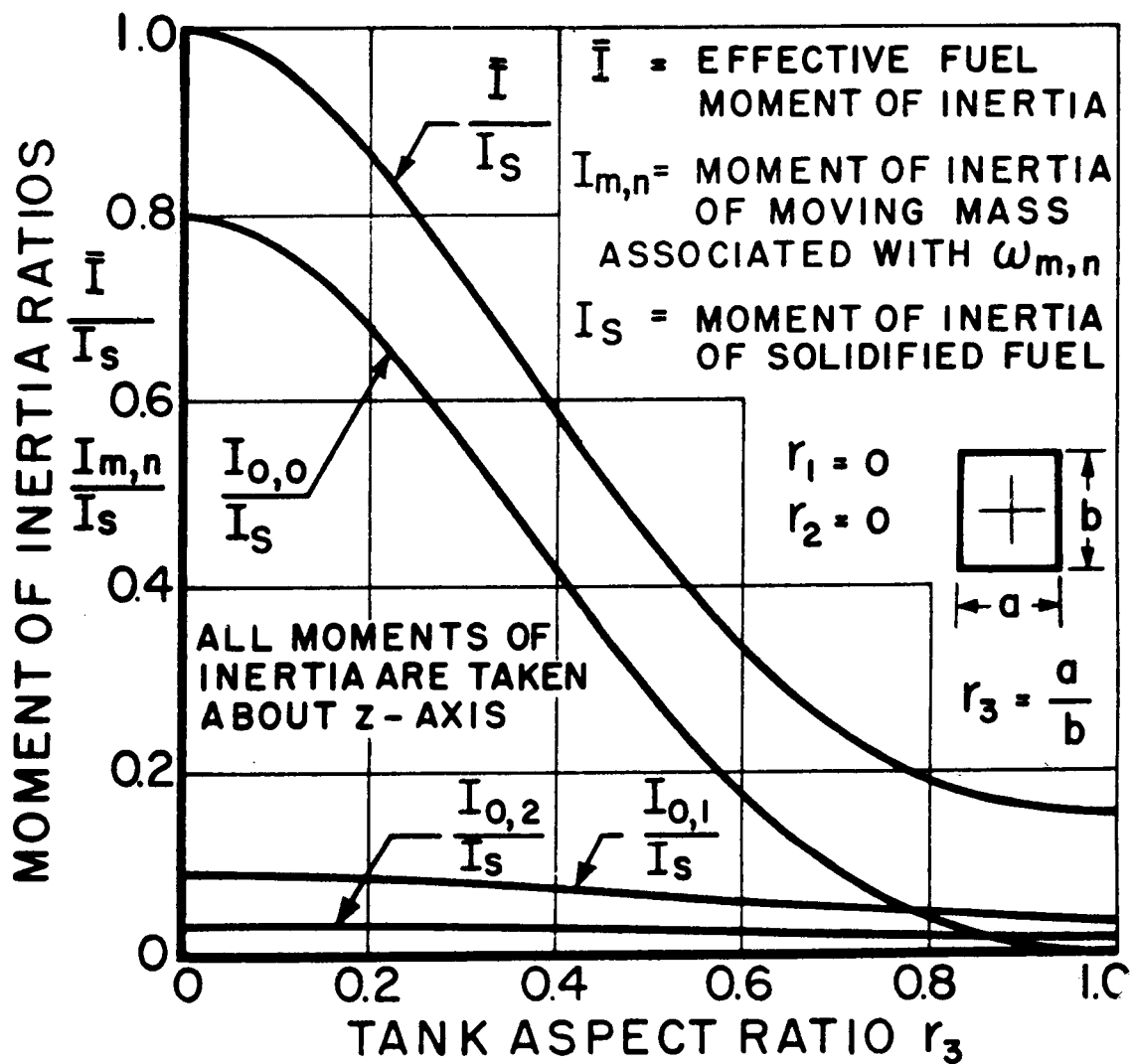
Rectangular Tank	Torsional Spring-Mass Model
Excitation: Harmonic Roll	

Roll about the z-axis, $\phi = \phi_0 \sin \omega t$.

$$M_z = I_s r_1^2 \omega^2 \phi_0 \sin \omega t \left[\frac{I}{I_s} + \sum_{m=0}^{\infty} \sum_{n=0}^{\infty} \frac{I_{mn}}{I_s} \left(\frac{\eta_{mn}^2}{\eta_{mn}^2 - 1} \right) \right]$$

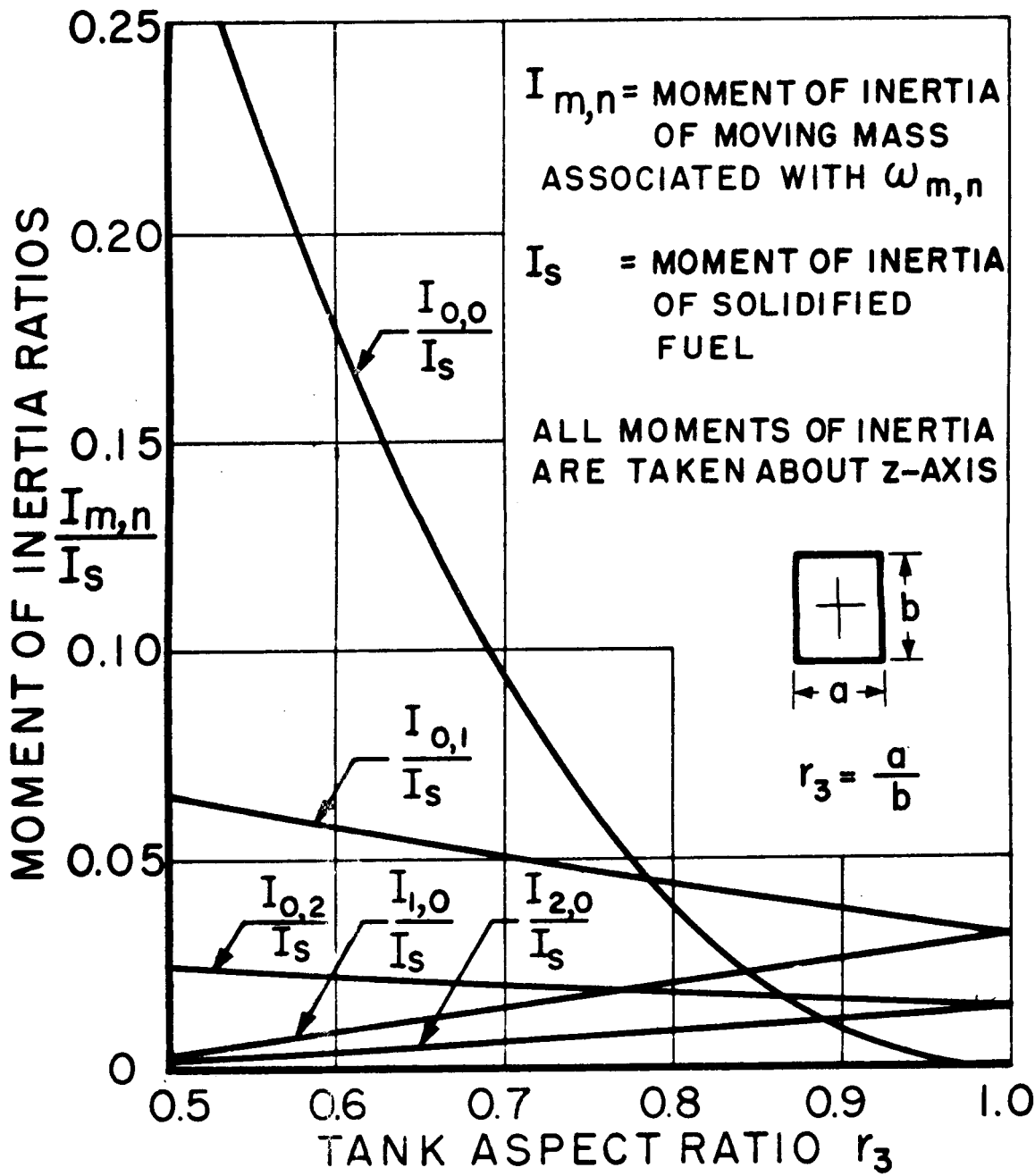
Table 4-59. Model Elements

Rectangular Tank	Torsional Spring-Mass Model
Excitation: Harmonic Roll	
Natural Frequency	$\omega_{mn}^2 = \frac{\pi g r_1}{h} \sqrt{r_3^2 (2m+1)^2 + (2n+1)^2}$ $\tanh \left[\pi r_1 \sqrt{r_3^2 (2m+1)^2 + (2n+1)^2} \right]$
Torsional Spring Constant	$k_{mn} = I_{mn} \omega_{mn}^2$
Moment of Inertia of Solidified Fluid	$I_s = \frac{m}{12} a^2 + b^2$
Effective Moment of Inertia of Fluid	$\frac{\bar{I}}{I_s} = 1 - \frac{4}{r_3^2 + 1} + \frac{768}{\pi^5 r_3 (r_3^2 + 1)} \sum_{n=0}^{\infty} \frac{\tanh \left[(2n+1) \pi r_3 / 2 \right]}{(2n+1)^5}$ <p style="text-align: right;">(fig. 4-49, 4-50)</p>
Moment of Inertia of Slosh Mass	$\frac{I_{mn}}{I_s} = \frac{768 \left[r_3^2 (2m+1)^2 - (2n+1)^2 \right]^2}{\pi^6 (1+r_3^2) (2m+1)^4 (2n+1)^4 \left[r_3^2 (2m+1)^2 + (2n+1)^2 \right]}$ $\frac{\tanh \left[\pi r_1 \sqrt{r_3^2 (2m+1)^2 + (2n+1)^2} \right]}{\pi r_1 \sqrt{r_3^2 (2m+1)^2 + (2n+1)^2}}$ <p style="text-align: right;">(fig. 4-49, 4-50)</p>
Moment of Inertia of Fixed Mass	$\frac{I}{I_s} = \frac{\bar{I}}{I_s} - \sum_{m=0}^{\infty} \sum_{n=0}^{\infty} \frac{I_{mn}}{I_s}$



Roll Moment of Inertia Ratios for Shallow Tank vs Tank Aspect Ratio.

Figure 4-49. Model Element Graph



Roll Moment of Inertia Ratios for Shallow Tank vs Tank Aspect Ratio.

Figure 4-50. Model Element Graph

V. Propellant Slosh Suppression

5.1 Anti-Slosh Devices

Table of Contents

5.1.1	Introduction.....	5-2
5.1.2	Design Requirements of an Anti-Slosh Device.....	5-3
5.1.3	Ring Baffles.....	5-5
5.1.3.1	Experimental.....	5-8
5.1.3.2	Analytical.....	5-31
5.1.3.3	Ring with Radial Clearance.....	5-88
5.1.3.4	Conic Section.....	5-89
5.1.3.5	Inverted Conic Section.....	5-94
5.1.4	Cruciform Baffles.....	5-97
5.1.5	Floats.....	5-98
5.1.5.1	Mat.....	5-98
5.1.5.2	Can.....	5-99
5.1.6	Partitions.....	5-105
5.1.6.1	Cross.....	5-105
5.1.6.2	Concentric.....	5-106
5.1.7	Pressure Distribution.....	5-107
5.1.7.1	Procedure I (28).....	5-107
5.1.7.2	Procedure II (18).....	5-108
5.1.7.3	Procedure III (83).....	5-112
5.1.8	Conclusions and Recommendations.....	5-125

5.1.1 Introduction. Sloshing becomes detrimental when the wave amplitudes of tanked propellants, agitated by oscillations, approach breaking height. This sloshing of the liquid exerts considerable forces on the missile structure, affects the controls and renders any liquid level measuring device inaccurate. This means that a sloshing damping device has to be provided. The term damping usually refers to the checking of a motion due to resistance, as by friction or any other similar cause. It is of especial significance in connection with the diminishing amplitude of an oscillation, as that of a liquid swinging inside a moving container. Unless energy is supplied during each cycle, the amplitude of the fluid motion falls off at each successive oscillation by an amount commonly expressed in terms of the decrement, or damping factor, which is the ratio of any one amplitude to that next succeeding it in the same sense and direction.

Many of the force and moment resultants given in Chapter IV require a damping factor before they can be evaluated. The accuracy of these equations and consequently their usefulness is therefore very much dependent on the value chosen for the damping parameter. When a large propellant tank has no damping devices the resistance to fluid motion at the container walls is generally accepted to be nil. That is, the fluid damping is negligible. However, when damping systems are introduced, the resulting damping factor depends on many variables and is thereby extremely difficult to obtain. For some damping devices, such as fixed ring baffles, a sound analytical approach can be effectively used while in most cases an experimental approach is the only way of obtaining a meaningful damping factor.

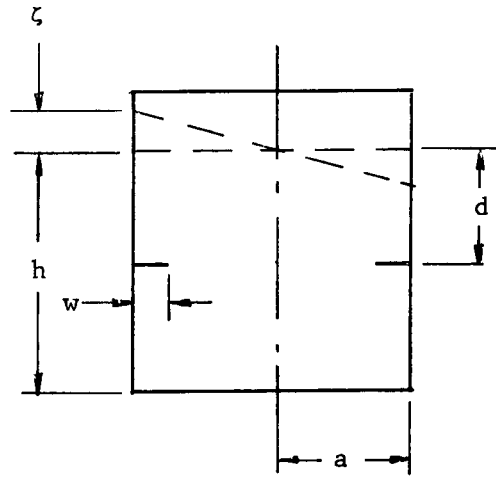
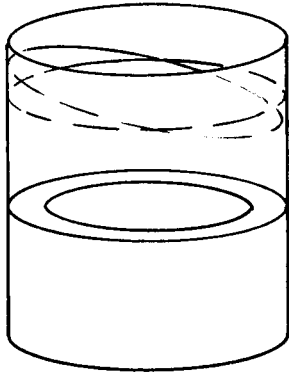
5.1.2 Design Requirements of an Anti-Slosh Device. Studies (40), (42) show that the depth below the undisturbed free surface at which the liquid no longer participates in surface oscillations is approximately equal to one-fourth the tank diameter. Therefore a damping device need only extend to such a depth. The liquid level, however, changes as the container empties thereby requiring either a damping device capable of moving down at a rate equal to the draining rate or a damping device which is fixed to the wall but extends to the bottom of the container. The first stipulation suggests some type of floating device, whereas the second suggests either longitudinal partitions or an evenly spaced baffle system covering the inner periphery of the tank and distributed throughout the depth of the liquid.

The amount of damping needed to stabilize a missile is determined from analog or digital computer studies of the over-all dynamic characteristics of the vehicle. In some cases, stability studies might indicate no need for anti-slosh baffles in a particular tank. Generally, however, the designer is faced with the problem of optimizing a damping system by integrating into his design the requirements that follow:

1. Produce a high damping effect.
2. Pay a minimum weight penalty.
3. Utilize minimum space.
4. Absorb the liquid forces and moments or transfer them uniformly to the tank structure, thereby avoiding points of high stress concentration.

5. Function throughout environmental changes, such as temperature.
6. Not interfere with other operations, such as the emptying of the container or the measurement of the liquid level.
7. Be easy to assemble.
8. Not cause damage to the tank or other built-in equipment during transportation of the missile.
9. Not interfere with cleaning operations.

Ring Baffles



where ζ = amplitude of liquid measured at the tank wall

h = depth of liquid

d = depth of ring below undisturbed free surface

a = radius of right circular cylinder

w = ring width

References: (32, 35, and 41).

Ring baffles are most effective against lateral slosh which has large vertical components of fluid velocity near the tank wall.

Investigations by Silveira, Stephens and Leonard (35) indicate that:

1. For a given baffle depth:
 - (a) The damping factor increases as the baffle width increases (fig. 5-10).
 - (b) The frequency increases as the baffle width decreases (fig. 5-15).

Ring Baffles (continued)

2. Based on the total surface of a baffle, the highest mean damping factor appears to be afforded by ring baffles as compared to the baffle types depicted in fig. (5-77).

Investigations by Garza and Abramson (32) indicate that:

1. For a given baffle depth:
 - (a) With the hole size constant:
 - (1) The frequency increases for increasing percent perforation (fig. 5-2).
 - (2) The damping factor increases for decreasing percent perforation (fig. 5-8).
 - (b) With the percent perforation constant:
 - (1) The frequency increases for increasing hole size (fig. 5-3).
 - (2) The damping factor increases for decreasing hole size (fig. 5-7).
2. Damping produced by perforated baffles is consistently lower than that produced by a solid baffle (fig. 5-7 and 5-8).

5.1:3, Ring Baffles. Because of the complexity of the boundary conditions, a theoretical approach for predicting the damping of a device is extremely limited. In particular, a fixed ring baffle is the only damping device for which an analytical approach exists. For this reason, it is necessary to resort to an experimental approach consisting of ground oscillation testing of a full scale or model tank containing the damping device to be evaluated. If the size of the model is small as compared to the prototype, the use of similitude theory is advisable in order to obtain reasonable similarity of fluid motion. Since it is generally not possible to model equal values of all dimensionless parameters affecting the fluid motion, an appropriate nondimensional modeling parameter must be chosen. Viscous forces and surface tension are small and can therefore be neglected whereas, forces resulting from both the velocity of the fluid and the inertial effects of acceleration cannot. Acceleration is of especial importance because of the three following effects on slosh phenomena:

1. During ground tests, the eigen frequencies remain constant, whereas, during flight conditions they vary as the square root of the longitudinal acceleration.
2. The wave amplitudes are approximately inversely proportional to the longitudinal acceleration.
3. The damping factor is proportional to the square root of the liquid amplitude.
4. The force and moment resultants are proportional to g .

Therefore, Froude's number, being the ratio of fluid velocity forces to inertia forces, is selected for the modeling parameter.

5.1.3.1 Ring Baffles: Experimental. Each of Articles 5.1.3.1.1 through 5.1.3.1.3 presents an analysis concerned with a particular reference from which experimental data in the form of graphs is presented. The analyses are composed of two parts; the first being concerned with experimental procedure and the second with interpretation of results. This information is meant to aid the designer in both evaluating data of a particular source and comparing data of different sources. Also, this information should be of use in similitude applications since most of the data is obtained from model studies.

5.1.3.1.1 Investigations by Garza and Abramson (32) are outlined below.

Fixed Ring Baffles

1. Baffle thickness: 0.018" to 0.030".
2. Ratio of baffle width to tank radius, $\frac{W}{R} = 0.157$.
3. Perforation:
 - (a) The hole size was 0.079" while the percent perforation was varied.
 - (b) The percent perforation was 30% while the hole size was varied.
4. Attachment to container: The baffles were secured to the tank by four 1/8" x 1/3" steel strips attached at 90° apart around the outer edge of the ring. They were supported through angle iron brackets bolted to the upper flange of the tank. The outer edge of the ring was turned down,

giving the ring an L type cross section which stiffened the ring considerably, but had little effect on damping (see Figure 5-1).

Container, Excitation and Instrumentation

The container was a rigid-wall circular cylindrical tank supported by four dynamometers. All tests were conducted for three amplitudes of translational excitation. Because of the rather significant effects of excitation amplitude, measurements were made for various values ranging from $0.00184 \leq \frac{x_0}{d} \leq 0.00823$, and then all data was presented in terms of RMS values. Table 5-1 gives the resonant frequencies for each of the various tests conducted.

Damping Factor

Experimental values of the damping factor γ_s were obtained from resonant peaks of experimental force response curves. Theoretical values of γ_s were calculated from Miles' equation (Article 5.1.3.2.1) using liquid surface amplitudes ζ_w , measured at the tank walls. Table 5-2 gives the damping values for each of the various tests conducted.

5.1.3.2 Investigations by Silveira, Stephens, and Leonard (35) are outlined below.

Baffles (Figure 5-76)

1. Baffle thickness

- (a) 12 inch tank: conic section, 1/16" Plexiglas; all others, 1/8" Plexiglas.

(b) 30 inch tank: fixed ring, 1/4" Plexiglas.

2. Ratio of baffle width to tank radius

(a) 12 inch tank: see Figure 5-77.

(b) 30 inch tank: $W/R = 0.076$.

3. Perforation

(a) Hole size, 1/8" diameter.

(b) Percent perforation, 50%.

Container Excitation and Instrumentation

Two containers were used: a 12" diameter tank of 1/8" Plexiglas and a 30" aluminum tank of 0.016" walls and 1/2" base. A paddle was used to excite the liquid in the fundamental mode and then removed when the amplitude was sufficient. Liquid response in the 12" tank was sensed by strain gages mounted on the torsion bars which are located between the base platform and the support ring, whereas the response in the 30" tank was measured by a load cell which replaced one of the three platform supports. The output signals from the strain gauges and the load cell were amplified and then fed into a dampometer to measure the damping and frequency of the liquid motion.

Damping Factor

The rate of decay of the moment resulting from the damped liquid oscillations was measured and the damping factor δ , representing the decay of oscillation, was defined as

$$\delta = \frac{1}{n} \log_e \frac{M_0}{M_n}$$

where n is the number of cycles over which the decay was measured, M_0 is the magnitude of the initial moment and M_n is the magnitude of the moment after n cycles.

General Comments

1. No graph is given for cruciform baffles since, for all but shallow depths, damping is independent of the fluid depth. Test results for the 90° and 45° positions (see Figure 5-77) are as follows: for $\frac{W}{R} = 0.169$, $\delta_{90} = 0.072$ and $\delta_{45} = 0.070$ and for $\frac{W}{R} = 0.337$, $\delta_{90} = 0.156$ and $\delta_{45} = 0.142$.
2. All data points presented represent the average of five or more measured values for the given condition.
3. For high values of baffle depth, the curves in Figures 5-9, 5-10, 5-11, 5-66, 5-67, and 5-69 approach the damping values for which no baffle is present.
4. In Figure 5-77, the mean damping factor for a particular baffle was obtained in the following manner: from the graph relating the damping factor to baffle depth, the area under the curve between $0.084 \frac{d}{R}$ above and $0.084 \frac{d}{R}$ below the maximum damping was divided by $0.168 \frac{d}{R}$.
5. The curves in Figures 5-12 and 5-14 are given by Miles' equation as presented in reference 33. It is

$$\delta = 5.66\pi e^{-4.6\frac{d}{R}} \left[\frac{R^2 - (R-W)^2}{R} \right]^{\frac{3}{2}} \left(\frac{\zeta_w}{R} \right)^{\frac{1}{2}}$$

If W^2 is neglected, then the damping factor becomes:

$$\delta = 5.66\pi e^{-4.6\frac{d}{R}} \alpha^{\frac{3}{2}} \left(\frac{\zeta_w}{R} \right)^{\frac{1}{2}}$$

which is identical to Miles' equation except that the constant multiplier is 5.66π instead of 2.83.

6. For high values of baffle depth, the curves in Figures 5-15, 5-16, 5-64, 5-65, and 5-68 approach, asymptotically, the first resonant frequency for a circular cylindrical tank containing no baffles.

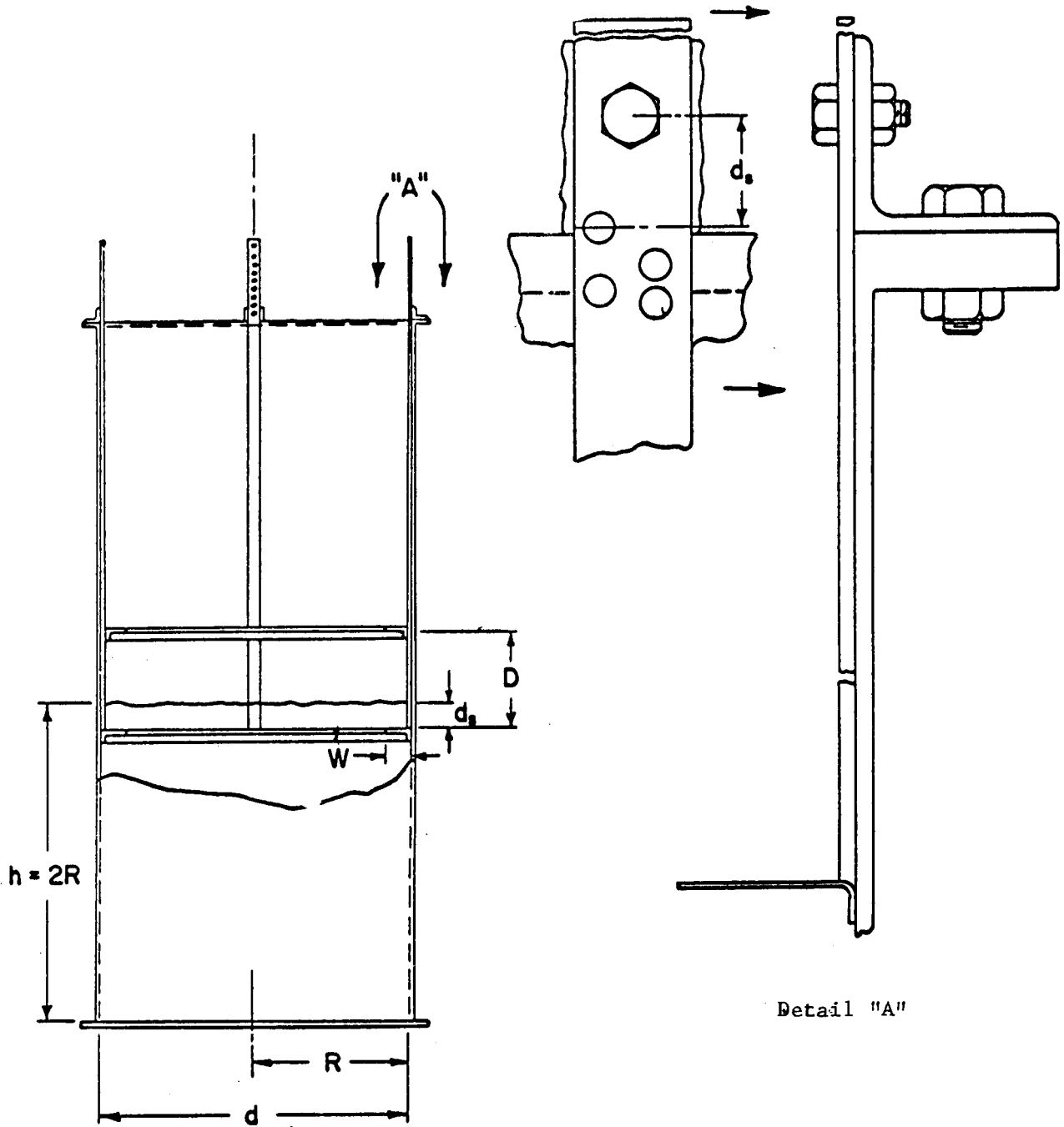


Figure 5.1 Details of baffle support arrangements and tank configuration. (32)

TABLE 5.1.

Liquid Resonant Frequency, (32)

W/R = 0.157

% Open Area	0	8%	16%	23%	30%	23%	30%	30%
Hole Diameter (in.)	0	0.079	0.079	0.079	0.079	0.040	0.040	0.02
Ring Depth d_s/R		$\omega^2 d/g$		$(X_0/d = 0.00184)$				
0	4.68	4.40	4.25	3.57	4.1	4.11	4.14	4.33
.025	4.19	3.19	3.47	3.30	3.88	3.20	3.43	3.26
.050	2.92	3.17	3.31	3.34	3.52	3.36	3.34	3.22
.075	3.01	2.90	3.27	3.32	3.47	3.26	3.34	3.32
.100	3.06	2.96	3.31	3.35	3.51	3.32	3.41	3.34
.125	2.97	3.19	3.40	3.36	3.49	3.31	3.43	3.35
.175	3.18	3.24	3.35	3.32	3.54	3.38	3.47	3.41
.250	3.40	3.36	3.40	3.45	3.56	3.52	3.54	3.42
.375	3.48	3.49	3.54	3.58	3.57	3.52	3.56	3.54
.450	3.47	3.54	3.62	3.58	3.58	3.59	3.62	3.54
		$\omega^2 d/g$		$(X_0/d = 0.00417)$				
0	4.43	3.84	3.76	3.73	3.65	3.81	4.16	3.87
.025	4.27	3.64	3.79	3.62	3.62	3.60	3.54	3.90
.050	3.71	3.29	3.40	3.54	3.50	3.44	3.66	3.55
.075	2.99	3.14	3.28	3.32	3.46	3.26	3.45	3.31
.100	2.94	3.15	3.28	3.35	3.45	3.28	3.38	3.30
.125	3.09	3.20	3.22	3.35	3.45	3.26	3.40	3.31
.175	3.09	3.24	3.26	3.38	3.51	3.26	3.45	3.34
.250	3.18	3.34	3.38	3.43	3.49	3.39	3.45	3.40
.375	3.33	3.46	3.40	3.43	3.42	3.52	3.45	3.44
		$\omega^2 d/g$		$(X_0/d = 0.00833)$				
0	3.96	3.84	3.73	3.54	3.52	3.58	3.28	3.49
.025	3.77	3.77	3.75	3.49	3.50	3.54	3.41	3.54
.050	3.58	3.58	3.51	3.49	3.47	3.47	3.40	3.49
.075	3.18	3.24	3.28	3.40	3.40	3.40	3.41	3.40
.100	2.97	3.22	3.28	3.31	3.38	3.24	3.34	3.36
.125	3.00	3.06	3.32	3.24	3.31	3.28	3.30	3.28
.175	3.07	3.13	3.28	3.31	3.31	3.28	3.30	3.32
.250	3.16	3.28	3.28	3.31	3.28	3.22	3.32	3.32
.375	3.30	3.32	3.31		3.24	3.30	3.36	3.32

TABLE 5.2

Ring Damping. (32)
 $W/R = 0.157$

% Open Area	0	8%	16%	23%	30%	23%	30%	30%
Hole Diameter (in.)	0	0.079	0.079	0.079	0.079	0.040	0.040	0.020
Ring Depth d_s/R		Damping Ratio,		$X_0/d = 0.00184$				
0	.060	.087	.084	.108	.087	.091	.110	.103
.025	.210	.132	.084	.106	.087	.114	.112	.116
.050	.137	.147	.071	.073	.055	.086	.086	.103
.075	.090	.1145	.070	.065	.050	.072	.082	.084
.100	.070	.0885	.069	.059	.045	.046	.050	.057
.125	.073	.067	.056	.049	.045	.059	.045	.053
.175	.060	.054	.056	.045	.040	.054	.033	.049
.250	.035	.040	.035	.047	.031	.032	.032	.042
.375	.027	.025	.026	.021	.022	.023	.022	.029
.450	.025	.022			.017	.023	.015	.023
		Damping Ratio,		$X_0/d = 0.00417$				
0	.101	.127	.101	.098	.082	.094	.102	.086
.025	.121	.126	.122	.108	.093	.110	.114	.109
.050	.173	.134	.119	.112	.089	.109	.106	.103
.075	.160	.112	.108	.084	.077	.104	.077	.089
.100	.110	.091	.090	.075	.064	.085	.068	.085
.125	.077	.102	.077	.064	.047	.077	.064	.078
.175	.072	.070	.072	.061	.050	.066	.054	.070
.250	.051	.061	.051	.049	.047	.051	.049	.055
.375	.039	.044	.038	.035	.040	.039	.032	.037
		Damping Ratio,		$X_0/d = 0.00833$				
0	.117	.122	.121	.111	.095	.110	.091	.114
.025	.146	.126	.124	.117	.087	.122	.106	.112
.050	.177	.134	.124	.109	.098	.126	.098	.118
.075	.158	.123	.114	.099	.084	.104	.086	.120
.100	.142	.115	.102	.093	.082	.093	.072	.093
.125	.116	.106	.093	.088	.078	.093	.082	.088
.175	.096	.096	.081	.078	.072	.079	.074	.072
.250	.082	.066	.067	.061	.057	.067	.058	.058
.375	.066	.048	.046		.026	.046	.038	.042

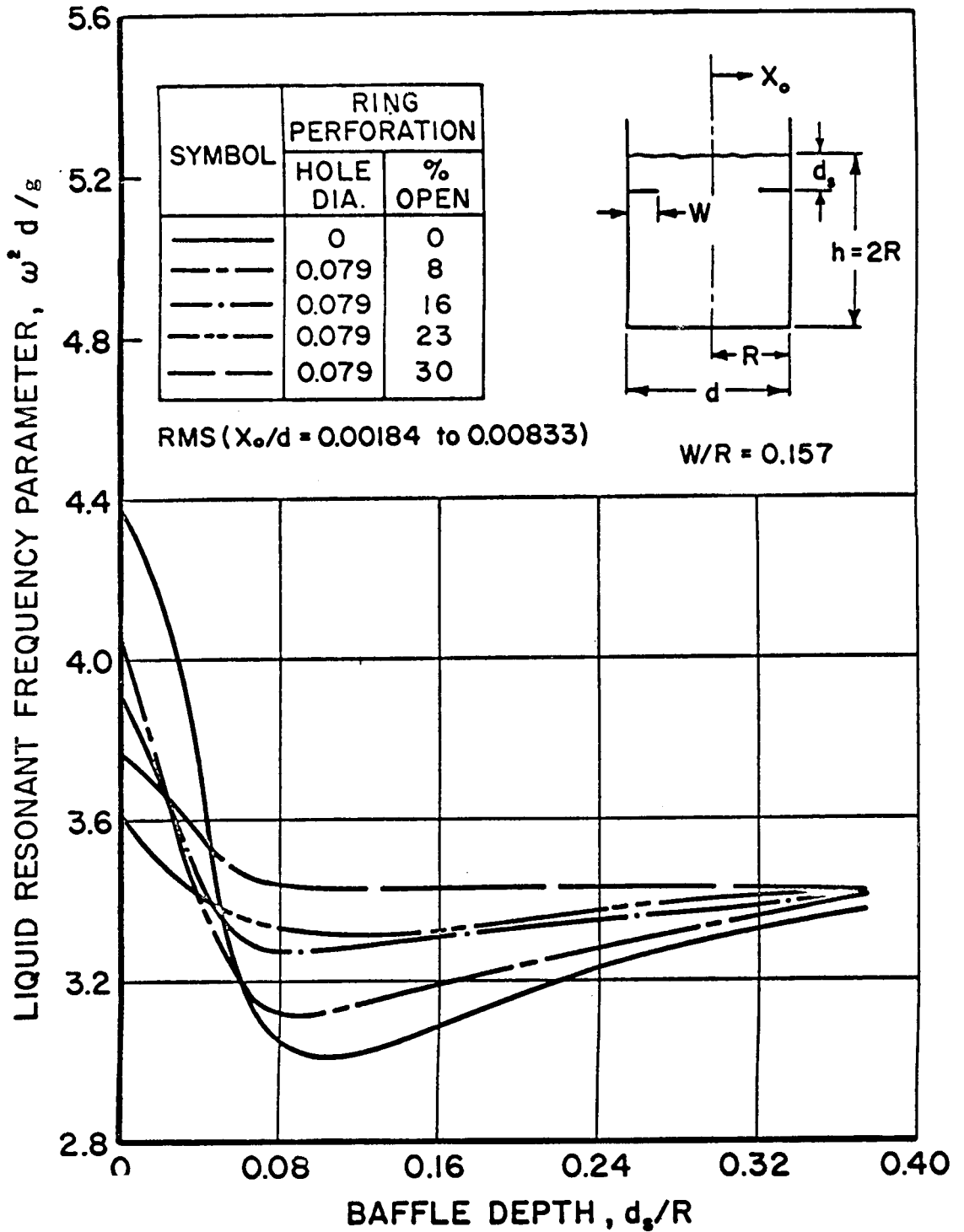


Figure 5.2 Effect of percent perforation on liquid resonant frequencies as a function of baffle depth. (32)

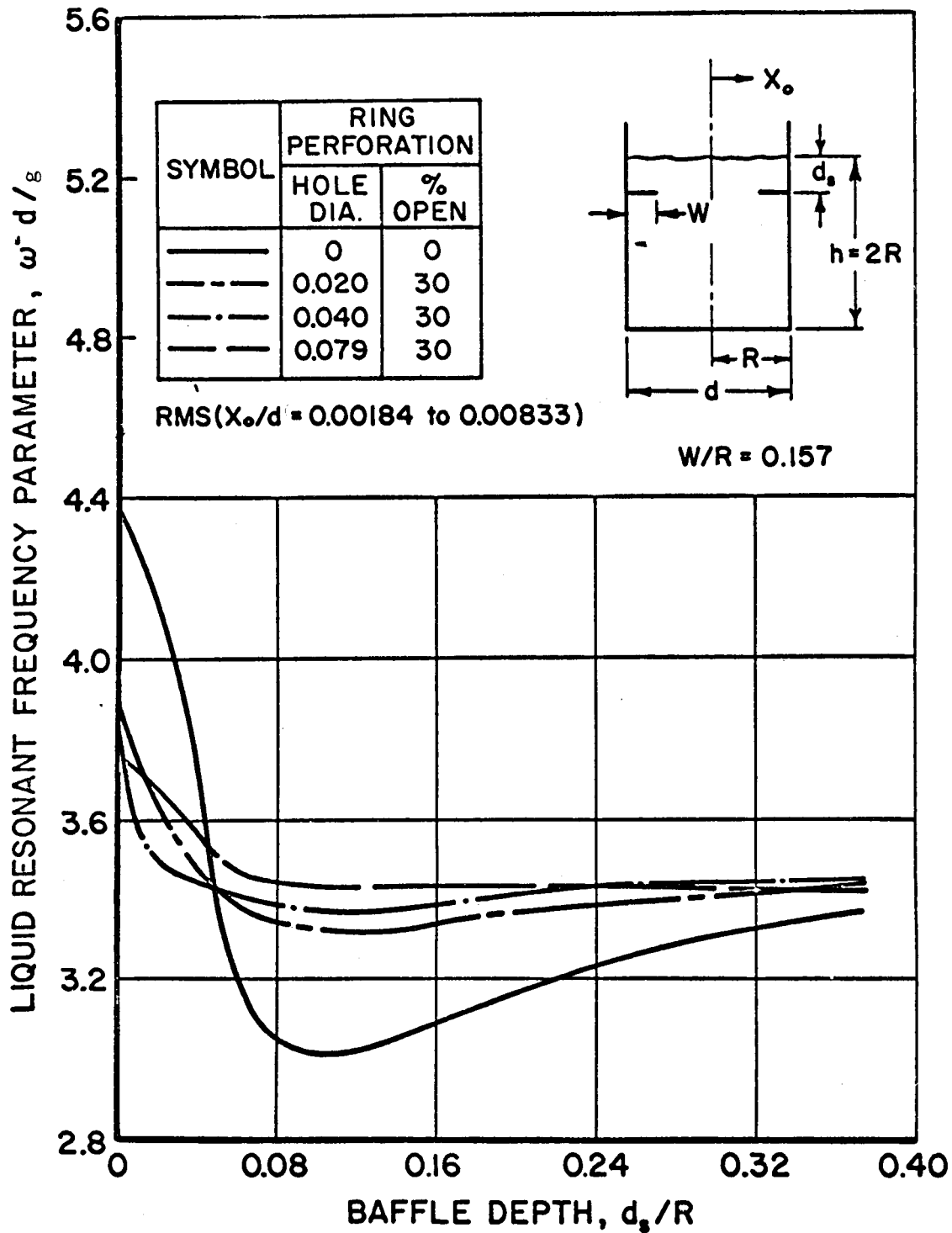


Figure 5.3 Effect of perforation hole size on liquid resonant frequencies as a function of baffle depth. (32)

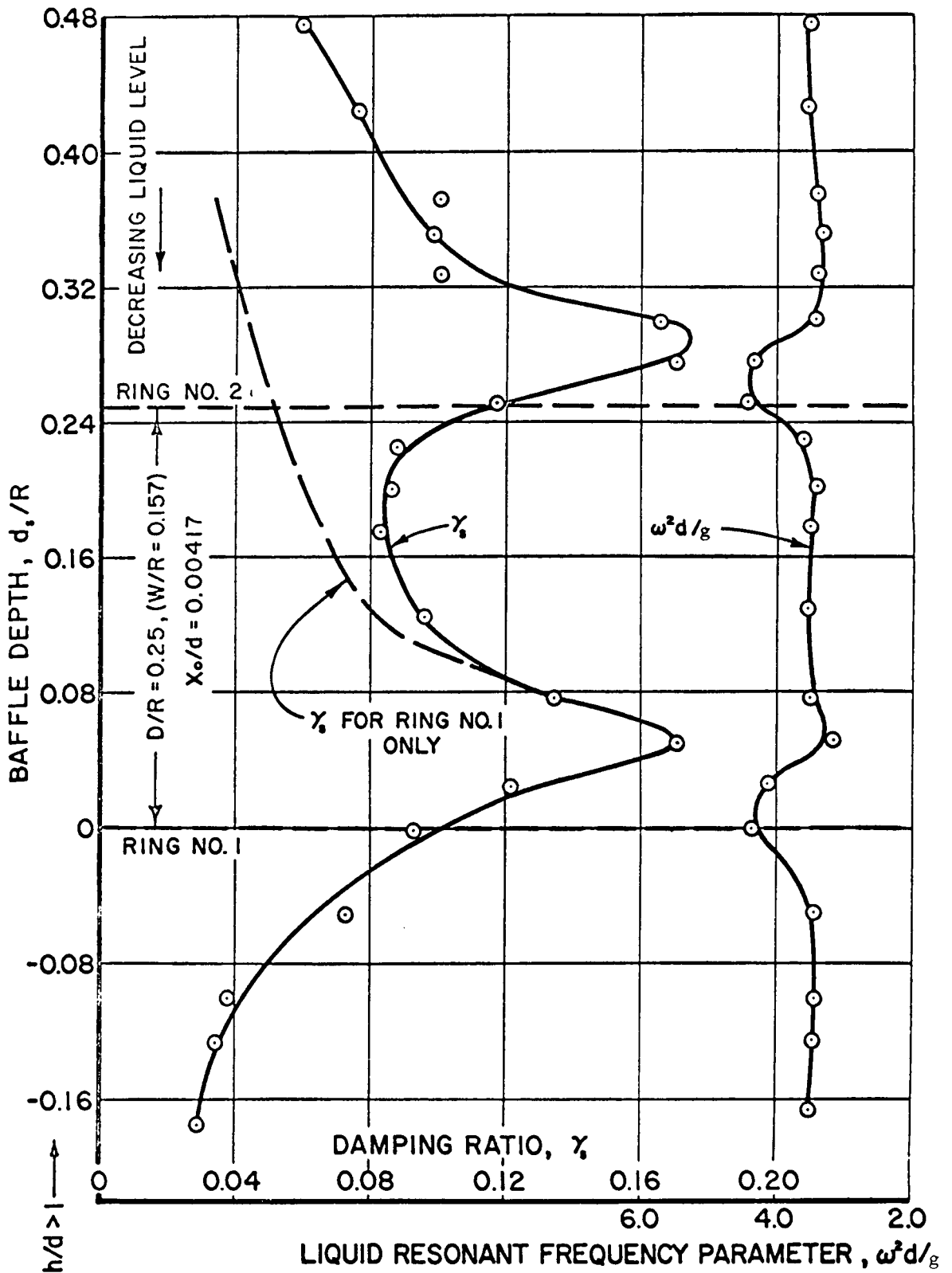


Figure 5.4 Effects of double rings as a function of baffle depth. (32)

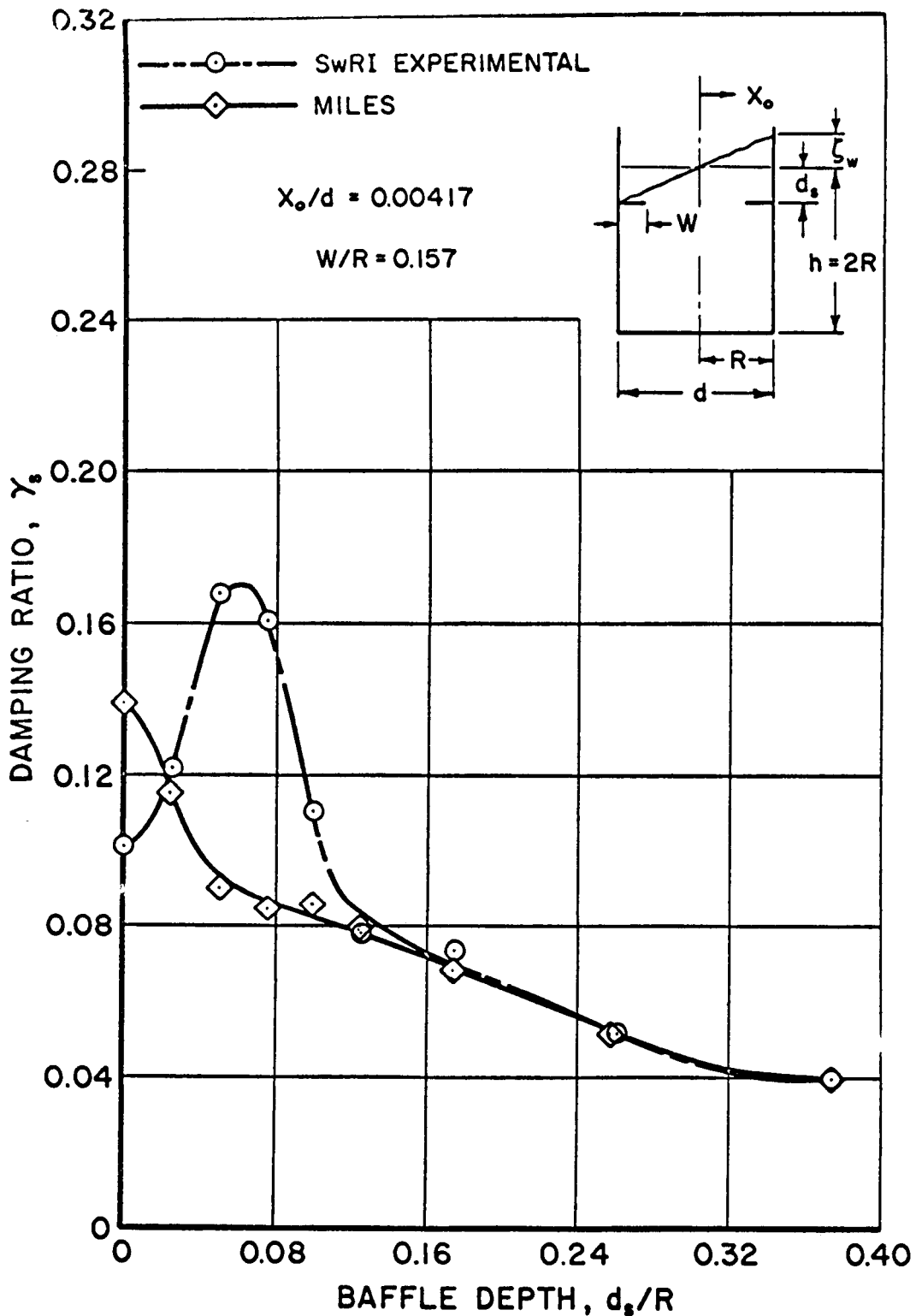


Figure 5.5 Comparison of theory and experiment for damping provided by a flat solid ring baffle as a function of baffle depth. (32)

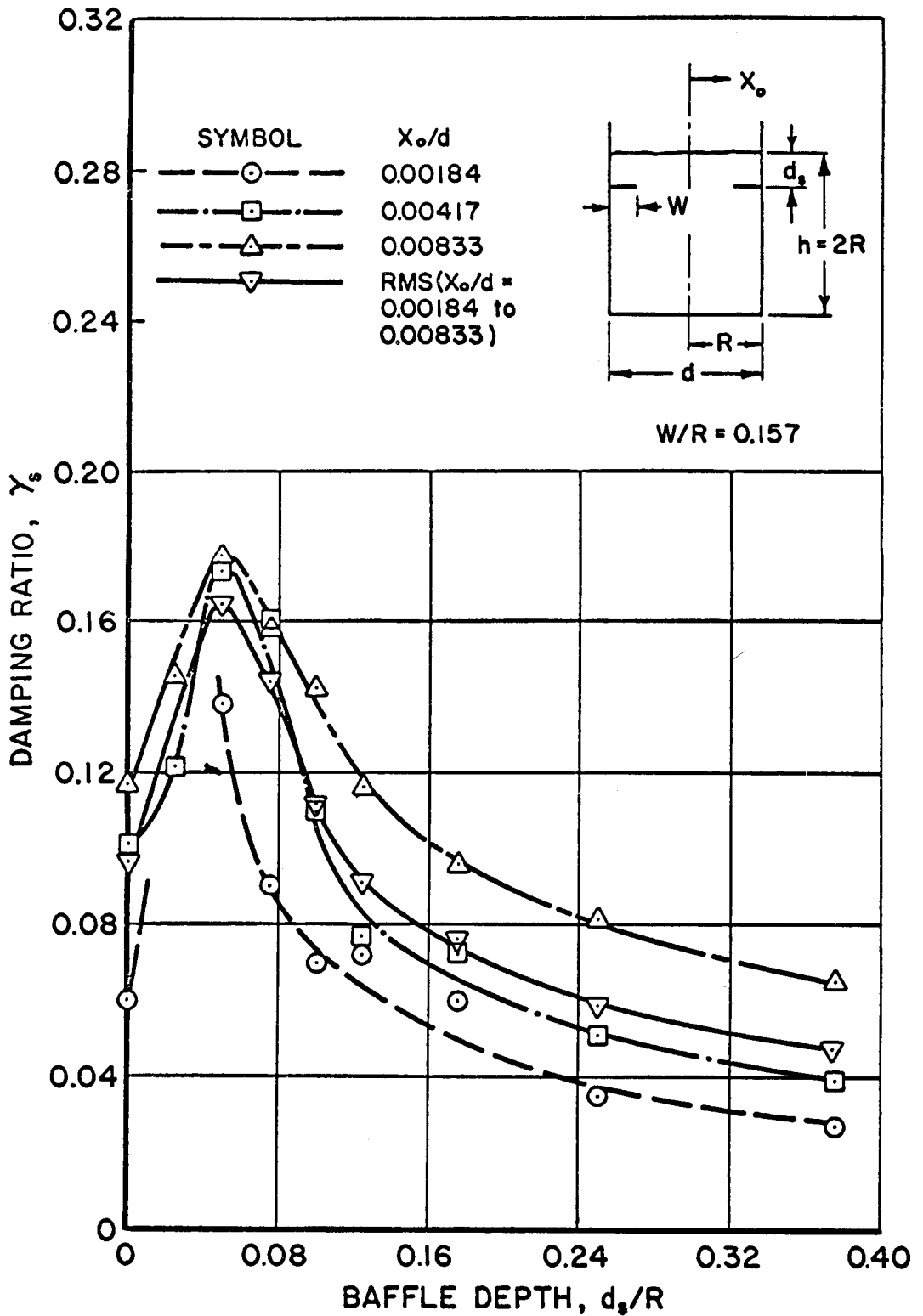


Figure 5.6 Effect of excitation amplitude on damping effectiveness of a solid flat ring baffle as a function of baffle depth. (32)

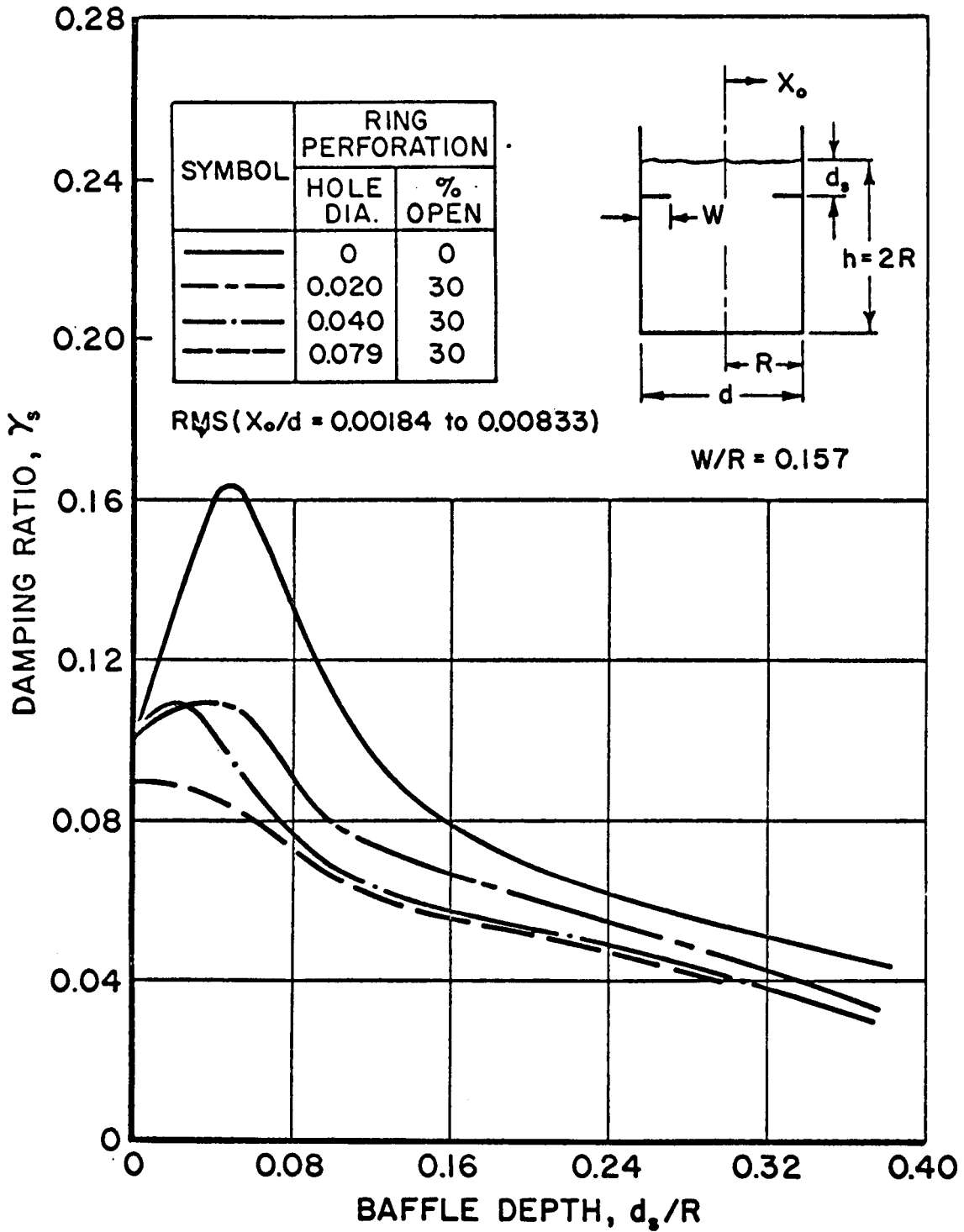


Figure 5.7 Effect of perforation hole size on damping effectiveness as a function of baffle depth. (32)

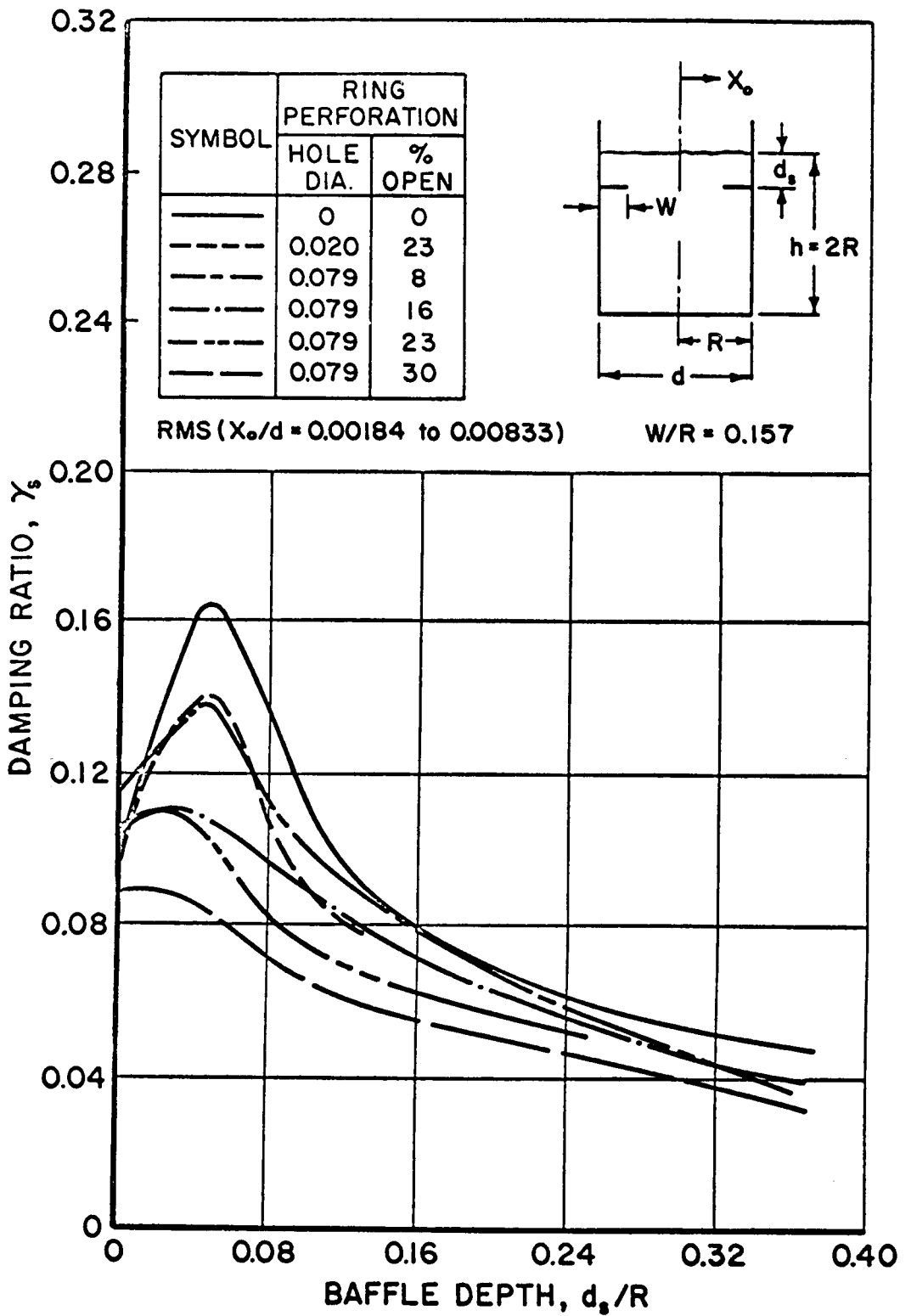
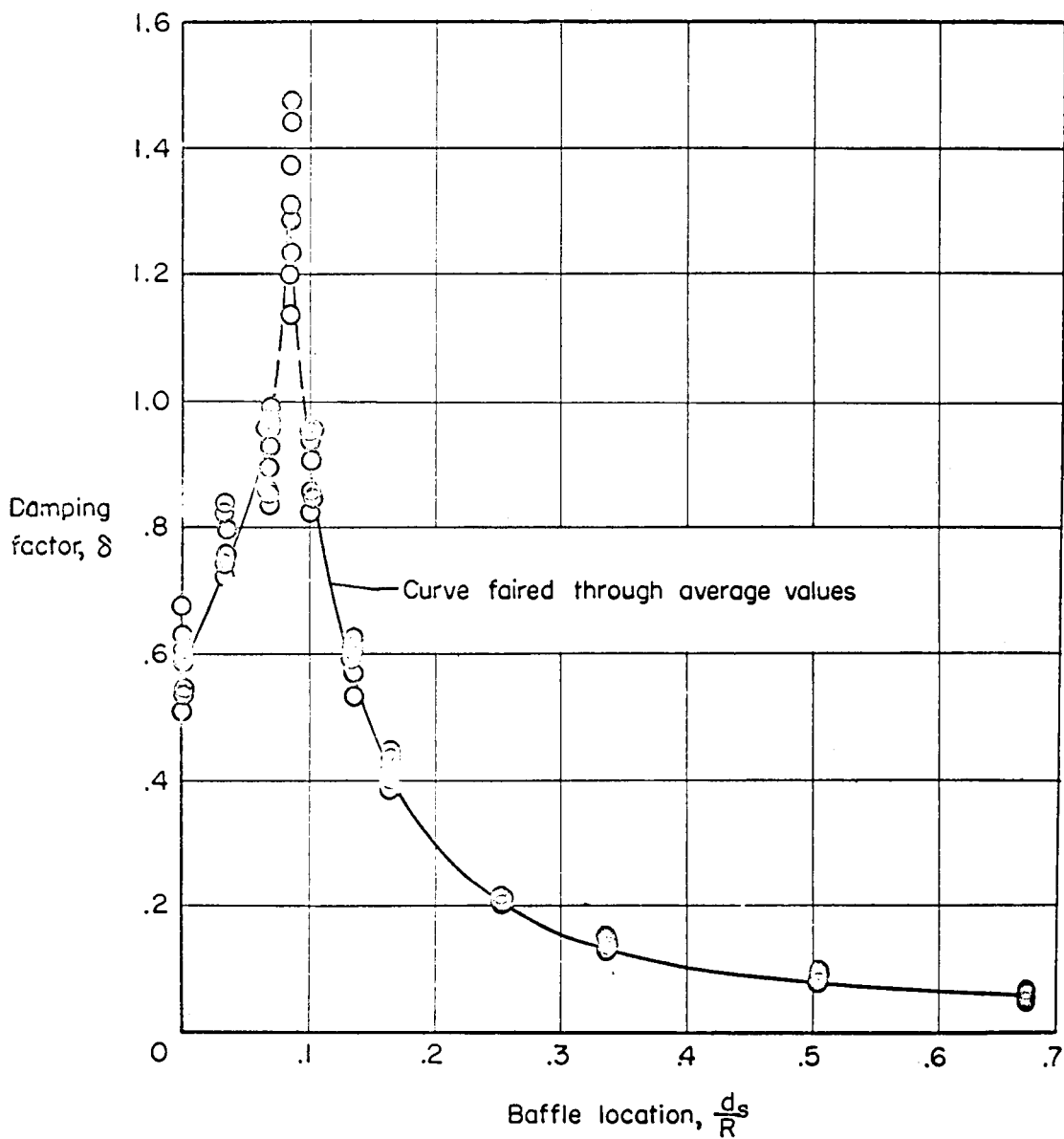
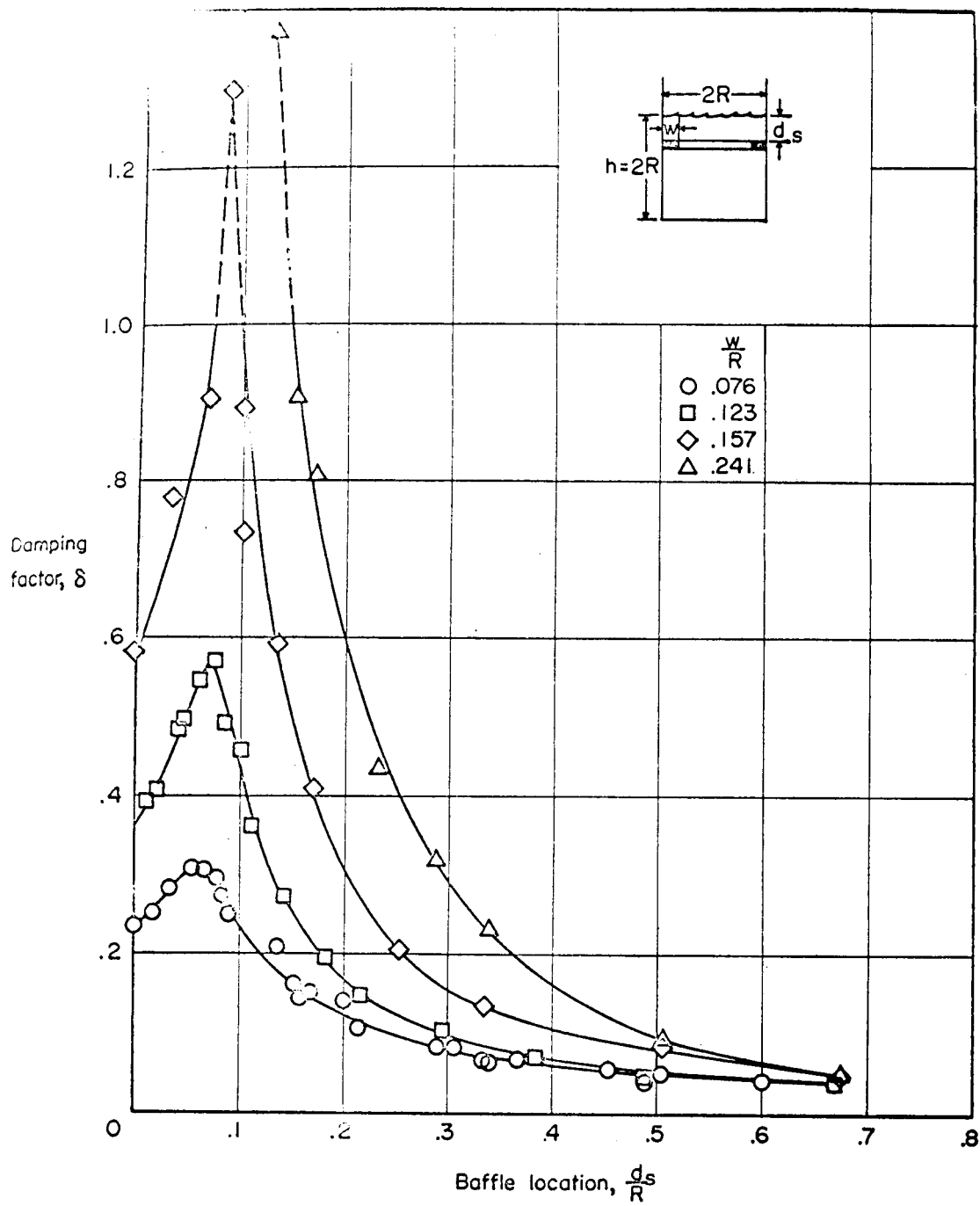


Figure 5.8 Effect of percent perforation on damping effectiveness as a function of baffle depth. (32)



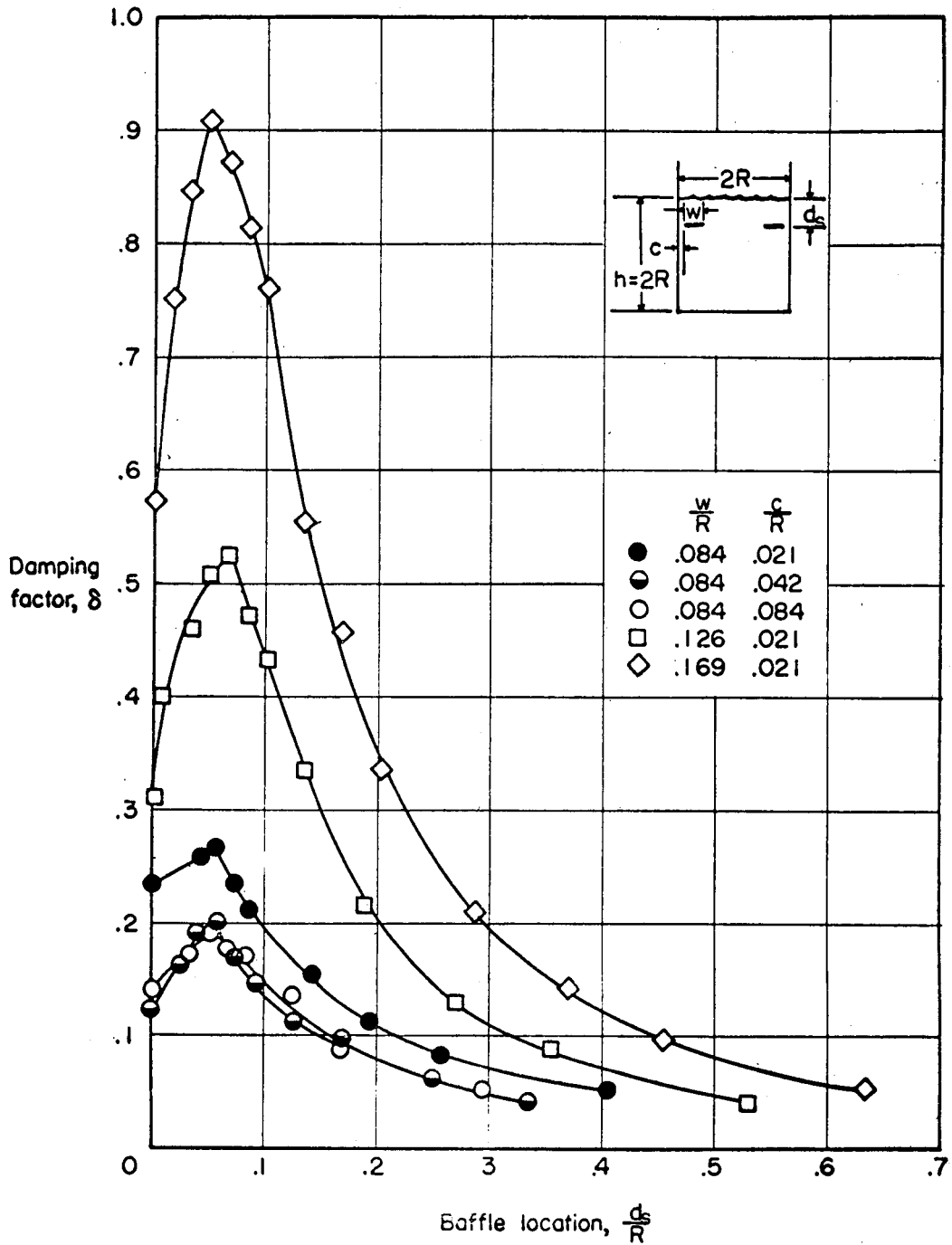
A typical distribution of data for a fixed-ring baffle as a function of baffle depth. $R = 6$ inches; $\frac{h}{R} = 2$. (35)

Figure 5-9



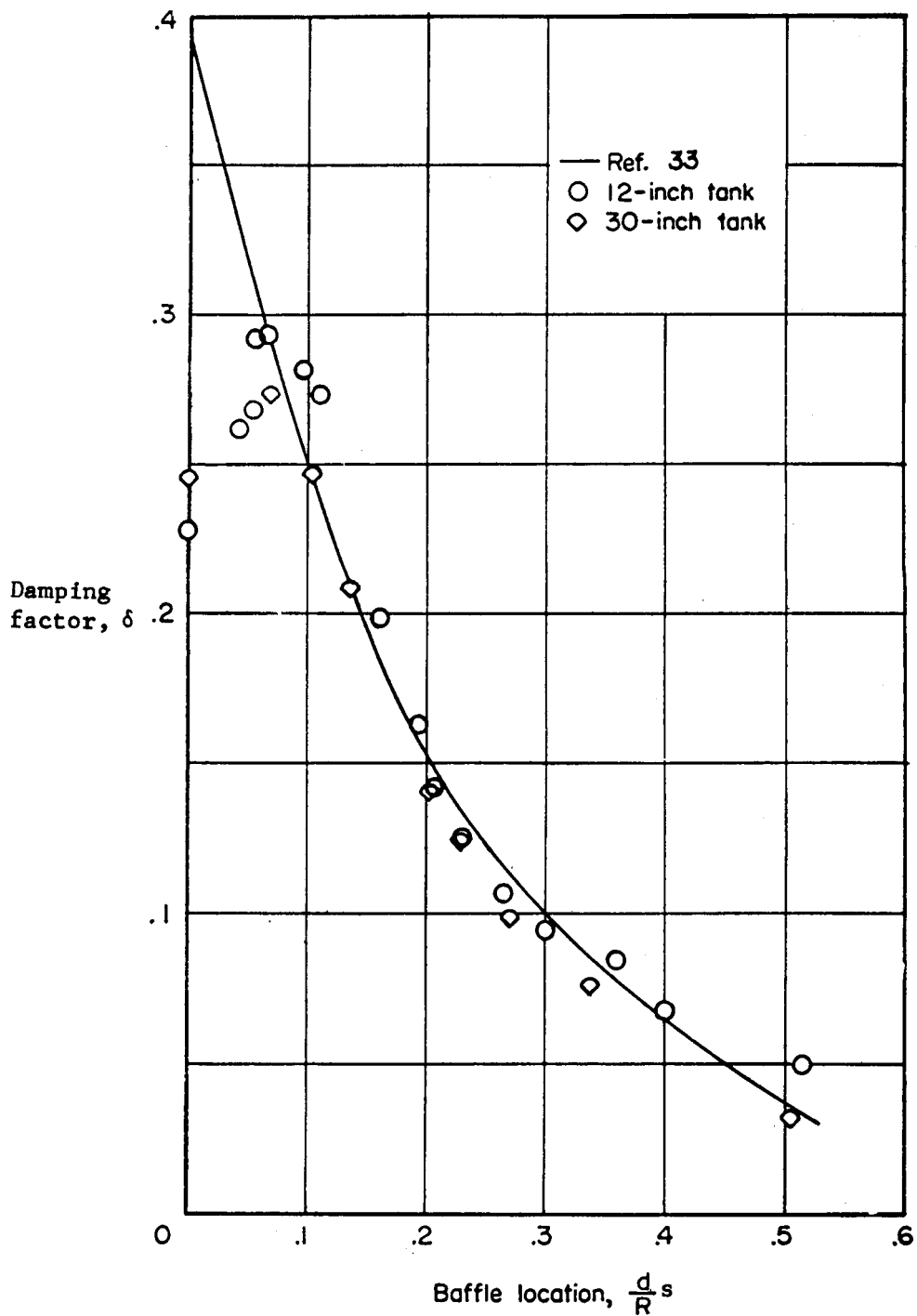
- Variation of damping factor with baffle location for fixed-ring baffle. $R = 6$ inches; $\frac{h}{R} = 2$. (35)

Figure 5-10



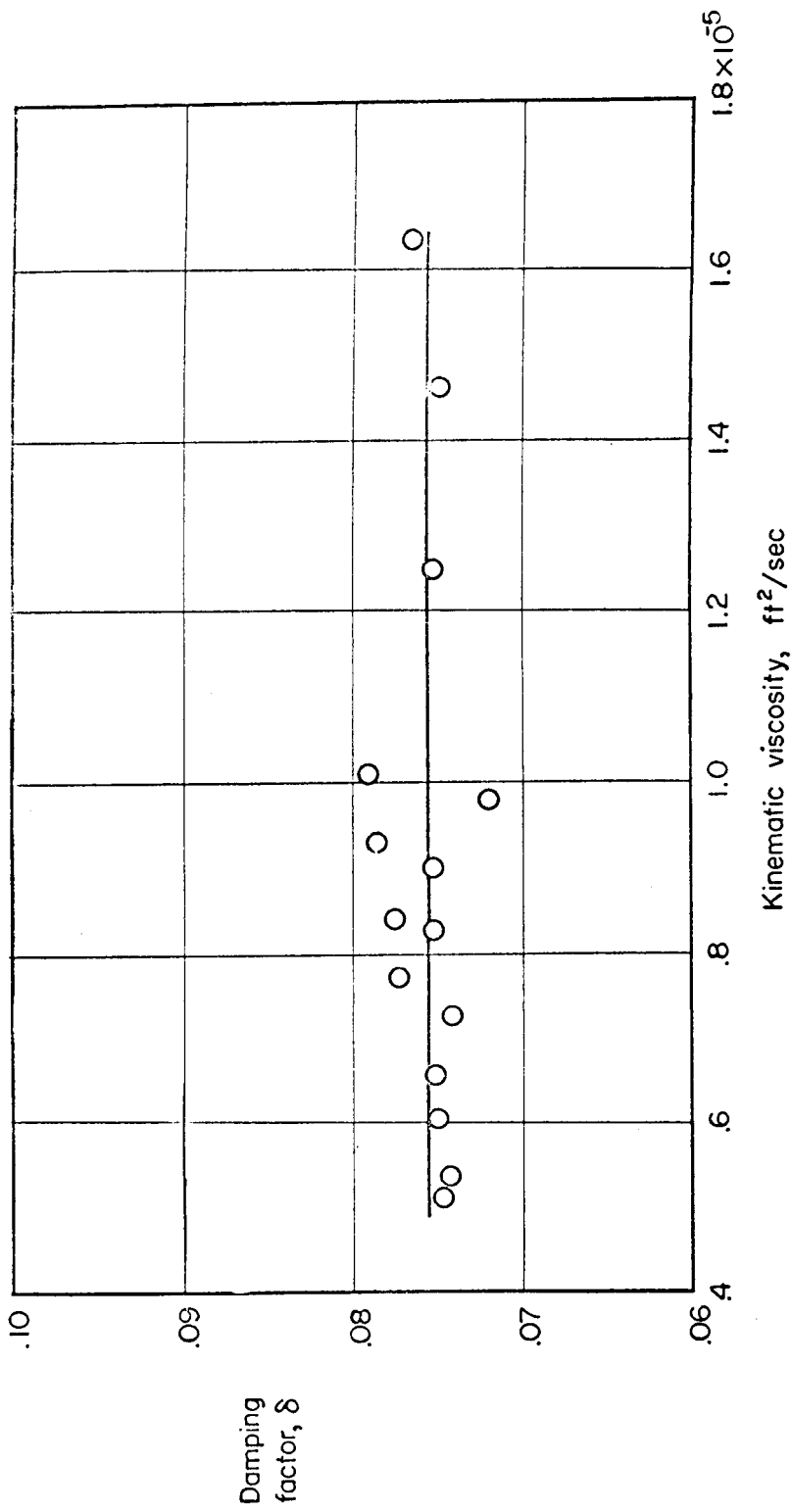
Variation of damping factor with baffle location for ring-with-radial-clearance baffle. $R = 6$ inches; $\frac{h}{R} = 2$. (35)

Figure 5-11



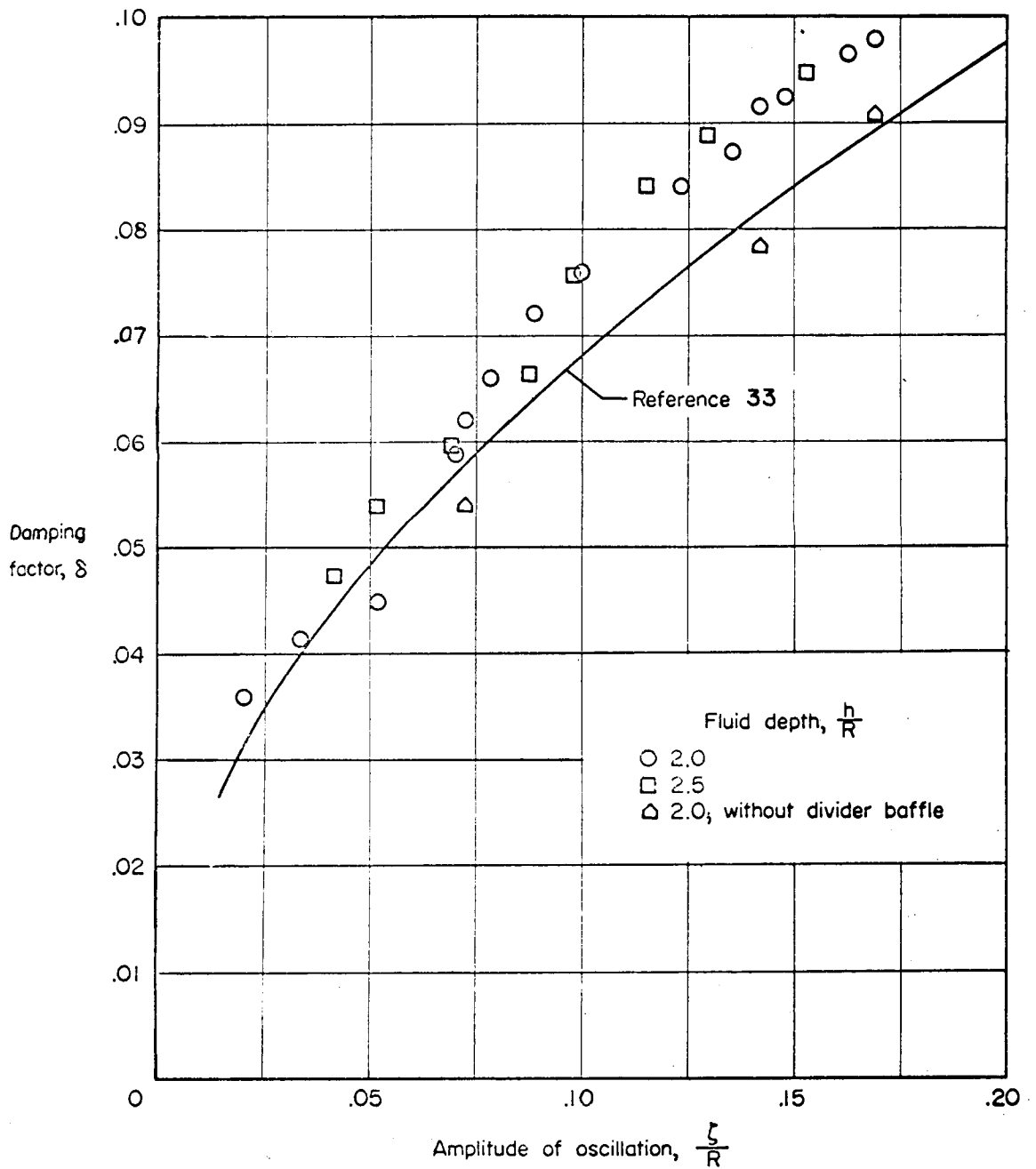
Variation of damping factor with baffle location in the 12- and 30-inch-diameter tanks. (35)

Figure 5-12



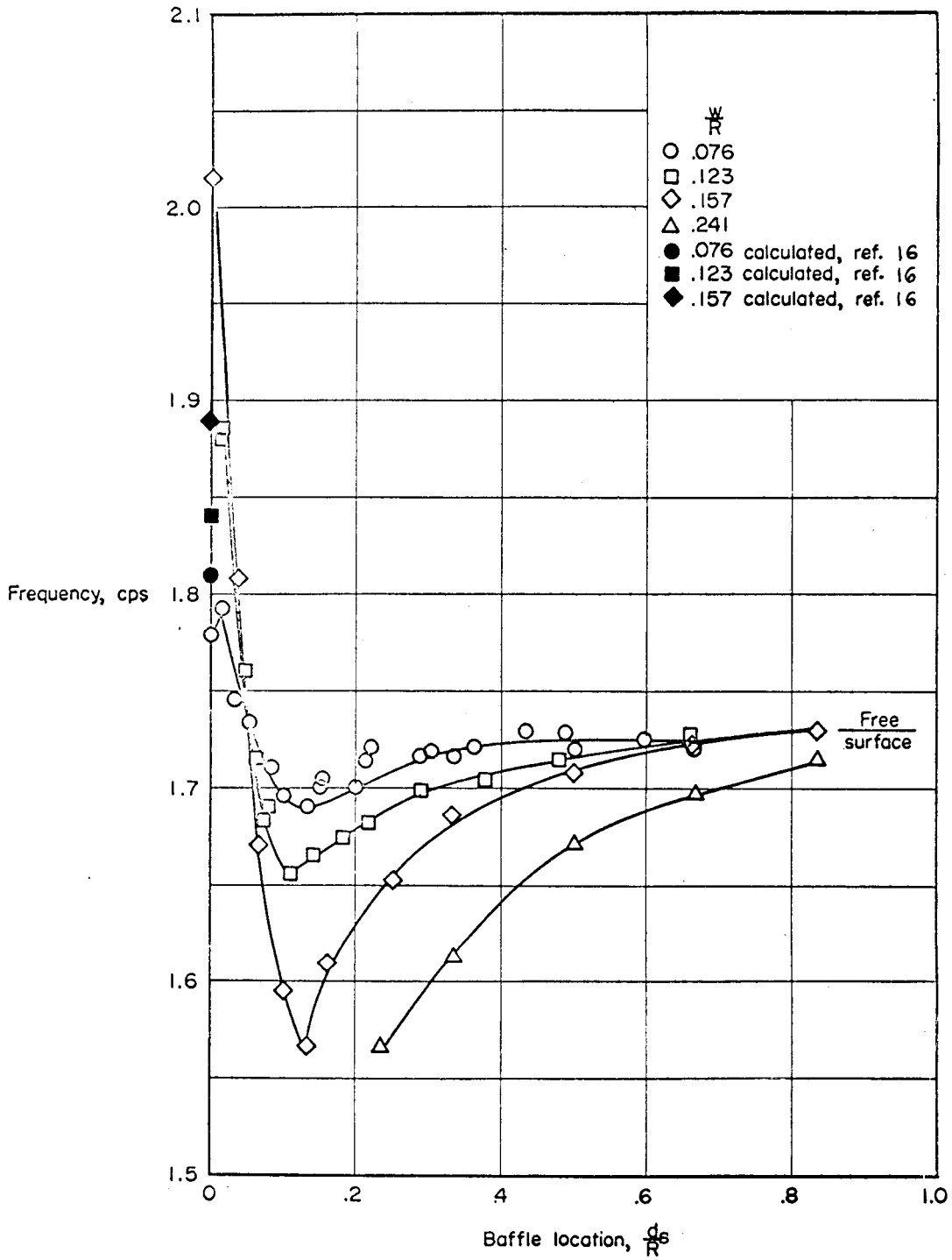
Variation of damping factor with kinematic viscosity of water for fixed-ring baffle mounted in 30-inch-diameter tank. $\frac{W}{R} = 0.076$. (35)

Figure 5-13



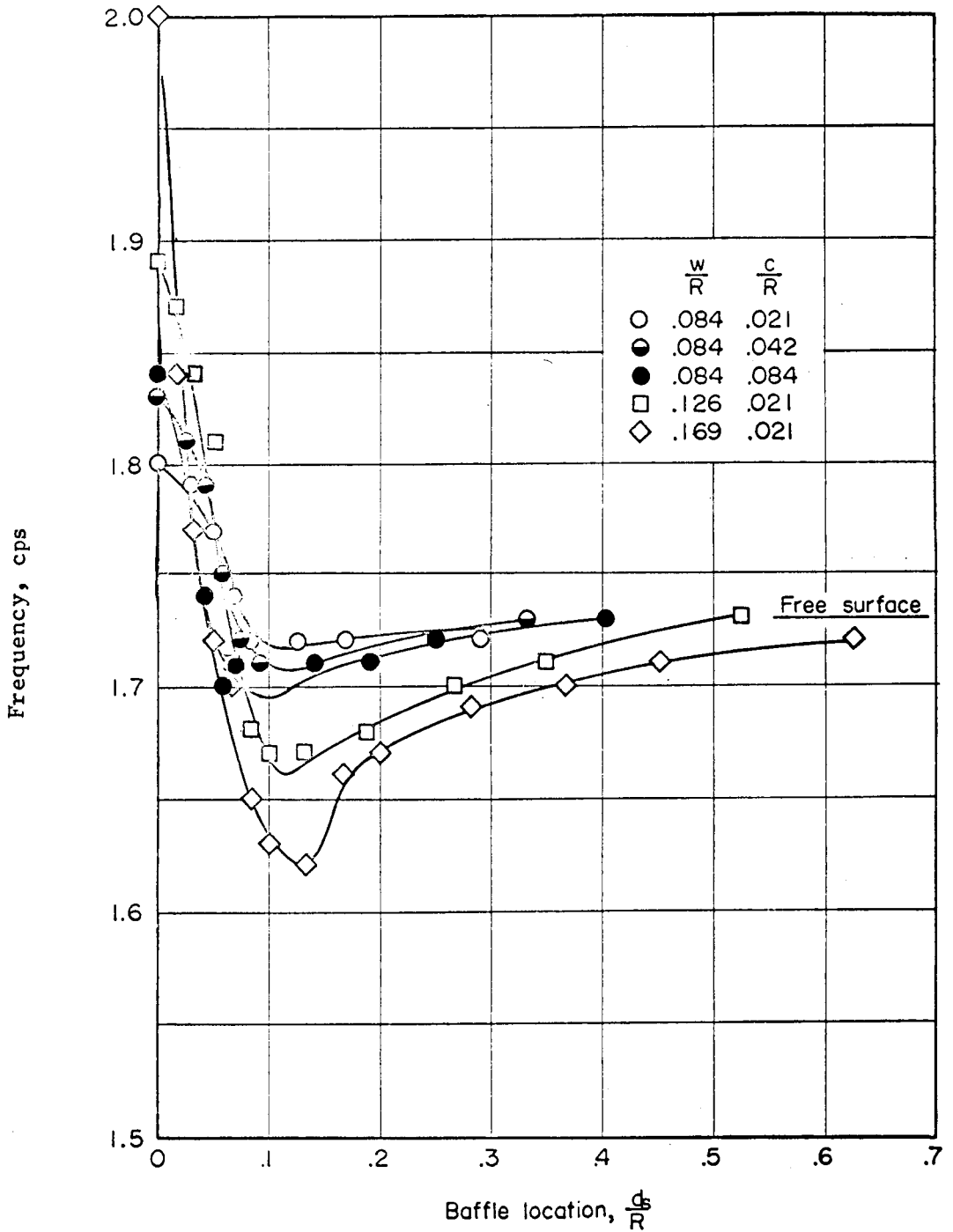
Variation of damping factor with amplitude of oscillation for fixed-ring baffle. $\frac{w}{R} = 0.076$; $\frac{d_s}{R} = 0.333$. (35)

Figure 5-14



Variation of frequency with baffle location for fixed-ring baffle. (35)

Figure 5-15



Variation of frequency with baffle location for ring-with-radial-clearance baffle. (35)

Figure 5-16

5.1.3.2 Ring Baffles: Analytical. Damping requirements are determined from stability studies of the vehicle in question. The designer must then determine the baffle width and spacing needed to yield a damping factor in the required range.

5.1.3.2.1 Miles' Analysis (28). According to Miles, the damping ratio of an annular ring baffle is

$$\gamma = 2.83 \alpha^{3/2} e^{-\frac{4.6d}{a}} (\zeta_1/a)^{1/2}, \quad \alpha \ll 1 \text{ and } \zeta_1 \ll a \quad (5-1)$$

where

$\alpha \pi a^2$ = ring baffle area

α = ratio of ring baffle area to cross-sectional area of tank

d = depth of ring baffle below undisturbed free liquid surface

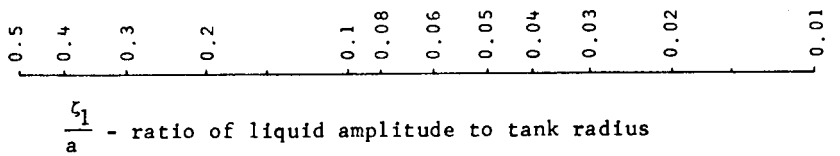
a = radius of circular cylindrical tank

ζ_1 = amplitude of liquid oscillations measured at the tank wall from undisturbed free liquid surface.

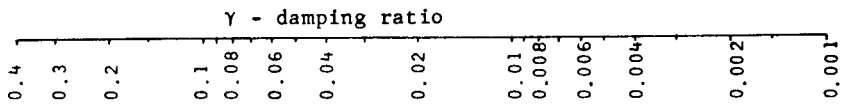
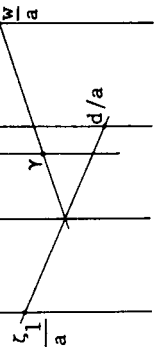
Within the restrictions on α and ζ_1 , this damping ratio relation was experimentally verified; however, Miles suggested that additional experimental confirmation would be desirable, both in order to establish the limits on α and ζ_1/a and to determine a more accurate value of the constant multiplier. Results are shown in Figures 5-17 to 5-29. A nomograph is shown on page 5-32. A line drawn between values of ζ_1/a and d/a determines a pivot point on the K-axis. A line drawn from this pivot point through a value of γ gives the corresponding value of W/a .

MILES' DAMPING RATIO

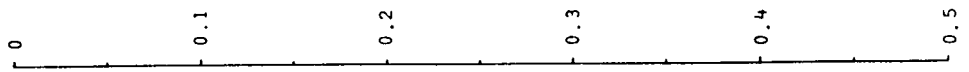
$$\gamma = 8 \left(\frac{\zeta_1}{a} \right)^{0.5} \left(\frac{w}{a} \right)^{1.5} e^{-4.6d/a}$$



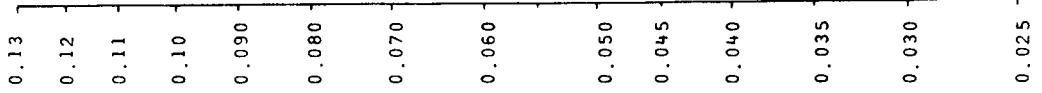
KEY



$\frac{a}{d}$ - ratio of baffle depth to tank radius



$\frac{a}{w}$ - ratio of baffle width to tank radius



DAMPING FACTOR VERSUS BAFFLE DEPTH FOR
 LIQUID AMPLITUDE $\zeta_w = 0.01g$ WITH THE BAFFLE
 WIDTH AS A PARAMETER (MILES FORMULA)

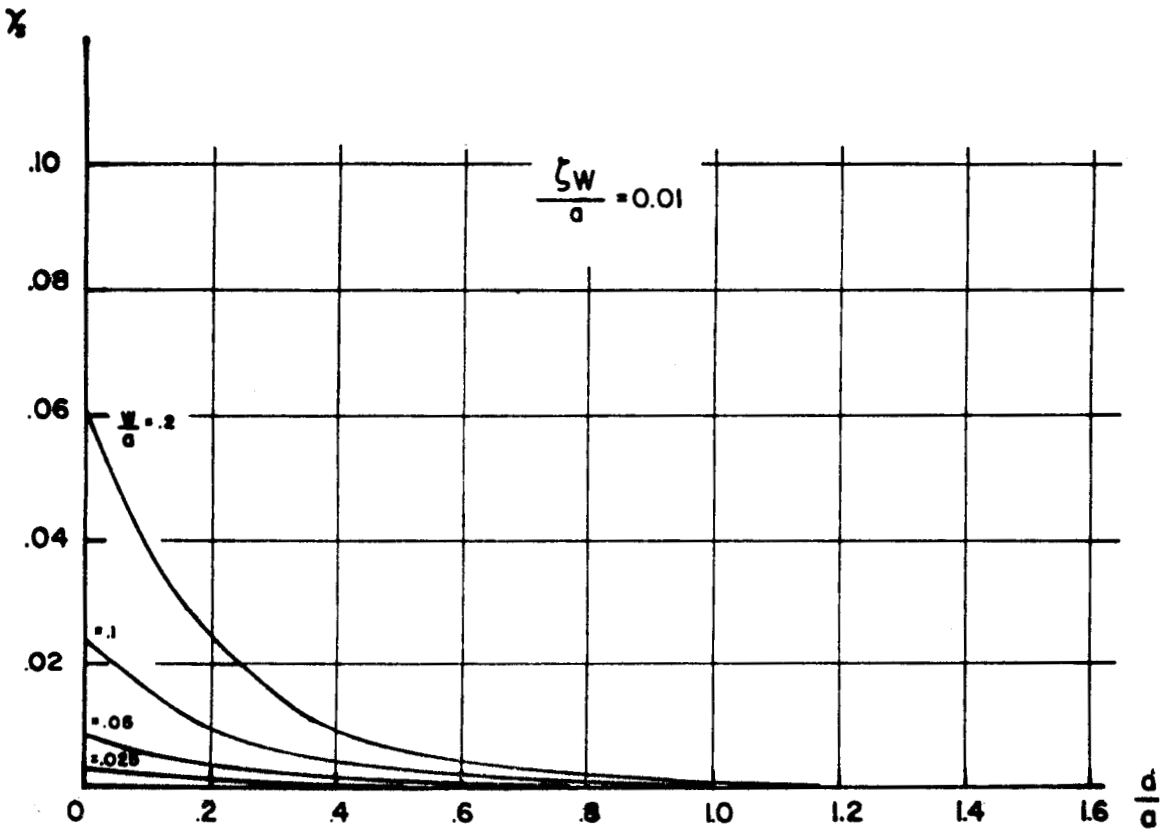


Figure 5-17

DAMPING FACTOR VERSUS BAFFLE DEPTH FOR
 LIQUID AMPLITUDE $\zeta_w = 0.050$ WITH THE BAFFLE
 WIDTH AS A PARAMETER (MILES FORMULA)

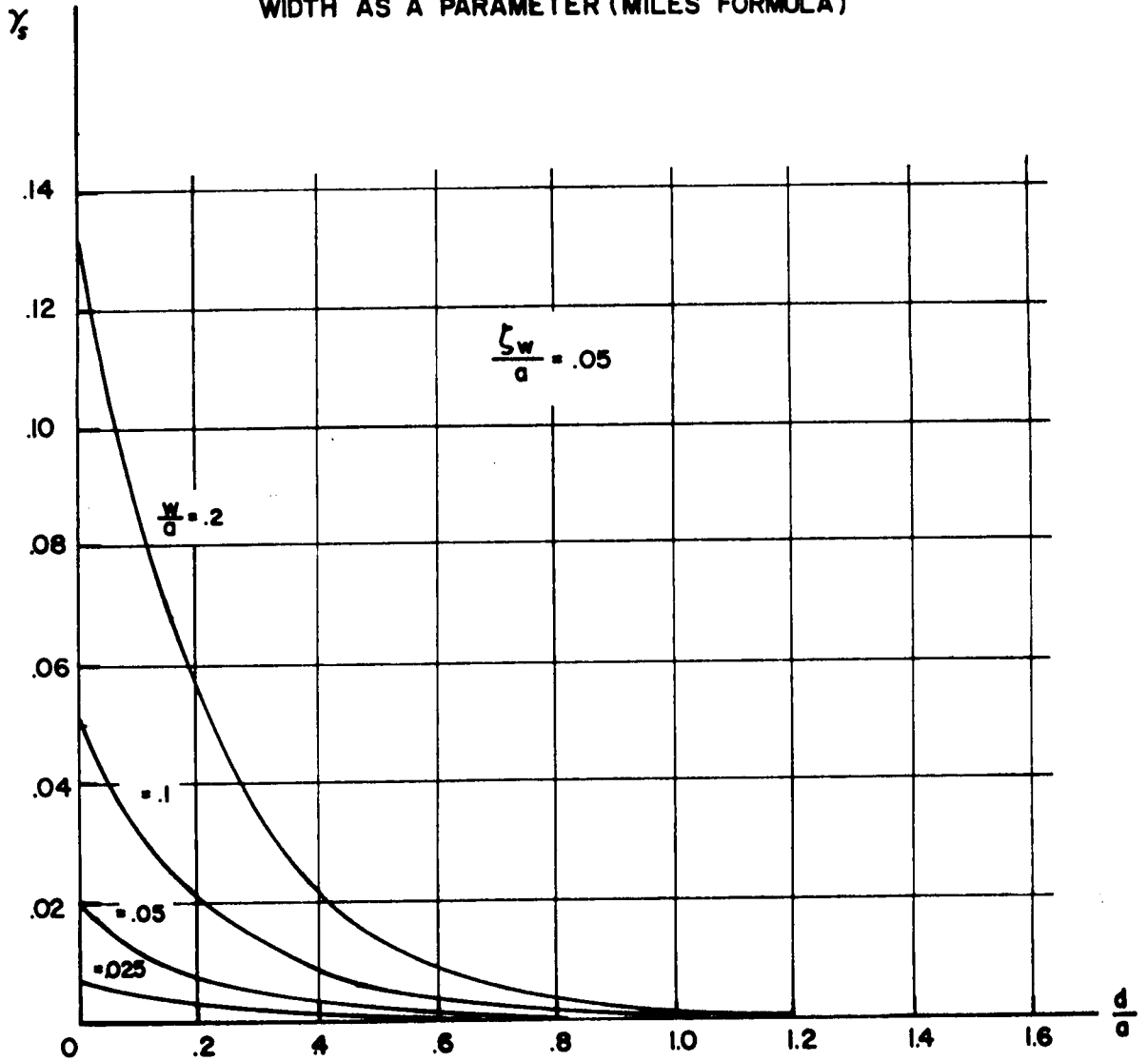


Figure 5-18

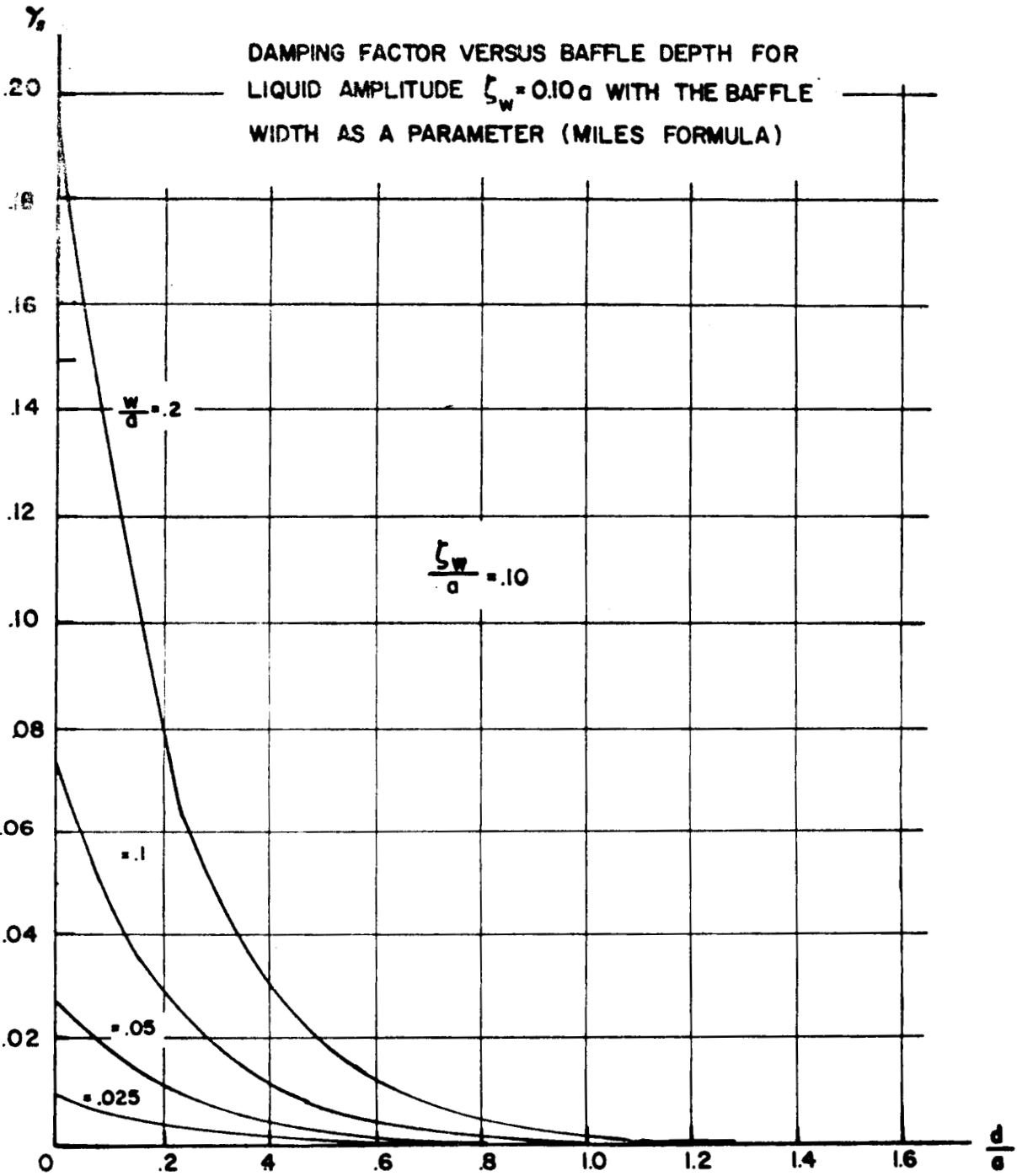


Figure 5-19

DAMPING FACTOR VERSUS BAFFLE DEPTH FOR
 LIQUID AMPLITUDE $\zeta_w = .20g$ WITH THE BAFFLE
 WIDTH AS A PARAMETER (MILES FORMULA)

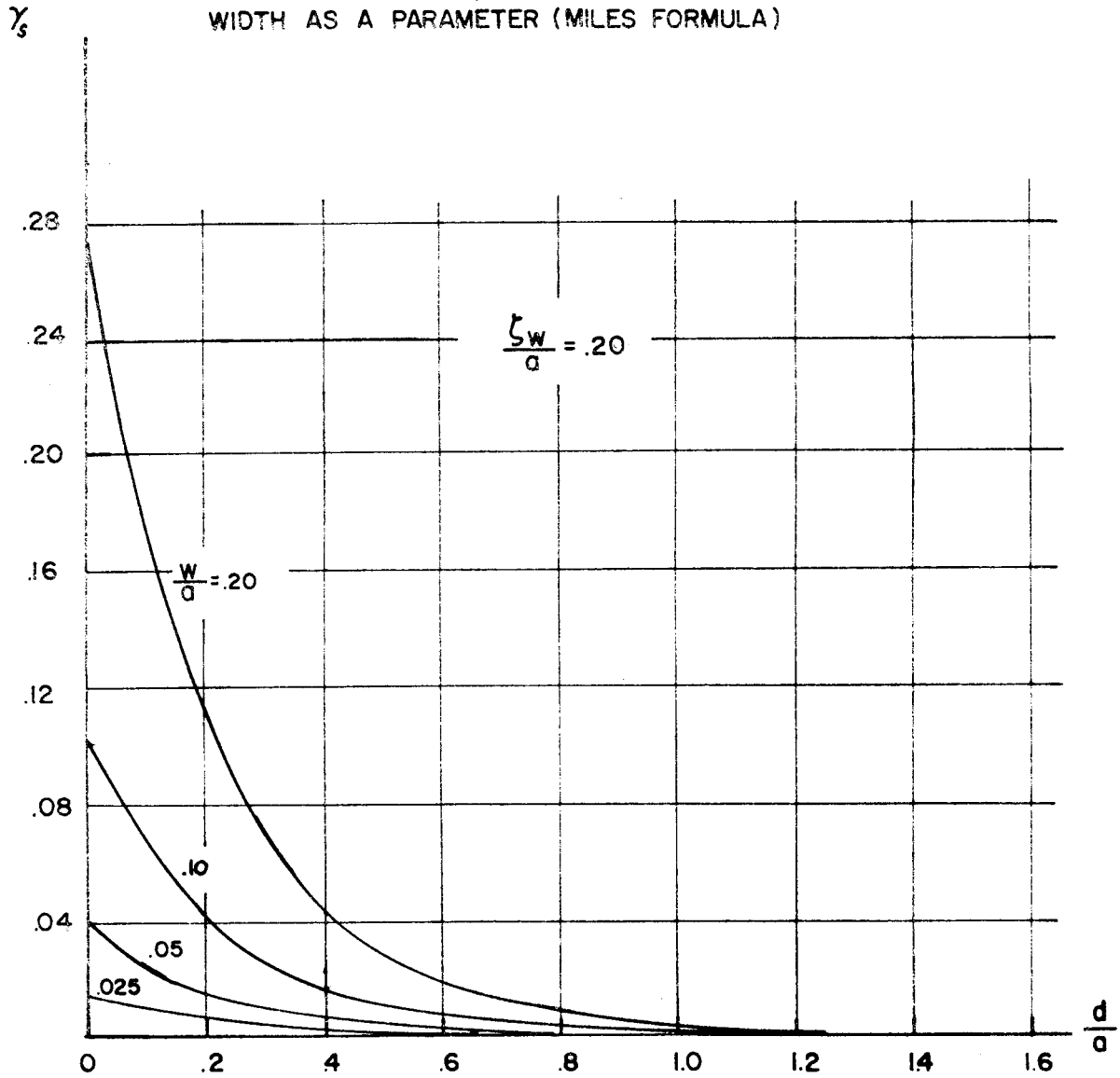


Figure 5-20

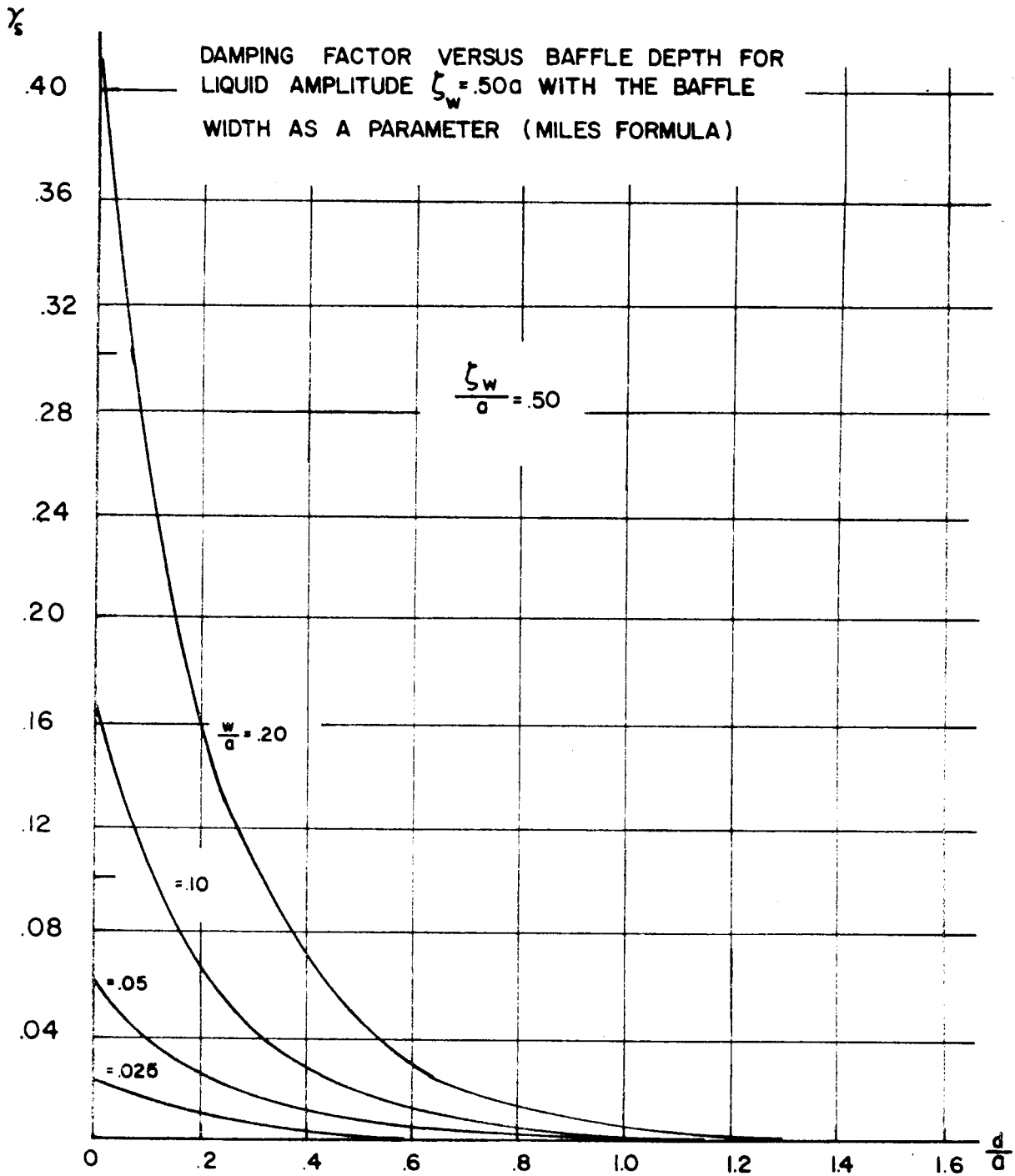


Figure 5-21

DAMPING FACTOR VERSUS BAFFLE DEPTH FOR WIDTH
 $W=0.025$ WITH LIQUID AMPLITUDE AS A PARAMETER
(MILES FORMULA)

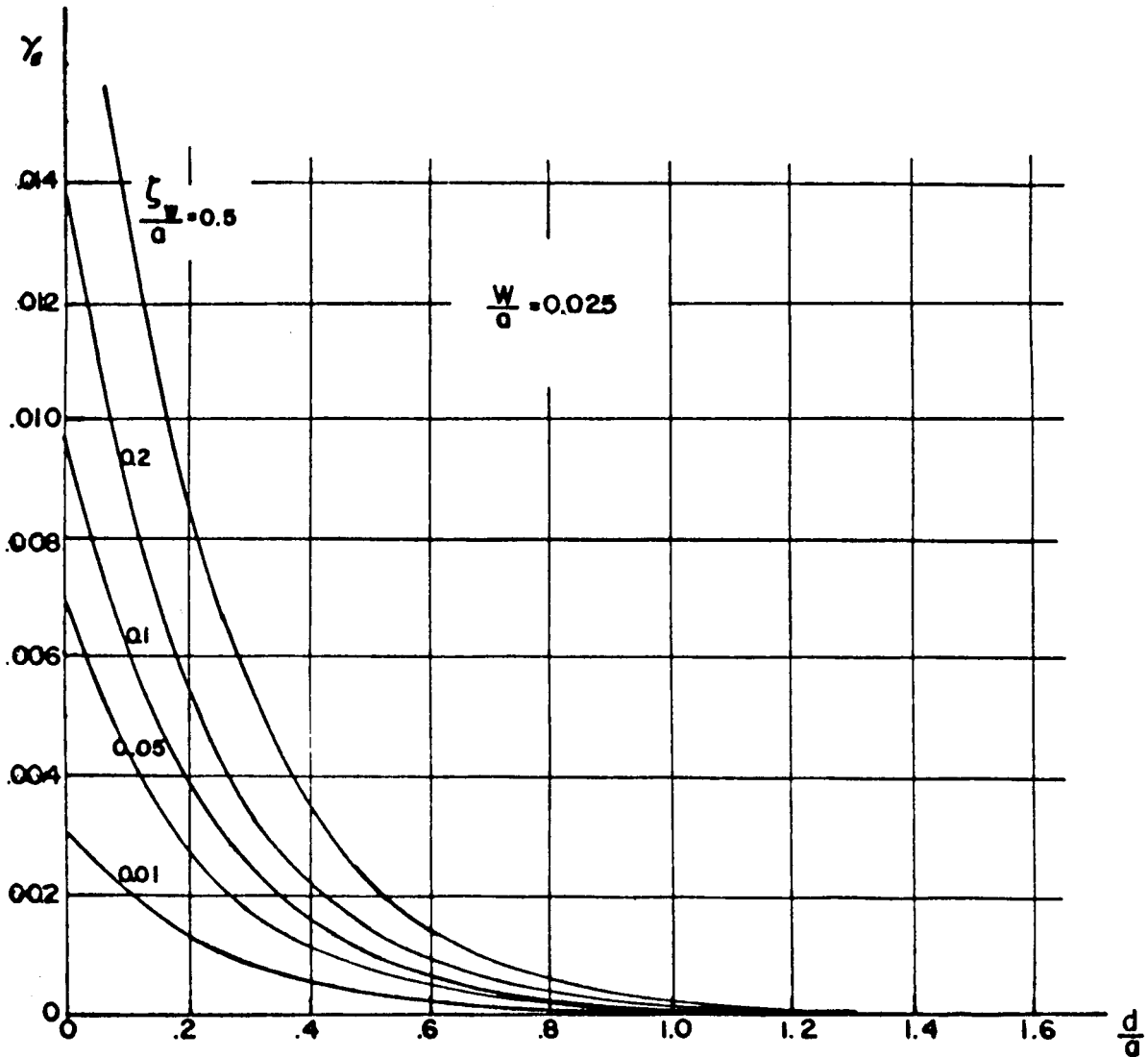


Figure 5-22

DAMPING FACTOR VERSUS BAFFLE DEPTH FOR WIDTH
 $W=0.05a$ WITH LIQUID AMPLITUDE AS A PARAMETER
(MILES FORMULA)

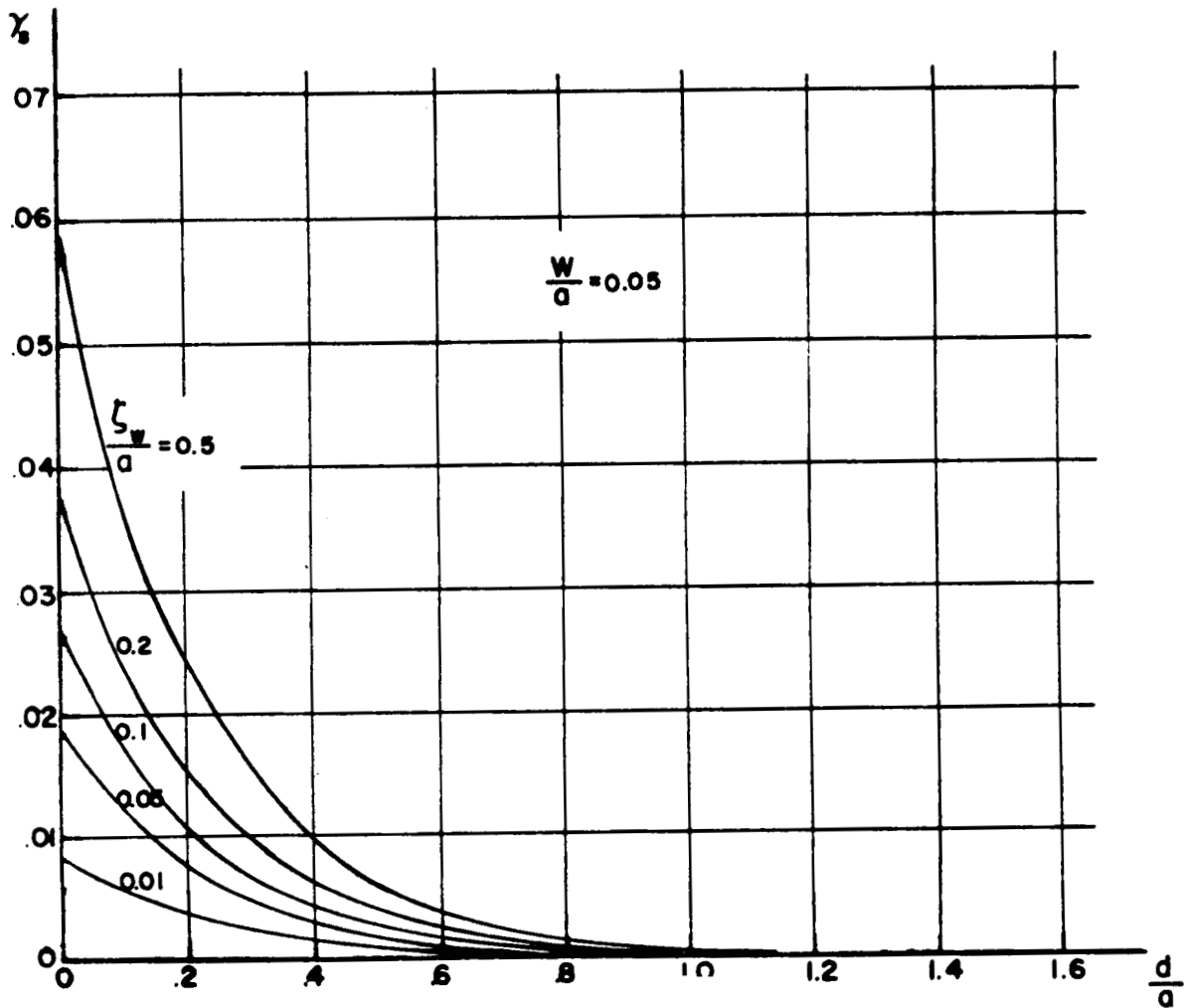


Figure 5-23

DAMPING FACTOR VERSUS BAFFLE DEPTH FOR WIDTH
 $W=0.10a$ WITH LIQUID AMPLITUDE AS A PARAMETER
(MILES FORMULA)

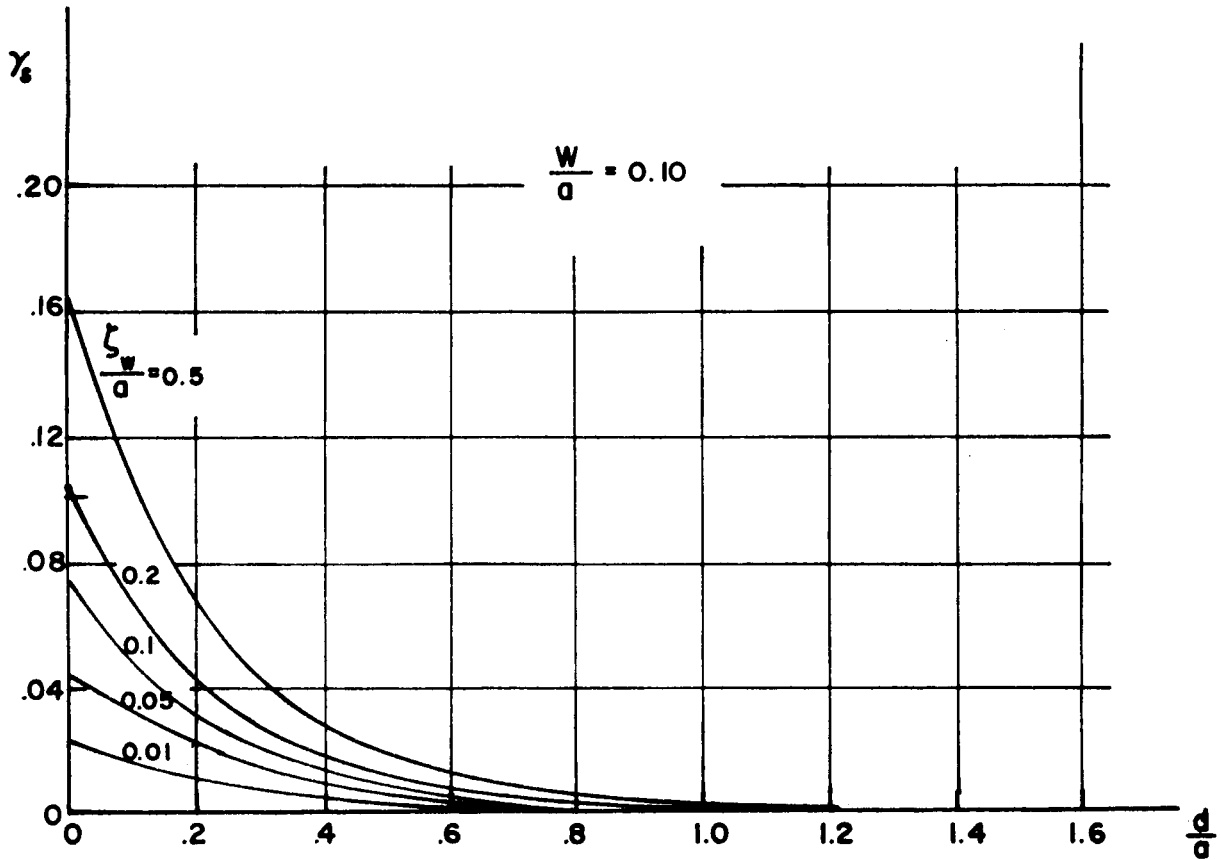


Figure 5-24

DAMPING FACTOR VERSUS BAFFLE DEPTH FOR WIDTH
 $W=0.20a$ WITH LIQUID AMPLITUDE AS A PARAMETER
(MILES FORMULA)

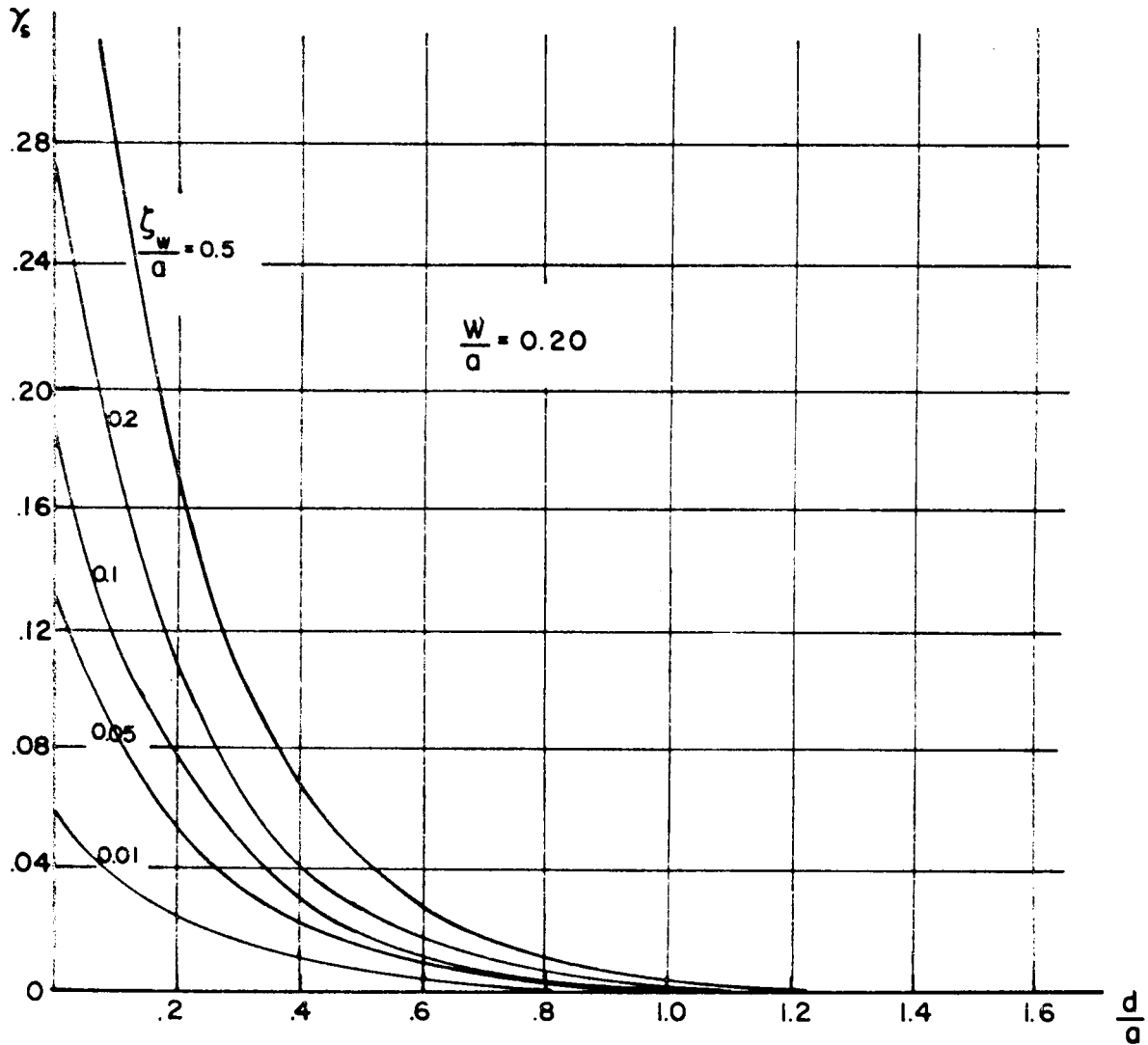


Figure 5-25

DAMPING FACTOR VERSUS SURFACE AMPLITUDE FOR BAFFLE
 WIDTH $W = .05a$ WITH BAFFLE LOCATION AS A PARAMETER
 (MILES FORMULA)

$$\frac{W}{a} = .05$$

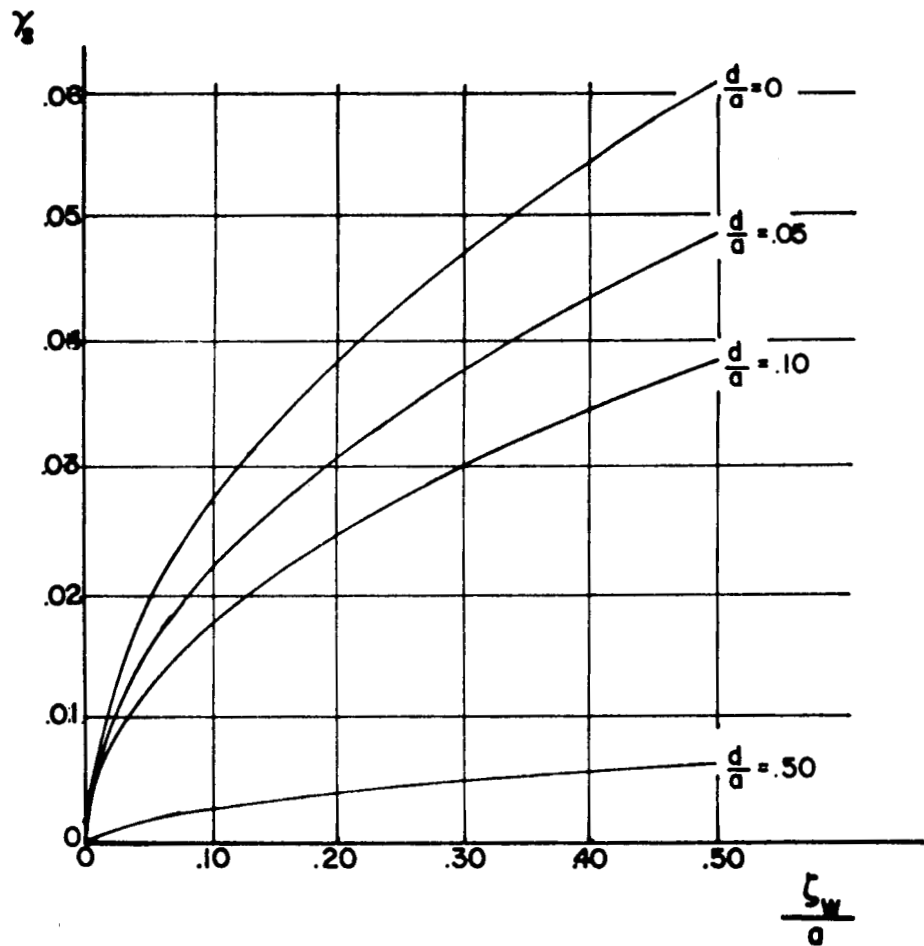


Figure 5-26

DAMPING FACTOR VERSUS SURFACE AMPLITUDE FOR BAFFLE
 WIDTH $W = .15a$ WITH BAFFLE LOCATION AS A PARAMETER
 (MILES FORMULA)

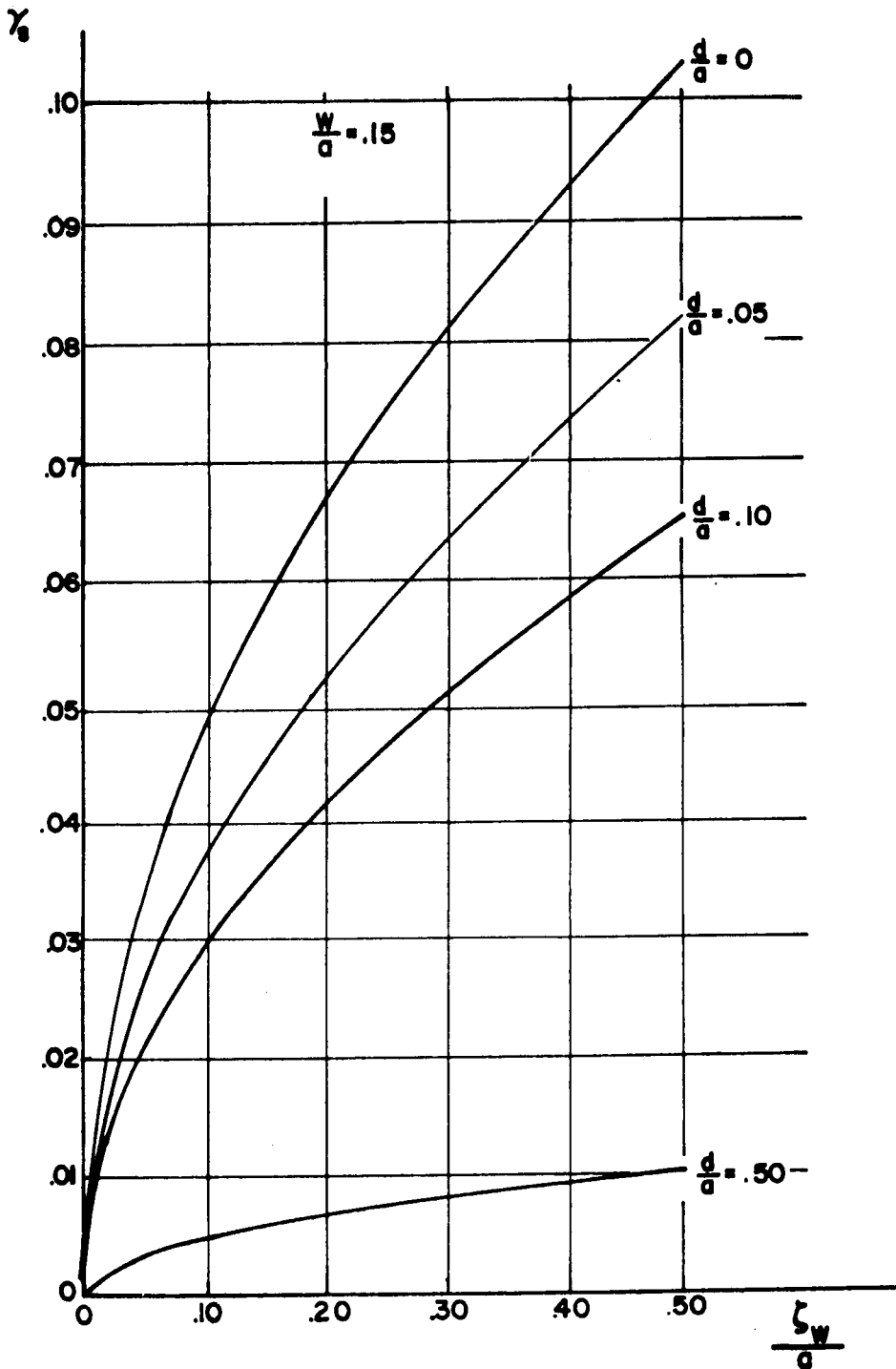


Figure 5-27

DAMPING FACTOR VERSUS BAFFLE WIDTH FOR
 $\zeta_w = .10a$ WITH LOCATION OF BAFFLE AS A
PARAMETER (MILES FORMULA)

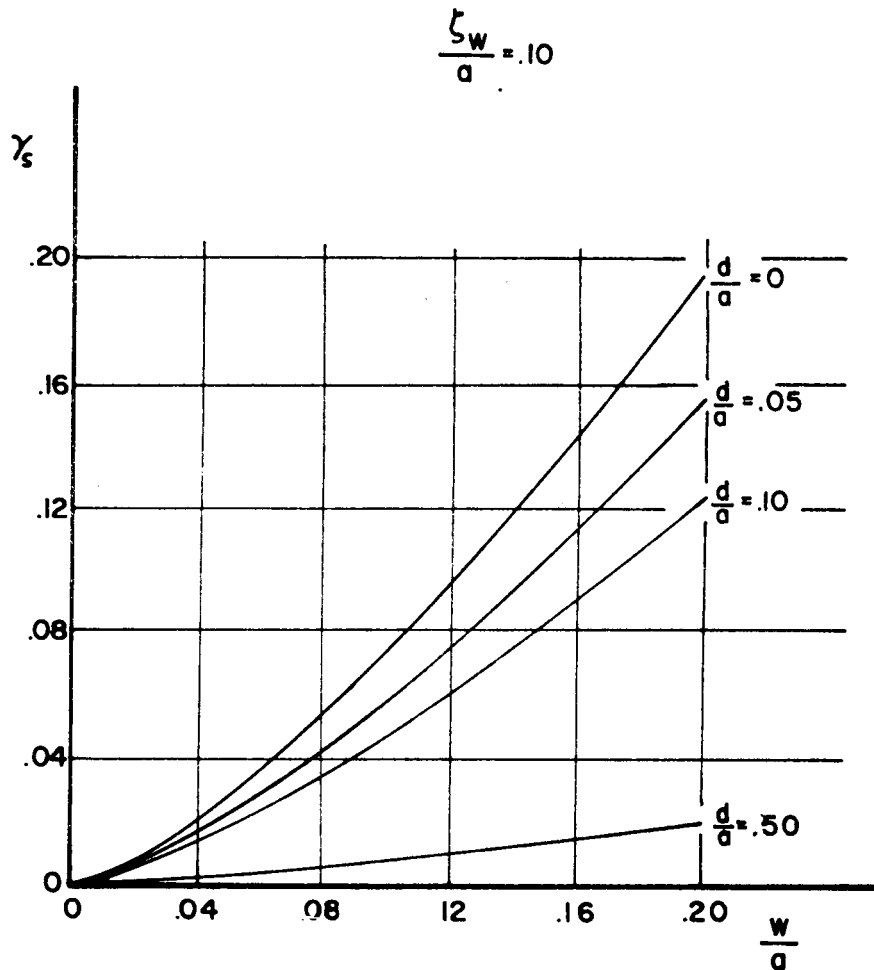


Figure 5-28

DAMPING FACTOR VERSUS BAFFLE WIDTH FOR
 $\zeta_w = .30a$ WITH LOCATION OF BAFFLE AS A
 PARAMETER (MILES FORMULA)

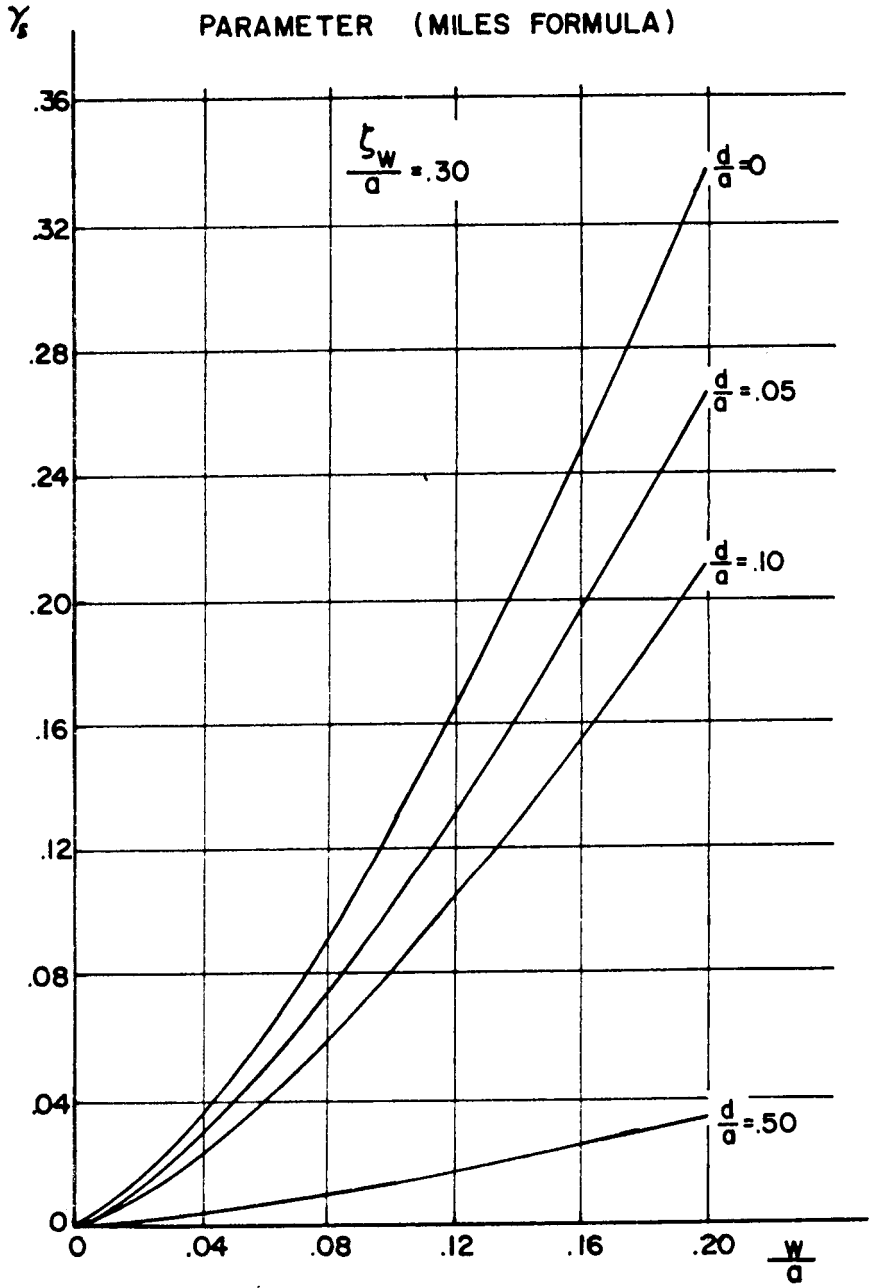


Figure 5-29

5.1.3.2.2 O'Neill's Extension (84). Within the scatter of experimental data, O'Neill showed that either of the following equations can be used for reasonable values of $\frac{\zeta_1}{a}$ and $\bar{F} = \frac{F}{\rho g a^3}$, for any ring submergence $\frac{d}{a} \geq 0$ and for ring widths corresponding to $\alpha \leq 0.25$

$$\begin{aligned} \gamma &= 2.83 e^{-4.60d/a} \alpha^{3/2} \left(\frac{\zeta_1}{a} \right)^{1/2} && \text{(Miles)} \\ \gamma &= 2.16 e^{-4.60d/a} \alpha^{3/2} \left(\frac{F}{\rho g a^3} \right)^{1/2} && (5-2) \end{aligned}$$

Equation (5-2) gives the damping factor in terms of the lateral liquid force F which is easier to measure than the wave amplitude ζ_1 .

5.1.3.2.3 Bauer's Extension (31). During sloshing, the baffles and the oscillating fluid are not in continuous contact with each other. There are parts of the oscillation cycle during which the fluid does not uniformly wet the entire surface of the baffles. For this reason, Miles (28) expression, Equation (5-1), gives a higher damping effect than that experimentally observed. To account for the deviation, an effective baffle area concept was herewith successfully employed. This effective baffle area is a function of the width w of the baffle, its location d below the liquid free surface, and the maximum amplitude of sloshing ζ_1 . The theoretical formula obtained agrees with experimental results.

In Equation (5-1), the baffle area ratio blocking the cross sectional area is defined as

$$\alpha = \frac{w}{a} \left[2 - \frac{w}{a} \right]$$

if the baffle is completely submerged during a slosh cycle. If the baffle is completely out of the liquid during a certain time of the slosh cycle, the effective baffle area is

$$\begin{aligned} \bar{\alpha} = & \frac{\frac{w}{a} \left(2 - \frac{w}{a} \right) - \frac{1}{2} \left(1 - \frac{d/a}{\zeta_1/a} \right) + \frac{2}{\pi} \frac{d/a}{\zeta_1/a} \ln \left[\frac{\zeta_1/a + (\zeta_1/a)^2 - (d/a)^2}{d/a} \right]}{\frac{1}{\pi} \frac{d/a}{(\zeta_1/a)^2} \sqrt{(\zeta_1/a)^2 - (d/a)^2} + \frac{1}{\pi} \arcsin \left(\frac{d/a}{\zeta_1/a} \right)} \\ & - \frac{\frac{1}{2} \frac{d/a}{\zeta_1/a} + \frac{1}{2} \left(1 - \frac{w}{a} \right)^2 \left\{ 1 - \frac{d/a}{\left(1 - \frac{w}{a} \right) \zeta_1/a} \right\}}{\dots} \end{aligned}$$

5.1.3.2.3 Bauer's Extension (31) (continued)

$$\begin{aligned}
 & - \frac{2}{\pi} \frac{\frac{d}{a} (1 - \frac{w}{a})}{\zeta_1/a} \ln \left[\frac{\zeta_1/a + \sqrt{(\zeta_1/a)^2 - (\frac{d/a}{1 - w/a})^2}}{\frac{d/a}{1 - w/a}} \right] \\
 & + \frac{1}{\pi} \frac{\frac{d}{a} (1 - \frac{w}{a})}{(\zeta_1/a)^2} \sqrt{(\zeta_1/a)^2 - \frac{(d/a)^2}{(1 - w/a)^2}} \\
 & - \frac{1}{\pi} (1 - \frac{w}{a})^2 \arcsin \left(\frac{d/a}{(1 - \frac{w}{a})\zeta_1/a} \right) + \frac{1}{2} (1 - \frac{w}{a}) \frac{d/a}{\zeta_1/a} \quad (5-3)
 \end{aligned}$$

If the baffle is completely submerged, i.e., $\frac{d}{a} \geq \frac{\zeta_1}{a}$, then the value of $\bar{\alpha}$ is equal to the underlined term (Equation 5-3). For the case of the baffle being out of the liquid during the slosh cycle in such a fashion that the inner rim of the ring baffle is not out of the fluid at any time, i.e.,

$$\frac{\zeta_1}{a} (1 - \frac{w}{a}) \leq \frac{d}{a} \leq \frac{\zeta_1}{a}$$

the underlined dotted terms are added to obtain the effective baffle area. For the case in which part of the baffle gets out of the liquid, i.e.,

$$\frac{d}{a} < \frac{\zeta_1}{a} (1 - \frac{w}{a})$$

the total formula applies. Thus, Miles Equation for a single flat ring baffle becomes

5.1.3.2.3 Bauer's Extension (31), (continued)

$$\gamma = 2.83 (\bar{\alpha})^{3/2} e^{-\frac{4.6d}{a}} (\zeta_1/a)^{1/2} \quad (5-4)$$

For a system of ring baffles, the damping factor can be obtained by superimposing the contribution of each baffle. The nth baffle at a location $d + (n-1)D$ below the free fluid surface exhibits an effective baffle area of

$$\begin{aligned} \bar{\alpha}_n = & \frac{w}{a} \left(2 - \frac{w}{a}\right) - \frac{1}{2} \left\{ 1 - \frac{\frac{d}{a} + (n-1) \frac{D}{a}}{\zeta_1/a} \right\} \\ & + \left(\frac{2}{\pi} \right) \left[\frac{\frac{d}{a} + (n-1) \frac{D}{a}}{\zeta_1/a} \right] \cdot \ln \left\{ \frac{\frac{\zeta_1}{a} + \sqrt{\frac{\zeta_1^2}{a^2} - \left(\frac{d}{a} + (n-1) \frac{D}{a}\right)^2}}{\frac{d}{a} + (n-1) \frac{D}{a}} \right\} \\ & - \left(\frac{1}{\pi} \right) \left[\frac{\frac{d}{a} + (n-1) \frac{D}{a}}{\zeta_1/a} \right] \cdot \sqrt{\left(\frac{\zeta_1}{a}\right)^2 - \left[\frac{d}{a} + (n-1) \frac{D}{a}\right]^2} \\ & + \left(\frac{1}{\pi} \right) \arcsin \left(\frac{\frac{d}{a} + (n-1) \frac{D}{a}}{\zeta_1/a} \right) - \left(\frac{1}{2} \right) \left(\frac{\frac{d}{a} + (n-1) \frac{D}{a}}{\zeta_1/a} \right) \\ & + \frac{1}{2} \left(1 - \frac{w}{a}\right)^2 \left\{ 1 - \frac{\frac{d}{a} + (n-1) \frac{D}{a}}{\left(1 - \frac{w}{a}\right) \zeta_1/a} \right\} \\ & - \frac{2}{\pi} \frac{\left[\frac{d}{a} + (n-1) \frac{D}{a}\right] \left(1 - \frac{w}{a}\right)}{\zeta_1/a} . \end{aligned}$$

5.1.3.2.3 Bauer's Extension (31) (continued)

$$\begin{aligned}
 & \ln \left[\frac{\frac{\zeta_1}{a} + \sqrt{\left(\frac{\zeta_1}{a}\right)^2 - \left[\frac{\frac{d}{a} + (n-1)\frac{D}{a}}{1 - \frac{w}{a}}\right]^2}}{\frac{\frac{d}{a} + (n-1)\frac{D}{a}}{1 - \frac{w}{a}}} \right] \\
 & + \frac{1}{\pi} \frac{\left[\frac{d}{a} + (n-1)\frac{D}{a}\right] (1 - \frac{w}{a})}{(\zeta_1/a)^2} \sqrt{\left(\frac{\zeta_1}{a}\right)^2 + \frac{\left[\frac{d}{a} + (n-1)\frac{D}{a}\right]^2}{(1 - \frac{w}{a})^2}} \\
 & - \frac{1}{\pi} (1 - \frac{w}{a})^2 \arcsin \left[\frac{\frac{d}{a} + (n-1)\frac{D}{a}}{(1 - \frac{w}{a})\zeta_1/a} \right] \\
 & + \frac{1}{2} (1 - \frac{w}{a}) \left[\frac{\frac{d}{a} + (n-1)\frac{D}{a}}{\zeta_1/a} \right] \tag{5-5}
 \end{aligned}$$

If

$$\frac{d}{a} + (n-1)\frac{D}{a} \geq \frac{\zeta_1}{a}$$

then

$$\bar{\alpha}_n = \alpha = \frac{w}{a} (2 - \frac{w}{a}) \tag{5-6}$$

because the complete baffle is submerged.

If

$$\frac{\zeta_1}{a} (1 - \frac{w}{a}) \leq \frac{d}{a} + (n-1)\frac{D}{a} \leq \frac{\zeta_1}{a}$$

then the underlined formula is added, while for the case

5.1.3.2.3 Bauer's Extension (31) (continued)

$$\frac{d}{a} + (n-1) \frac{D}{a} < \frac{\zeta_1}{a} \left(1 - \frac{w}{a}\right)$$

the complete formula applies.

For a baffle located above the undisturbed liquid surface, the same formula can be applied approximately with a slight modification.

If the baffle is completely out of the liquid, i.e.,

$$\frac{\zeta_1}{a} \leq \frac{d^*}{a},$$

where $d^* = (D - d)$ is the distance of the baffle above the undisturbed liquid surface, the baffle area subjected to the fluid is $\bar{\alpha}^* = 0$. The value D is the distance between baffles. For

$$\frac{d^*}{a} < \frac{\zeta_1}{a} \leq \frac{d^*/a}{1 - \frac{w}{a}} \quad \text{and} \quad \frac{\zeta_1}{a} \geq \frac{d^*/a}{1 - \frac{w}{a}},$$

i.e., only a part of the baffle is subjected to the liquid during a slosh cycle, then the effective baffle area contributing to the damping is

$\bar{\alpha}^* = \alpha - \bar{\alpha}$. For the m th baffle, this is

$$\bar{\alpha}_m^* = \frac{1}{2} \left(1 - \frac{m \frac{D}{a} - \frac{d}{a}}{\zeta_1/a}\right) - \frac{2}{\pi} \frac{\left(m \frac{D}{a} - \frac{d}{a}\right)}{\zeta_1/a} \ln \left[\frac{\frac{\zeta_1}{a} + \sqrt{\left(\frac{\zeta_1}{a}\right)^2 - \left[m \frac{D}{a} - \frac{d}{a}\right]^2}}{m \frac{D}{a} - \frac{d}{a}} \right] +$$

5.1.3.2.3 Bauer's Extension (31) (continued)

$$\begin{aligned}
 & + \frac{1}{\pi} \frac{\left[m \frac{D}{a} - \frac{d}{a} \right]}{(\zeta_1/a)^2} \sqrt{\left(\frac{\zeta_1}{a} \right)^2 - \left(m \frac{D}{a} - \frac{d}{a} \right)^2} - \frac{1}{\pi} \arcsin \left[\frac{m \frac{D}{a} - \frac{d}{a}}{\zeta_1/a} \right] + \\
 & + \frac{1}{2} \frac{\left(m \frac{D}{a} - \frac{d}{a} \right)}{\zeta_1/a} - \frac{1}{2} \left(1 - \frac{w}{a} \right)^2 \left\{ 1 - \frac{\left(m \frac{D}{a} - \frac{d}{a} \right)}{\left(1 - \frac{w}{a} \right) \zeta_1/a} \right\} + \\
 & + \frac{2}{\pi} \frac{\left(m \frac{D}{a} - \frac{d}{a} \right) \left(1 - \frac{w}{a} \right)}{\zeta_1/a} \ln \frac{\frac{\zeta_1}{a} + \sqrt{\left(\frac{\zeta_1}{a} \right)^2 - \left(\frac{m \frac{D}{a} - \frac{d}{a}}{\left(1 - \frac{w}{a} \right)^2} \right)}}{\left(m \frac{D}{a} - \frac{d}{a} \right) \left(1 - \frac{w}{a} \right)} \\
 & - \frac{1}{\pi} \frac{\left[m \frac{D}{a} - \frac{d}{a} \right] \left(1 - \frac{w}{a} \right)}{(\zeta_1/a)^2} \sqrt{(\zeta_1/a)^2 - \left[\frac{m \frac{D}{a} - \frac{d}{a}}{\left(1 - \frac{w}{a} \right)} \right]^2} + \\
 & + \frac{1}{\pi} \left(1 - \frac{w}{a} \right)^2 \arcsin \left\{ \frac{\left(m \frac{D}{a} - \frac{d}{a} \right)}{\left(1 - \frac{w}{a} \right) \zeta_1/a} \right\} - \frac{1}{2} \left(1 - \frac{w}{a} \right) \frac{\left[m \frac{D}{a} - \frac{d}{a} \right]}{\zeta_1/a} .
 \end{aligned}$$

(5-7)

5.1.3.2.3 Bauer's Extension (31) (continued)

If the value

$$m \frac{D}{a} - \frac{d}{a} \geq \frac{\zeta_1}{a},$$

then $\bar{\alpha}_m^* = 0$, while for the case where a partial part of the baffle is only subjected to the liquid during one slosh cycle, the effective area contributing to damping is presented by the underlined part of the formula. This means that this part is used for

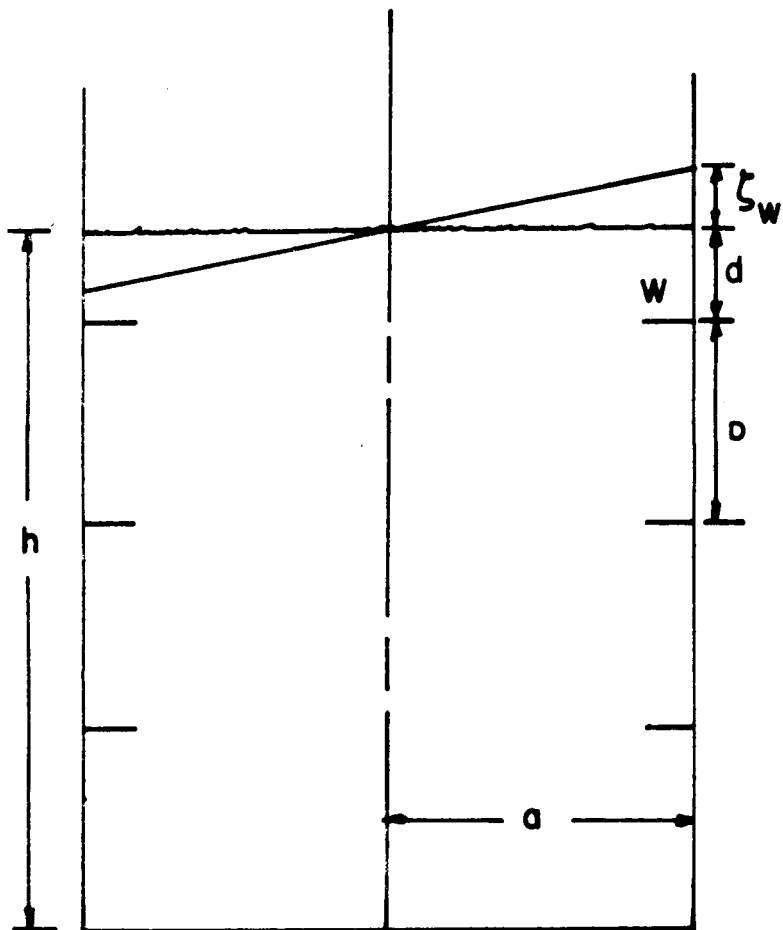
$$\frac{\zeta_1}{a} \left(1 - \frac{w}{a}\right) \leq \frac{D}{a} - \frac{d}{a} \leq \frac{\zeta_1}{a}.$$

$$m \frac{D}{a} - \frac{d}{a} \leq \frac{\zeta_1}{a} \left(1 - \frac{w}{a}\right),$$

the total formula is applied for the effective area. Thus the total damping of n baffles of width w submerged into the undisturbed liquid and m baffles of the same width outside of the undisturbed fluid, all of which are apart from each other by the value D , is given by

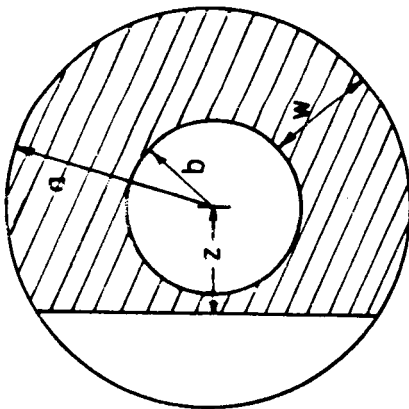
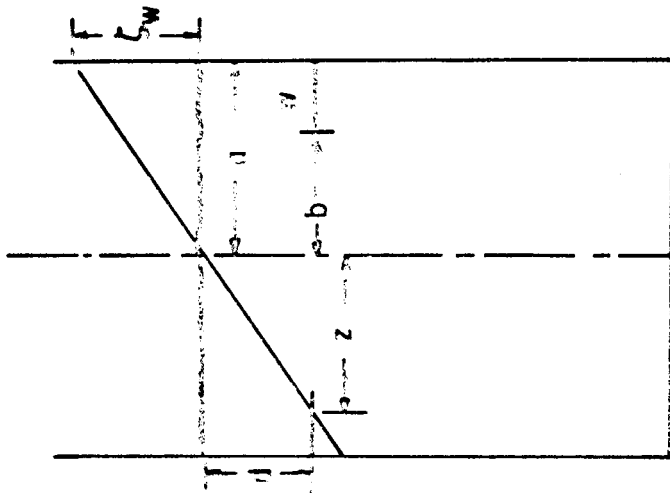
$$\gamma_s = 2.83 \sqrt{\frac{\zeta_1}{a}} \left\{ \sum_{n=1}^N e^{-4.6 \left[\frac{d}{a} + (n-1) \frac{D}{a} \right]} \cdot \bar{\alpha}_n^{3/2} + \sum_{m=1}^M e^{-4.6 \left(m \frac{D}{a} - \frac{d}{a} \right)} \bar{\alpha}_m^{*3/2} \right\}. \quad (5-8)$$

The result of this investigation can be seen in Figures 5-31 to 5-63.



TANK CONFIGURATION AND BAFFLE ARRANGEMENT

Figure 5-30



ANNULAR RING BAFFLE PARTIALLY OUT OF LIQUID
DURING SLOSH CYCLE

Figure 5-31

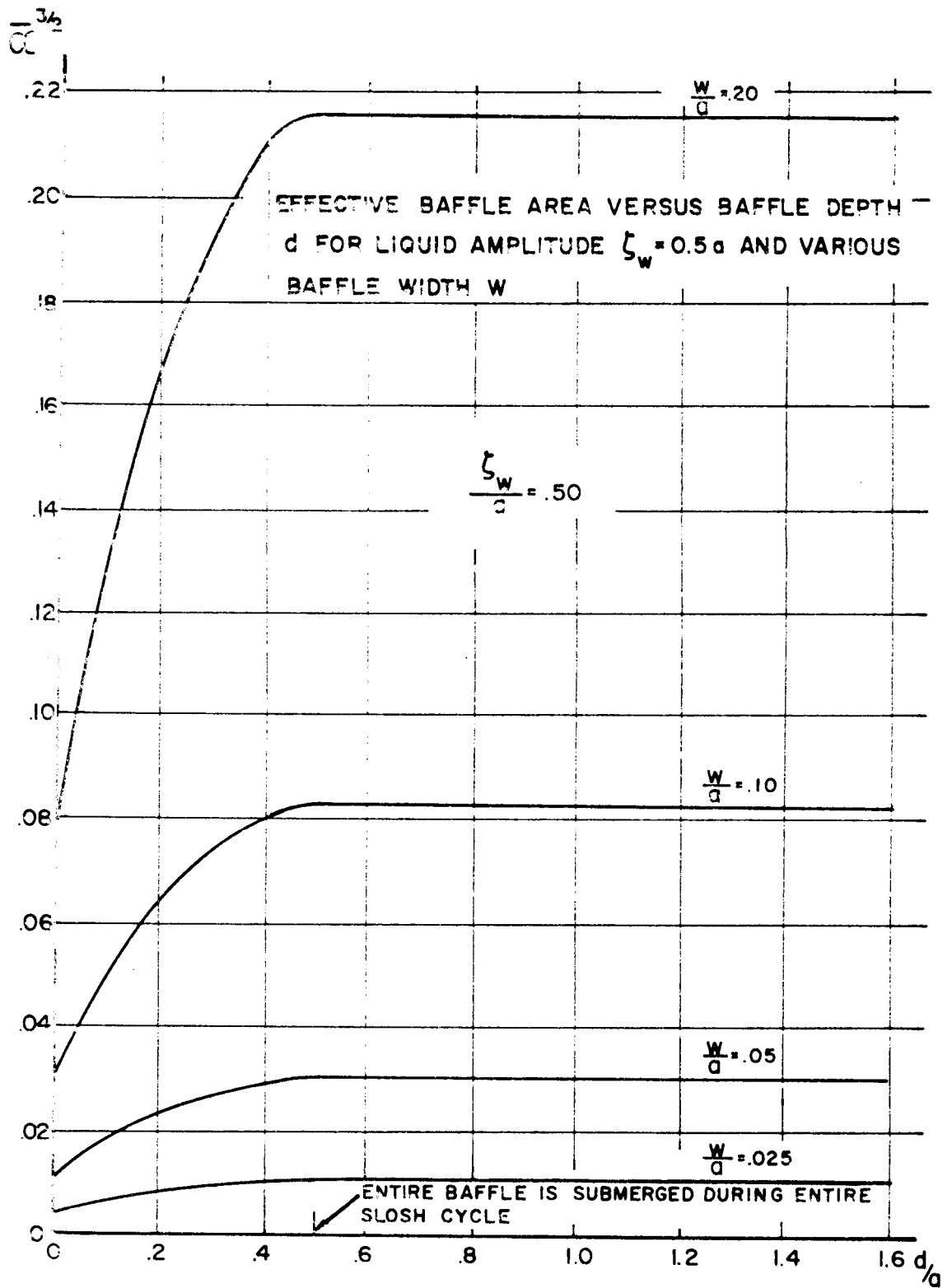


Figure 5-32

EFFECTIVE BAFFLE AREA VERSUS BAFFLE DEPTH
 d FOR LIQUID AMPLITUDE $\zeta_w = 0.5d$ AND VARIOUS
 BAFFLE WIDTH W

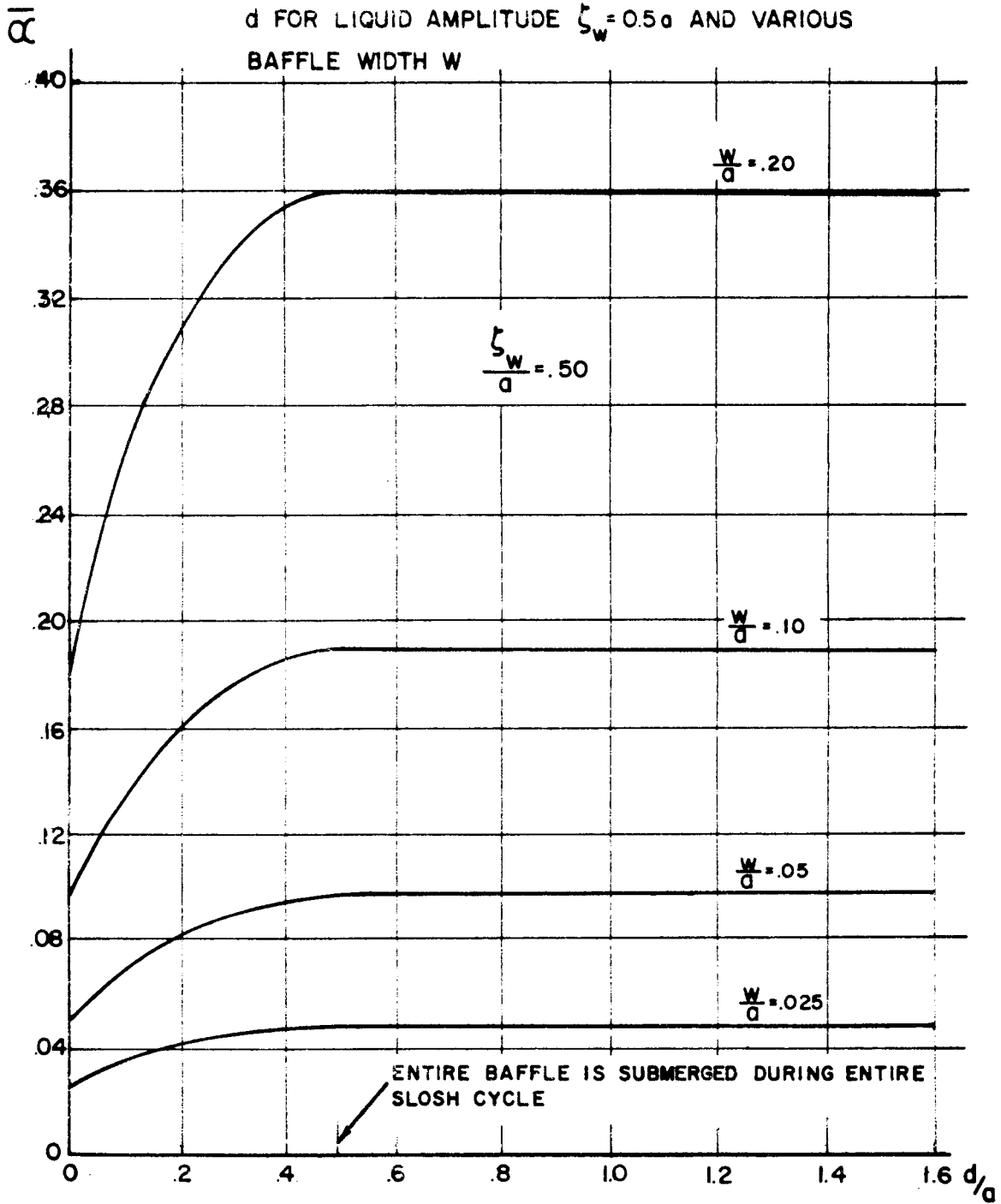


figure 5-33

EFFECTIVE BAFFLE AREA VERSUS BAFFLE DEPTH
 d FOR CONSTANT BAFFLE WIDTH $w=0.1a$ AND
 VARIOUS SURFACE AMPLITUDE ζ_w

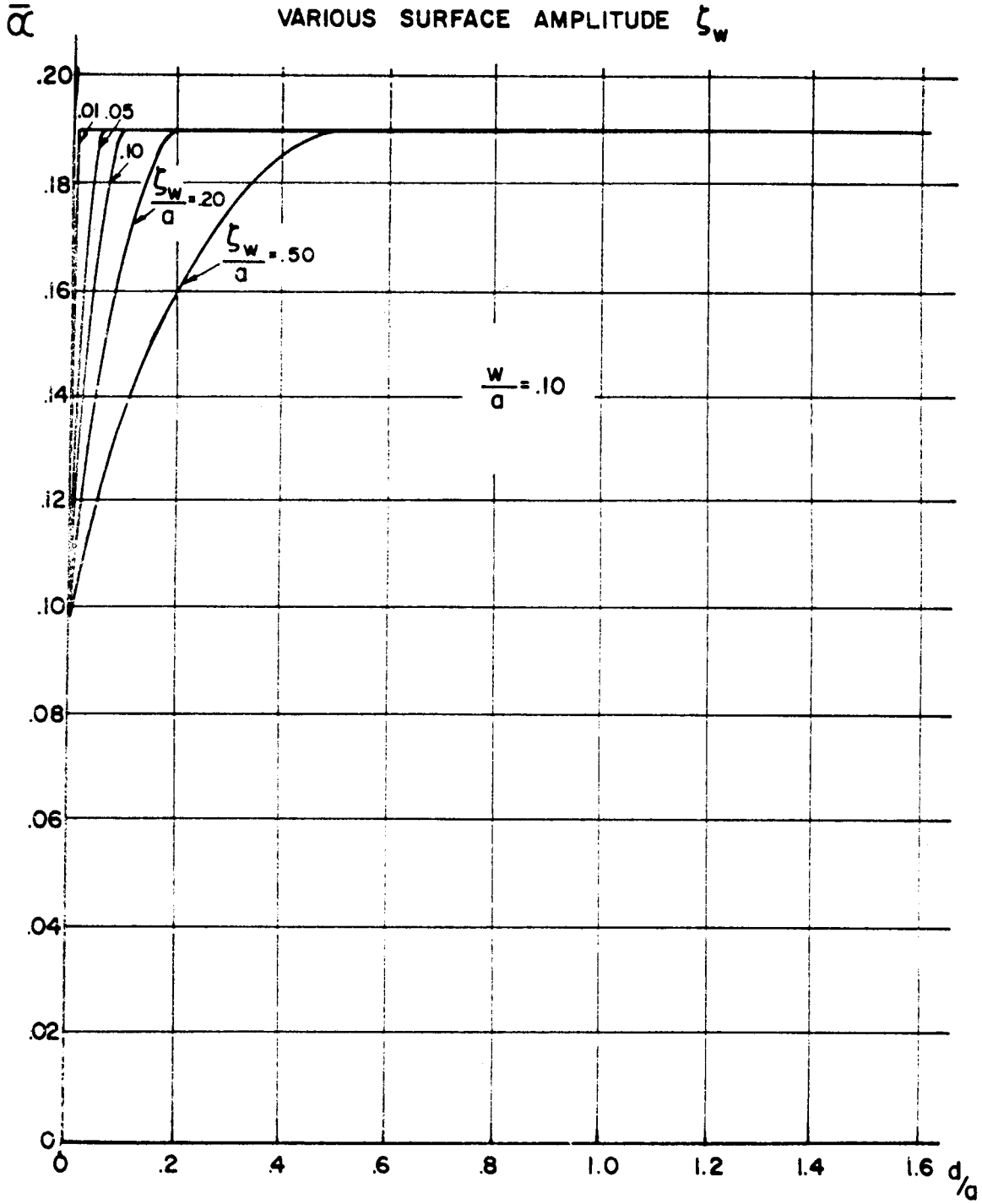


Figure 5-34

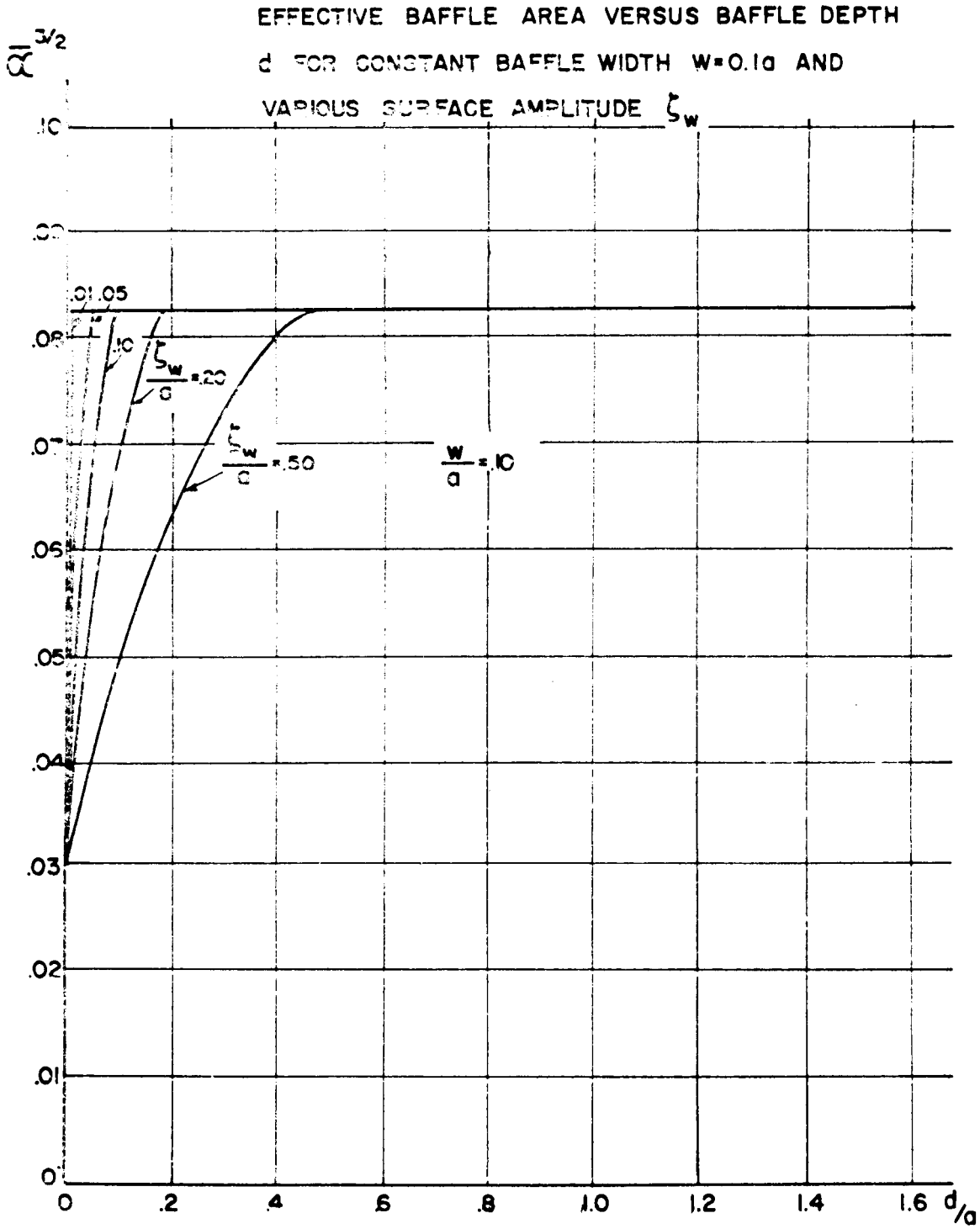


Figure 5-35

DAMPING FACTOR VERSUS BAFFLE DEPTH FOR
 LIQUID AMPLITUDE $\zeta_w = 0.01a$ WITH THE BAFFLE
 WIDTH AS A PARAMETER (MILES FORMULA)

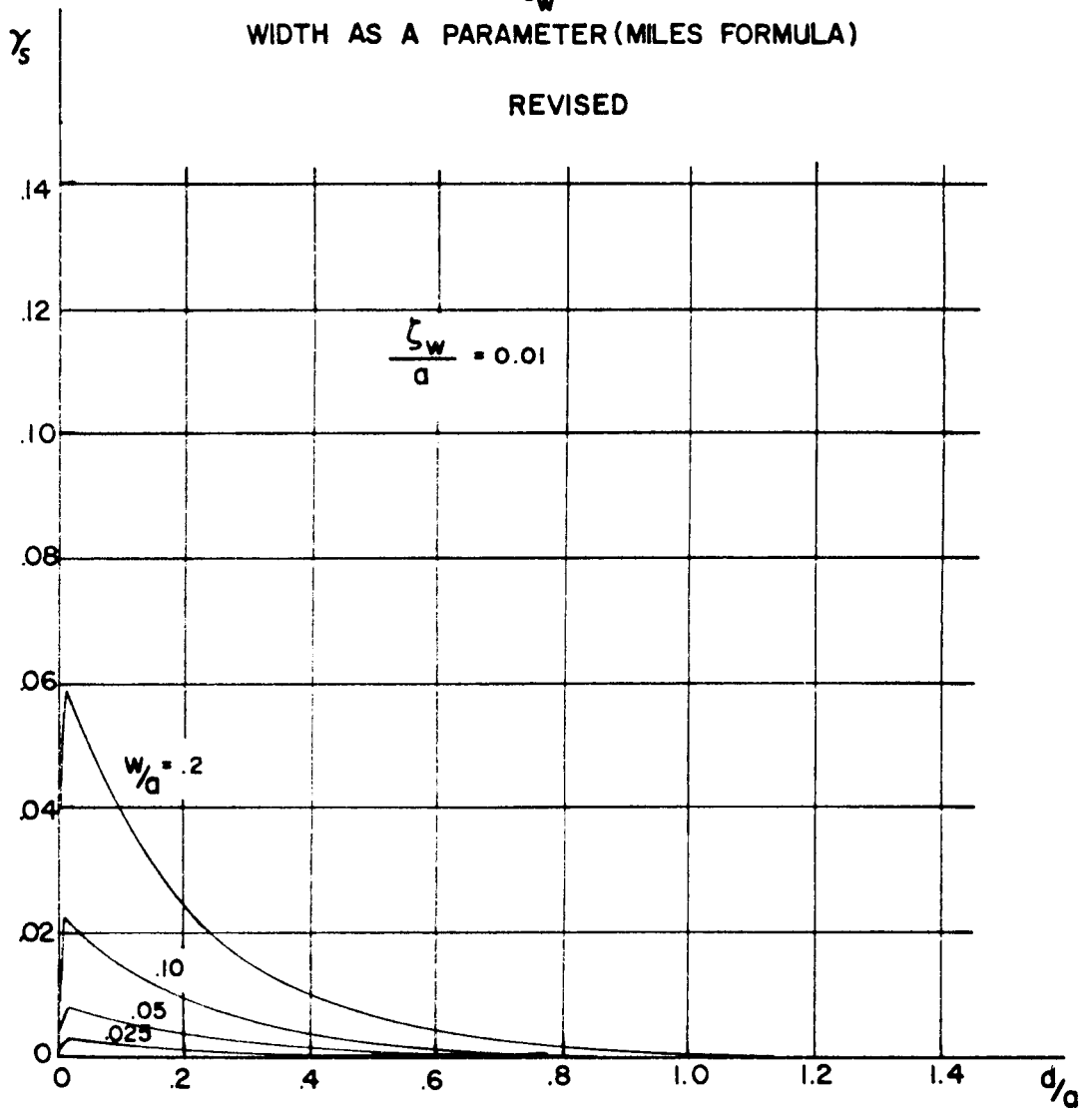


Figure 5-36

DAMPING FACTOR VERSUS BAFFLE DEPTH FOR
 LIQUID AMPLITUDE $\zeta_w = 0.05a$ WITH THE BAFFLE
 WIDTH AS A PARAMETER (MILES FORMULA)
 REVISED

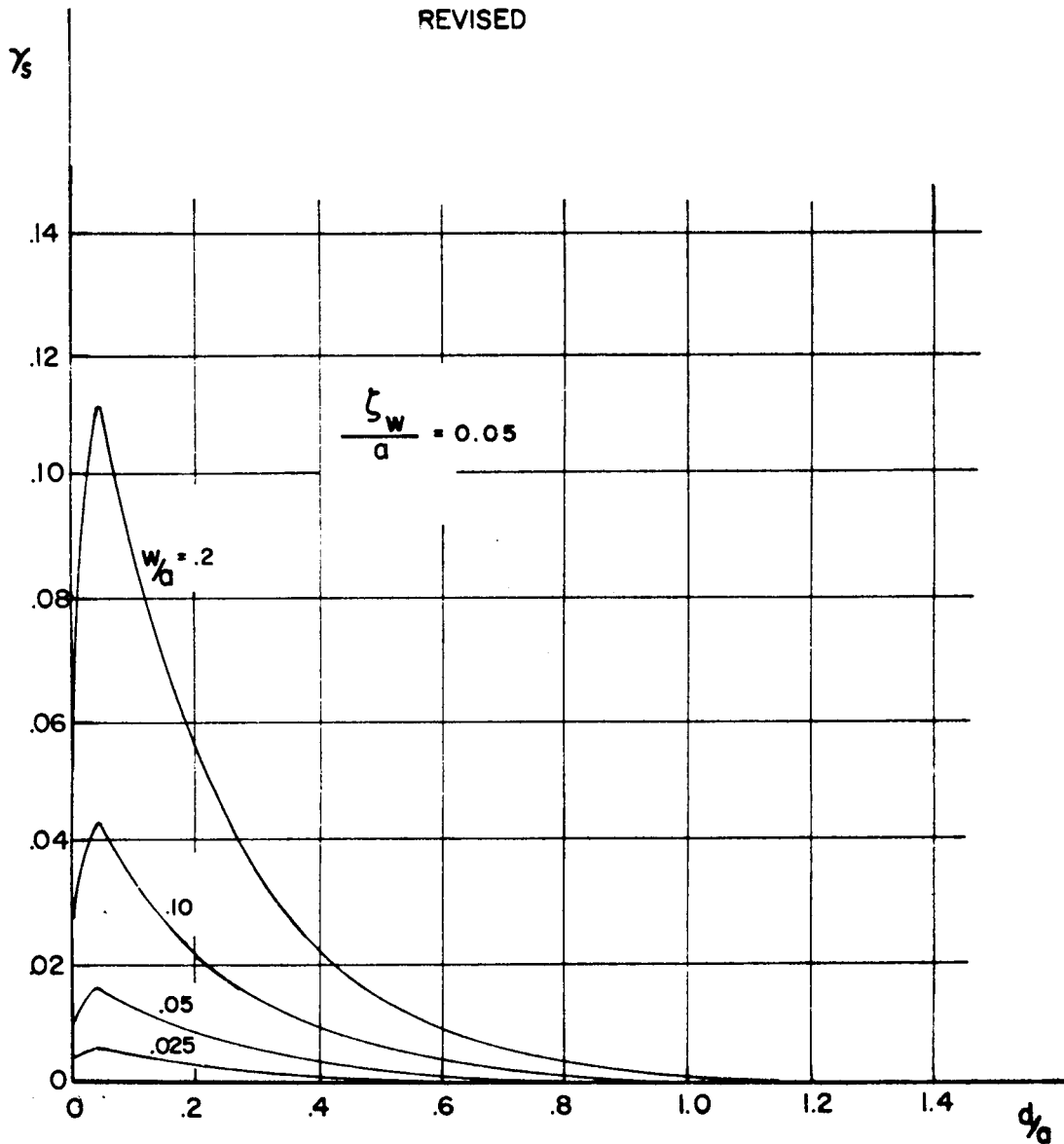


Figure 5-37

DAMPING FACTOR VERSUS BAFFLE DEPTH FOR
 LIQUID AMPLITUDE $\zeta_w = 0.10g$ WITH THE BAFFLE
 WIDTH AS A PARAMETER (MILES FORMULA)
 REVISED

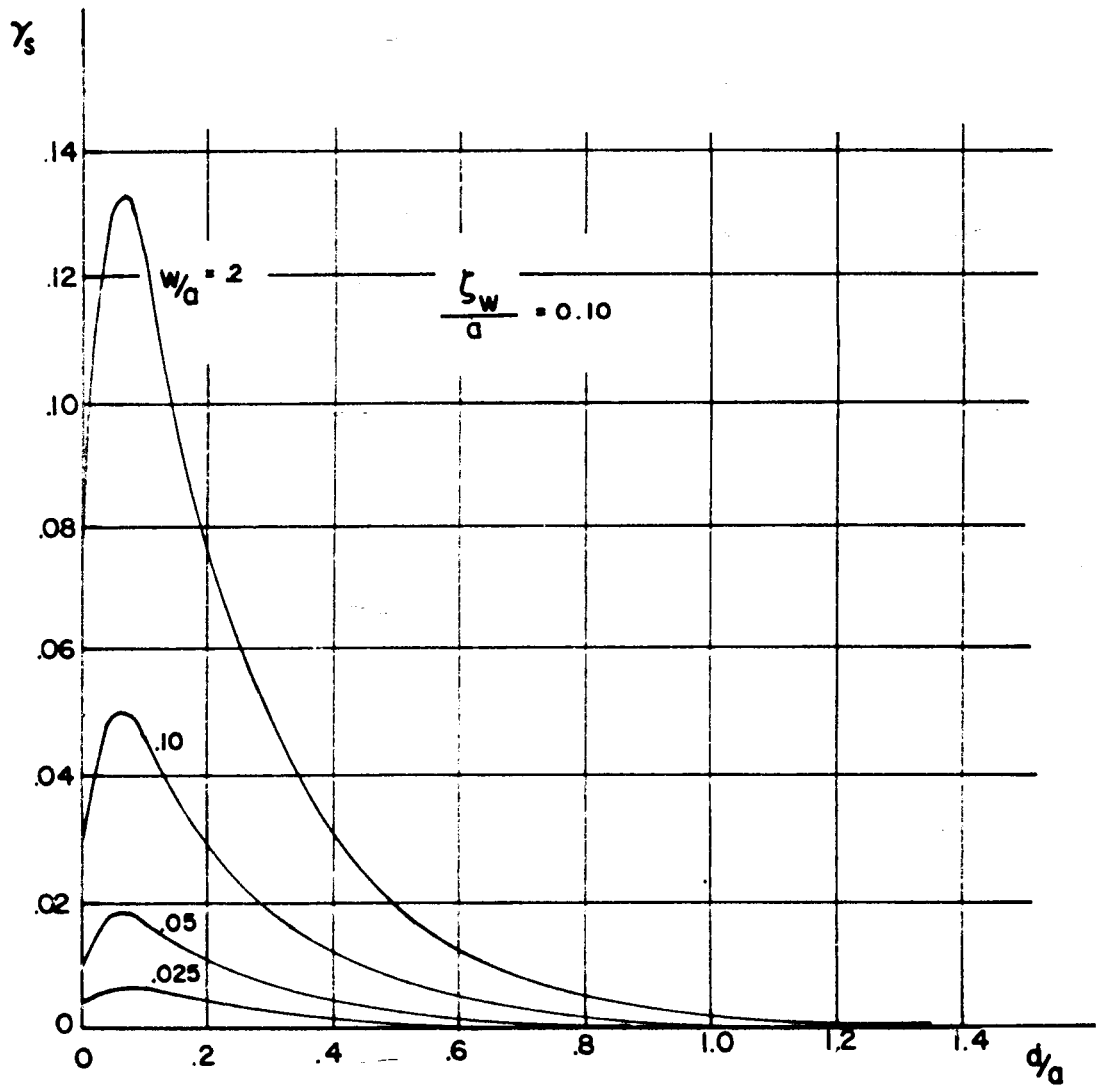


Figure 5-38

DAMPING FACTOR VERSUS BAFFLE DEPTH FOR
 LIQUID AMPLITUDE $\zeta_w = 0.20a$ WITH THE BAFFLE
 WIDTH AS A PARAMETER (MILES FORMULA)
 REVISED

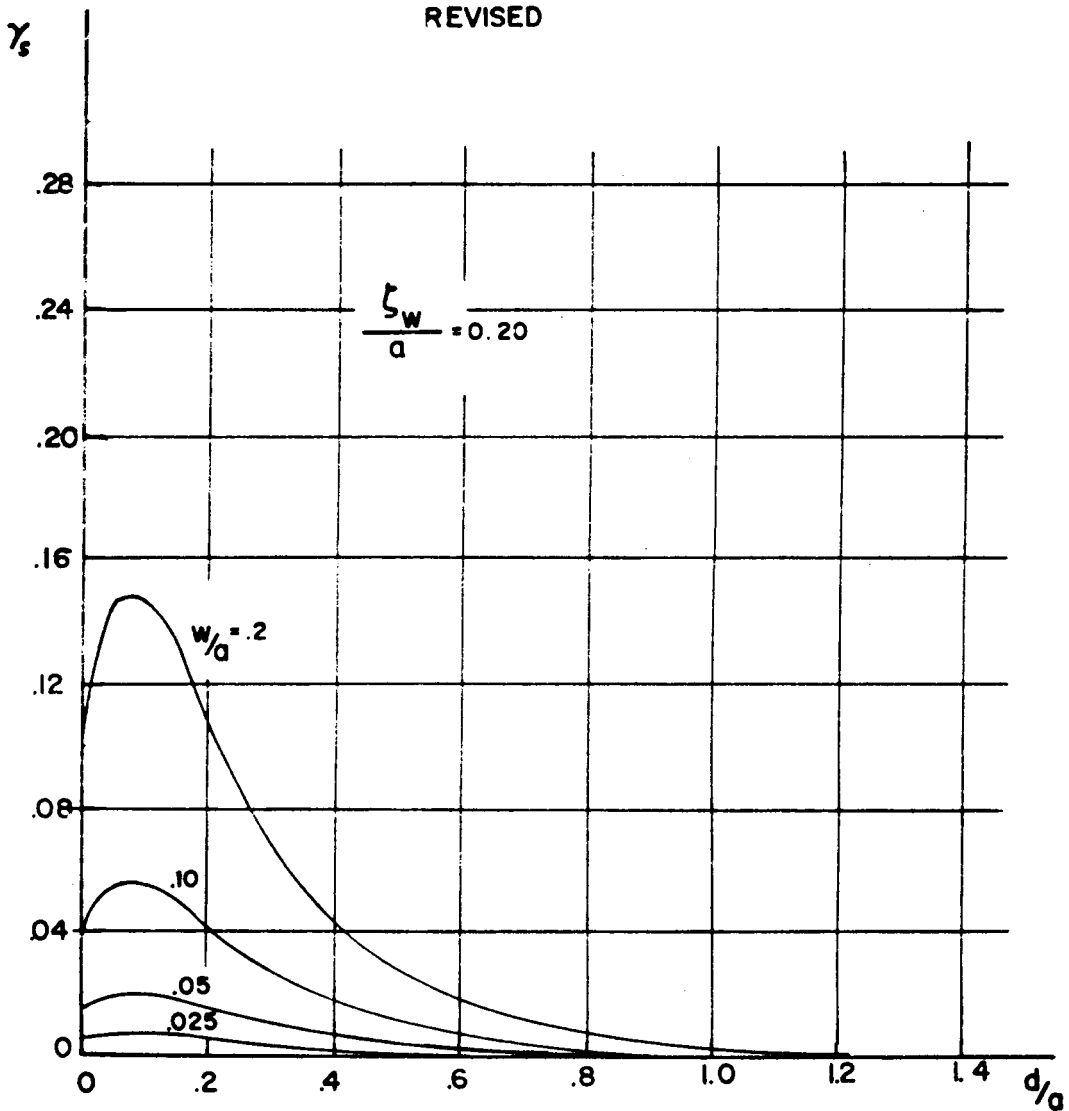


Figure 5-39

DAMPING FACTOR VERSUS BAFFLE DEPTH FOR
 LIQUID AMPLITUDE $\zeta_w = 0.50a$ WITH THE BAFFLE
 WIDTH AS A PARAMETER (MILES FORMULA)
 REVISED

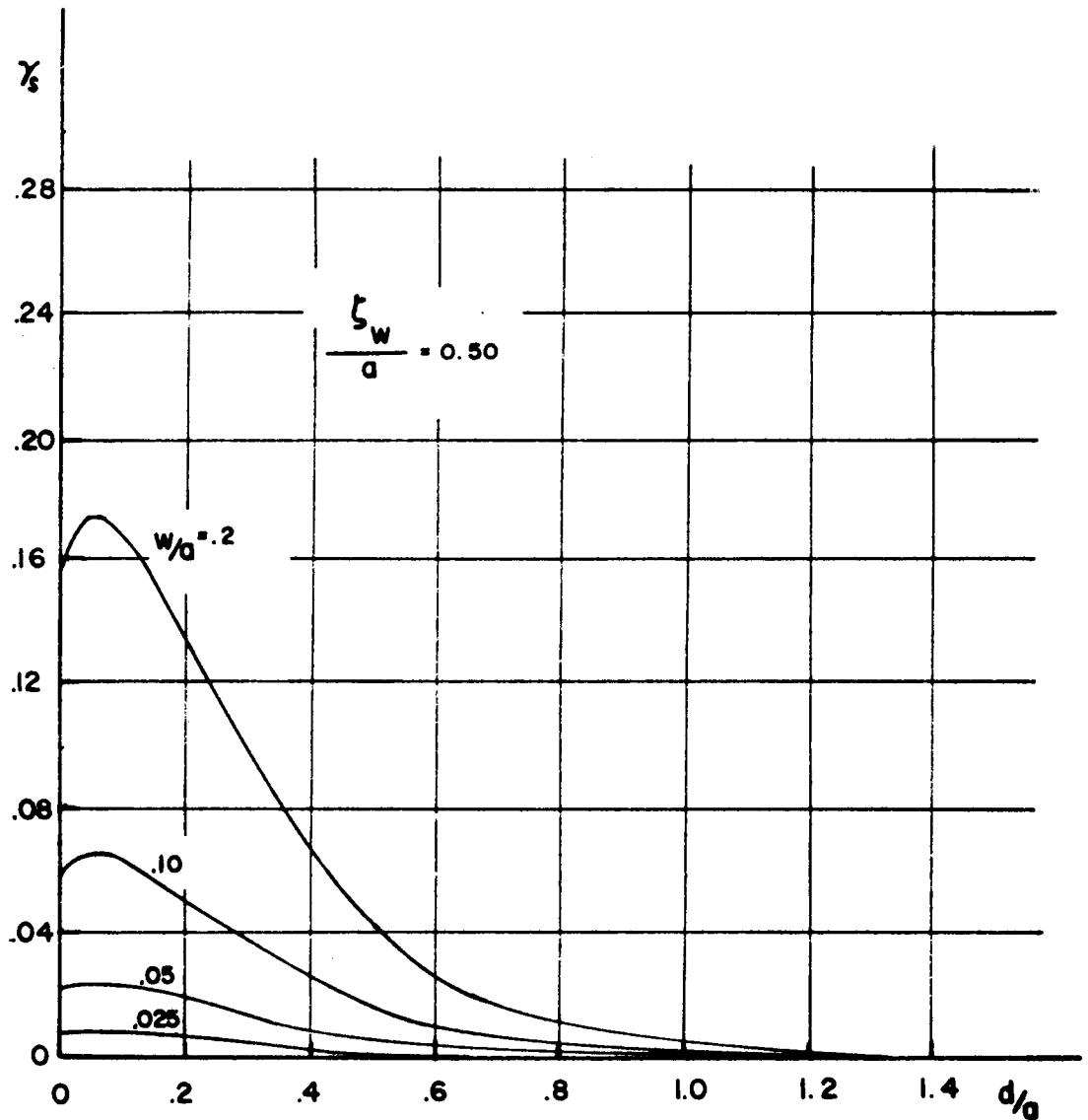


Figure 5-40

DAMPING FACTOR VERSUS BAFFLE DEPTH FOR WIDTH
W=0.025a WITH LIQUID AMPLITUDE AS A PARAMETER
(MILES FORMULA)

REVISED

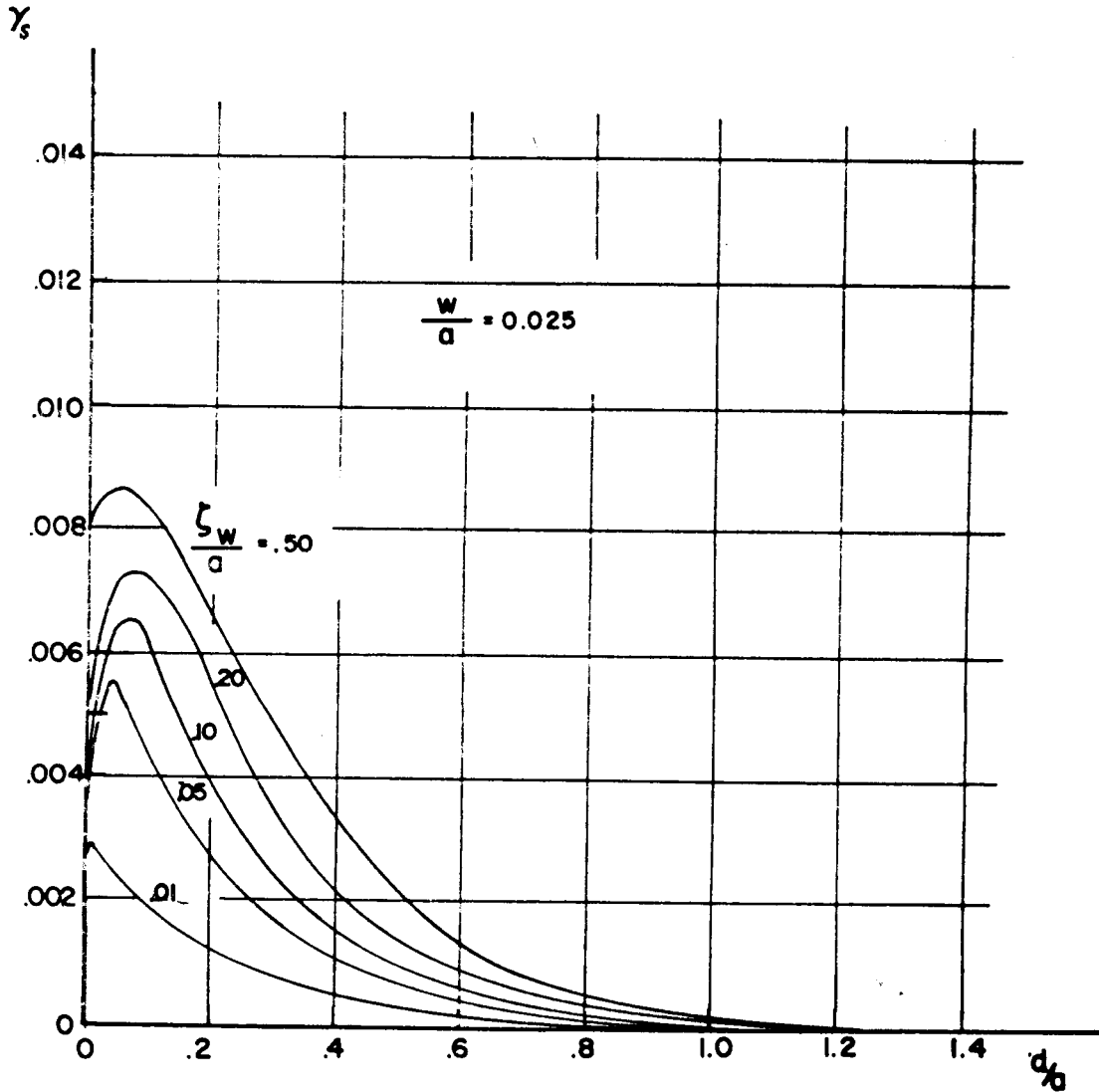


Figure 5-41

DAMPING FACTOR VERSUS BAFFLE DEPTH FOR WIDTH
 $W=0.05a$ WITH LIQUID AMPLITUDE AS A PARAMETER
(MILES FORMULA)
REVISED

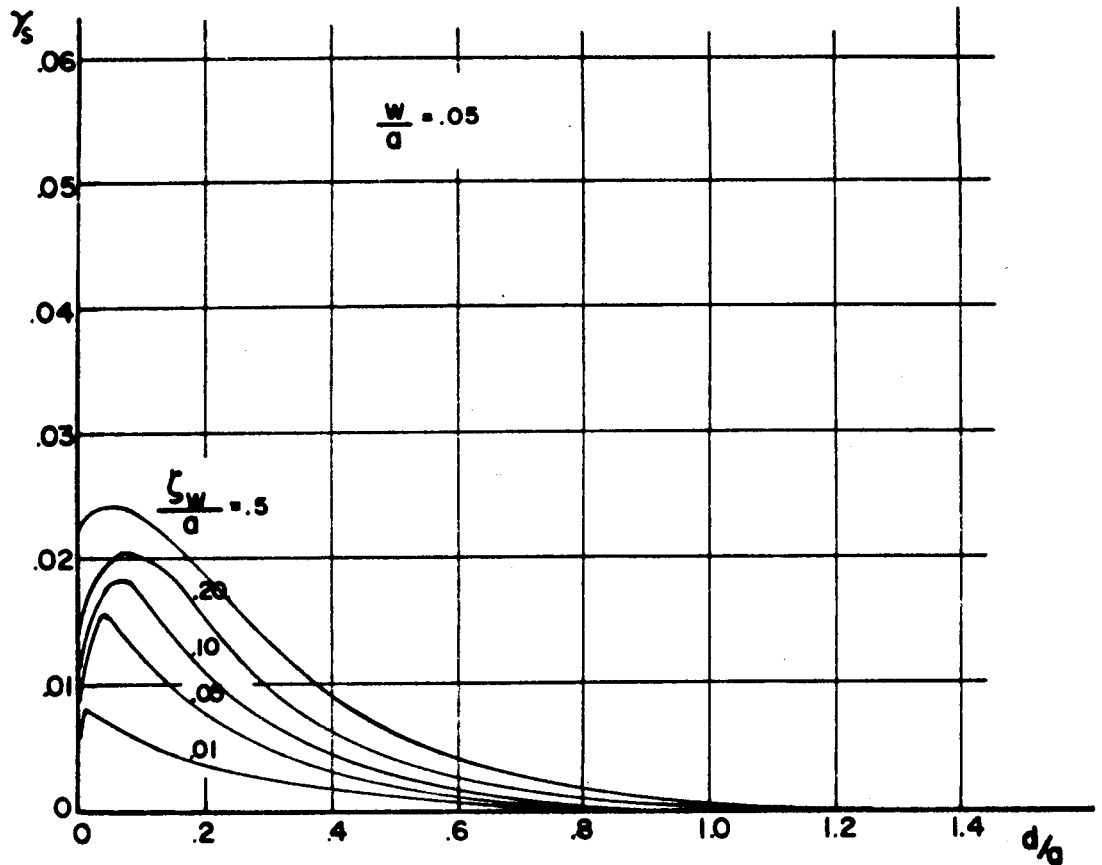


Figure 5-42

DAMPING FACTOR VERSUS BAFFLE DEPTH FOR WIDTH
 $W = .10g$ WITH LIQUID AMPLITUDE AS A PARAMETER
(MILES FORMULA)

REVISED

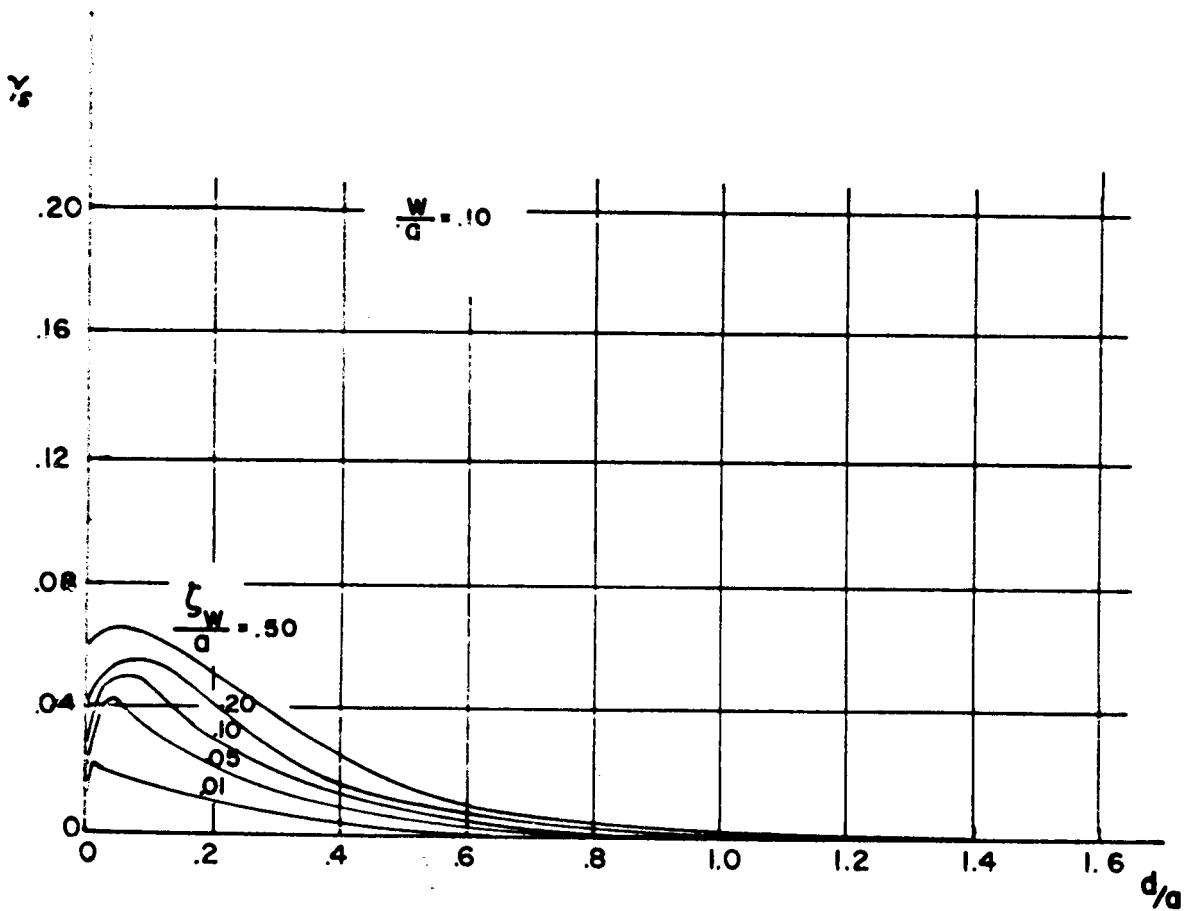


Figure 5-43

DAMPING FACTOR VERSUS BAFFLE DEPTH FOR WIDTH
 $W=0.20a$ WITH LIQUID AMPLITUDE AS A PARAMETER
(MILES FORMULA)

REVISED

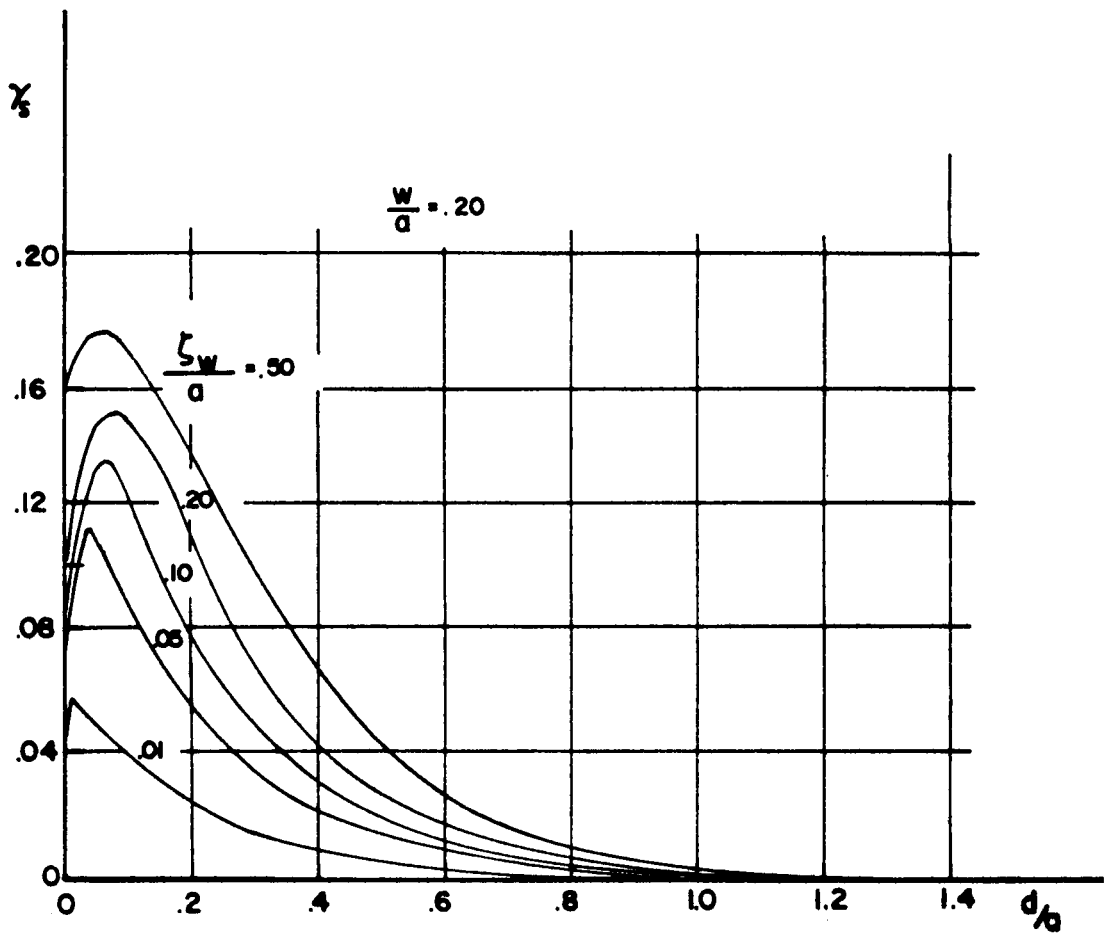


Figure 5-44

DAMPING FACTOR VERSUS SURFACE AMPLITUDE FOR
 BAFFLE WIDTH $W = .05a$ WITH BAFFLE LOCATION AS
 A PARAMETER (MILES FORMULA)

REVISED

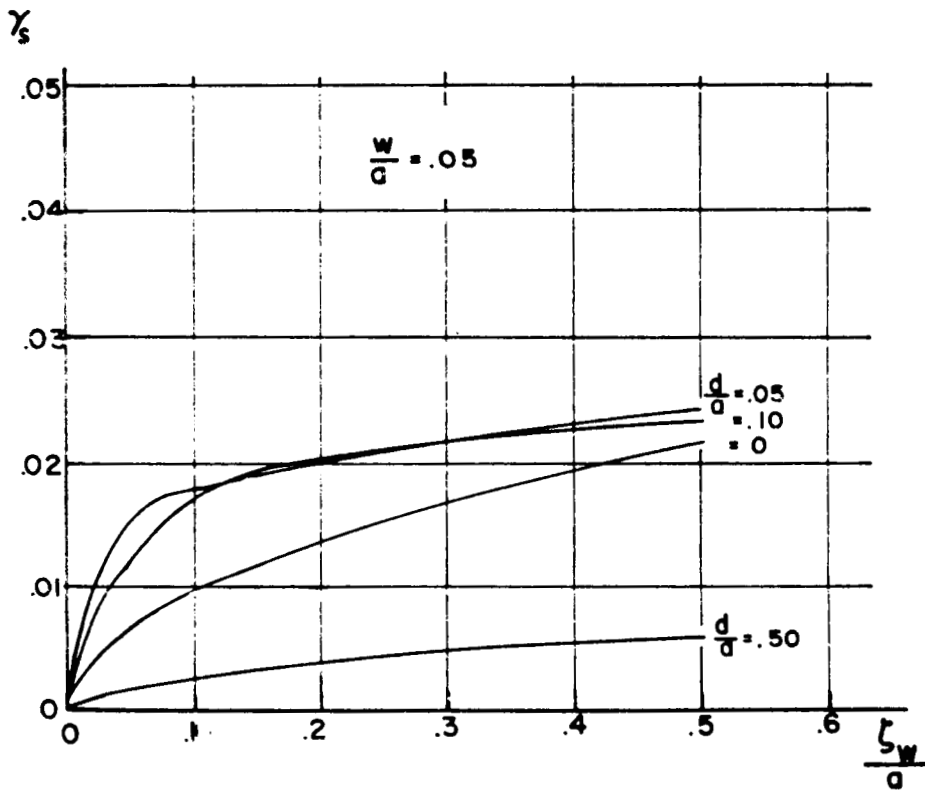


Figure 5-45

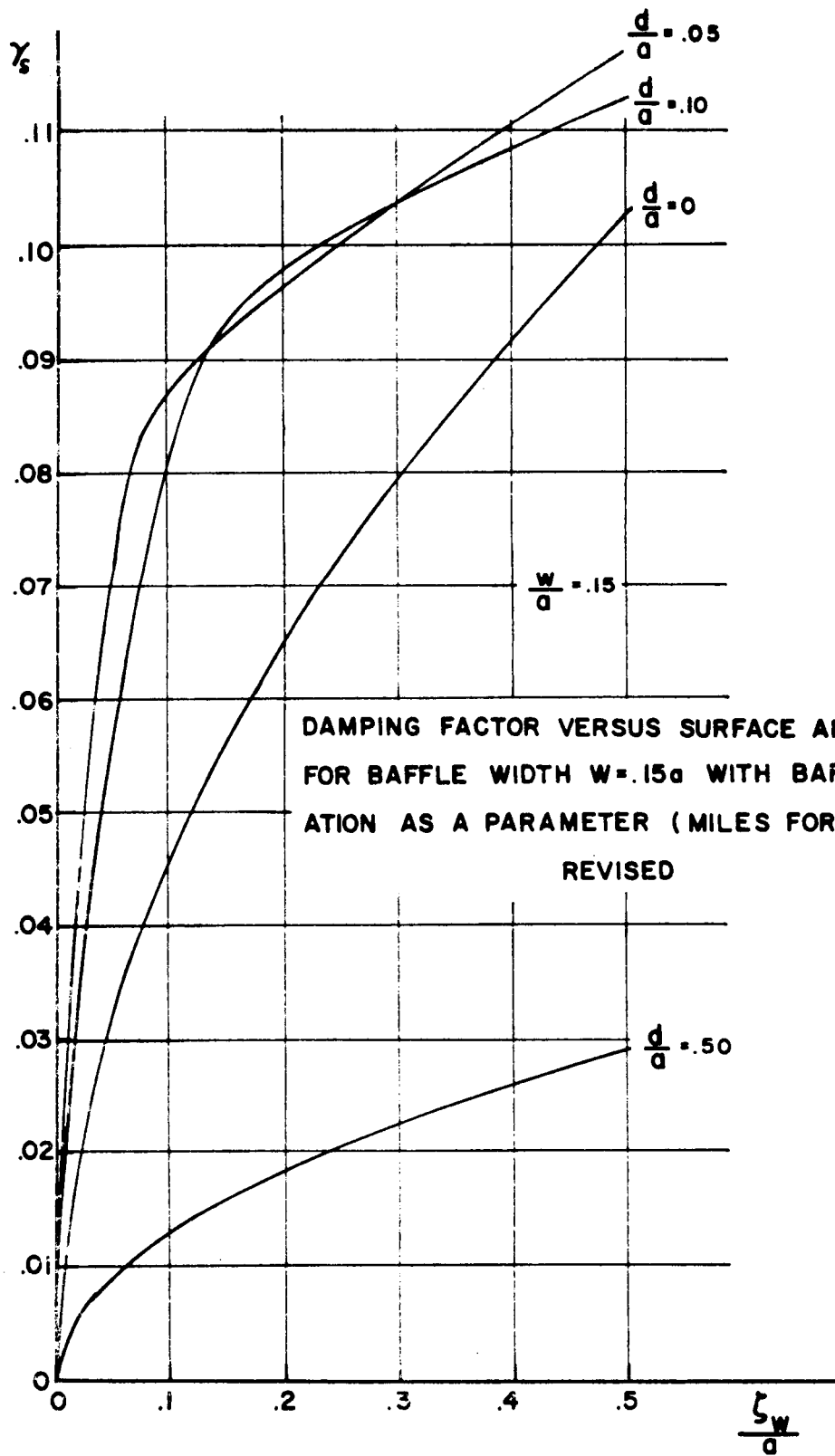


Figure 5-46

DAMPING FACTOR VERSUS BAFFLE WIDTH FOR
 $\zeta_w = .10a$ WITH LOCATION OF BAFFLE AS A PARAMETER
(MILES FORMULA)
REVISED

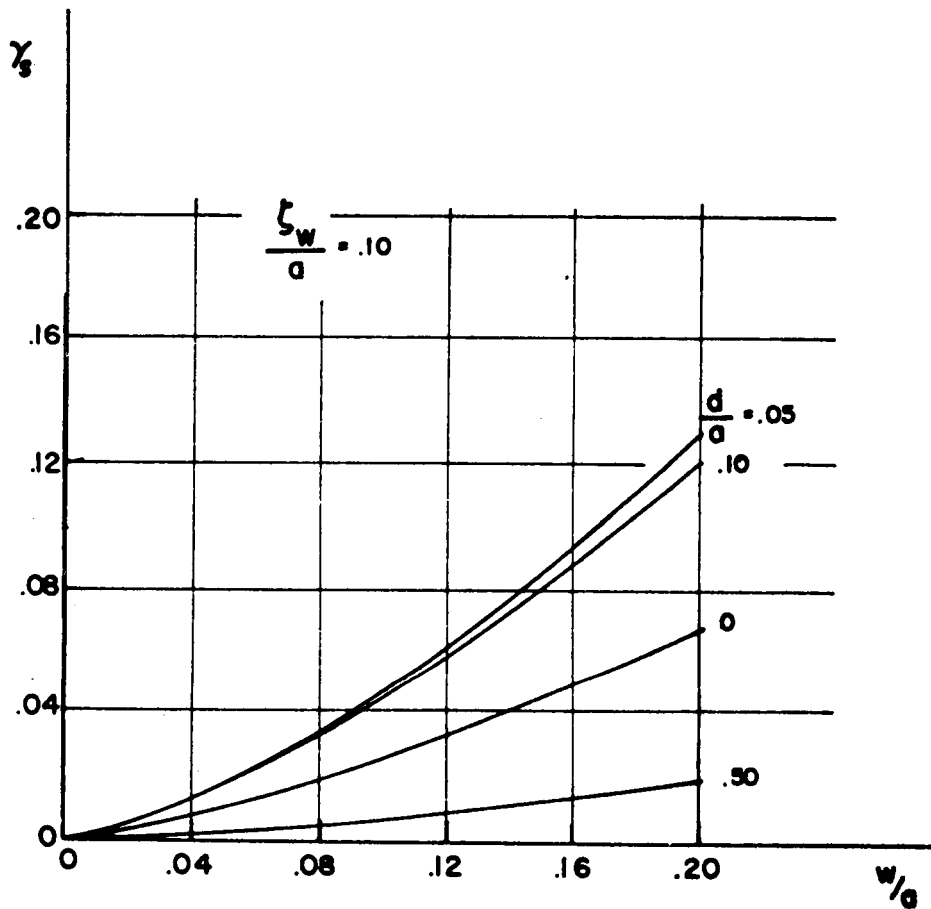


Figure 5-47

DAMPING FACTOR VERSUS BAFFLE WIDTH FOR
 $\zeta_w = .30a$ WITH LOCATION OF BAFFLE AS A PARAMETER
 (MILES FORMULA)
 REVISED

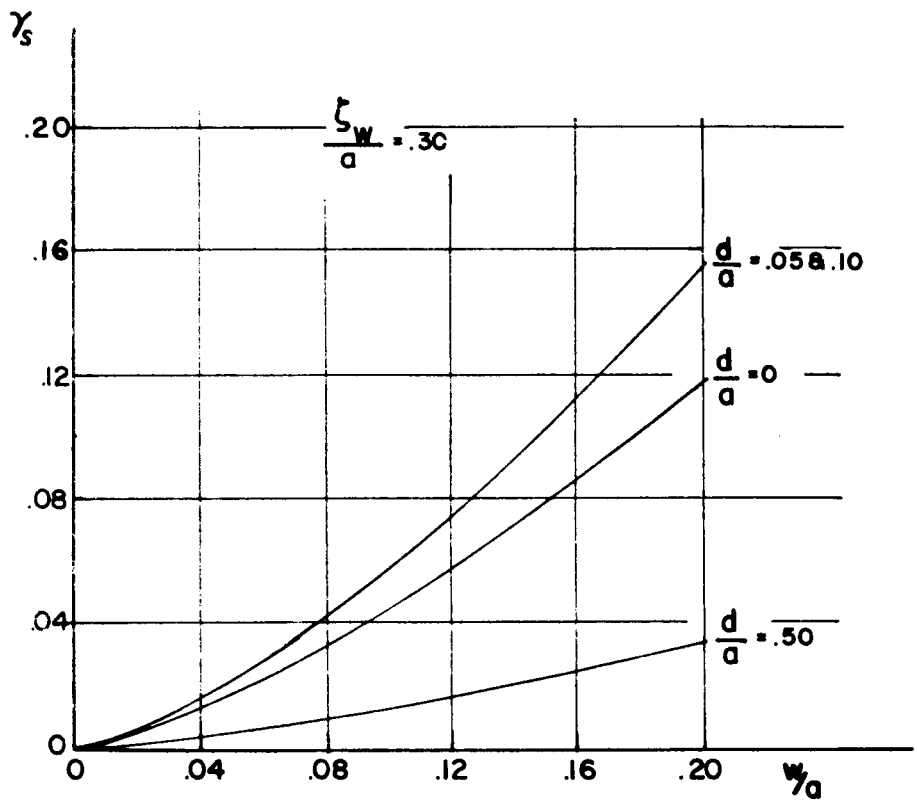


Figure 5-48

DAMPING FACTOR VERSUS BAFFLE DEPTH FOR
 VARIOUS BAFFLE WIDTHS AND A LIQUID AMPLITUDE
 OF $\zeta_w = 0.01a$ AND A BAFFLE DISTANCE FROM EACH
 OTHER $D = 0.2a$

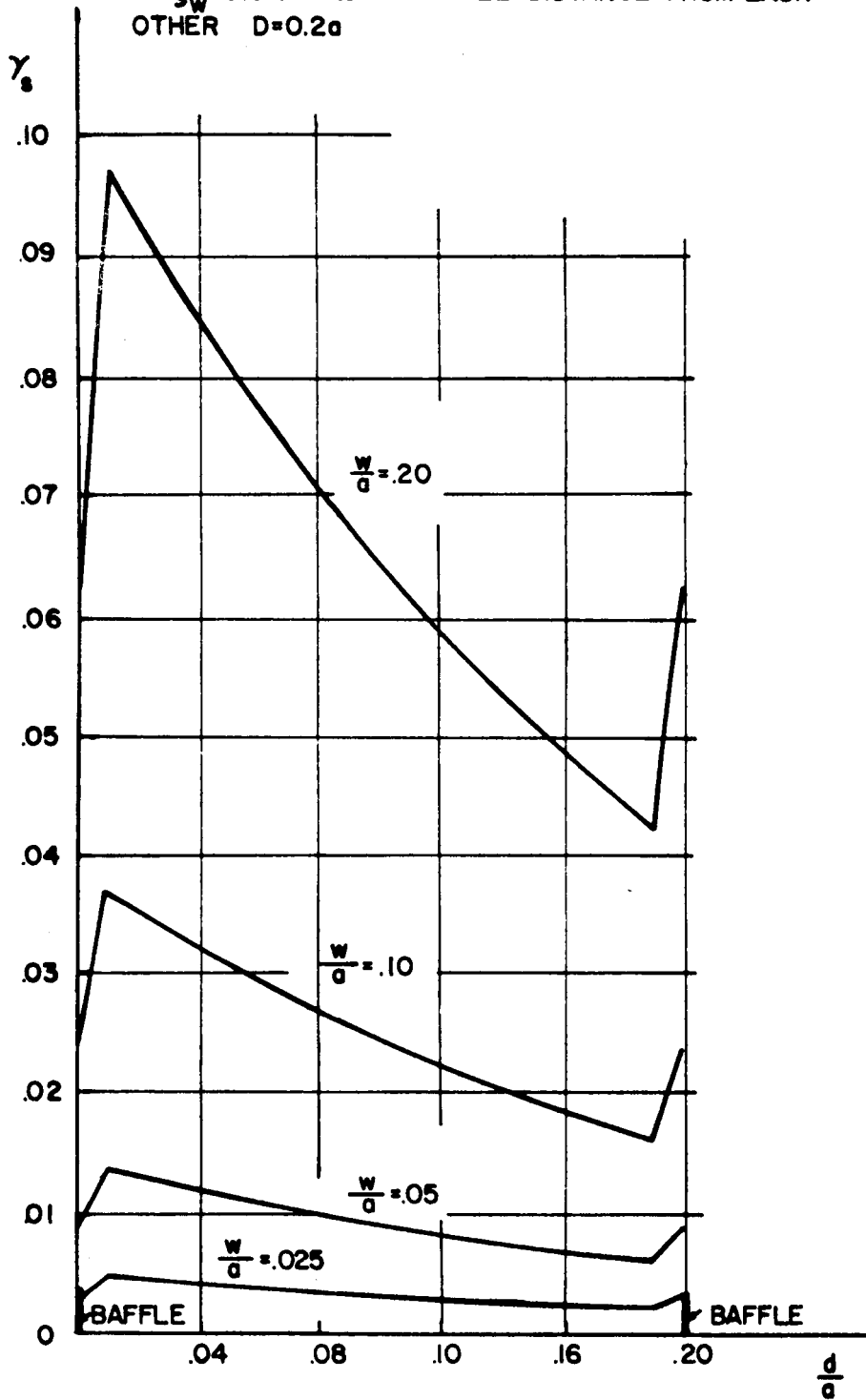


Figure 5-49

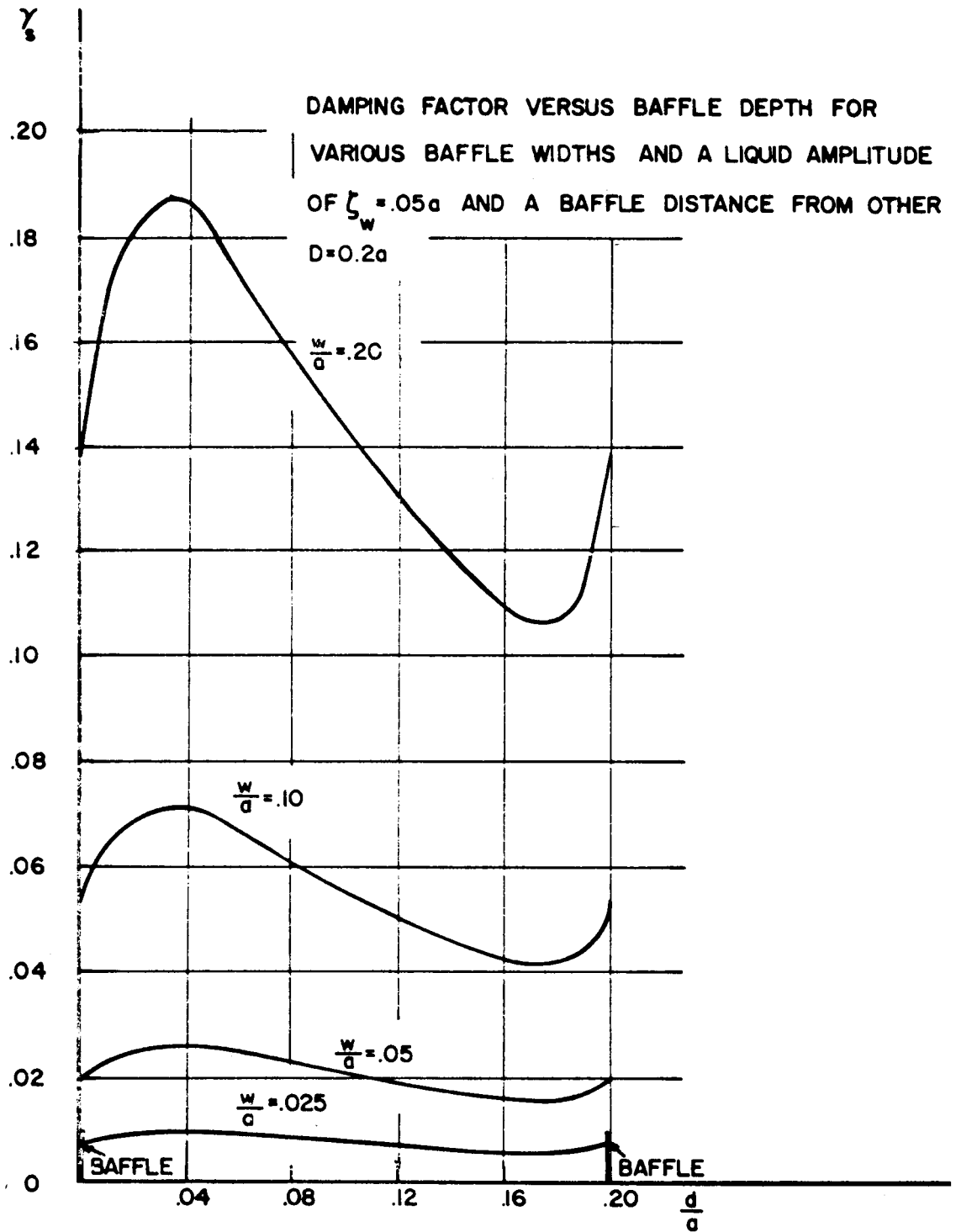


Figure 5-50

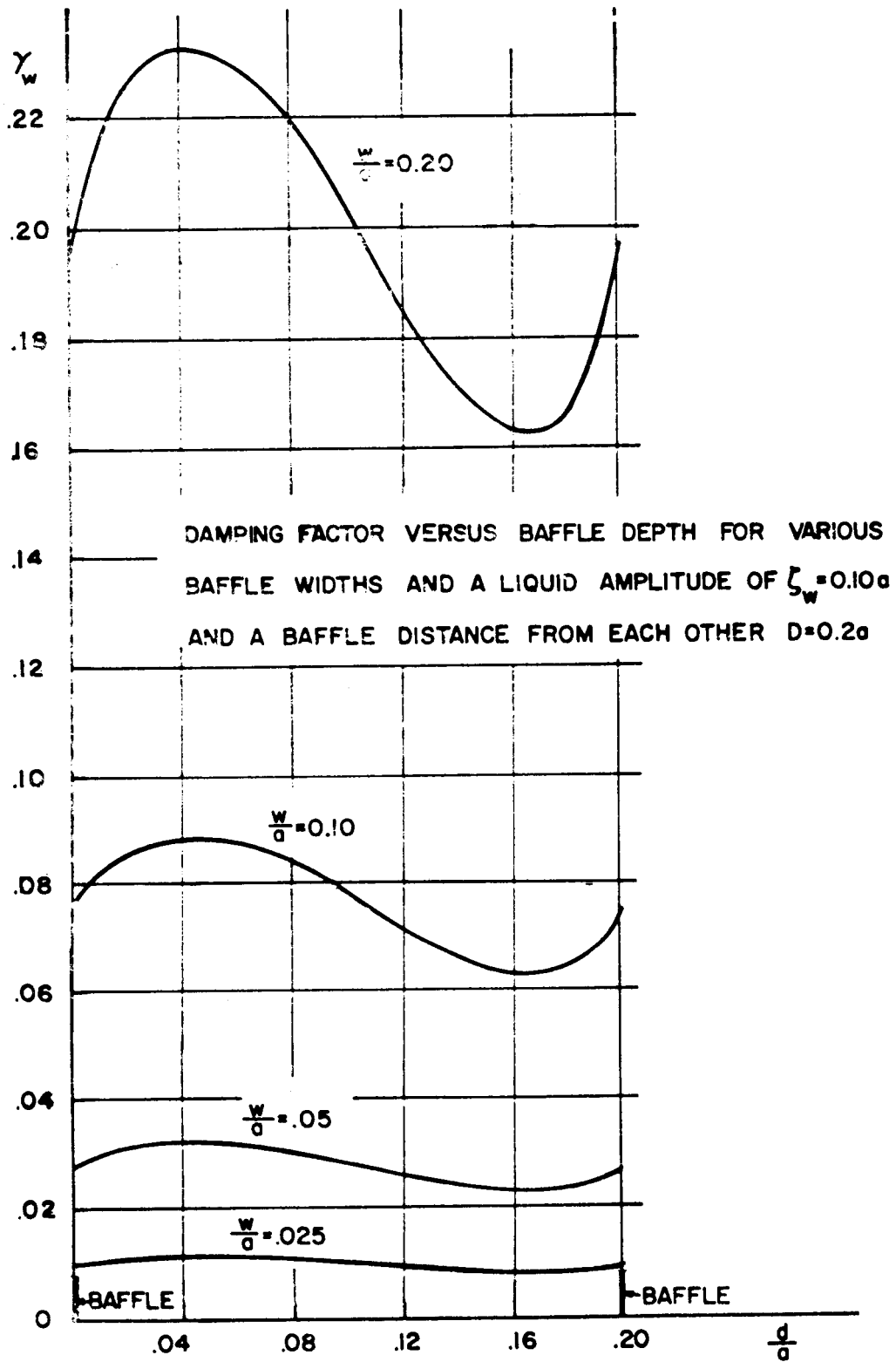


Figure 5-51

DAMPING FACTOR VERSUS BAFFLE DEPTH FOR VARIOUS
 BAFFLE WIDTHS AND A LIQUID AMPLITUDE OF $\zeta_w = 0.2a$
 AND A BAFFLE DISTANCE FROM EACH OTHER $D = 0.2a$

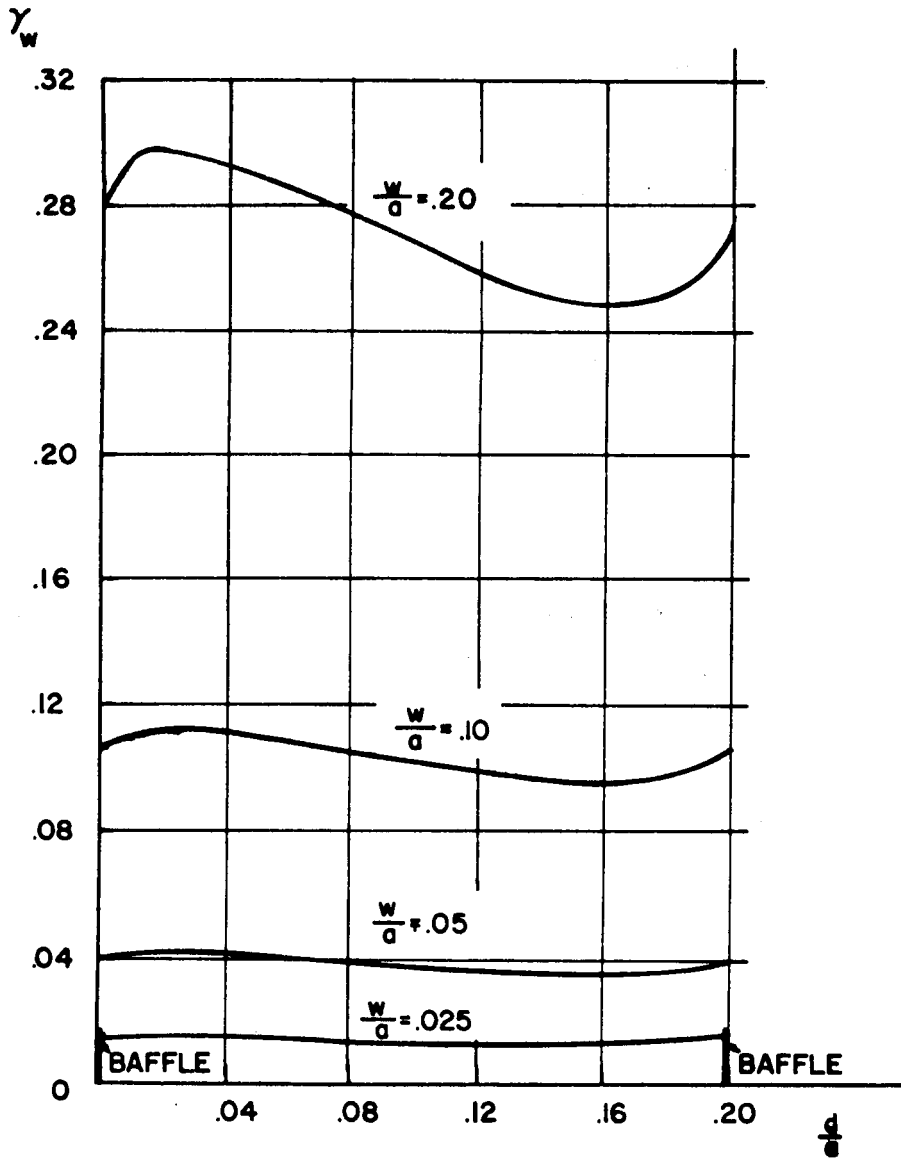


Figure 5-52

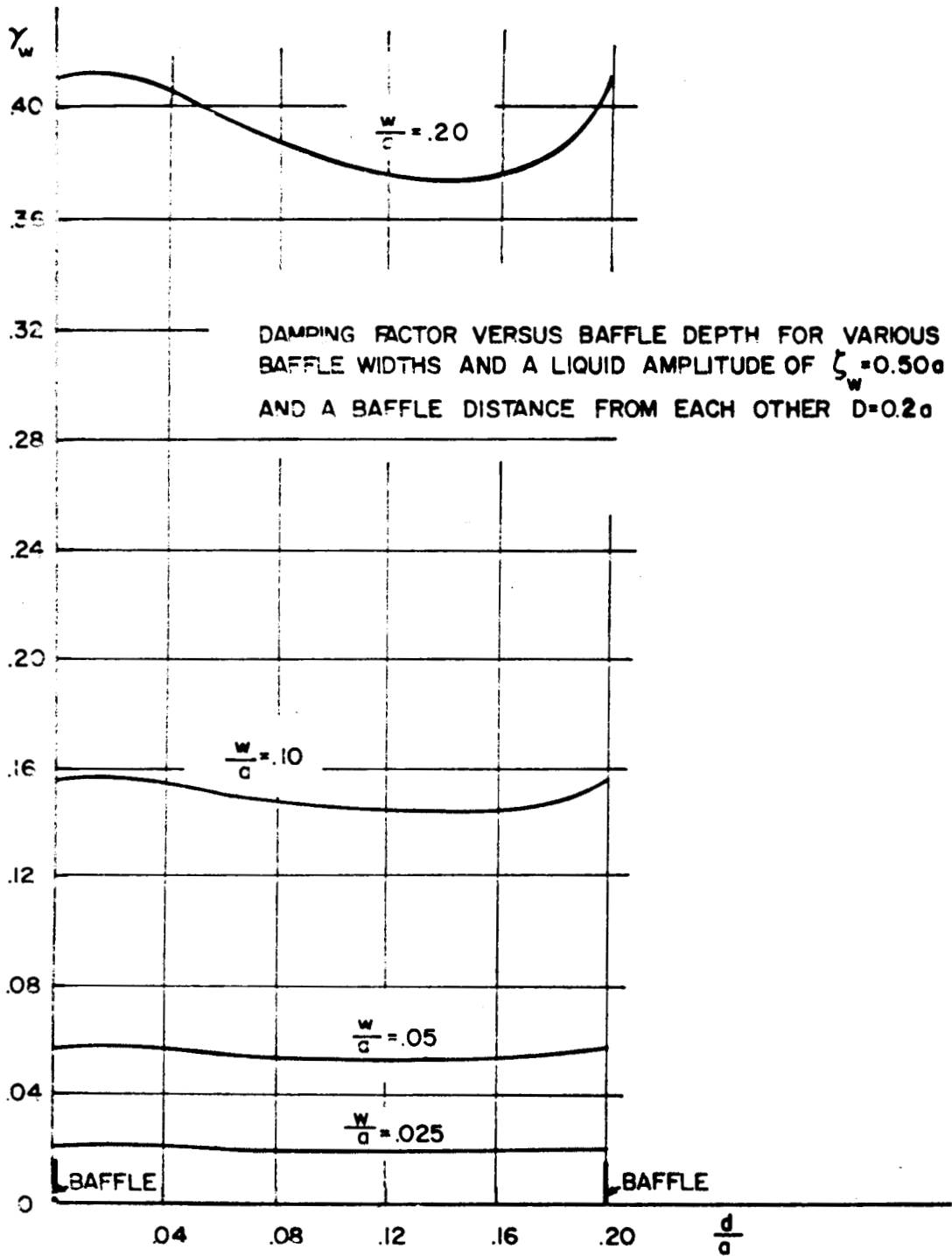


Figure 5-53

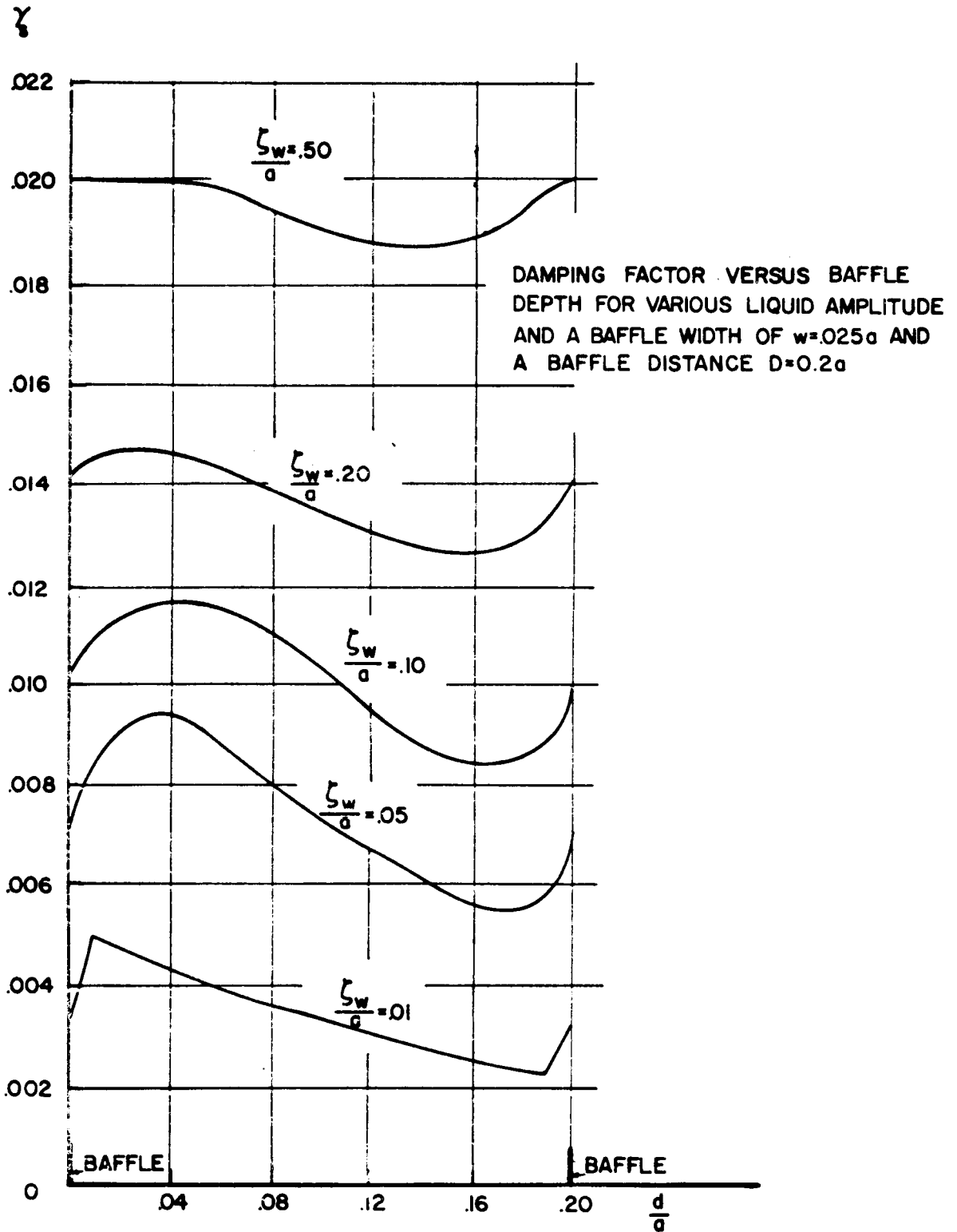


Figure 5-54

DAMPING FACTOR VERSUS BAFFLE DEPTH FOR VARIOUS
 LIQUID AMPLITUDE AND A BAFFLE WIDTH OF $w=.05a$
 AND A BAFFLE DISTANCE $D=0.2a$

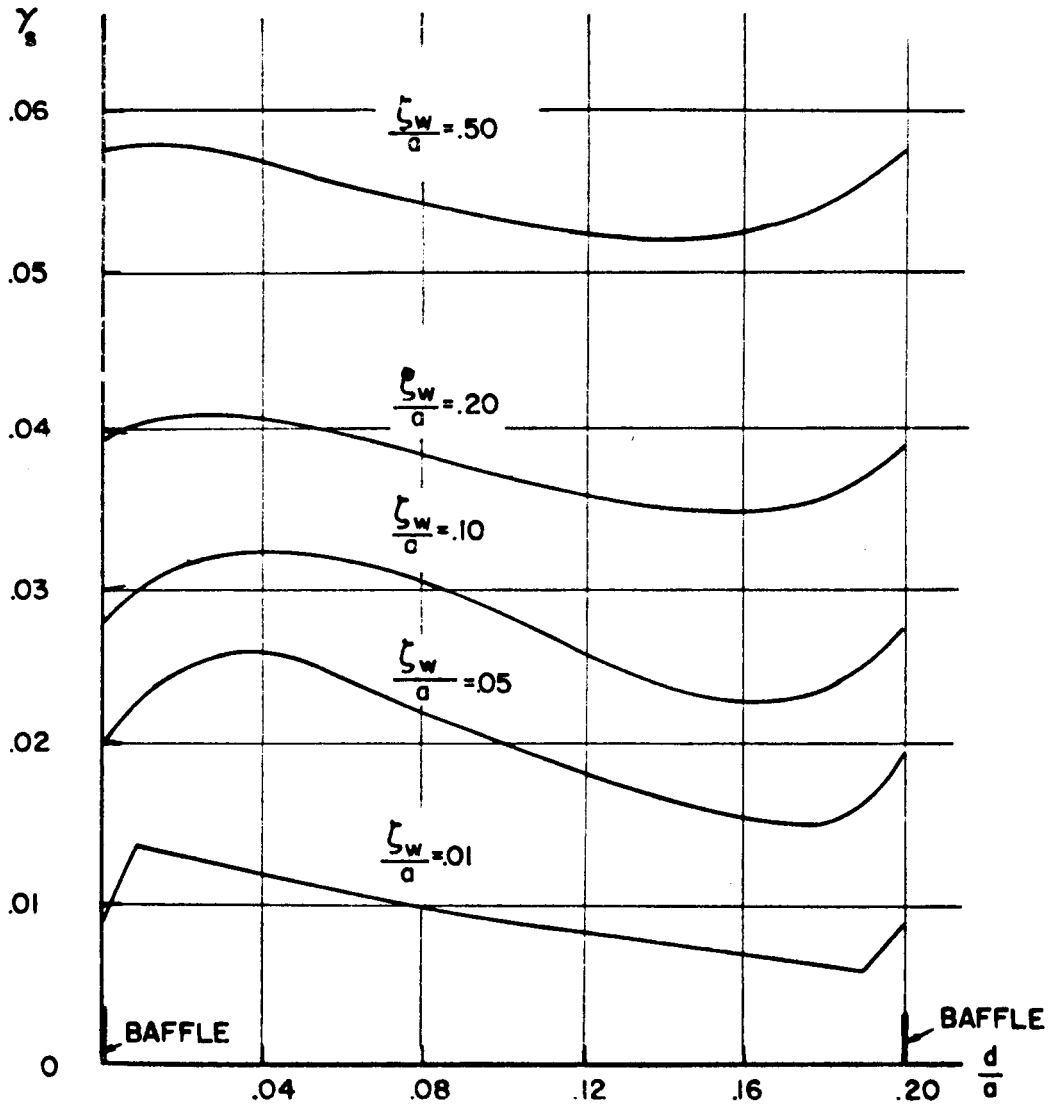


Figure 5-55

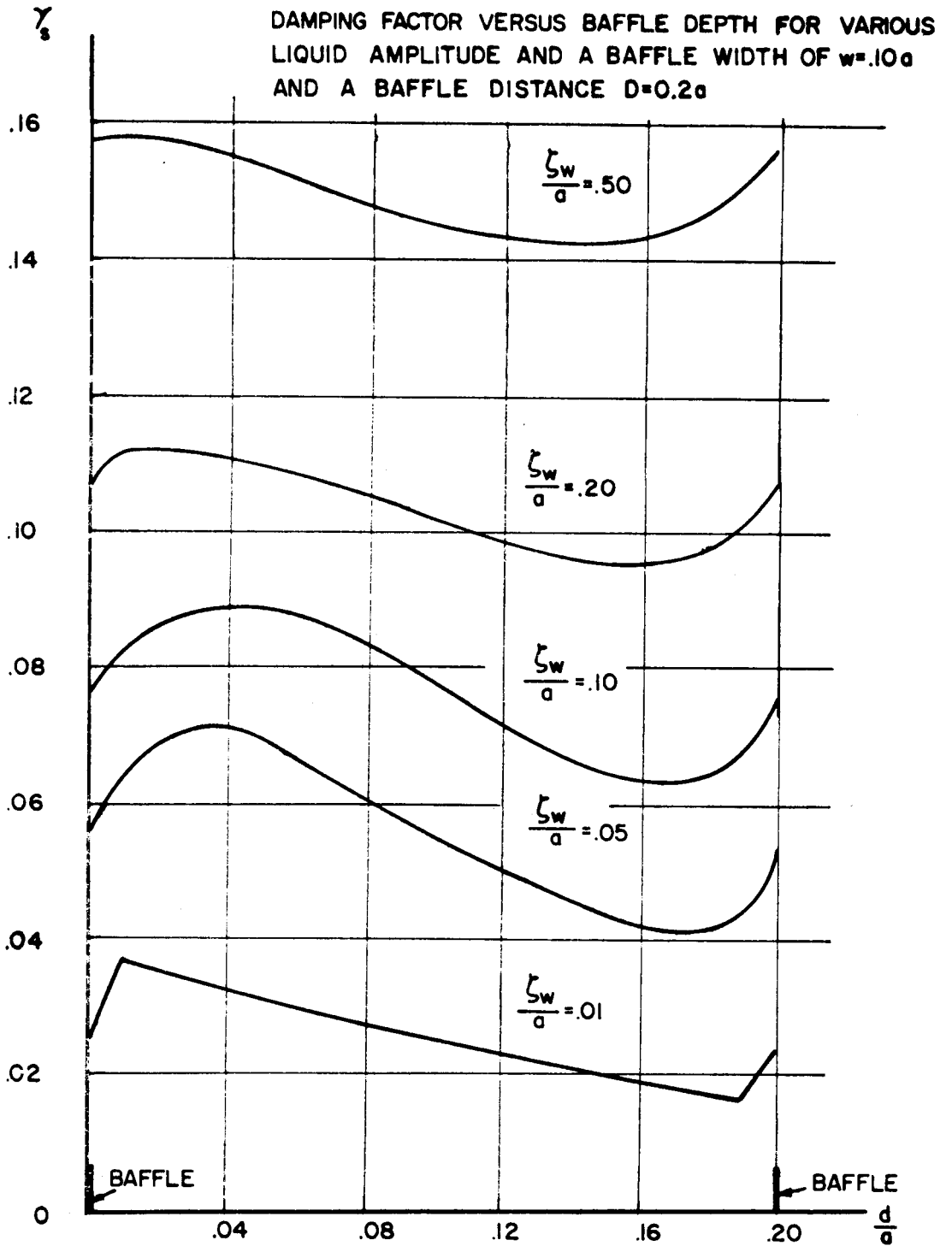


figure 5-56

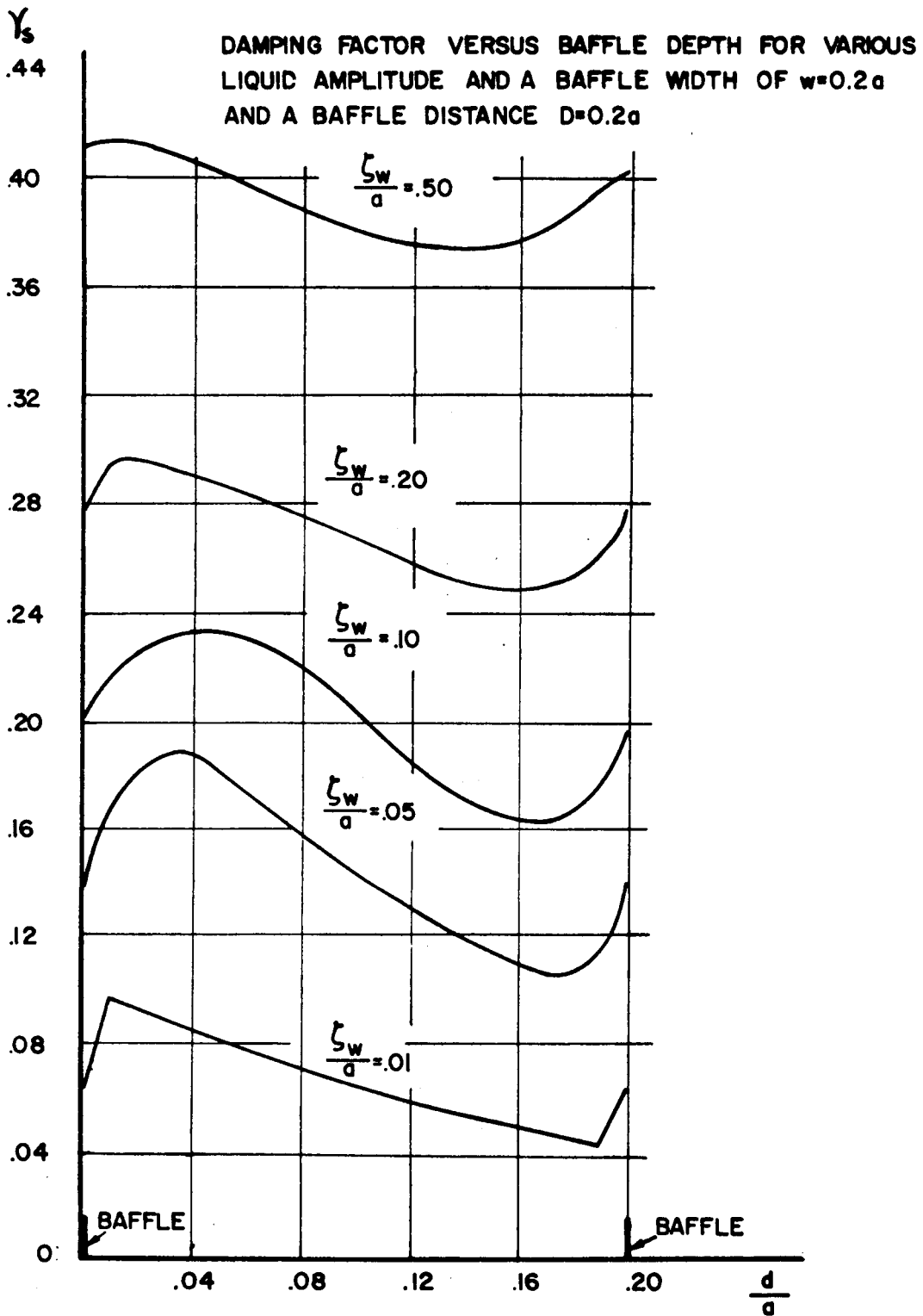


Figure 5-57

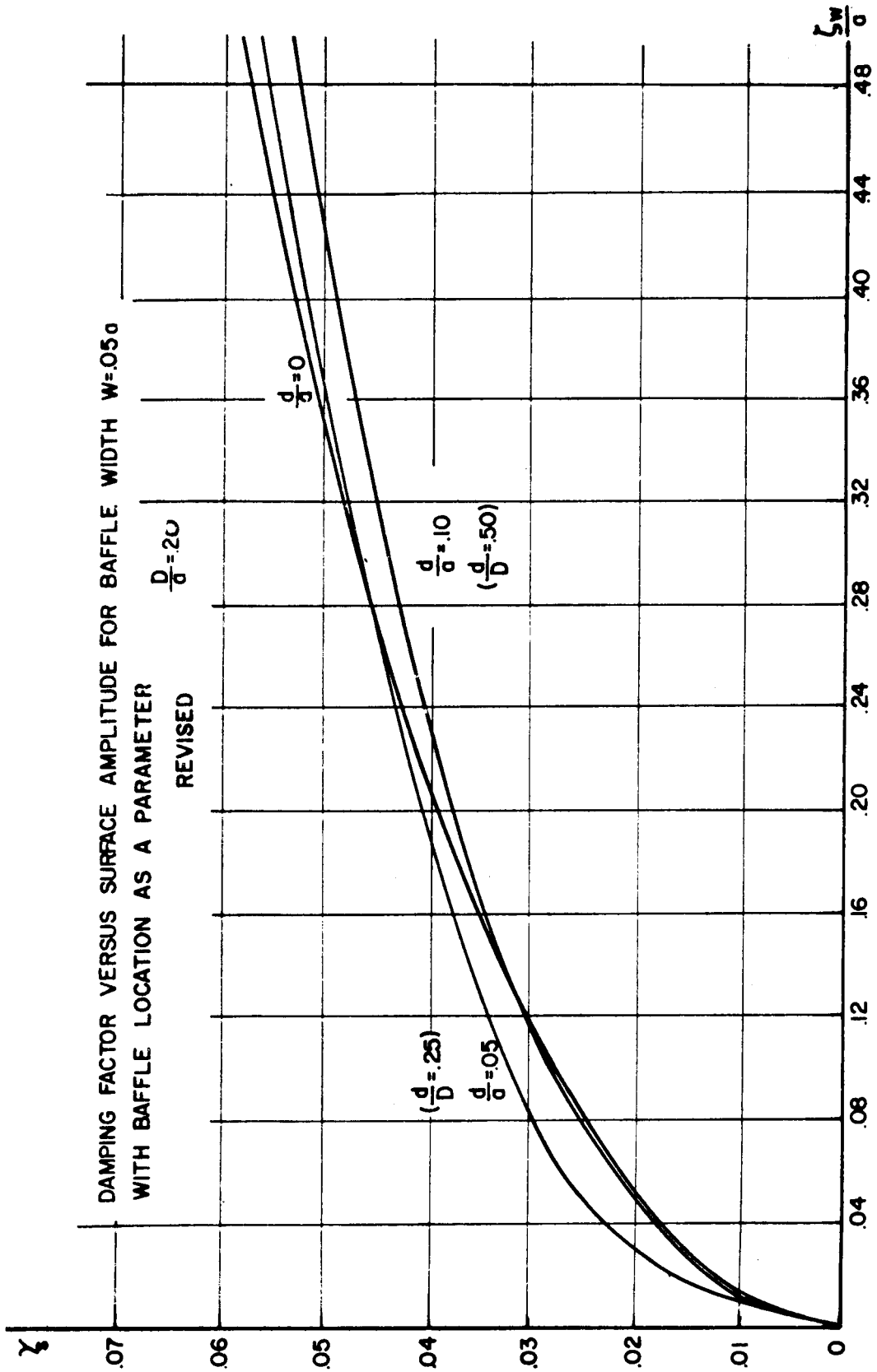


Figure 5-58

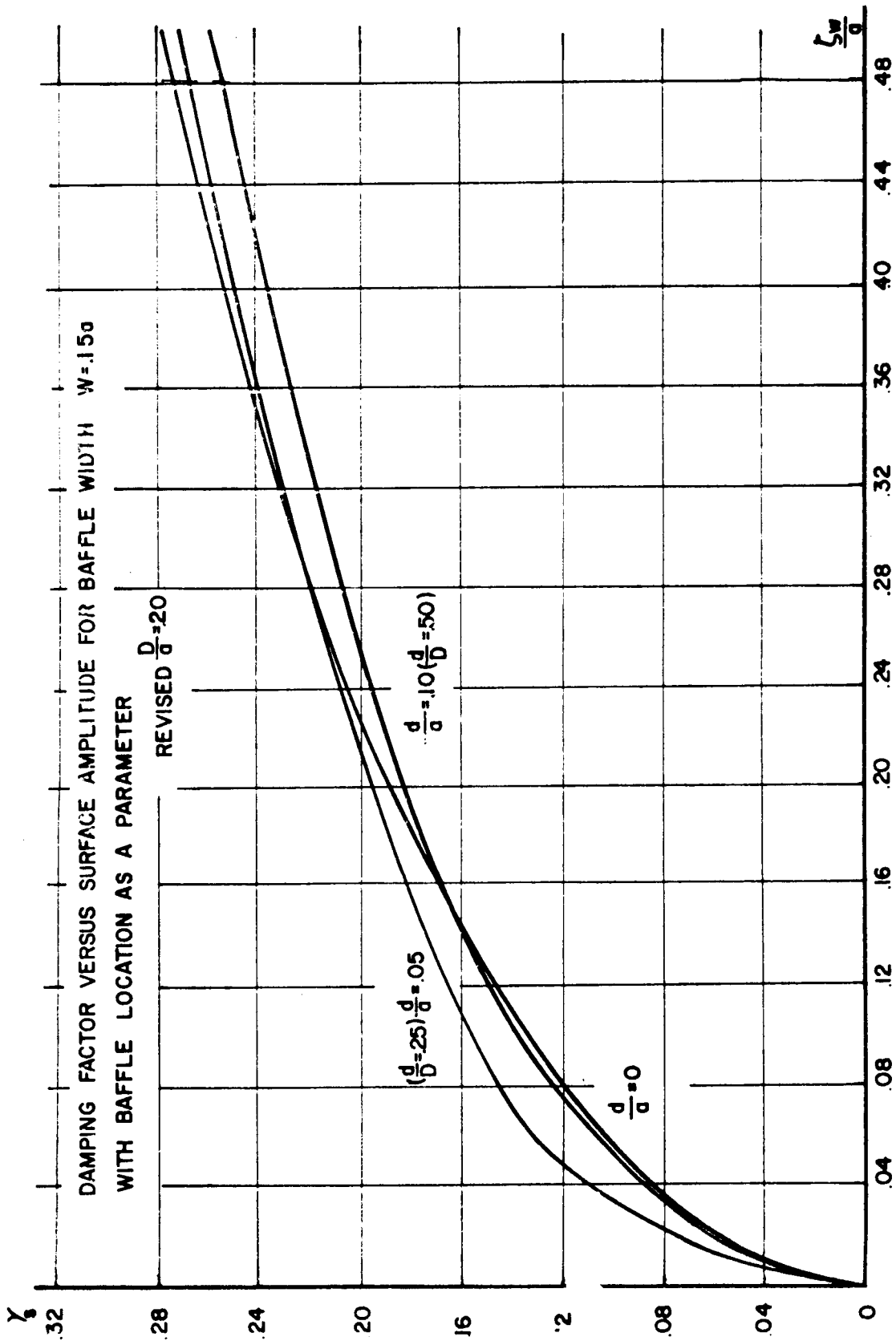


Figure 5-59

DAMPING FACTOR VERSUS BAFFLE WIDTH FOR $\zeta_w = .10a$
 WITH LOCATION OF BAFFLE AS A PARAMETER

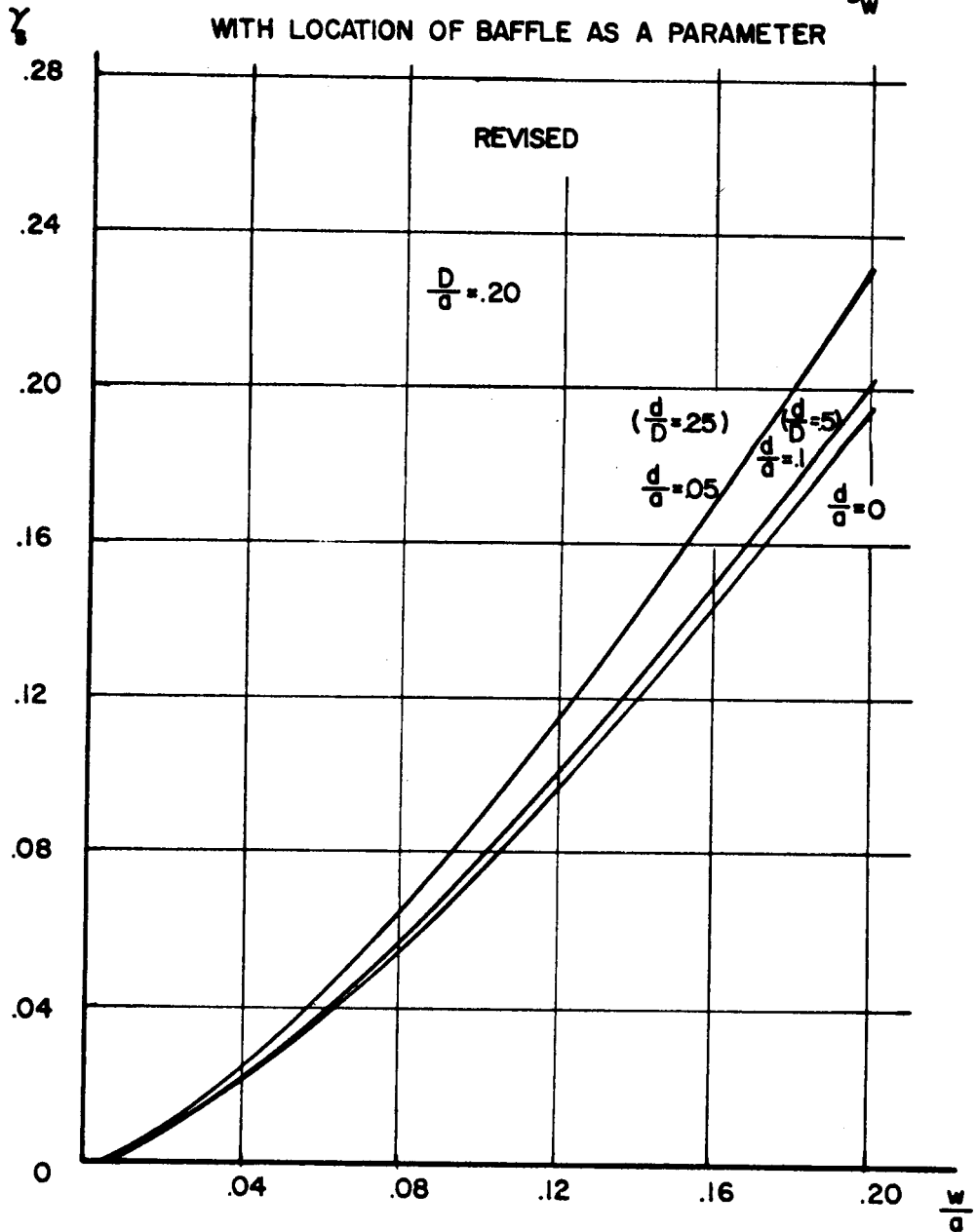


Figure 5-60

DAMPING FACTOR VERSUS BAFFLE WIDTH FOR $\zeta_w = .3a$
 WITH LOCATION OF BAFFLE AS A PARAMETER

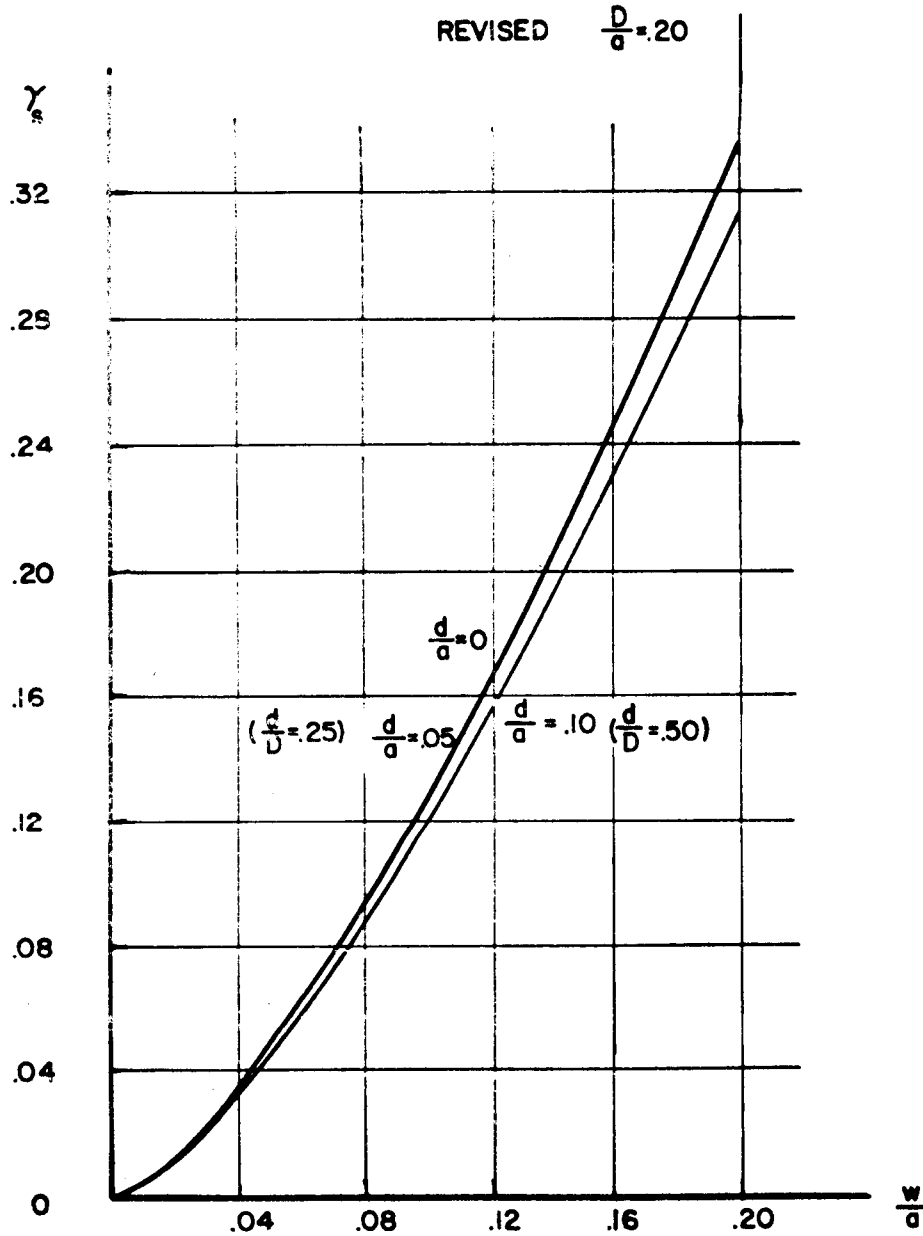


Figure 5-61

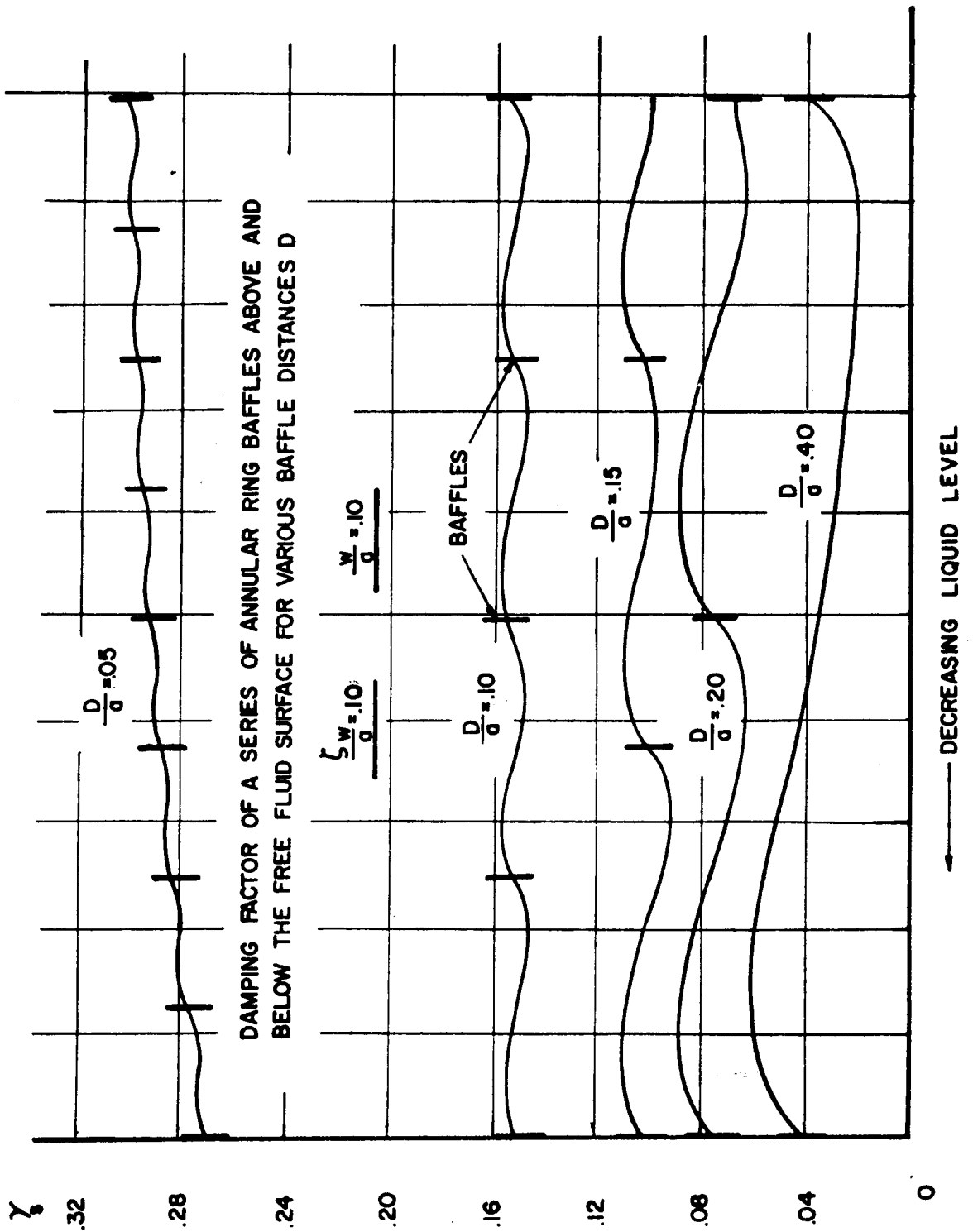


Figure 5-62

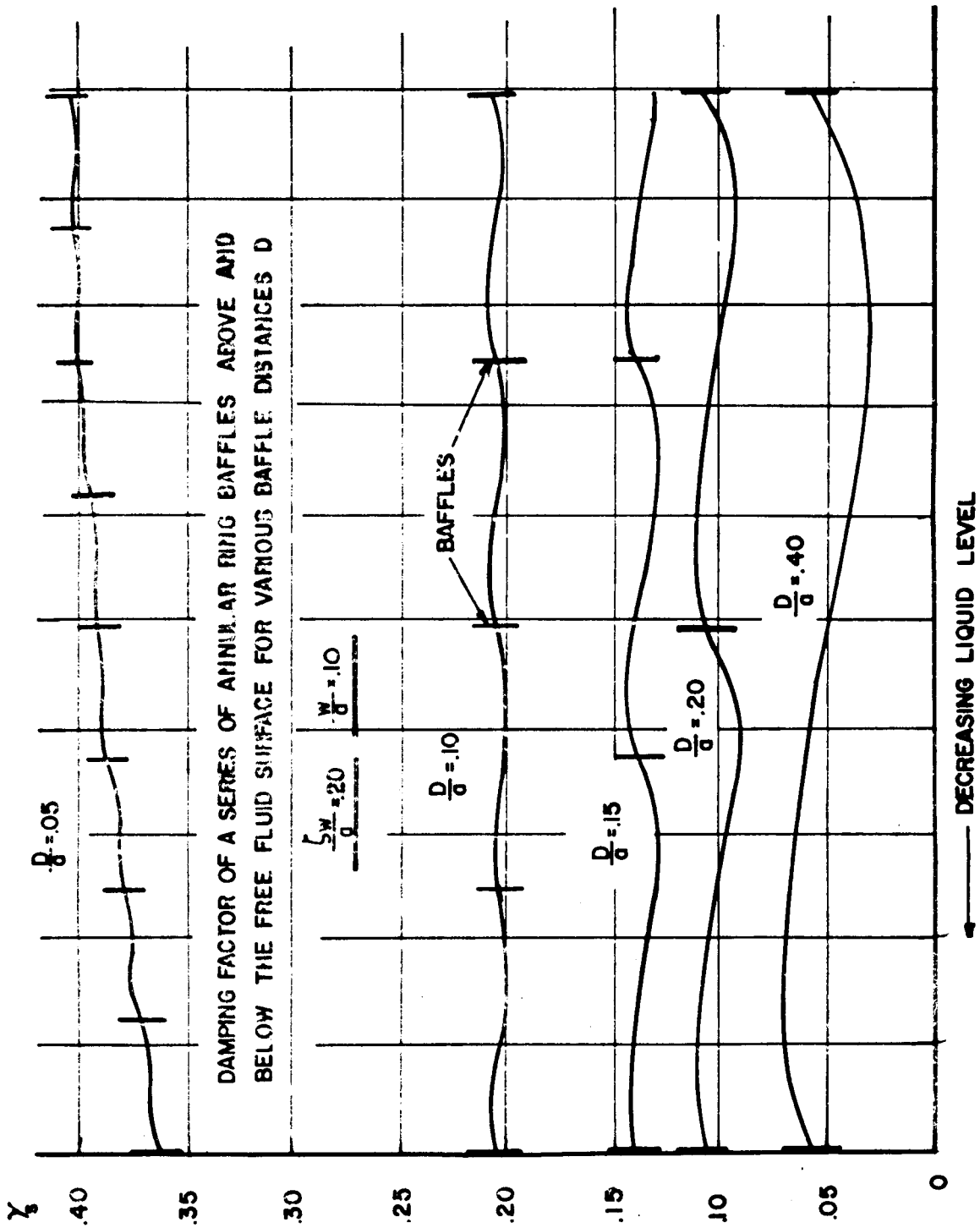
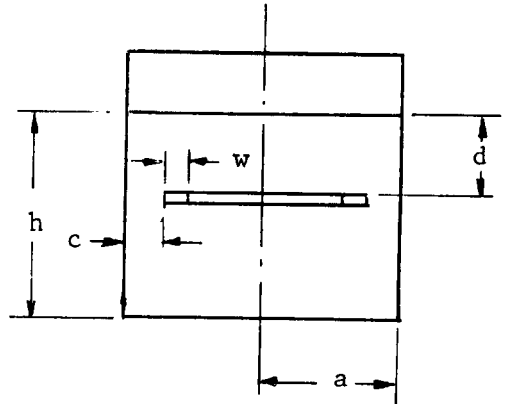
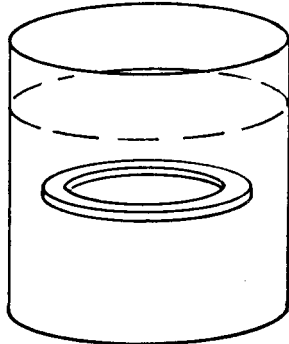


Figure 5-63

5.1.3.3 Ring with Radial Clearance



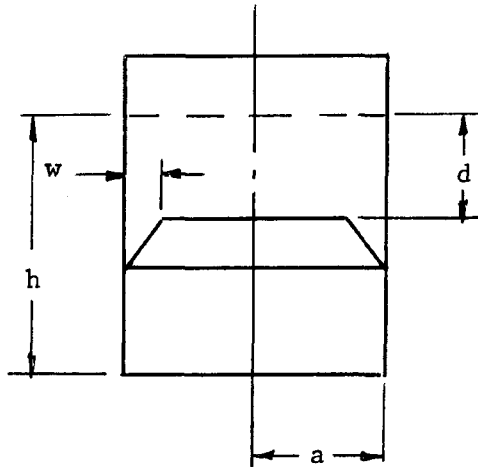
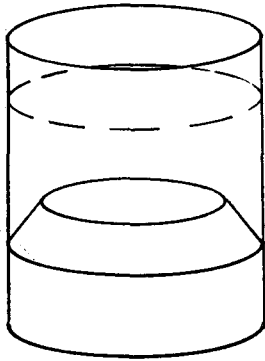
where h = depth of liquid
 d = depth of baffle
 a = radius of right circular cylinder
 w = ring width
 c = radial clearance

References: (35)

Investigations by Silveira, Stepes and Leonard (35) show that for a given baffle depth:

1. With the radial clearance constant:
 - (a) The damping factor increases as the baffle width increases (Figure 5-11)
 - (b) The frequency increases as the baffle width decreases (Figure 5-16).
2. With the baffle width constant:
 - (a) The damping factor decreases as the radial clearance increases (Figure 5-11)
 - (b) The frequency increases as the radial clearance decreases (Figure 5-16).

5.1.3.4 Conic Section



where h = depth of liquid

d = depth of conic section below undisturbed free-surface

a = radius of right circular cylinder

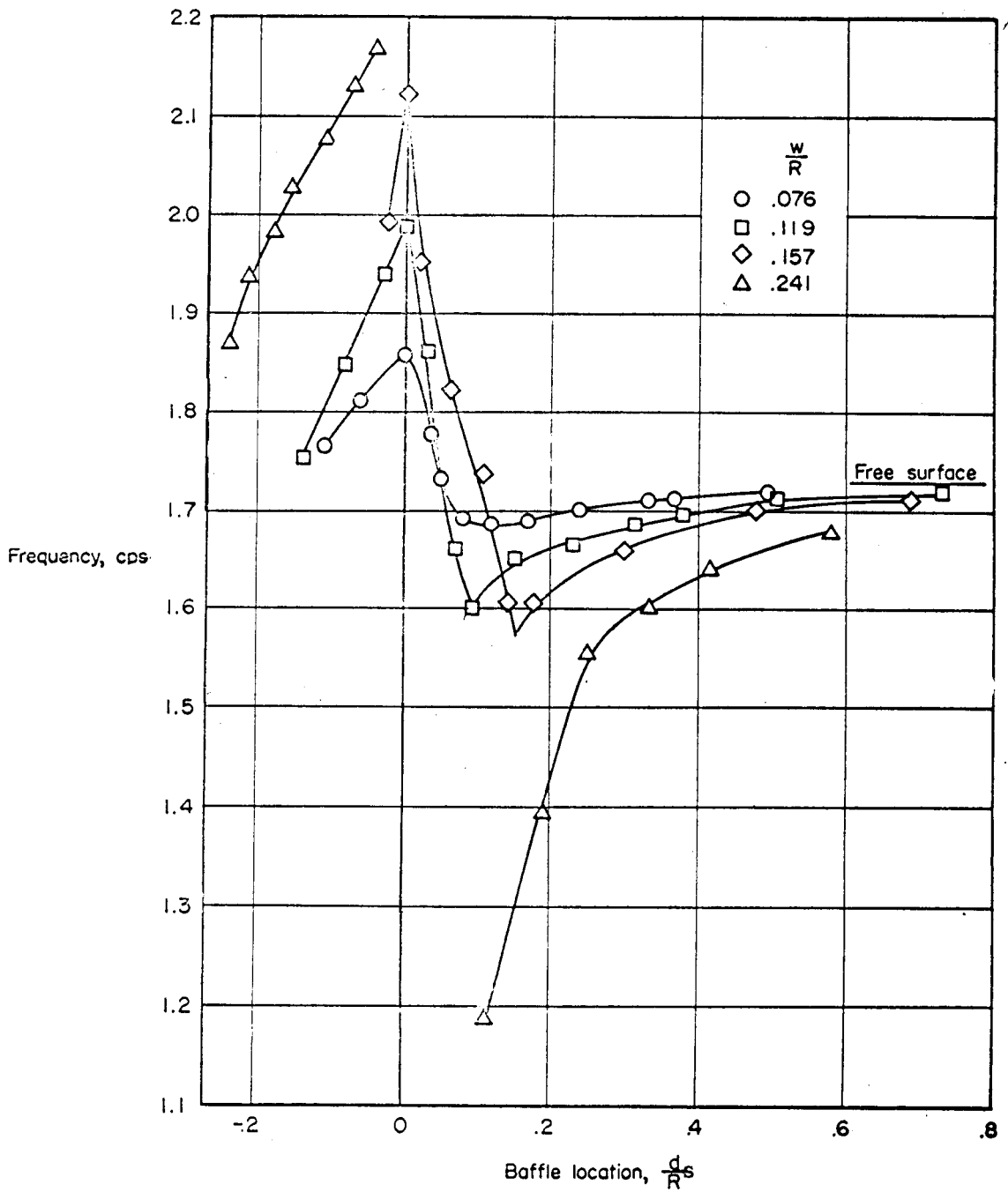
w = conic section width

References: (35, 42, 43, and 83)

Investigations by Silveira, Stephens and Leonard (35) show that:

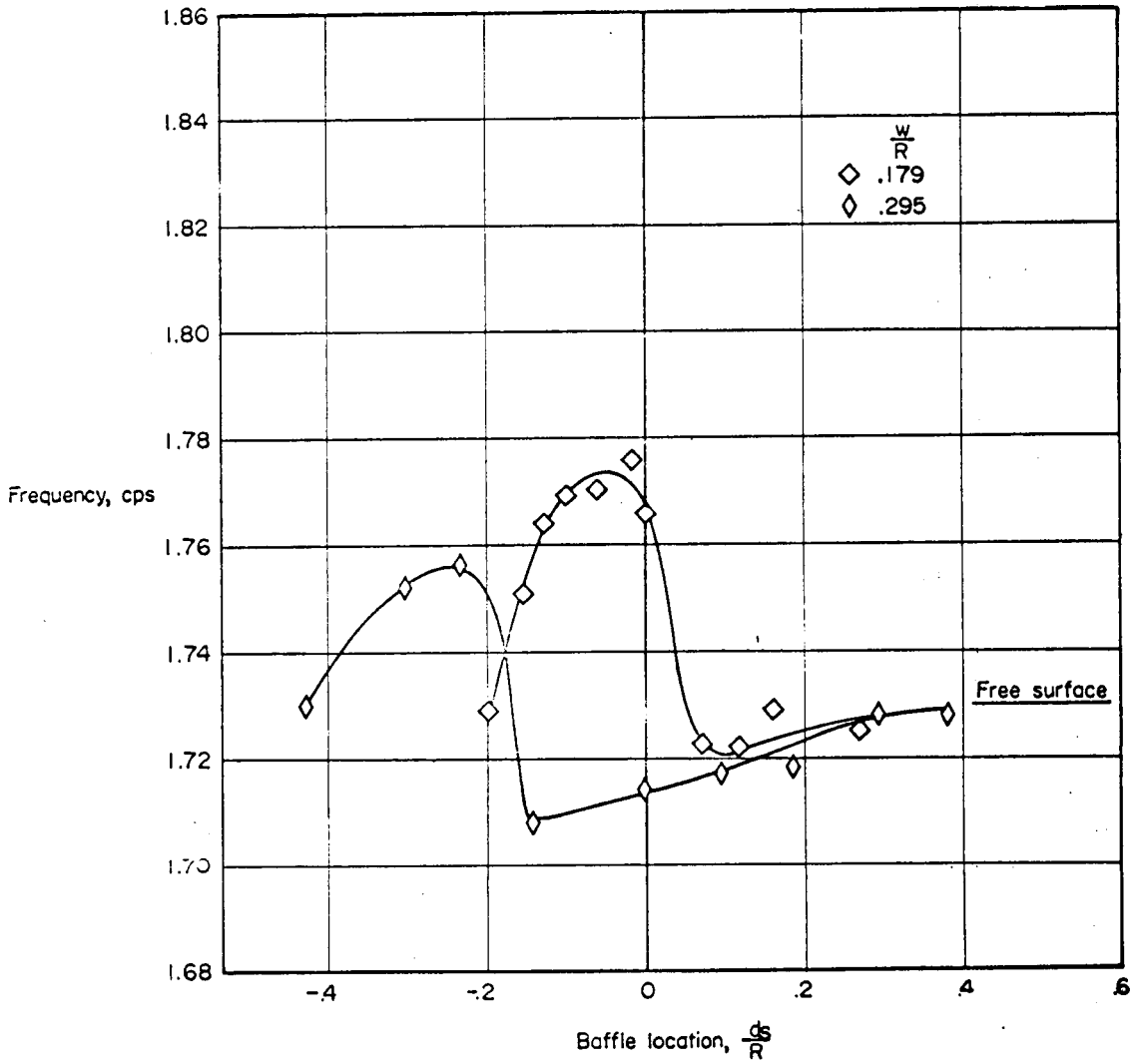
1. For a given baffle depth:
 - (a) The damping factor of a perforated and nonperforated conic section increases as the baffle width increases (Figure 5-68).
 - (b) The frequency for a perforated and nonperforated conic section increases as the baffle width decreases (Figure 5-64 and 5-67).
2. Although the damping provided by the conic sections is slightly higher than that for the ring baffles, the surface area of a conic section having the same baffle width as that of the ring baffle is considerably higher.

Investigations by Liu (83) give a conformal mapping solution for the pressure distribution on the conic section (article 5.1.7.3):



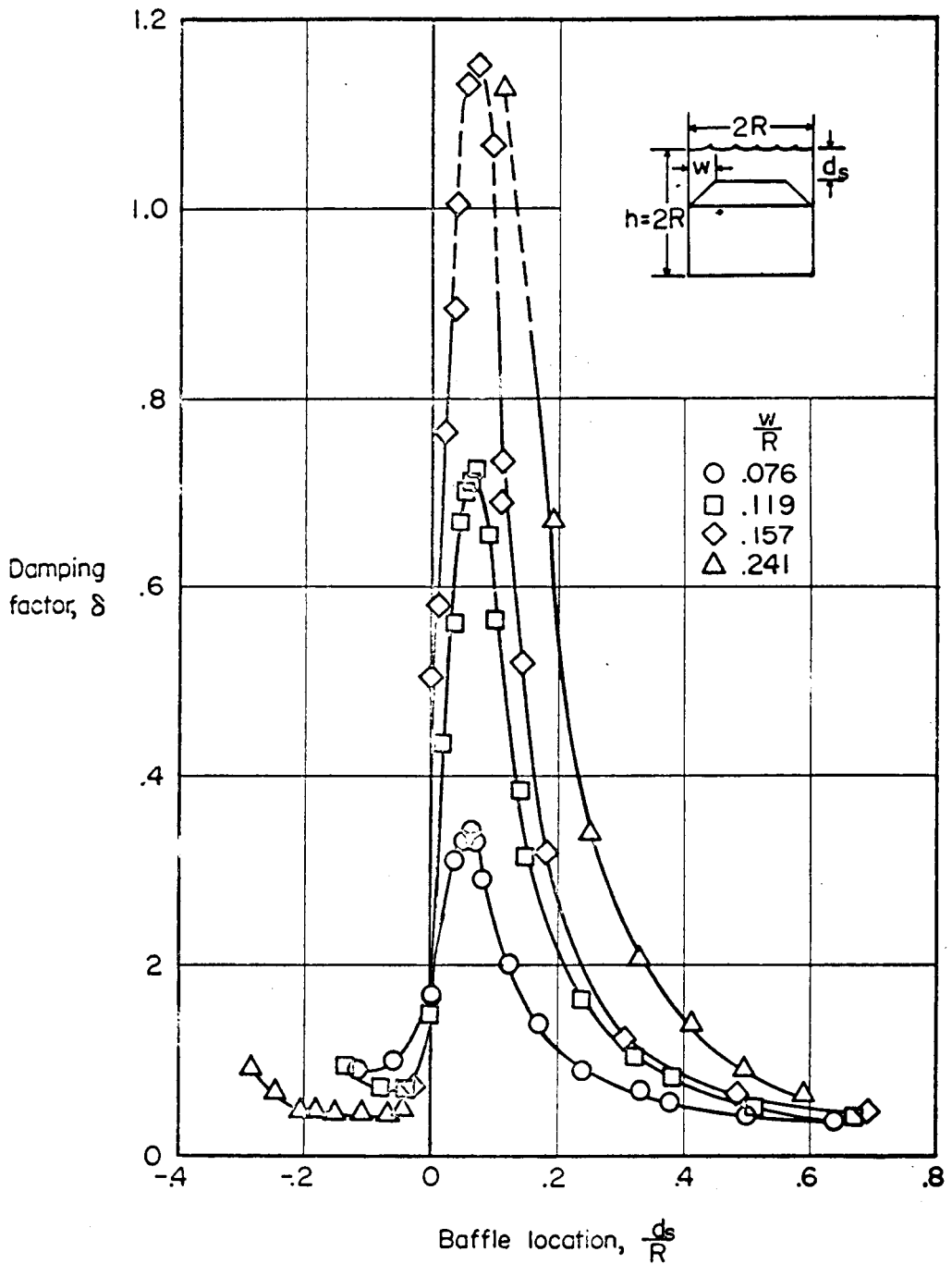
Variation of frequency with baffle location for conic-section baffle. (35)

Figure 5-64



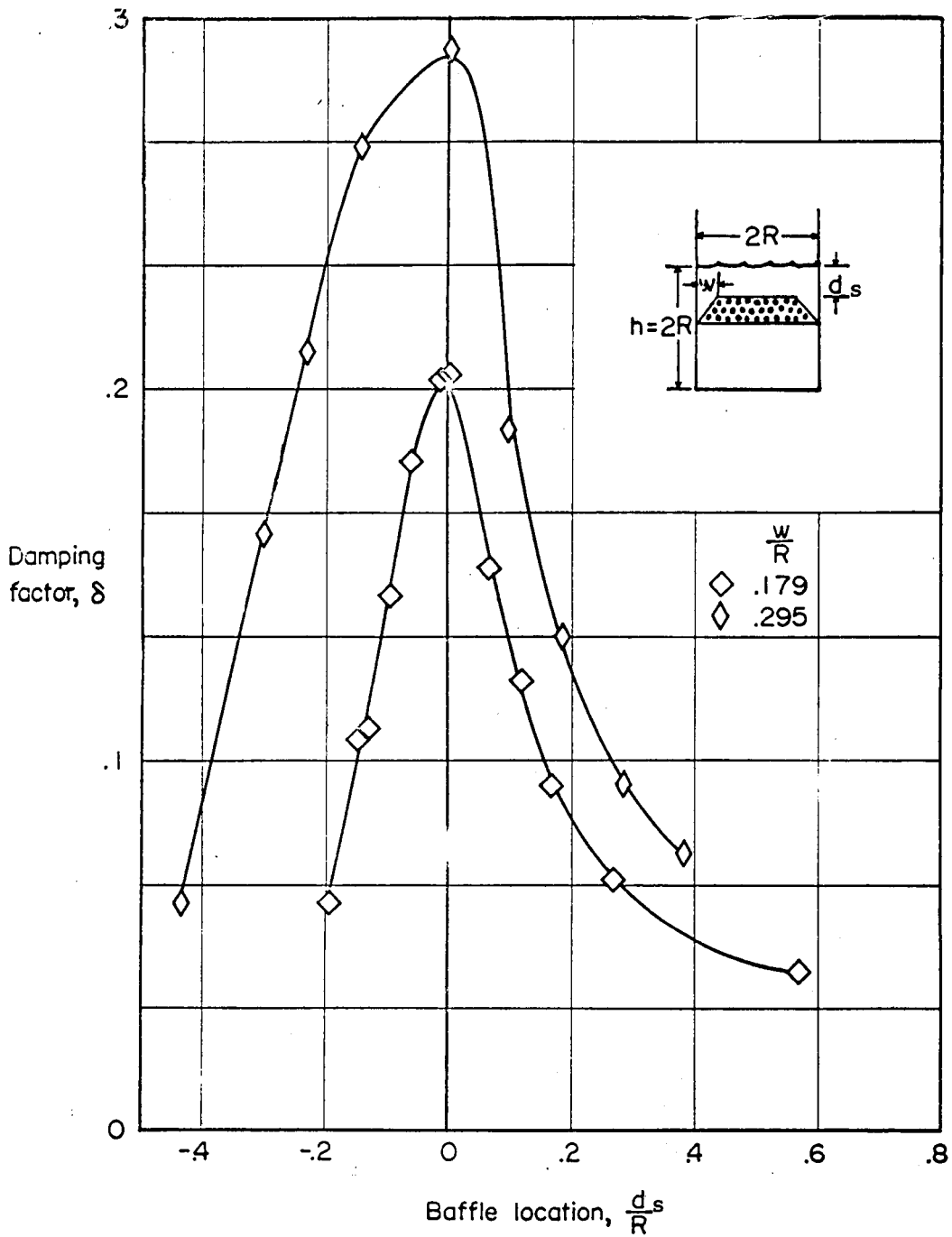
Variation of frequency with baffle location for perforated-conic-section baffle. (35)

Figure 5-65



Variation of damping factor with baffle location for conic-section baffle. $R = 6$ inches; $\frac{h}{R} = 2$. (35)

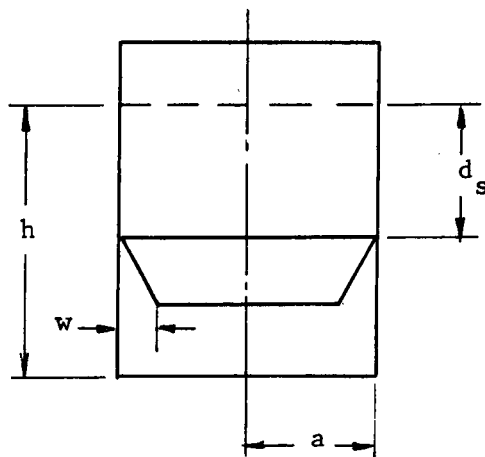
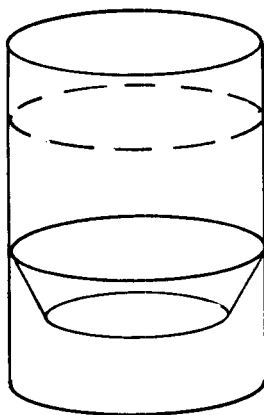
Figure 5-66



Variation of damping factor with baffle location for perforated-conic-section baffle. $R = 6$ inches; $\frac{h}{R} = 2$. (35)

Figure 5-67

5.1.3.5 Inverted Conic Section

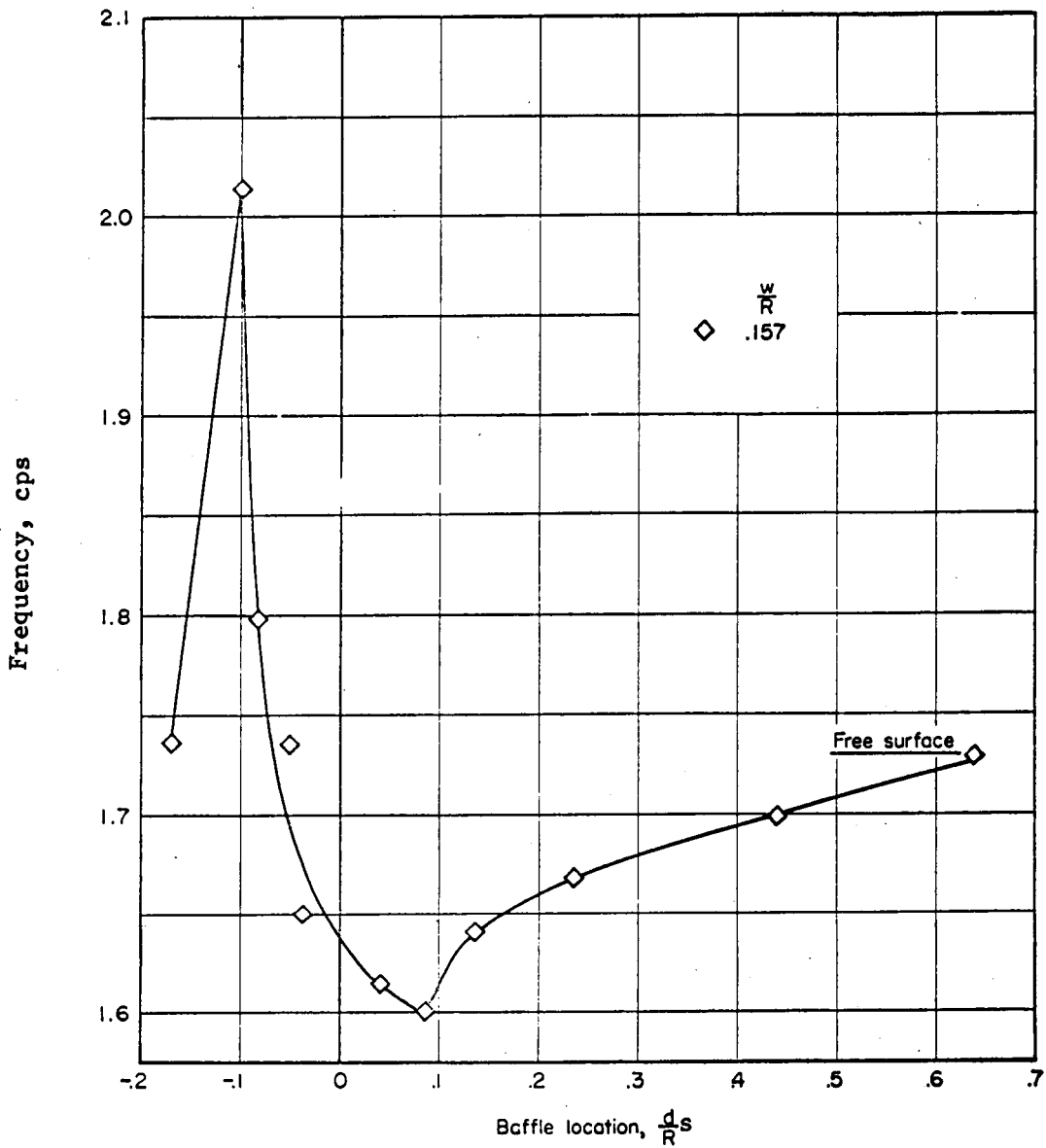


where h = depth of liquid
 a = radius of circular cylindrical tank
 d_s = depth of baffle
 w = inverted conic section width

References: (35, 42, and 83)

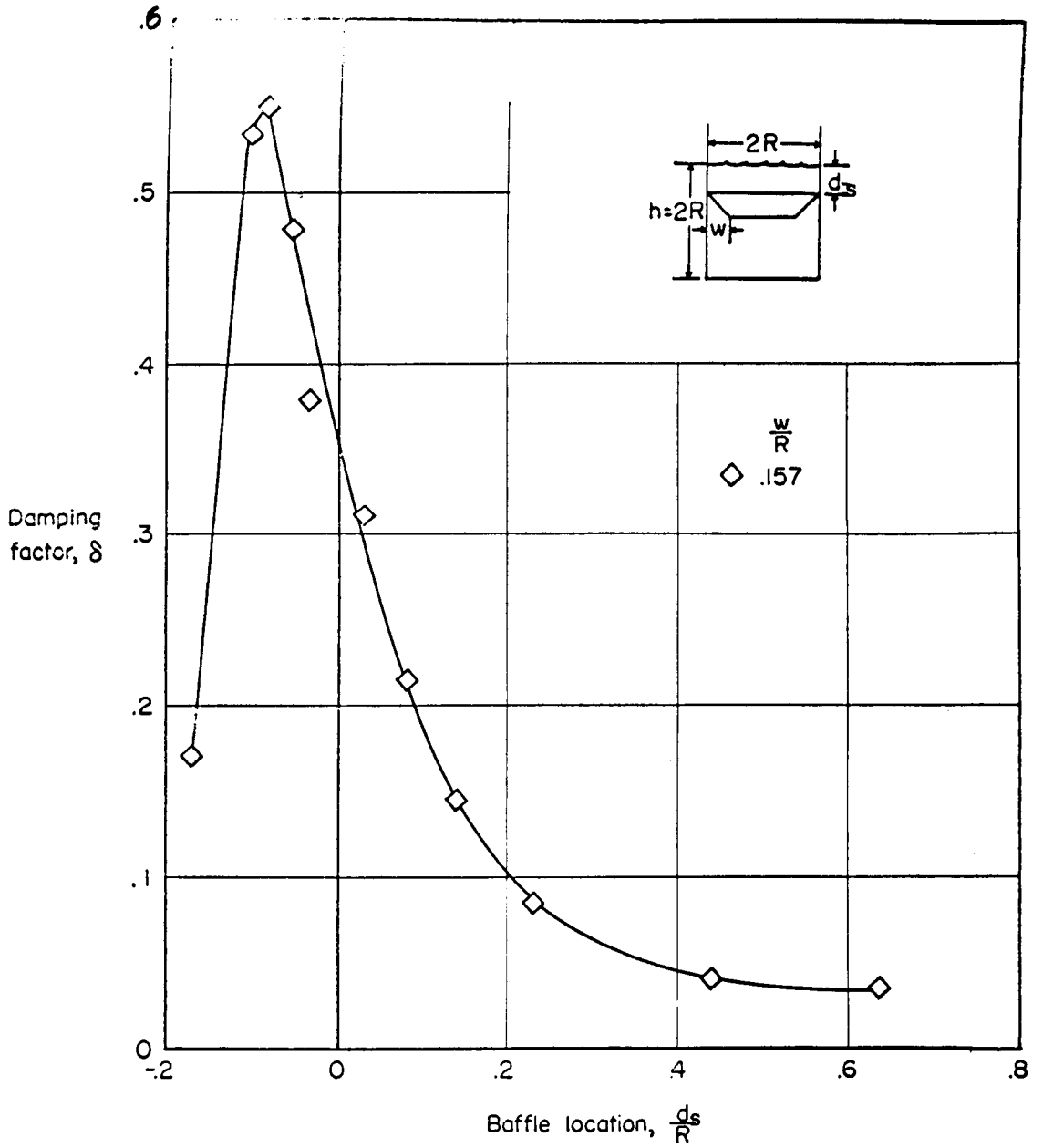
of Investigations by Silveira, Stephens and Leonard (35) show the effect/baffle width on both the frequency and the damping factor as a function of baffle depth (Figures 5.68 and 5.69).

Investigations by Liu (83) give a conformal mapping solution for the pressure distribution on the baffle.



Variation of frequency with baffle location for inverted-conic-section baffle. (35)

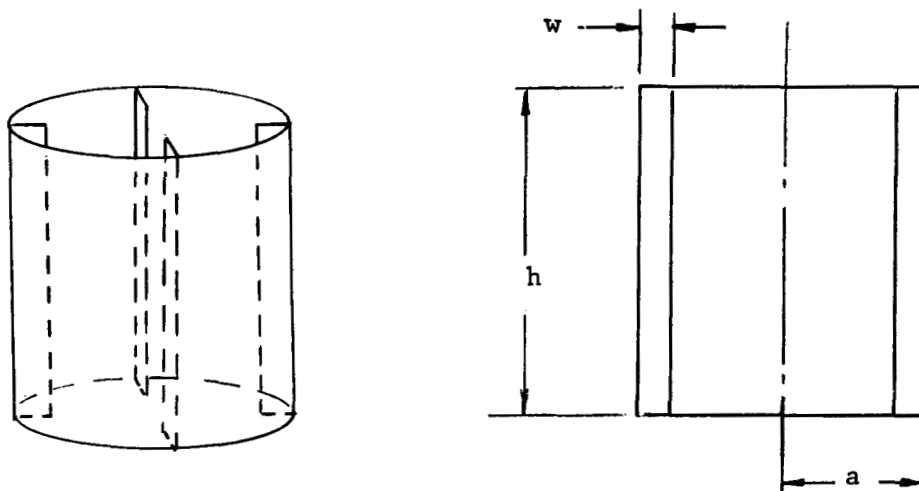
Figure 5-68



Variation of damping factor with baffle location for inverted-conic-section baffle. $R = 6$ inches; $\frac{h}{R} = 2$. (35)

Figure 5-69

5.1.4 Cruciform Baffle



where h = depth of liquid

a = radius of right circular cylinder

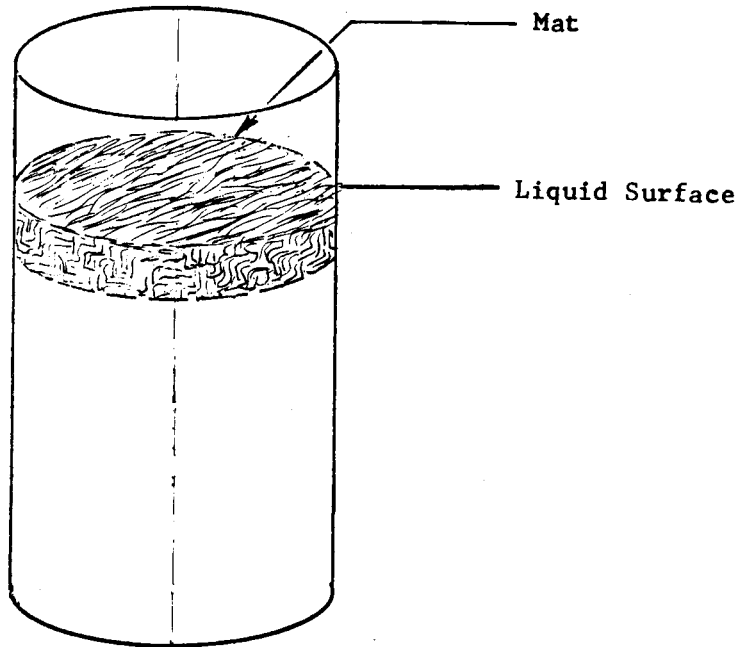
w = cruciform width

References: (35)

Cruciform baffles are most effective against rotary slosh which has large horizontal components of fluid velocity near the tank wall. Cruciform baffles are also slightly effective against lateral slosh since large horizontal fluid velocities exist where the node line of the first slosh mode intersects the tank walls.

Investigations by Silveira, Stephens and Leonard (35) indicate, as would be expected, that damping is independent of fluid depth except for shallow fluid depths.

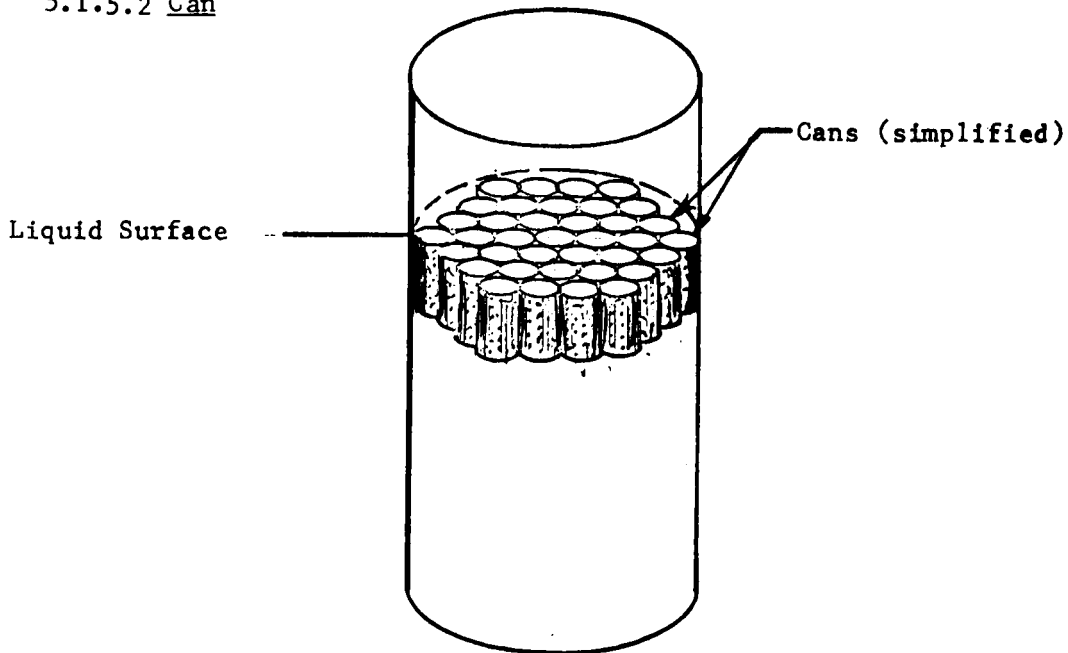
5.1.5.1 Mat



References: (40, 42, 43)

Investigations by Eulitz (40) have been made using commercial coco-fiber mats cut into a shape corresponding to the cross-sectional area of the tank. Several layers were used to attain the required thickness and hollow, airtight aluminum spheres were inserted between the layers to provide the necessary buoyancy. The device was highly effective in damping the liquid amplitude; however, because of the following, it is impractical for missile application. The inner walls of a propellant tank are usually obstructed by stiffener rings, pipelines and other equipment. Therefore, if a floating device is to be used, it must be capable of adapting to the changing cross-sectional area of the container.

5.1.5.2 Can



References: (40, 42, 43)

Investigations by Eulitz (40) have been made using cans made of perforated sheet metal and enclosing a hollow air-tight metal ball of slightly smaller diameter, which provides the necessary buoyancy. The optimum dimensions of a can necessary for adequate buoyancy and thereby the total number of cans is determined in the following manner. The fraction of submerged volume of the enclosed ball λ is given by

$$\lambda = \frac{(4)\sqrt{3}(\delta\gamma n)}{3D} [3 + (3 + n) P]$$

where δ = the thickness of the can wall

γ = the specific gravity of the can material

n = the number of cans along a tank diameter

D = the tank diameter

P = the percent perforation

For a particular set of values δ , γ and P , a graph of λ vs. D can be plotted consisting of a family of curves corresponding to various values of n (for example, see Figure 5-73). The curve passing nearest to the intersection of the desired mean values of $\lambda = 0.5$ and the tank diameter D under consideration will give the optimum value of n . The total number of cans is then determined by

$$N = \frac{1}{4} (3n^2 + 1)$$

5.1.5.2 Can (continued)

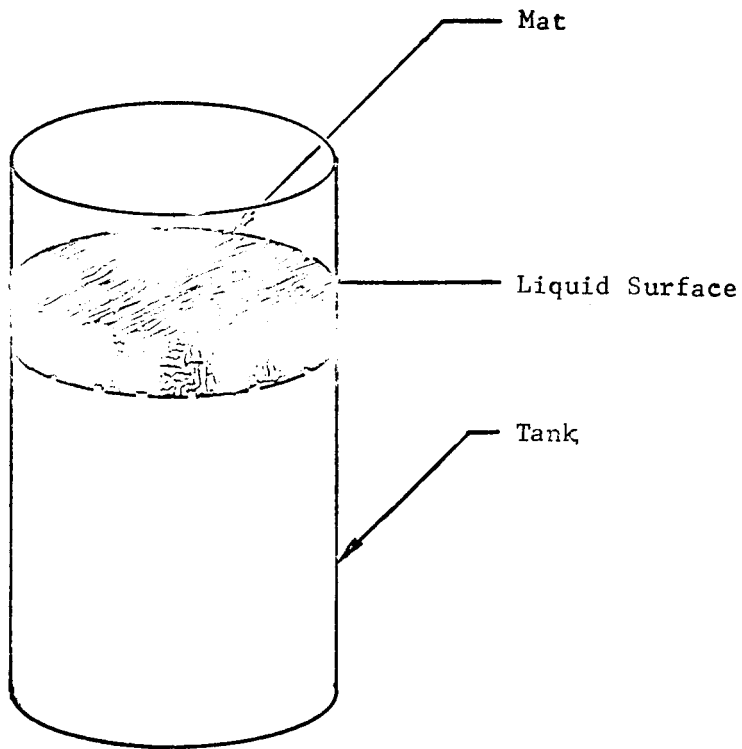
and the can diameter is given by

$$d_1 = \frac{D}{n}$$

The cans are made of perforated aluminum sheet enclosing a hollow air-tight aluminum ball, of slightly smaller diameter, which provides the necessary buoyancy (Figures 5-70 and 5-71). The size and number of cans used in the tests are indicated by $n = 7$ or $N = 37$ (see Figure 5-72).

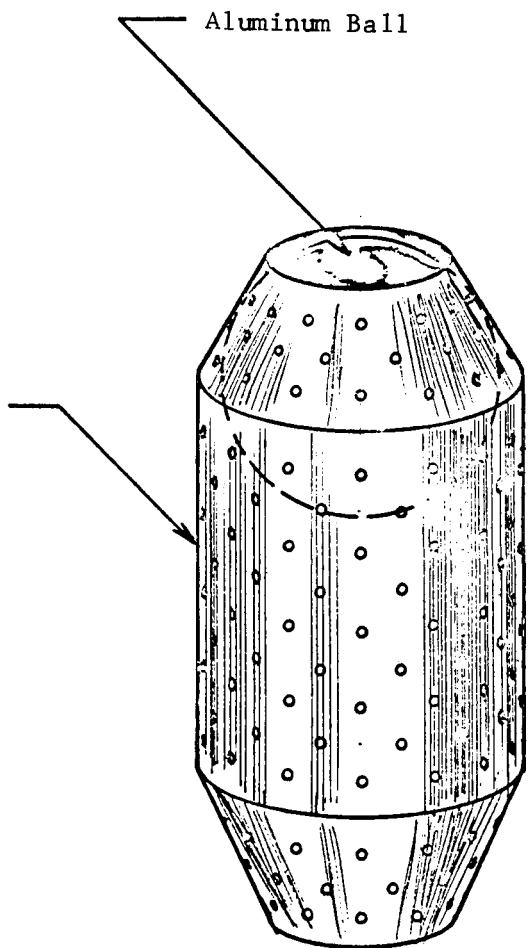
The containers are rigid-wall circular cylindrical tanks of diameter 17.5 and 25 inches, respectively.

The optimum dimensions of the can necessary for adequate buoyancy, and thereby the total number of cans, is determined as follows: the desired value of λ the fraction of submerged volume of the aluminum ball, is 0.5. Figure 5-73 gives an equation for λ as a function of the thickness of the can wall δ , the specific gravity of the can material γ , the percent perforation P , the tank diameter D and the number of cans along a tank diameter n . The curves shown in Figure 5-73 enable the designer to determine the values for n and N corresponding to $\lambda \approx 0.5$ as a function of D for a set of values of δ , γ and P . Note that the notation used in Figures 5-71, 5-72, and 5-73 is applicable only to these figures.



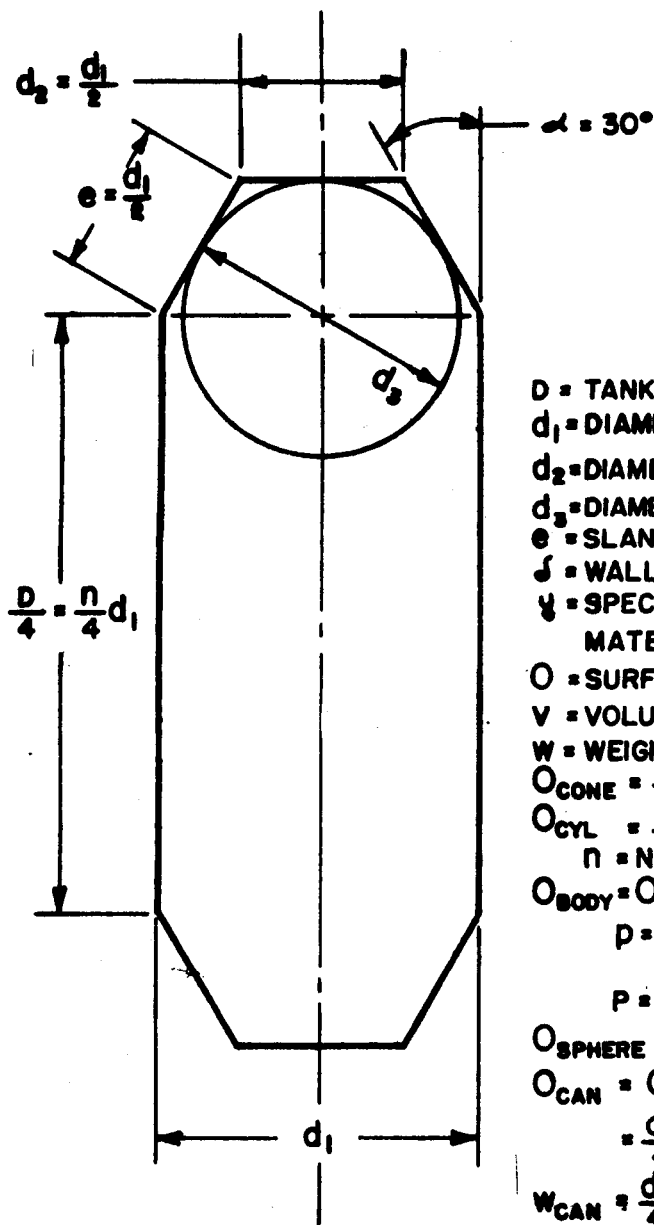
Mat Type Device

Perforated Cylindrical Body



Single "Can" Device

Figure 5-70 Mat type device and single can. (40)



- D = TANK DIAMETER
- d_1 = DIAMETER OF THE CYLINDRICAL BODY
- d_2 = DIAMETER OF THE CONE OPENING
- d_3 = DIAMETER OF THE ALUMINUM BALL = $\frac{d_1}{2} \sqrt{3}$
- e = SLANT HEIGHT OF THE CONE
- δ = WALL THICKNESS OF THE CAN
- γ = SPECIFIC GRAVITY OF THE CAN MATERIAL
- O = SURFACE OF THE CAN
- V = VOLUME OF THE CAN MATERIAL = O · δ
- W = WEIGHT OF THE CAN MATERIAL = O · δ · γ
- $O_{\text{CONE}} = \frac{3}{8} d_1^2 \pi$ (eq.5)
- $O_{\text{CYL}} = \frac{1}{4} d_1^2 \pi n$ (eq.4)
- n = NUMBER OF BODIES UPON D
- $O_{\text{BODY}} = O_{\text{CYL}} + 2 O_{\text{CONE}} = \frac{d_1^2}{4} \pi (3+n)p$
- $p = \frac{100-P}{100}$ (eq.6)
- P = PERFORATION IN %
- $O_{\text{SPHERE}} = \frac{3}{4} d_1^2 \pi$ (eq.7)
- $O_{\text{CAN}} = O_{\text{BODY}} + O_{\text{SPHERE}}$
- $= \frac{d_1^2}{4} \pi [3 + (3+n)p]$ (eq.8)
- $W_{\text{CAN}} = \frac{d_1^2}{4} \pi [3 + (3+n)p] \delta \gamma$ (eq.9)

Typical dimensions of cans. (40)

Figure 5-71

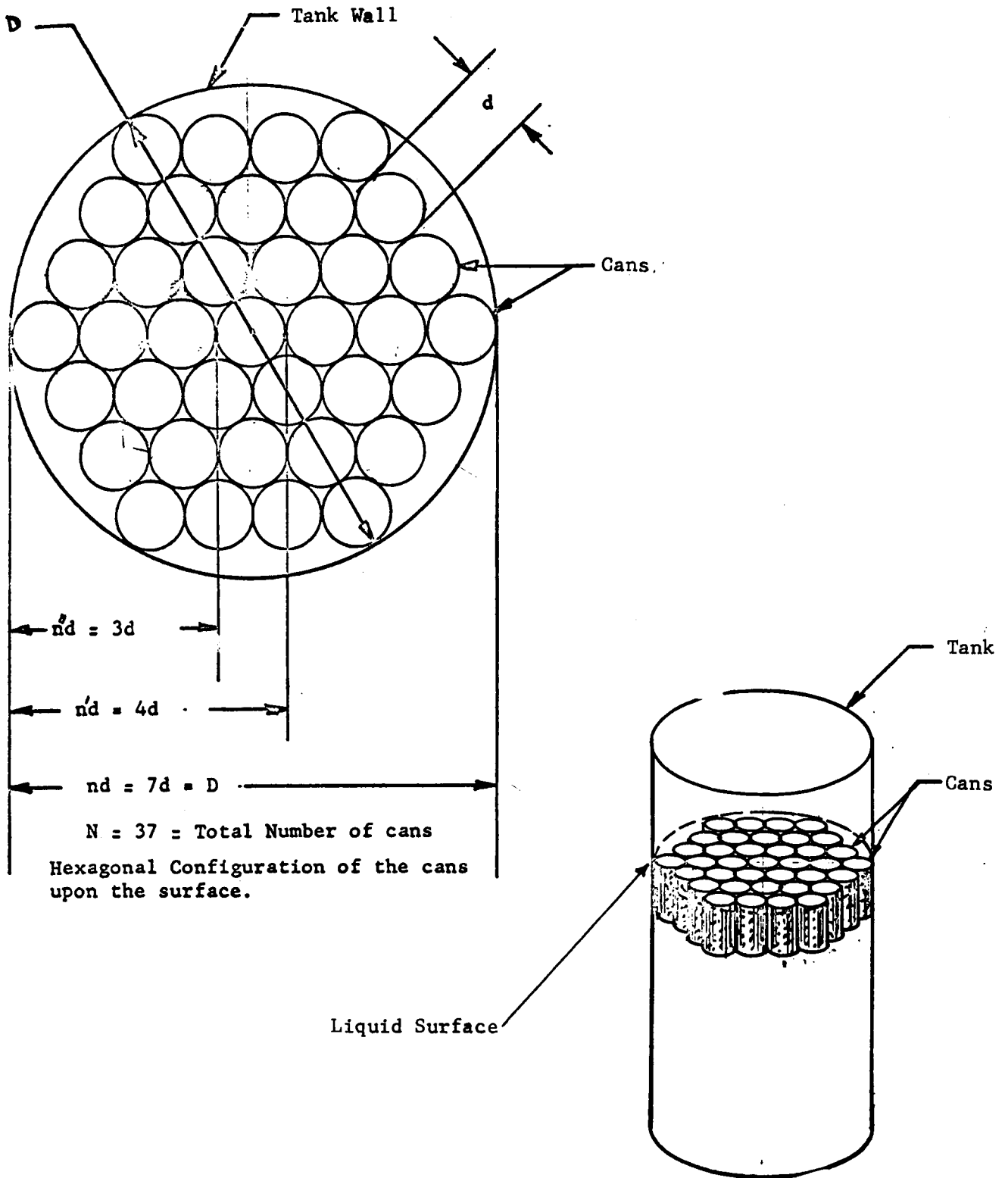


Figure 5-72 Distribution of cans within a tank. (40)

$$\lambda = \frac{4\sqrt{3}}{3D} \frac{\delta Y n}{[3 + (3 + n)P]}$$

$\delta = 0.1 \text{ cm} = 0.04 \text{ in}$

$Y = 2.7$

$P = 0.75 \text{ g/cm}^3$

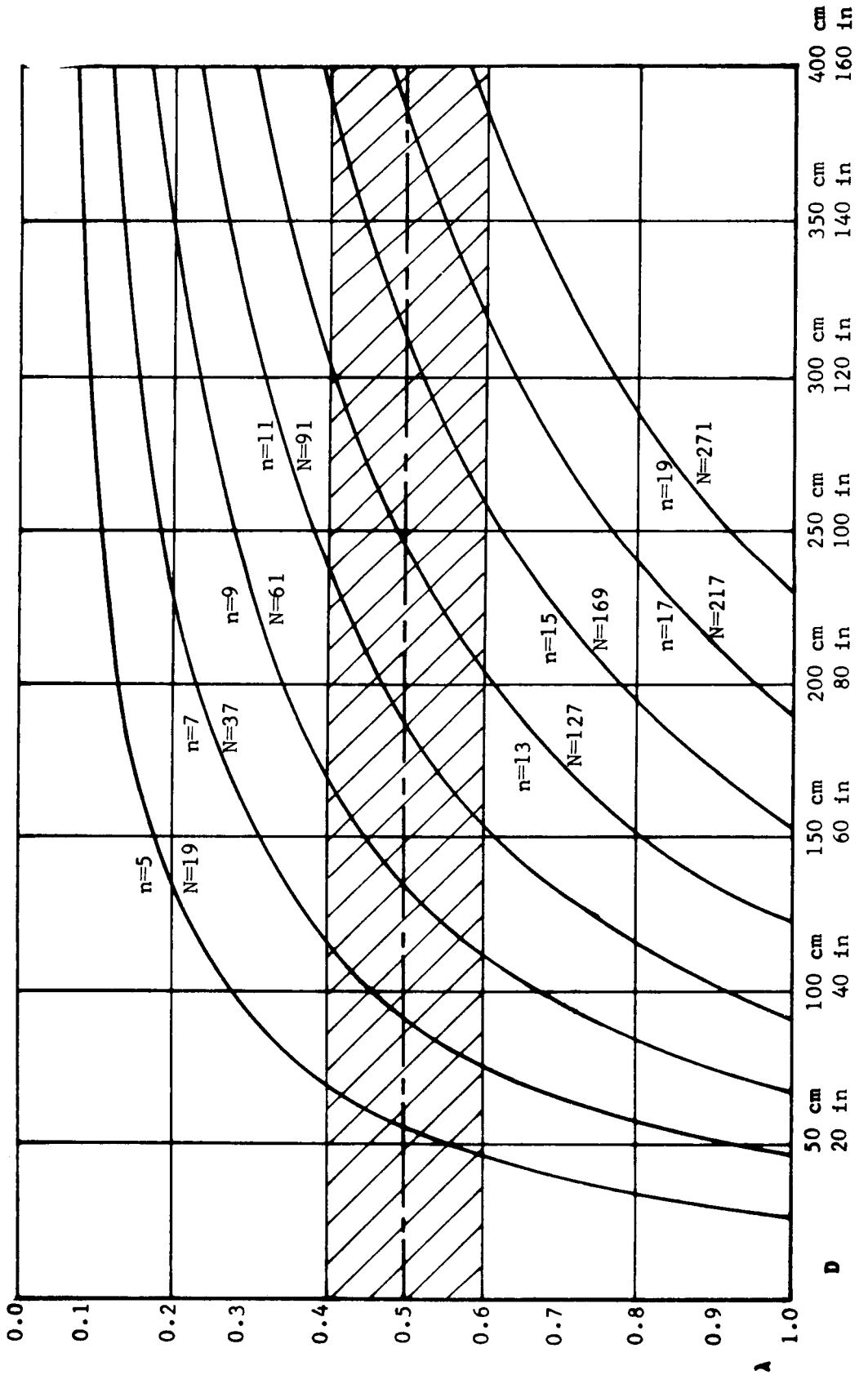
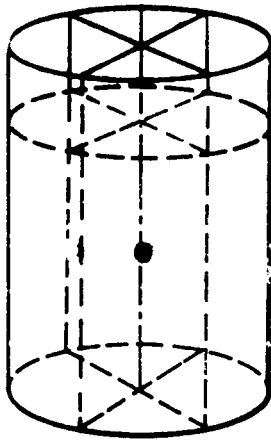


Figure 5-73 Optimum Number of Cans for Circular Cylindrical Tank. (40)

5.1.6.1 Cross Partitions

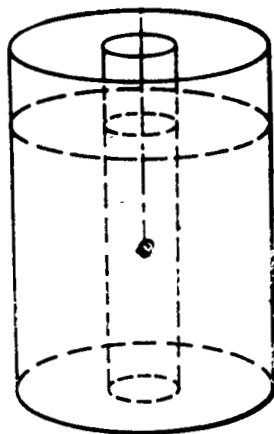


References: (4, 58)

Investigations by Bauer (4) indicate that cross partitions have a greater effect on the eigen frequencies than do concentric partitions. For the quarter-sectored tank, the oscillating propellant takes on various modes of vibration. Also, in the case of a quarter-sectored tank, the vibrating liquid mass is reduced to more than one-half of that of a circular cylindrical tank.

Investigations by Garza (58) indicate the effect of hole size on the frequency as a function of percent perforation (Figure 5-78 and 5-79) and the effect of both percent perforation and frequency on the damping ratio as a function of the excitation amplitude (Figure 5-80 and 5-81).

5.1.6.2 Concentric Partitions



References: (4, 52)

5.1.7 Pressure Distribution. The designer of a baffle system is interested in finding the pressure history of the fluid acting on the baffles because after the spacing and width of the baffles have been optimized, integration of the pressure will give the moments to be expected during flight. Thus, with the forces and moments acting on the baffle determined, the baffle material and its thickness can be chosen to withstand the load exerted on the baffles by the oscillating fluid, insuring, also, that the system pays a minimum weight penalty from the addition of the baffles.

5.1.7.1 Procedure I (28). The force per unit area on the ring is given by

$$\begin{aligned} p(\theta, t) &= C_D \cdot \frac{1}{2} \rho w^2 \\ &= C_D \frac{\rho}{2} \omega^2 f^2(-d) \cos^2 \theta \sin^2(\omega t) \end{aligned} \quad (5-9)$$

where w is the vertical component of the fluid velocity, $f(z) = \sinh k(z+h)$, $\sinh(kh)$ and C_D is the local drag coefficient. Its value may be obtained from the empirical relation

$$C_D = 15 \sqrt{\frac{U T}{D}}, \quad 2 \leq \frac{U T}{D} \leq 20$$

and

$$C_D = 2, \quad \frac{U T}{D} \geq 100$$

where $\frac{U T}{D}$ is the "period-parameter"; U_m denotes the timewise maximum velocity, T the period, D the plate width, and

$$\frac{U T}{D} = \frac{[\omega \zeta_1 f(-d) \cos \theta] (2\pi/\omega)}{\alpha a} = \frac{2\pi f(-d)}{\alpha} \left(\frac{\zeta_1}{a} \right) \cos \theta$$

Substituting $\omega^2 = kg \tanh(kh)$ into Eq. (5-9) and expressing the maximum pressure on the baffle as an equivalent head of the liquid, we have

$$Z_{\max} = \frac{P_{\max}}{\rho g} = \frac{1}{2} k a \tanh(kh) f^2(-d) (C_D)_{\max} \left(\frac{\zeta_1^2}{a} \right) \quad (5-10)$$

5.1.7.2 Procedure II (18). Analytical research has shown that the motion of the free surface of tanked liquid propellants is normal to the undisturbed liquid free surface. Thus, the maximum pressure and moments exerted by the liquid on the baffles occur when the mean free surface is at baffle level. That is, when the baffle depth, with respect to the free surface, is zero ($d = 0$).

The dynamic pressure of the fluid acting at any point on a baffle in a cylindrical tank can be expressed as

$$p = \frac{2kg\zeta_1 \rho \cos \theta}{144 (\epsilon_1^2 - 1)} \left[\frac{J_1(\epsilon_1 \frac{r}{a})}{J_1(\epsilon_1)} \right] e^{-\frac{\epsilon_1 d}{a}} \quad (5-11)$$

where

- p = dynamic pressure, psi
- kg = longitudinal acceleration, ft/sec²
- ρ = mass density of the liquid, #m/ft³
- a = radius of the cylinder, ft
- ϕ_1 = angle corresponding to sloshing amplitude
- $\zeta_1 = a \phi_1$, maximum amplitude of sloshing, ft
- θ = angular coordinate

5.1.7.2 Procedure II (18) (continued).

It can be seen from Equation (5-11) that the maximum positive pressure and maximum negative pressure will occur at $\theta = 0$, $r=a$ and $\theta = 180^\circ$, $r=a$, respectively. The analytical expression for the moments acting on the baffle is obtained from the dynamic pressure. It has the following form:

$$M_B(S) \cong \left[\frac{\pi}{4} \rho (a^4 - a_o^4) S^2 X(S) - \sum_{n=1}^{\infty} \left(\frac{S^4 X(S)}{S^2 + \omega_n^2} \right) \left[\frac{2\pi a^4 \cosh\left(\frac{\epsilon_n}{a}\right)(h-d)}{\epsilon_n^2 (\epsilon_n^2 - 1) \cosh\left(\frac{\epsilon_n h}{a}\right)} \right] \left[K\left(\frac{a_o}{a}, \epsilon_n\right) \right] \right] \quad (5-12)$$

where

$$K\left(\frac{a_o}{a}, \epsilon_n\right) = \left\{ 1 - \left(\frac{a_o}{a}\right) \left[\frac{J_1\left(\frac{\epsilon_n a_o}{a}\right)}{J_1(\epsilon_n)} \right] + \left(\frac{a_o}{a}\right)^2 (\epsilon_n) \left[\frac{J_1'\left(\frac{\epsilon_n a_o}{a}\right)}{J_1(\epsilon_n)} \right] \right\} = \text{constant}$$

S = Laplace transformation operation

a_o = Inner radius of annular baffle, ft

For a circular cylindrical tank of arbitrary size it is convenient to express Equation (5-12) as a ratio of the baffle moment to the product of longitudinal acceleration kg and sloshing amplitude ζ_1 . That is,

$$\frac{|M_{B_1}|}{\rho a^3 k |\zeta_1|} = \left[\frac{g e^{-\frac{\epsilon_1 d}{a}}}{4} \right] K\left(\frac{a_o}{a_1}, \epsilon_1\right) \quad (5-13)$$

where

$|M_{B_1}|$ = absolute value of the moment on the baffle corresponding to the first oscillation mode ($n = 1$)

5.1.7.2 Procedure II (18) (continued)

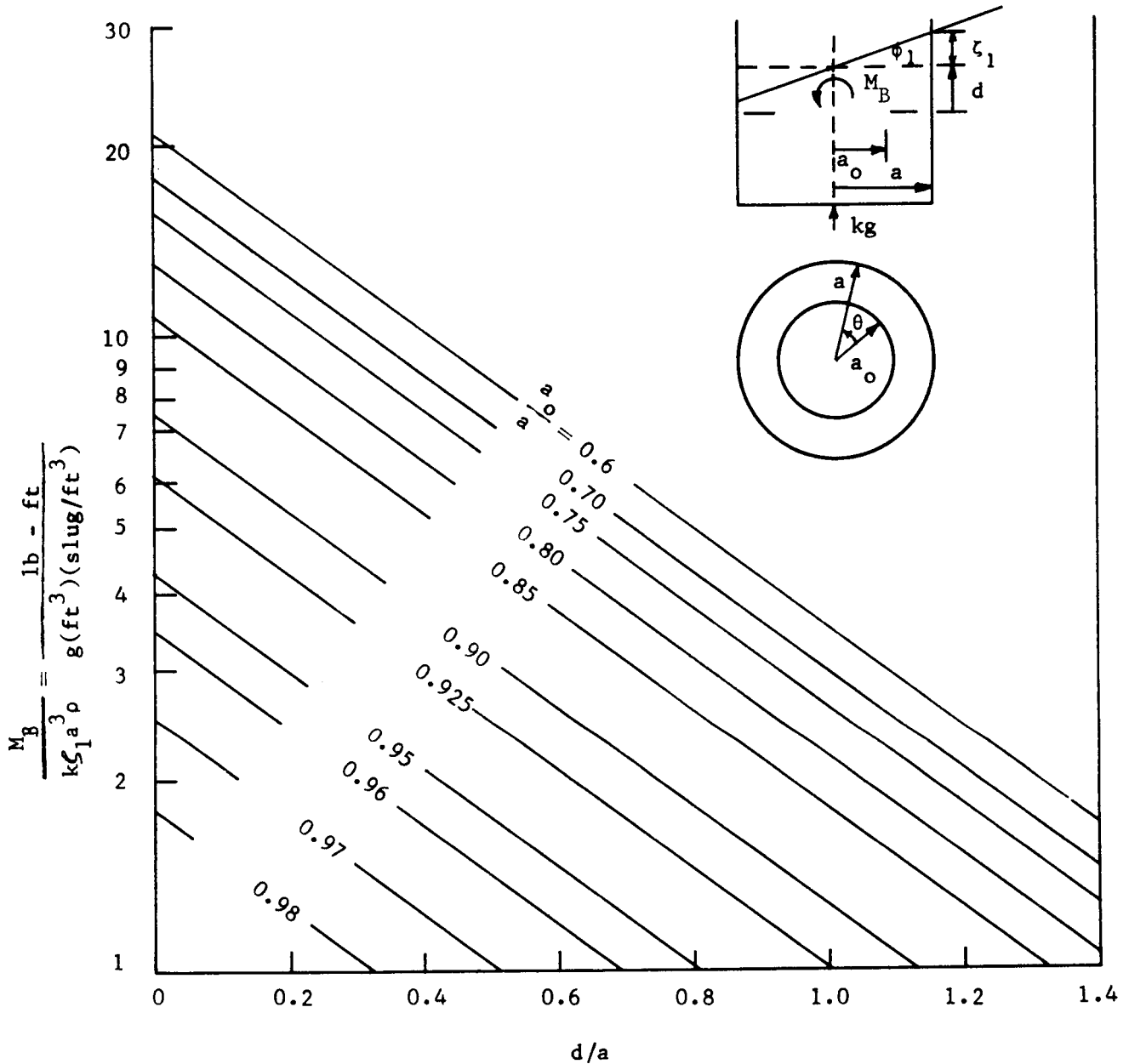
Graphical representation of Equation (5-13) can be found in Figure (5-74). It shows the baffle moment as a function of baffle width. The curves in this figure are valid only for fluid depth greater than one radius of the tank measured from the bottom. That is, $\frac{h}{a} > 1$. For $\frac{h}{a} < 1$, the following correction factor is recommended:

$$CF = \frac{e^{\frac{\epsilon_1 d}{a}}}{\cosh \frac{\epsilon_1 d}{a} + \sinh \frac{\epsilon_1 d}{a} \tanh \frac{\epsilon_1 d}{a}}$$

Then, the corrected moment expression becomes

$$M'_{B1} = CF \left\{ M_{B1} \left[\text{Equation (5-13)} \right] \right\} \quad (5-14)$$

$$\frac{M_B}{k\zeta_1 a^3 \rho} = \frac{\pi}{4} g e^{-\frac{\epsilon_1 d}{a}} \left[1 - \frac{a_0}{a} \frac{J_1(\epsilon_1 \frac{a_0}{a})}{J_1(\epsilon_1)} + \left(\frac{a_0}{a}\right)^2 \epsilon_1 \frac{J_1'(\epsilon_1 \frac{a_0}{a})}{J_1(\epsilon_1)} \right]$$



Moments Produced on Ring Baffles (18)

Figure 5-74

5.1.7.3 Procedure III (83). Conformal mapping is used to transform the geometrically complex representation of the baffle and the tank wall into a simple plane for which a solution to the Bernoulli equation for incompressible, nonviscous, unsteady flow is readily obtainable. Since this equation gives the velocity and pressure distribution on the baffle in the transformed plane it is then a simple matter to take the inverse transformation to find the solution in the original plane.

The transformation is obtained by using the Christoffel-Schwarz expression defined as

$$z = A \int_0^w (w-u_1)^{\alpha_1-1} (w-u_2)^{\alpha_2-1} \dots (w-u_k)^{\alpha_k-1} dw + B \quad (5-15)$$

where

$$z = F(w) = x + iy$$

$$w = u + iv$$

x, y = Cartesian coordinates in z -plane

u, v = Cartesian coordinates in w -plane

A = Constant which determines the scale factor and rotation of the polygon

B = Constant which determines the origin of the w -plane

$\pi\alpha_k$ = Interior angles of the polygon formed by the tank wall and the baffles in the z -plane

u_k = Vertices of the polygon on the u -axis

The pressure distribution applicable to all three cases herewith given is as follows:

5.1.7.3 Procedure III (83) (continued)

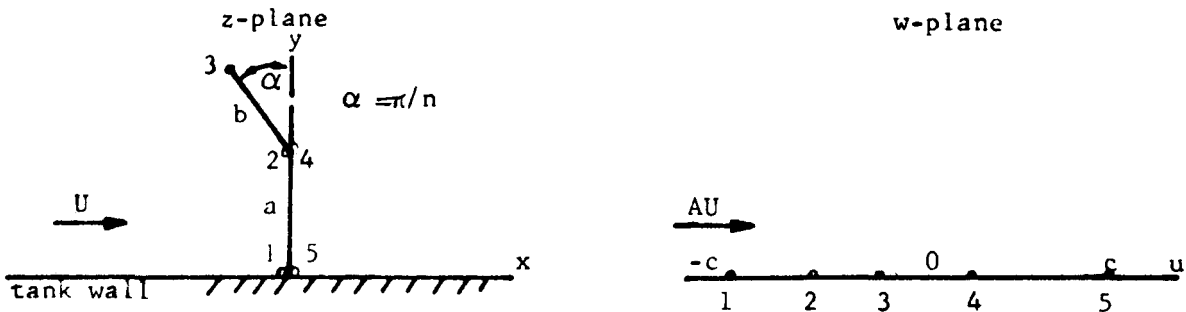
$$p(u,v) = \rho \left\{ |U| \omega \left[\operatorname{Re} F(w) - Au \right] - |U|^2 \left(\frac{3}{2} - 2ARF + \frac{A^2 R}{2K} \right) \right\} \quad (5-16)$$

where ω is the circular frequency, ρ the density of the fluid, U the velocity of the fluid acting on the baffle and f , K , and R are parameters depending on the geometry of the system.

Baffle Type I. The baffle-tank wall system in the z -plane is mapped onto the w -plane by the transformation

$$z = A \int_0^w (w+c)^{-1/2} (w-u_2)^{-1/n} (w-u_3)(w-u_4)^{1/n} (w-c)^{-1/2} dw + B \quad (5-17)$$

The result is shown in the figure for Baffle Type I below.



Baffle Type I

5.1.7.3 Procedure III (83) (continued)

The parameters and constants for the pressure distribution given in Equation (5-16) are as follows:

$$K(u,o) = \frac{\sqrt{2A}}{2(c^2 - u^2)} \left| \frac{u-u_4}{u-u_2} \right|^{1/n}$$

$$R(u,o) = \frac{\sqrt{2}}{2A(u-u_3)^2} \left| \frac{u-u_2}{u-u_4} \right|^{1/n}$$

$$f(u,o) = \beta \sin(\theta_3/n)$$

$$g(u,o) = -\beta \cos(\theta_3/n)$$

$$A = b/I_2 \quad B = b_1 + ib_2$$

$$\theta_3(u,o) = \begin{cases} 0 & \text{for } -c \leq u \leq u_2, u_4 \leq u \leq c \\ \pi & \text{for } u_2 \leq u \leq u_4 \end{cases}$$

$$\beta(u,o) = \sqrt{2(c^2 - u^2)} (u-u_3)$$

$$I_o = \int_0^{u_3} |F'(w)| dw$$

$$I_2 = \int_{u_2}^{u_3} (w+c)^{1/2} (w-u_2)^{-1/n} (u_3-w)(u_3-w)^{1/n} (c-w)^{-1/2} dw$$

$$b_1 = -b(1+I_o/I_2) \sin \alpha ; b_2 = b(1+I_o/I_2) \cos \alpha + a$$

The constants u_2, u_3, u_4 can be determined from the integral expression for I_2 above and from the following definite integrals:

$$\begin{aligned}
 I_1 &= \int_{-c}^{u_2} (w+c)^{-1/2} (u_2-w)^{-1/n} (u_3-w)(u_4-w)^{1/n} (c-w)^{-1/2} dw \\
 I_3 &= \int_{u_3}^{u_4} (w+c)^{-1/2} (w-u_2)^{-1/n} (w-u_3)(u_4-w)^{1/n} (c-w)^{-1/2} dw \\
 I_4 &= \int_{u_4}^{u_5} (w+c)^{-1/2} (w-u_2)^{-1/n} (w-u_3)(w-u_4)^{1/n} (c-w)^{-1/2} dw
 \end{aligned}
 \tag{5-18}$$

where $I_1, I_2, I_3,$ and I_4 are definite integrals which are proportional to the length of the sides of the polygon ABCDE corresponding to polygon 12345 in the transformation for Baffle Type I. Thus,

$$\frac{\overline{BC}}{\overline{AB}} = \frac{I_2}{I_1} = \frac{b}{a} = \lambda_2 \quad \frac{\overline{CD}}{\overline{AB}} = \frac{I_3}{I_1} = \frac{b}{a} = \lambda_3 \quad \frac{\overline{DE}}{\overline{AB}} = 1 = \lambda_4$$

The unknown constants u_2, u_3, u_4 can be determined by finite difference techniques by using the simultaneous equations

$$I_k(u_2, u_3, u_4) = \lambda_k I_1(u_2, u_3, u_4) \quad , \quad k = 2, 3, 4 \tag{5-19}$$

For example: let u_2^*, u_3^* and u_4^* be the solution of the above equation and take $u_2^{(o)}, u_3^{(o)}$ and $u_4^{(o)}$ as the initial values differing little from the exact solution u_2^*, u_3^* and u_4^* . We expand equation (5-19) in a Taylor's series in powers of the differences $\alpha_k^{(1)} = u_k^* - u_k^{(o)}$ and terminate at the first order terms, thus obtaining the first approximation

5.1.7.3 Procedure III (83) (continued)

$$I_k^{(0)} + \sum_{j=2,3,4} \alpha_j^{(1)} I_{k,u_j}^{(0)} = \lambda_k \left[I_1^{(0)} + \sum_{j=2,3,4} \alpha_j^{(1)} I_{1,u_j}^{(0)} \right] \quad k=2,3,4 \quad (5-20)$$

where

$$I_{k,u_j}^{(m)} = \left[\frac{\partial I_k}{\partial u_j} \right]_{u_j = u_j^{(m)}}$$

The partial derivatives which have limits not depending on u_2 , u_3 and u_4 may be obtained by direct differentiation, i.e., performing the partial differentiation, then integrating. Those that have u_2 , u_3 and u_4 as limits are computed numerically by using

$$I_{k,u_j}^{(m)} = \left[I_k(u_j^{(m)} + \Delta u) - I_k^{(m)} \right] / \Delta u, \quad (5-21)$$

where Δu is a small increment. Solving for $\alpha_j^{(1)}$ simultaneously from equation (5-20) and using the second approximation,

$$u_j^{(1)} = u_j^{(0)} + \alpha_j^{(1)}, \quad j=2, 3, 4$$

in equation (5-20), we obtain

$$I_k^{(1)} + \sum_{j=2,3,4} \alpha_j^{(2)} I_{k,u_j}^{(1)} = \lambda_k \left[I_1^{(1)} + \sum_{j=2,3,4} \alpha_j^{(2)} I_{1,u_j}^{(1)} \right] \quad k=2,3,4.$$

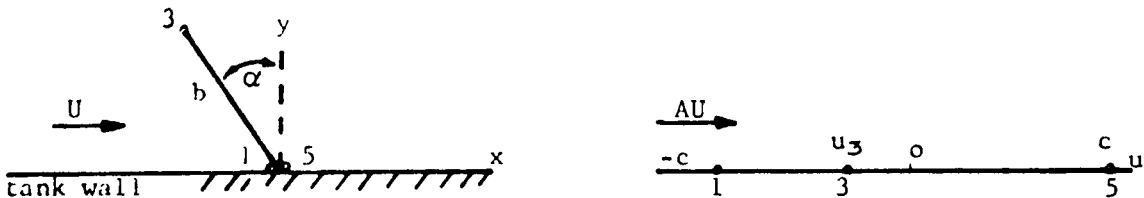
The above process is carried out until $u_k^{(m)}$'s converge.

5.1.7.3 Procedure III (83) (continued)

Special Case: Baffle Type IA. This is a special case of Baffle Type I for which $a = 0$, $u_2 = -c$, and $u_4 = c$. The transformation becomes

$$z = A \int_0^w (c+w)^{-\frac{(n+2)}{2n}} (w-u_3)(w-c)^{-\frac{(n-2)}{2n}} dw + B \quad (5-22)$$

The results are shown in the figure for Special Case Ia below.



Special Case Ia

For this case, the parameters and constants needed to obtain the pressure distribution (Equation 5-16) are the following:

$$K(u,0) = \frac{\sqrt{2}}{2} A (c+u)^{-\frac{(n+1)}{n}} (c-u)^{-\frac{(n-1)}{n}}$$

$$R(u,0) = \frac{\sqrt{2}}{2A} \left[\frac{c+u}{c-u} \right]^{1/n} (u-u_3)^{-2}$$

$$f(u,0) = - \sqrt{2(c^2-u^2)} (u-u_3) \sin \alpha \quad (5-23)$$

$$g(u,0) = - \sqrt{2(c^2-u^2)} (u-u_3) \cos \alpha$$

5.1.7.3 Procedure III (83) (continued)

$$A = b/I_2$$

$$B = b_1 + ib_2$$

$$\text{Re}F(u,0) = A \sin \alpha \int_0^u (c+u)^{-(n+2)/2n} (u-u_3) (c-u)^{-(n-2)/2n} du + b_1$$

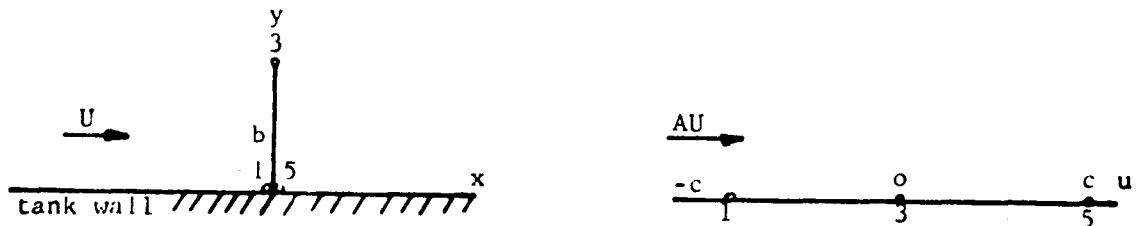
$$\text{Im}F(u,0) = -A \cos \alpha \int_0^u (c+u)^{-(n+2)/2n} (u-u_3) (c-u)^{-(n-2)/2n} du + b_2$$

The pressure distribution for Case IA is shown in figure (5-75).

Special Case: Baffle Type IB. This is a special case of Baffle Type I for which $\alpha = 0$, $u_2 = -c$, $u_3 = 0$, $u_4 = c$, and $\frac{1}{n} = 0$. The transformation becomes

$$z = A \int_0^w \frac{wdw}{\sqrt{w^2 - c^2}} = A \sqrt{w^2 - c^2}. \quad (5-24)$$

The results are shown in the figure for special Case IB below.



Special Case Ib

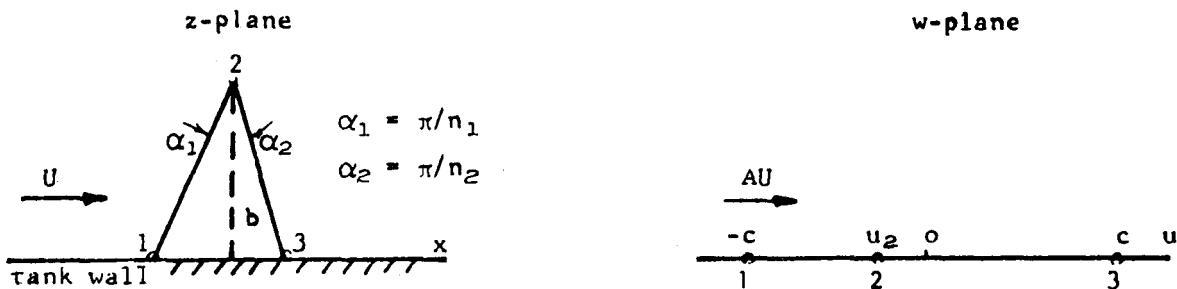
The pressure distribution is well known. It is parabolic in shape with the maximum disturbance pressure occurring at the base of the baffle and the minimum (zero) at the tip of the baffle.

5.1.7.3 Procedure III (83) (continued)

Baffle Type II. The baffle-tank system ($n_1 = n_2 = n$, $u_2 = 0$) in the z -plane is mapped onto the w -plane by the transformation

$$z = A \int_0^w (c+w)^{-\frac{(n_1-2)}{2n_1}} (w-u_2)^{1-\frac{1}{n_1}-\frac{1}{n_2}} (w-c)^{-\frac{(n_2-2)}{2n_2}} dw + B \quad (5-25)$$

The results of this transformation is shown in the figure below.



Baffle Type II

The parameters and constants given in Equation (5-16) can be obtained as follows:

$$\frac{dz}{dw} = AK' (\sin \alpha_1 + i \cos \alpha_1) = K(f + ig)$$

$$\frac{dw}{dz} = \frac{1}{AK'} (\sin \alpha_1 - i \cos \alpha_1) = R(f - ig) \quad (5-26)$$

$$-c \leq u \leq u_2$$

5.1.7.3 Procedure III (83) (continued)

$$\frac{dz}{dw} = AK' (\sin \alpha_2 - i \cos \alpha_2) = K(f + ig)$$

$$\frac{dw}{dz} = \frac{1}{AK'} (\sin \alpha_2 + i \cos \alpha_2) = R(f - ig) \quad (5-27)$$

$$-u_2 \leq u \leq c$$

$$K' = (c+u)^{-\frac{(n_2-2)}{2n_2}} |u-u_2|^{-\frac{1}{n_1} - \frac{1}{n_2}} (c-u)^{-\frac{(n_2-2)}{2n_2}}$$

$$A = \frac{b}{I_1 \cos \alpha_1} \quad I_1 = \int_{-c}^{u_2} K' du$$

$$b_1 = b \left(\tan \alpha_2 - \frac{\sin \alpha_2}{\cos \alpha_1} \frac{I_c}{I_1} \right), \quad I_c = \int_0^c K' du$$

$$b_2 = b \left(\frac{\cos \alpha_2}{\cos \alpha_1} \frac{I_c}{I_1} \right) \quad (5-28)$$

The constant u_2 can be found from

$$\frac{\cos \alpha_1}{\cos \alpha_2} I_1 = I_c - I_2, \quad I_2 = \int_0^{u_2} K' du$$

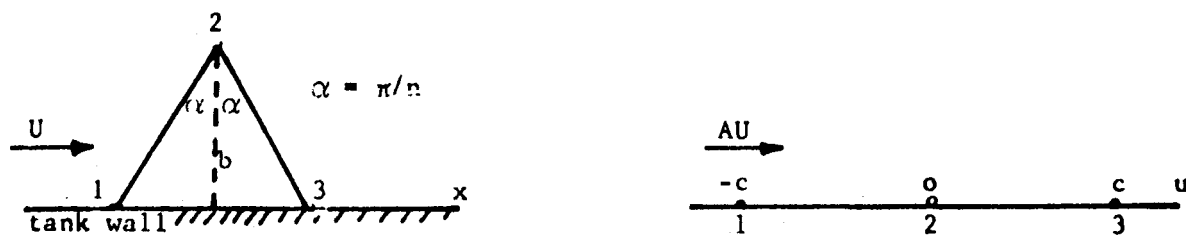
5.1.7.3 Procedure III (83) (continued)

Special Case: Baffle Type IIA. Same as Baffle Type II

but $\alpha = \alpha_1 = \alpha_2$. The transformation becomes

$$z = A \int_0^w \left[(w^2 - c^2)^{-\frac{(n-2)}{2n}} (w)^{\frac{(n-2)}{n}} \right] dw + ib \quad (5-29)$$

The results are shown in the figure below



Baffle Type IIA

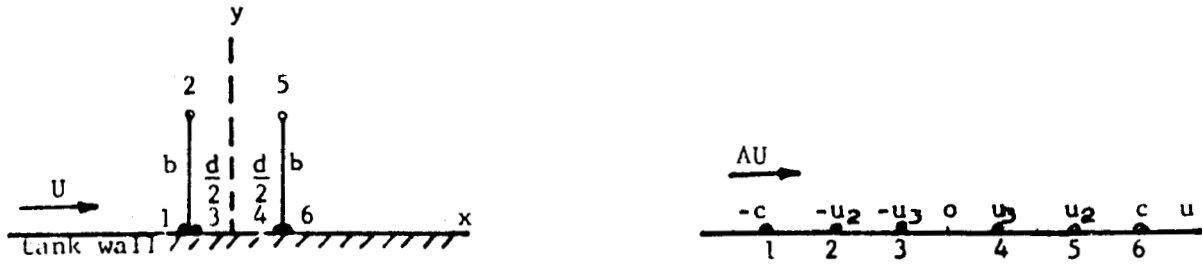
Baffle Type III. The transformation from the z-plane

to the w-plane is given by

$$z = A \int_0^w \frac{(w^2 - u_2^2) dw}{\sqrt{(w^2 - c^2)(w^2 - u_3^2)}} \quad (5-30)$$

5.1.7.3 Procedure III (83)(continued)

and the results shown in the figure below.



BAFFLE TYPE III

The parameters and constants given in Equation (5-16) are as follows:

$$\frac{dz}{dw} = A \frac{(u^2 - u_2^2)}{\sqrt{(c^2 - u^2)(u^2 - u_3^2)}} (0 - i) = K(f + ig)$$

$$\frac{dw}{dz} = \frac{1}{A} \frac{\sqrt{(c^2 - u^2)(u^2 - u_3^2)}}{(u^2 - u_2^2)} (0 + i) = R(f - ig) \quad (5-31)$$

for $u_3 \leq |u| \leq c$

$$\frac{dz}{dw} = A \frac{(u^2 - u_2^2)}{\sqrt{(c^2 - u^2)(u_3^2 - u^2)}} (1 + io) = K(f + ig)$$

$$\frac{dw}{dz} = \frac{1}{A} \frac{\sqrt{(c^2 - u^2)(u_3^2 - u^2)}}{u^2 - u_2^2} (1 - io) = R(f - ig) \quad (5-32)$$

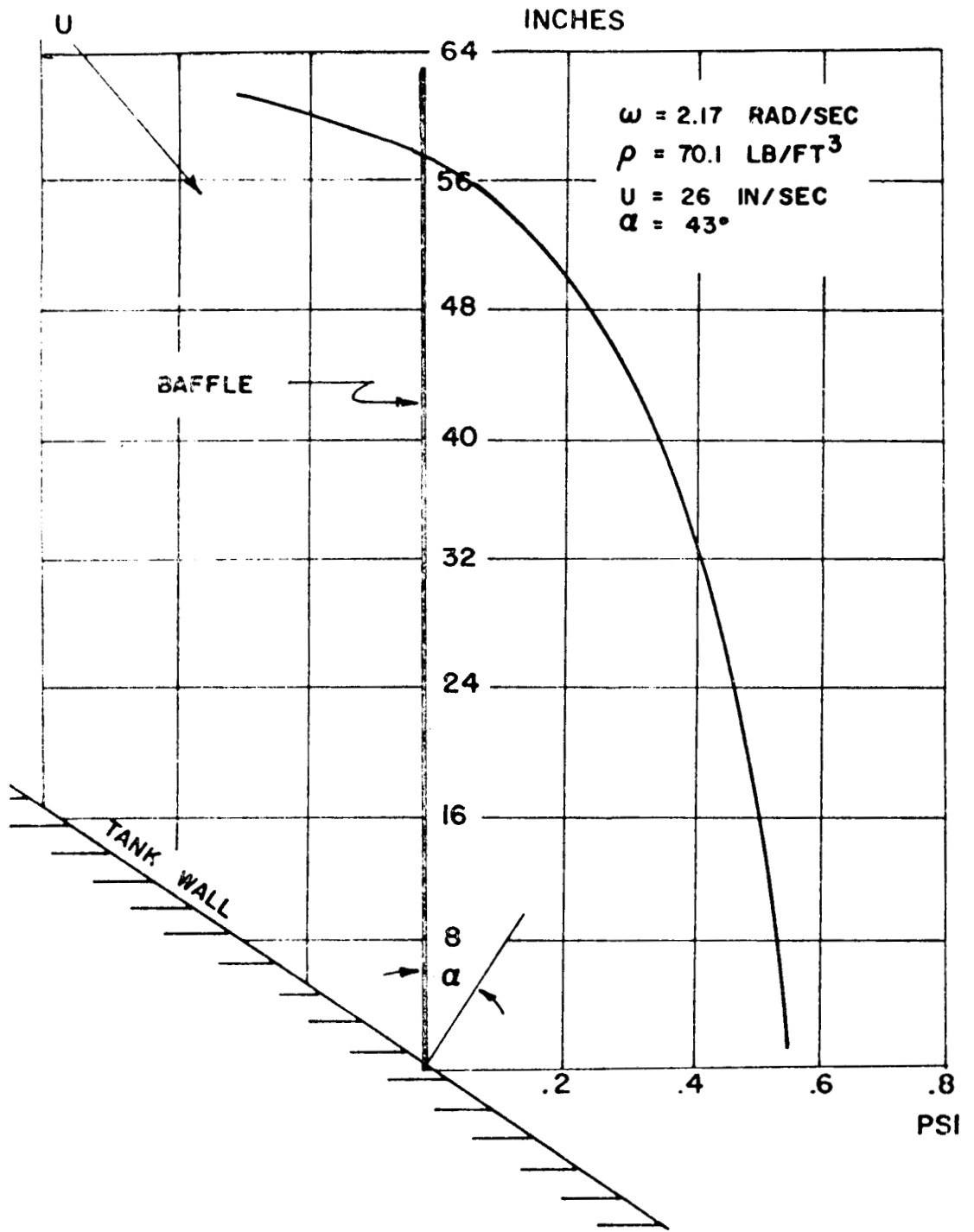
for $|u| \leq u_3$

5.1.7.3 Procedure III (83) (continued)

The constants u_2 , u_3 , and A are determined simultaneously from the equations

$$\begin{aligned}
 K_1/K_2 &= d/2b, & K_2 &= K_3, & A &= d/2K_1, & B &= 0 \\
 K_1 &= \int_0^{u_3} \frac{(u_2^2 - u^2) du}{\sqrt{(c^2 - u^2)(u_3^2 - u^2)}} \\
 K_2 &= \int_{u_3}^{u_2} \frac{(u_2^2 - u^2) du}{\sqrt{(c^2 - u^2)(u_3^2 - u^2)}} \\
 K_3 &= \int_{u_2}^c \frac{(u^2 - u_2^2) du}{\sqrt{(c^2 - u^2)(u^2 - u_3^2)}}
 \end{aligned} \tag{5-33}$$

Special Case: Baffle Type IIIA. The results are identical with Special Case Baffle Type IB but with $u_3 = u_2 = 0$.



PRESSURE ON A SLANT BAFFLE (83).

Figure 5-75

5.1.8 Conclusions and Recommendations

In choosing a damping system, the designer should start with solid ring baffles and use Miles' expression, Equation (5-1), for his first approximation of the damping factor. The reason is that Miles' equation is simple in format and in nature and a rather rapid "ball-park figure" for the spacing and width of the baffles can be obtained. Bauer's extension (article 5.1.3.2.3) would then give more accurate results and optimum conditions. The pressure acting on the baffle (Equations 5-10, 5-11, and 5-16) will permit the optimization of the thickness and material of each baffle and thus the calculation of the total weight added by the damping system.

Results

1. The maximum frequency occurs when the baffle is located at the undisturbed free liquid surface, i.e., $\frac{d_s}{R} = 0$ (Figures 5-2 and 5-3).
Note: The curves in Figures 5-2 and 5-3, for high values of $\frac{d_s}{R}$, approach asymptotically, the first resonant frequency for a circular cylindrical tank containing no baffles.
2. Agreement between experimental values of the damping factor and those obtained from Miles' equation is good except in the range of $0 < \frac{d_s}{R} < 0.125$ (Figure 5-5).
3. With the hole size constant and for a given baffle depth:
 - (a) The frequency increases for increasing percent perforation (Figure 5-2).

Results (continued)

- (b) The damping factor increases for decreasing hole size (Figure 5-8).
- 4. With the percent perforation constant and for a given baffle depth:
 - (a) The frequency increases for increasing hole size (Figure 5-3).
 - (b) The damping factor increases for decreasing hole size (Figure 5-7).
- 5. The frequency of a solid fixed ring baffle is higher than that of a perforated baffle for $\frac{d_s}{R} \leq 0.05$ and lower for $\frac{d_s}{R} \leq 0.05$ (Figures 5-2 and 5-3).
- 6. Damping produced by perforating baffles is consistently lower than that produced by a solid baffle (Figure 5-7 and 5-8).
- 7. The damping factor increases as the excitation amplitude increases (Figure 5-6).
- 8. For a given baffle depth:
 - (a) The damping factor of a fixed ring, conic section and perforated conic section increases as the baffle width increases (Figures 5-10, 5-67, and 5-68).
 - (b) With the radial clearance constant, the damping factor of a ring-with-radial-clearance increases as its baffle width increases (Figure 5-11).
 - (c) With the baffle width constant, the damping factor of a ring-with-radial-clearance decreases as the radial clearance increases (Figure 5-11).

9. The damping factor is independent of kinematic viscosity and increases as the excitation amplitude increases (Figures 5-13 and 5-14).
10. Agreement between experimental values of the damping factor and those obtained in Miles' equation is good except for $0 < \frac{d_s}{R} \leq (0.8 - 1.2)$, (Figures 5-12 and 5-14).
11. For a given baffle depth:
 - (a) The frequency for a fixed ring, conic section, and perforated conic section increases as the baffle width decreases (Figures 5-15, 5-64, and 5-66).
 - (b) With the radial clearance constant, the frequency increases as the baffle width decreases (Figure 5-16).
 - (c) With the baffle width constant, the frequency increases as the radial clearance decreases (Figure 5-16).
12. During propellant loading, the cans erected smoothly and arranged themselves in the required configuration even though they were randomly placed in the tank bottom before starting the filling operation. For this reason, they operated as good anti-vortex devices.
13. The devices floated perfectly and yielded high damping effects.
14. Draining the liquid while the tank was oscillating did not change the damping effect.
15. An inherent disadvantage of cans is that they are free to move when the container is empty, i.e., they are loose bodies during the transportation of the missile and can thereby cause damage to the inner tank structure.

16. The dashed parts of the curves in Figures 5-9, 5-10, and 5-67 indicate that, because of the turbulent nature of the liquid in the regions of higher damping, an uncertainty existed in defining the exact location of maximum damping.
17. A divided baffle which extended down to the ring baffle was used for most of the tests in Reference (35). This tended to increase the value of the damping as seen in Figure 5-14.

Conclusions

1. Fixed ring baffles can be perforated with holes of relatively small diameter, thereby reducing the baffle area by as much as 23% with no appreciable loss in damping effectiveness. Such reduction in baffle area may be effectively used for additional baffles thus increasing the minimum damping ratio value with no appreciable increase in baffle weight.
2. For an excitation amplitude $\frac{x_o}{d} = 0.00417$, the baffle above the liquid surface adds to damping only when the distance $\frac{d_s}{R} < 0.125$ and the baffle below the surface contributes to damping only when $0 \leq \frac{d_s}{R} \leq 0.375$. The baffle spacing for some minimum γ_s can be determined by adding the depth of the submerged baffle to the depth of $\frac{d_s}{R} = 0.125$ for which the upper baffle is still effective.
3. Fixed ring baffles can efficiently introduce liquid damping into propellant tanks.
4. Fixed ring baffles are not very efficient for shifting the liquid resonant frequency.

Conclusions (continued)

5. Based on the total surface area of a baffle, the highest mean damping factor of the baffles tested appears to be afforded by the fixed ring baffle (Figure 5-78).

Summarizing, the following remarks are pertinent.

1. Bauer's extension to Miles' equation can be used without further experimental verification except for a check of the final product.

2. Ring baffles provide little frequency effect.

3. Solid ring baffles with small diameter perforations (about 20% open area) can effectively be used to reduce baffle weight addition without an appreciable loss in damping effectiveness.

4. Conical rings offer greater degree of damping than floating cans, except where the cans carefully cover the liquid surface.

5. The amount of damping produced by both floating cans and conical rings is strongly dependent upon excitation amplitude.

6. Cans are the only suitable type of float. However, ring baffles are more reliable and appear to give greater damping.

7. Floats, like baffles, are used mostly to damp liquid motion however, floats are like partitions, in that their effect on frequency and damping is constant for all shallow depths.

8. Subdivision by radial walls is much more effective in reducing the amount of sloshing than subdivision by concentric walls. In the case of a quarter-sectored tank the vibrating liquid mass is reduced to more than 1/2 that of a circular cylinder.

9. Ring baffles are far better as damping devices than conic, inverted conic or cruciform baffles.

10. Cross partitions have a greater effect on the eigen-frequencies than do concentric partitions.

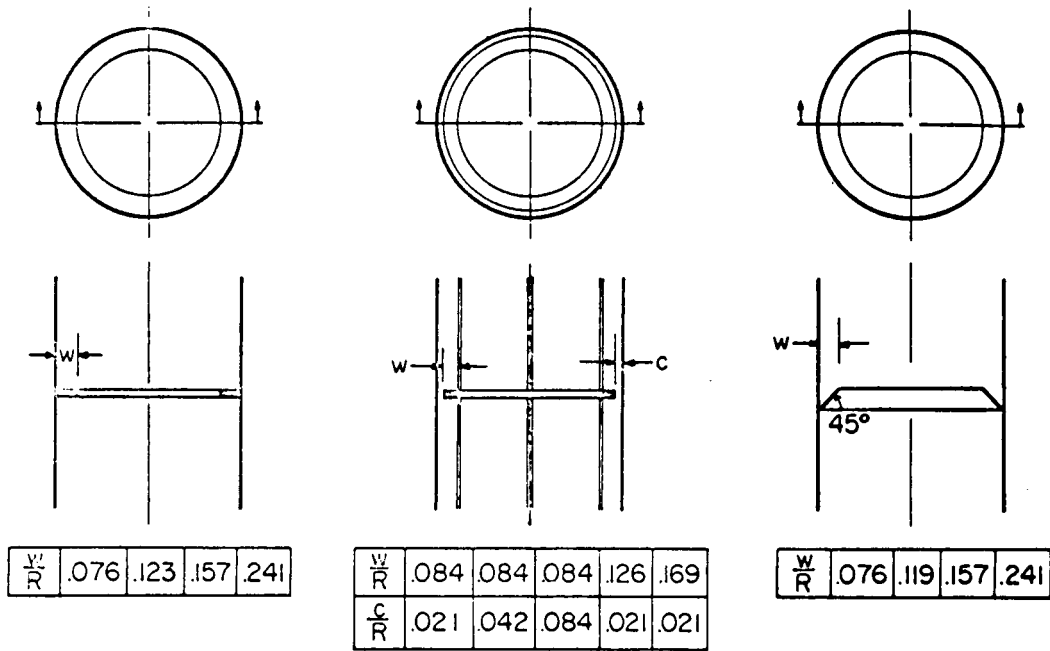
11. Floats should cover the entire cross-sectional area and fill the zone of oscillation, i.e., to a depth of one-fourth the tank diameter.

12. Floats should be capable of following the changing liquid level.

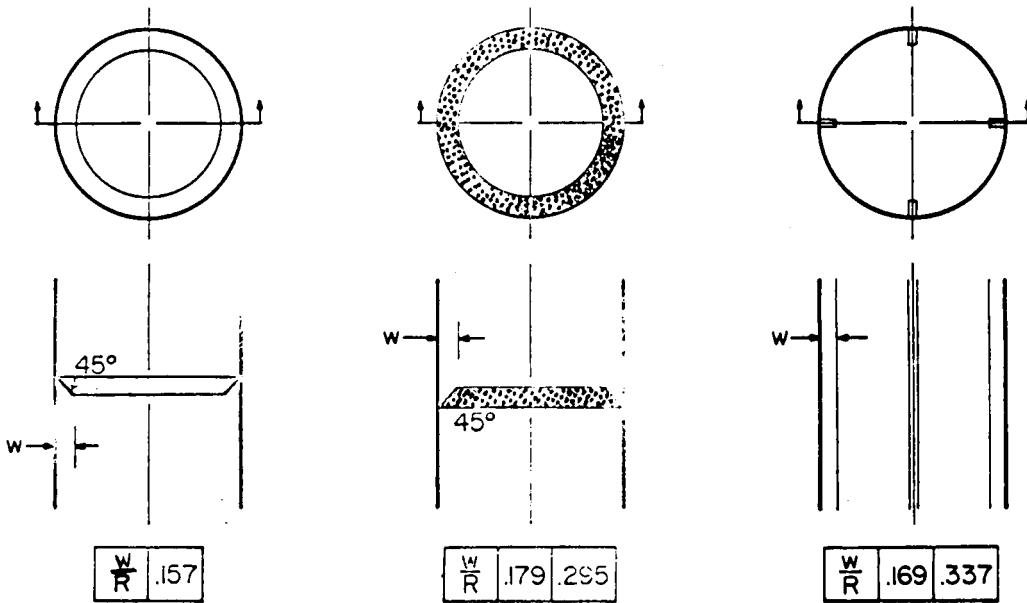
13. Floats should be capable of adapting to the changing cross-sectional area of the container, i.e., the float should not catch-on or cling to stiffener rings, pipelines or other equipment obstructing the inner walls of the tank.

14. Floats should not change the moment of inertia of the liquid when subjected to roll excitations about the longitudinal axis of the container.

15. Partitions should divide the total liquid mass into approximately equal partial masses thereby effectively reducing the tank diameter.



(a) Fixed ring. (b) Ring with radial clearance. (c) Conic section.



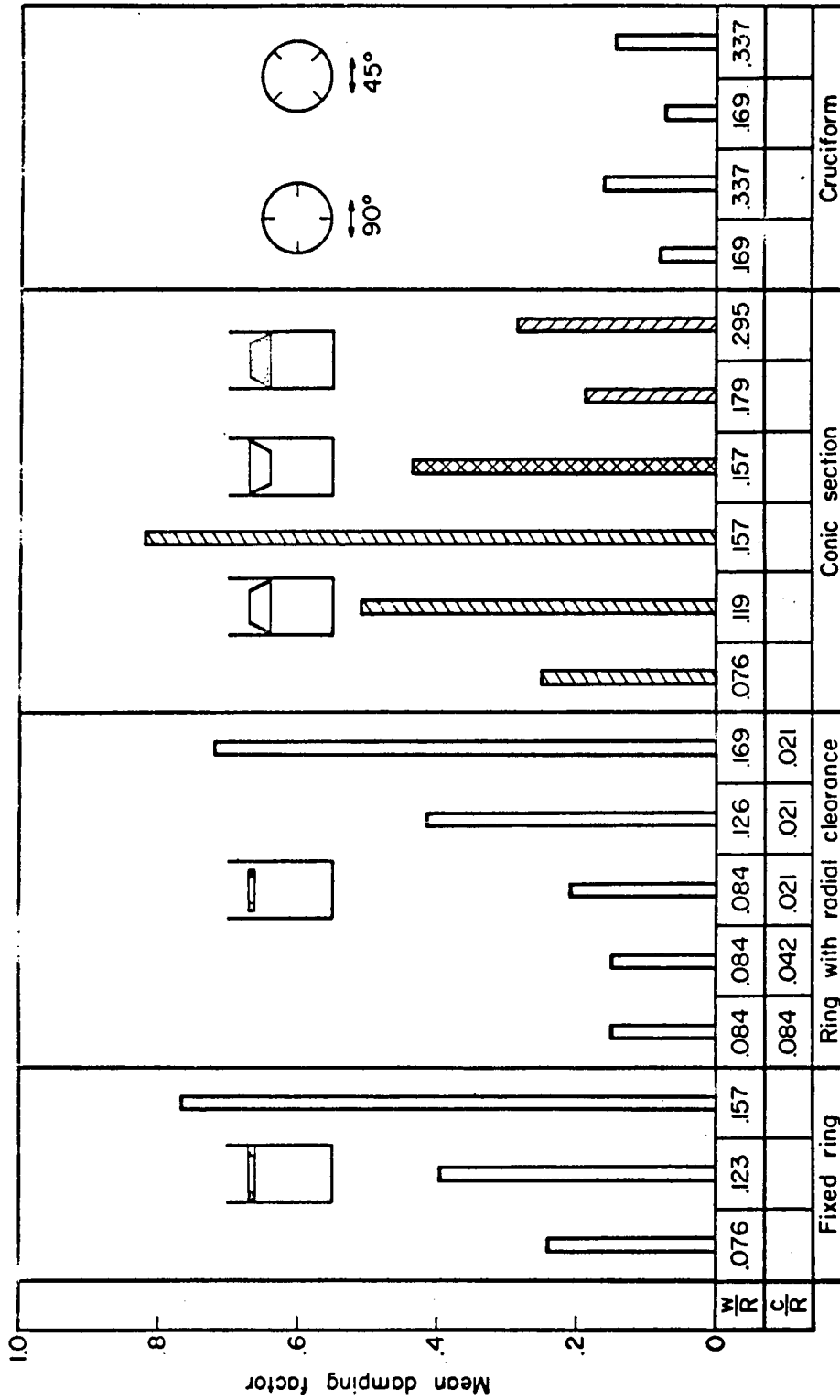
(d) Inverted conic section.

(e) Perforated conic section.

(f) Cruciform.

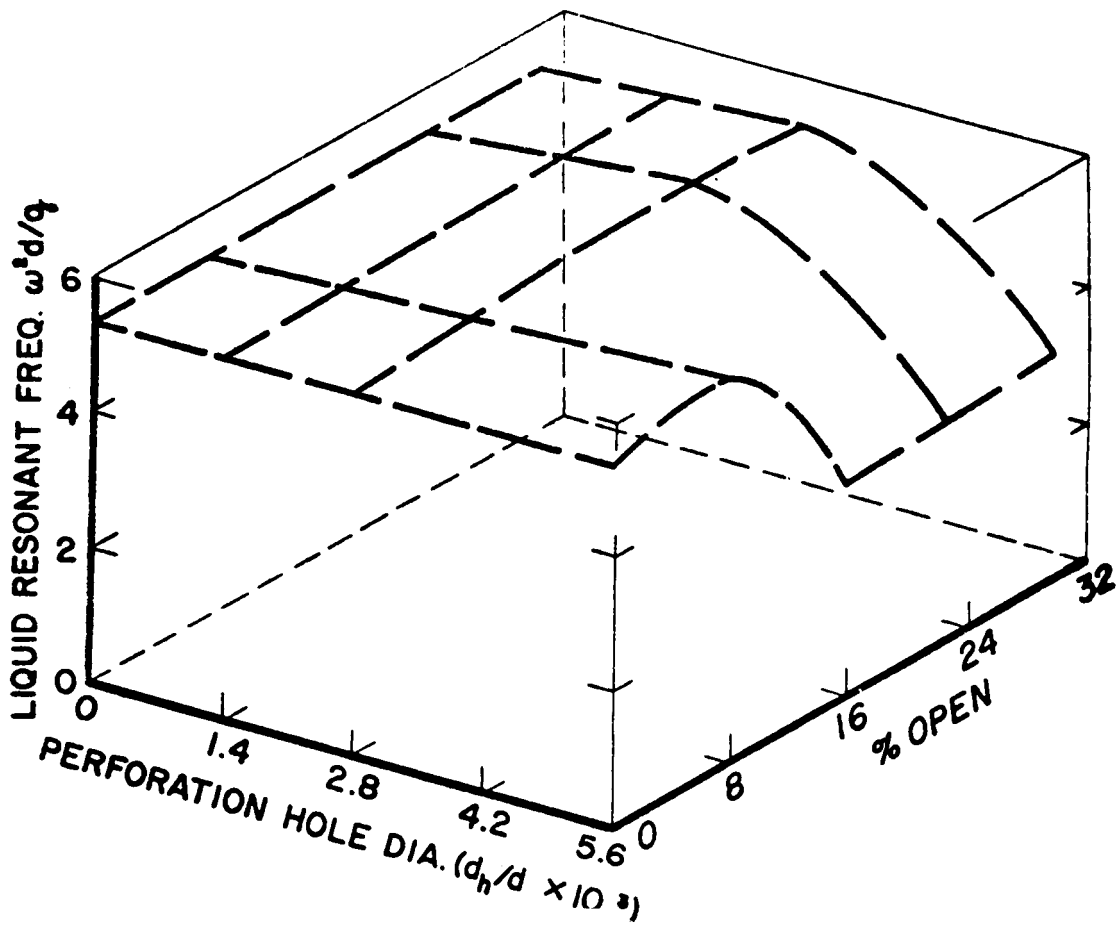
Baffle configurations. (35)

Figure 5-76



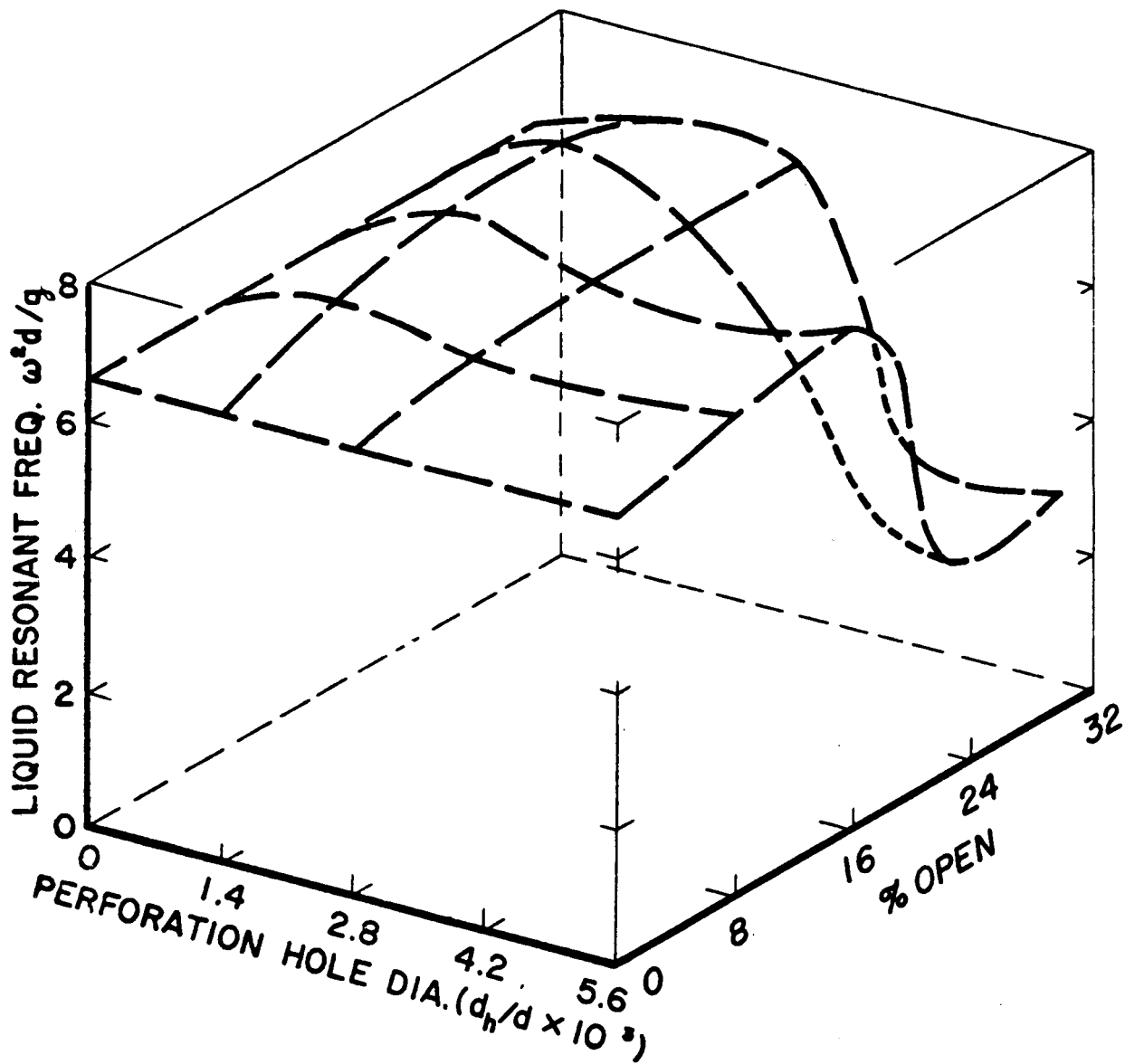
Comparison of baffles. (35)

Figure 5-77



Effect of hole size and percent perforation on resonant frequency for a quarter sector tank. (58)


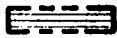

Figure 5-78

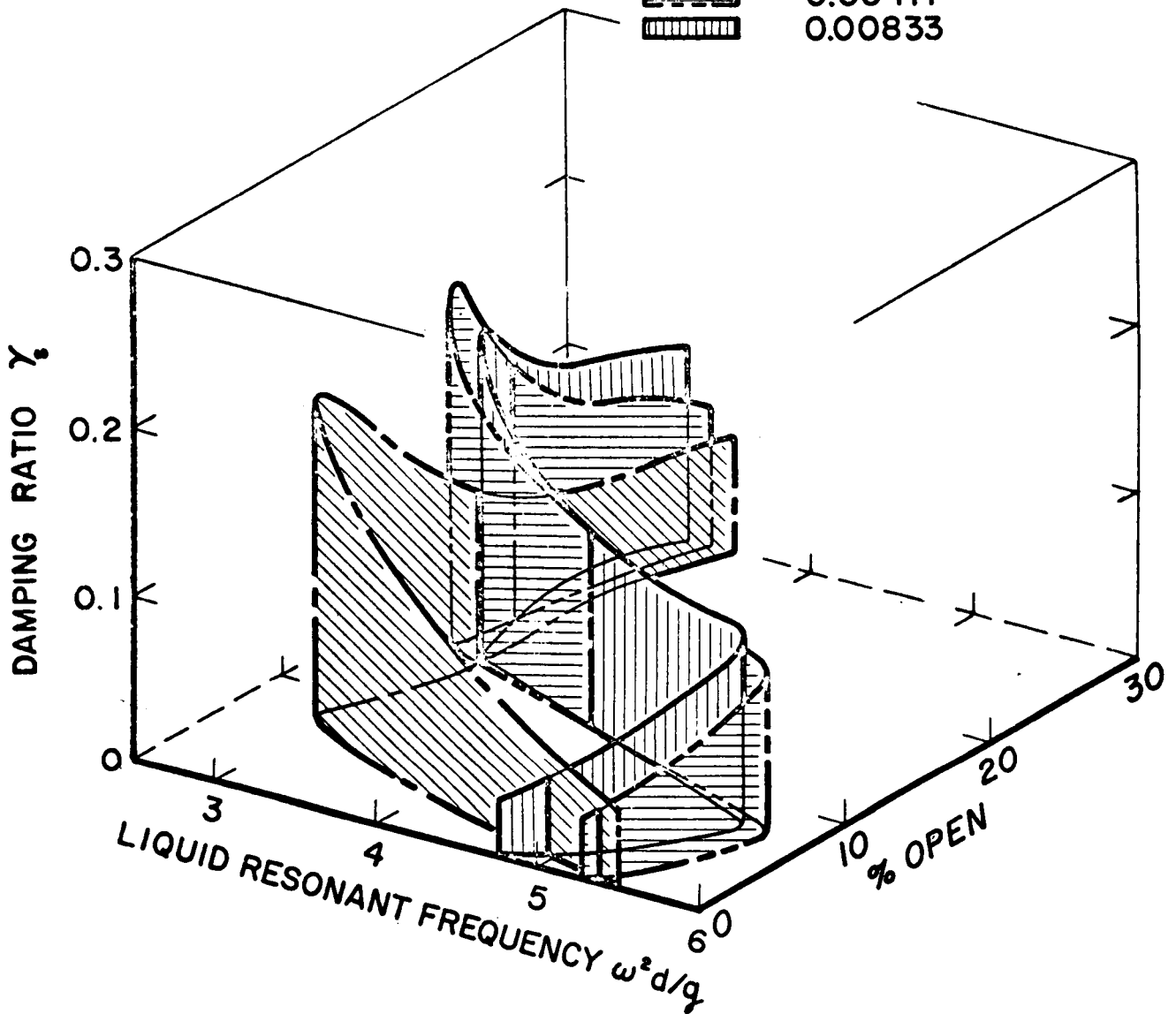


Effect of hole size and percent perforation on resonant frequency for an eighth sector tank. (58)

Figure 5-79

90° SECTOR TANK
 PERFORATION HOLE DIA. $d_h/d = 0.0056$

SYMBOL	X_0/d
	0.00187
	0.00417
	0.00833



Effect of percent perforation and resonant frequency on the damping ratio as a function of excitation amplitude for a quarter sector tank.(58)

Figure 5-80

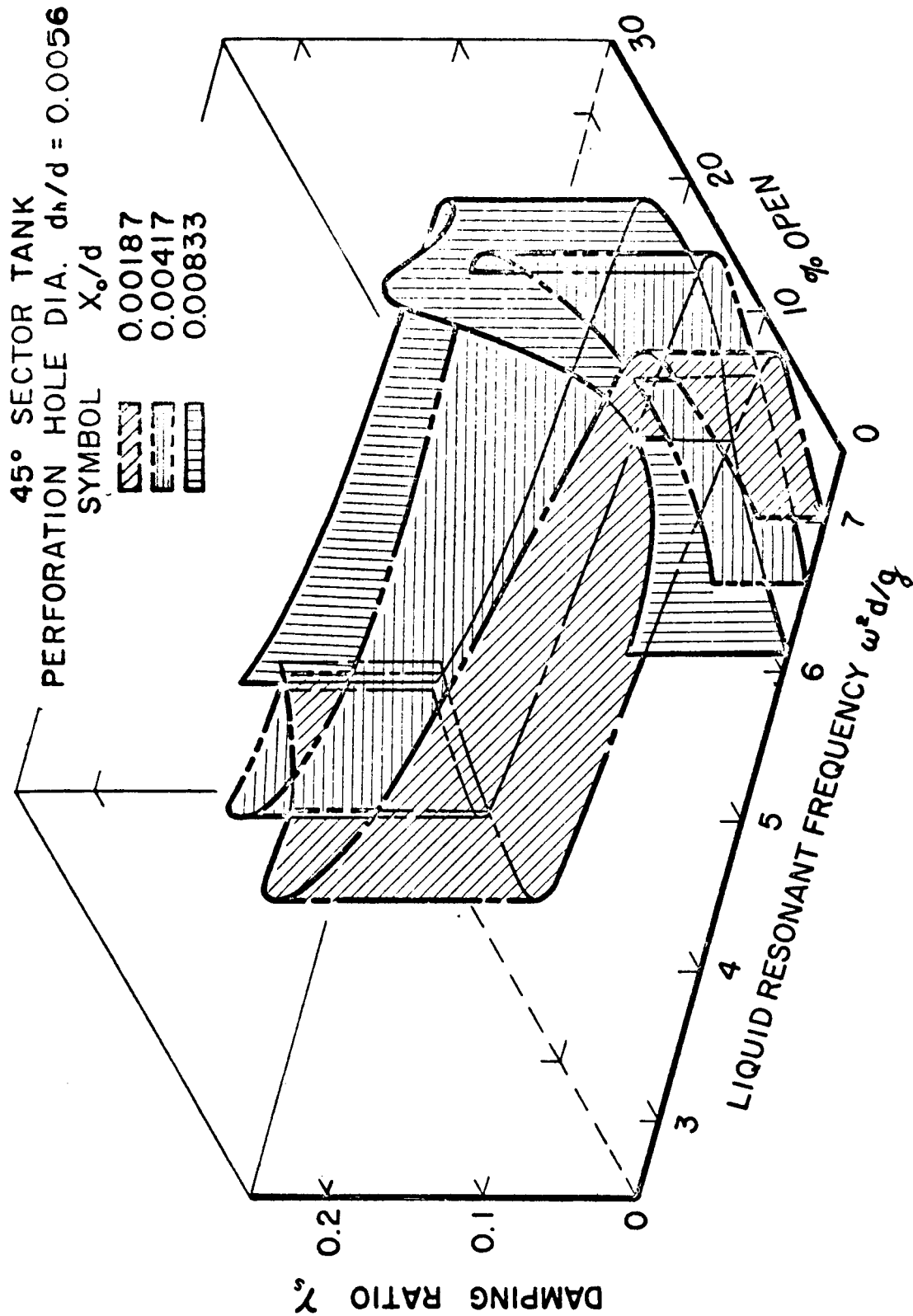


Figure 5-81. Effect of percent perforation and resonant frequency on the damping ratio as a function of excitation amplitude for an eighth sector tank. (58)

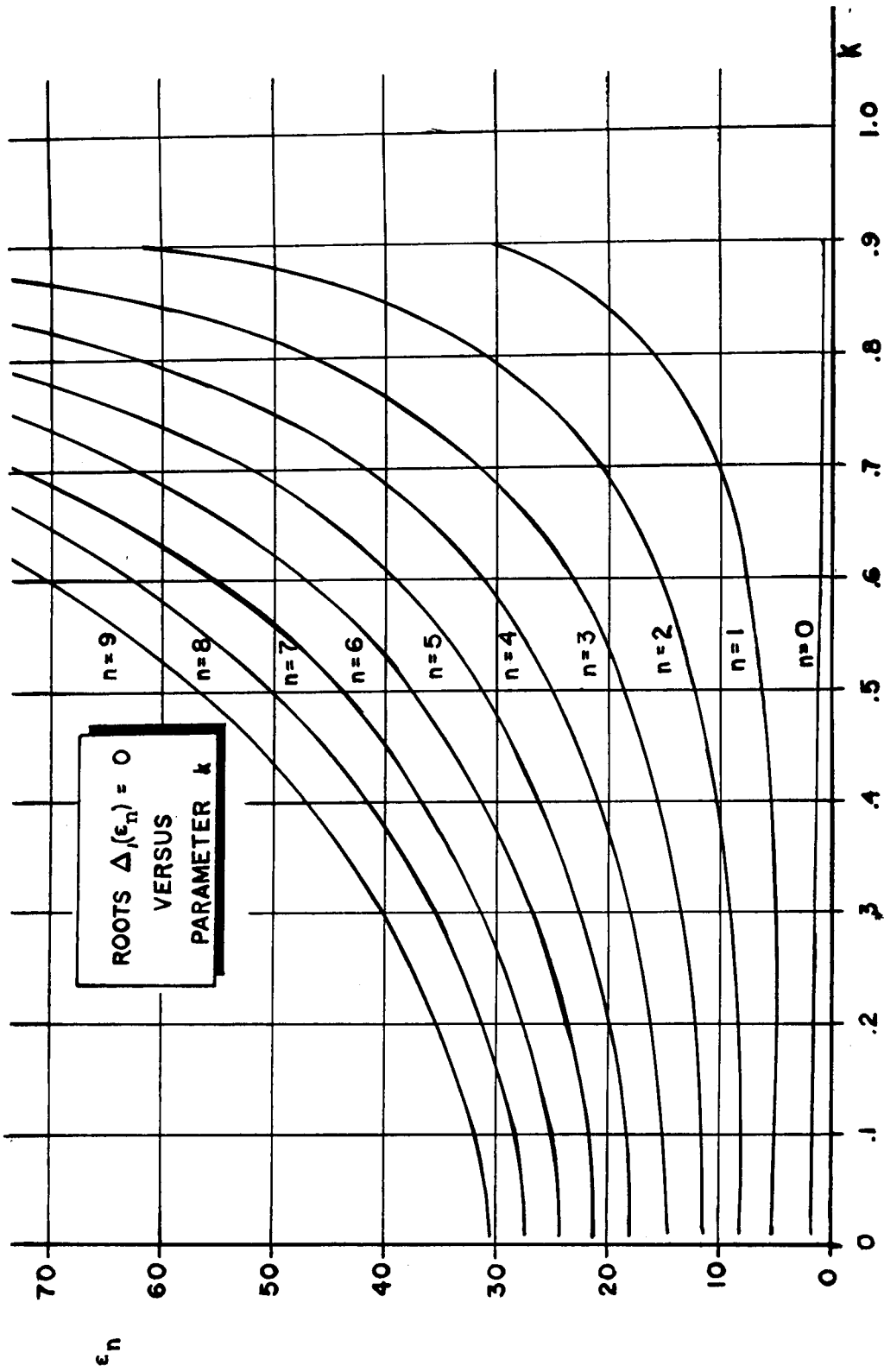


FIGURE A-1

ROOTS ϵ_{mn} ($m=1$) OF $\Delta_1(\epsilon_{mn}) = J_1'(k\epsilon_{mn}) Y_1'(k\epsilon_{mn}) - J_1'(k\epsilon_{mn}) Y_1'(\epsilon_{mn}) = 0$.

TABLE A-1
CONTAINER VELOCITY POTENTIAL FOR CIRCULAR CYLINDRICAL TANK OR DERIVATIVE THEREOF.

Excitation	ϕ_1 - Container Velocity Potential
Translation in the x-direction, $x = x_0 e^{i\omega t}$	$\phi_1 = i\omega r x_0 e^{i\omega t} \cos\phi = i\omega r x \cos\phi$
Translation in the y-direction, $y = y_0 e^{i\omega t}$	$\phi_1 = i\omega r y_0 e^{i\omega t} \sin\phi = i\omega r y \sin\phi$
Pitching about the x-axis, $\chi = \chi_0 e^{i\omega t}$	$\phi_1 = i\omega z \chi_0 e^{i\omega t} \sin\phi = i\omega z \chi \sin\phi$
Pitching about the y-axis, $\theta = \theta_0 e^{i\omega t}$	$\phi_1 = i\omega z \theta_0 e^{i\omega t} \cos\phi = i\omega z \theta \cos\phi$
Roll about the z-axis, $\phi = \phi_0 e^{i\omega t}$	$\phi_1 = i\omega r^2 \phi_0 e^{i\omega t} = i\omega r^2 \phi$

TABLE A-2
CONTAINER VELOCITY POTENTIAL FOR RECTANGULAR TANK.

Excitation	ϕ_1 - Container Velocity Potential
Translation in the x-direction, $x = x_0 \sin\omega t$	$\phi_1 = \omega x x_0 \sin\omega t$
Pitching about the y-axis, $\theta = \theta_0 \sin\omega t$	$\phi_1 = \omega x z \theta_0 \cos\omega t$
Roll about the z-axis, $\phi = \phi_0 \sin\omega t$	$\phi_1 = \omega x y \phi_0 \cos\omega t$

TABLE A-3

ZEROS ϵ_{mn} ($m=1$) OF THE FIRST DERIVATIVE OF THE BESSEL
 FUNCTION OF THE FIRST ORDER AND FIRST KIND [$J_1'(\epsilon_{mn}) = 0$].

n	ϵ_n	n	ϵ_n	n	ϵ_n
0	1.84119	11	36.89000	22	71.45677
1	5.33144	12	40.03341	23	74.60000
2	8.53631	13	43.17665	24	77.74383
3	11.70600	14	46.31957	25	80.88514
4	14.86359	15	49.46238	26	84.02718
5	18.01553	16	52.60507	27	87.16914
6	21.16440	17	55.74758	28	90.31228
7	24.31145	18	58.89000	29	93.45301
8	27.45751	19	62.03234	30	96.59499
9	30.60194	20	65.17465	31	99.73675
10	33.74397	21	68.31682		

TABLE A-4
 ROOTS ϵ_{mn} OF THE FIRST DERIVATIVE OF THE BESSEL
 FUNCTION OF ORDER $2m$ AND OF THE FIRST KIND [$J'_{2m}(\epsilon_{mn}) = 0$].

$\frac{m}{n}$	0	1	2	3	4	5	6	7	8	9
0	3.832	3.054	5.318	8.105	9.648	11.716	13.821	15.917	18.104	20.189
1	7.016	6.706	9.282	11.735	14.115	16.448	18.745	21.015	23.261	25.495
2	10.173	9.969	12.682	15.268	17.774	20.223	22.629	25.002	27.317	29.670
3	13.324	13.170	15.964	18.697	21.229	23.761	26.246	28.694	31.112	33.504
4	16.471	16.348	19.196	21.932	24.587	27.182	29.729	32.237	34.712	37.160
5	19.616	19.513	22.401	25.184	27.889	30.535	33.131	35.689	38.212	40.707
6	22.760	22.672	25.590	28.410	31.155	33.842	36.481	39.079	41.643	44.178
7	25.904	25.826	28.768	31.618	34.397	37.118	39.792	42.426	45.052	47.595
8	29.047	28.978	31.939	34.813	37.620	40.371	43.075	45.740	48.371	50.971
9	32.189	32.127	35.104	38.000	40.830	43.607	46.338	49.030	51.687	54.315

TABLE A-5

ROOTS ϵ_{mn} OF THE FIRST DERIVATIVE OF THE BESSEL FUNCTION
 OF ORDER $4m$ AND OF THE FIRST KIND $[J'_{4m}(\epsilon_{mn}) = 0]$.

	1	3	5
0	5.31756	13.82109	22.26759
1	9.28240	18.74485	27.71172
2	12.68191	22.62927	31.97366
3	15.96411	26.24604	35.87393
4	19.19603	29.72898	39.58453
5	22.40103	33.13145	43.17654

TABLE A-6

ROOTS ϵ_{mn} ($m=1$) OF THE DETERMINANT

$$\Delta_1(\epsilon_{mn}) = J_1'(\epsilon_{mn}) Y_1'(\epsilon_{mn}) - J_1'(\epsilon_{mn}) Y_1'(\epsilon_{mn}) = 0$$

WHERE J_1' AND Y_1' ARE THE FIRST DERIVATIVES OF

THE BESSEL FUNCTIONS OF ORDER 1 AND OF

THE FIRST AND SECOND KIND RESPECTIVELY.

$k \backslash n$	0	.1	.2	.3	.4	.5	.6	.7	.8	.9
0	1.8412	1.8035	1.7051	1.5821	1.4618	1.3547	1.2621	1.2824	1.1134	1.0532
1	5.3314	5.1371	4.9609	5.1374	5.6592	6.5649	8.0411	10.5919	15.7781	31.4470
2	8.5363	8.1992	8.4331	9.3084	10.6834	12.7066	15.8013	21.0041	31.4513	62.8481
3	11.7060	11.3588	12.1650	13.6837	15.8481	18.9427	23.6239	31.4558	47.1504	94.2645
4	14.8636	14.6344	15.9932	18.1159	21.0488	25.2025	31.4632	41.9190	62.8510	125.6750
5	18.0155	17.9864	19.8616	22.5707	26.2641	31.4721	39.3076	52.3845	78.5549	157.0880
6	21.1644	21.3837	23.7502	27.0369	31.4859	37.7459	47.1552	62.8523	94.2601	188.5022
7	24.3114	24.8081	27.6498	31.5092	36.7119	44.0223	55.0047	73.3212	109.9662	219.9170
8	27.4575	28.2497	31.5563	35.9855	41.9403	50.3005	62.8553	83.7910	125.6728	251.3320
9	30.6019	31.7027	35.4675	40.4643	47.1704	56.5797	70.7066	94.2612	141.3797	282.7473

Table A-7. Liquid Displacements

Circular Cylindrical Tank	Excitation: Harmonic Translation and/or Pitching
---------------------------	--

Translation in the x-direction, $x = x_0 e^{i\omega t}$

$$\zeta = \frac{\omega^2}{g} x_0 e^{i\omega t} \cos \phi \left[r + \sum_{n=0}^{\infty} \frac{2a J_1(\rho_n)}{(\epsilon_n^2 - 1)(\eta_n^2 - 1) J_1(\epsilon_n)} \right]$$

Pitching about the y-axis, $\theta = \theta_0 e^{i\omega t}$

$$\zeta = -\omega^2 \theta_0 e^{i\omega t} \cos \phi \left\{ \frac{hr}{2g} + \sum_{n=0}^{\infty} \frac{2a J_1(\rho_n)}{(\epsilon_n^2 - 1)(\eta_n^2 - 1) J_1(\epsilon_n)} \left[\frac{2}{\omega^2 \cosh \kappa_n} + \frac{h}{2g} - \frac{1}{\omega^2} \right] \right\}$$

Table A-8. Liquid Displacements

Quarter-Sector Tank	Excitation: Harmonic Translation and/or Pitching
---------------------	--

Translation in the x-direction, $x = x_0 e^{i\omega t}$

$$\zeta = \frac{\omega^2}{g} x_0 e^{i\omega t} \left[r \cos \phi + \sum_{m=0}^{\infty} \sum_{n=0}^{\infty} \frac{a_m b_{mn} J_{2m}(\rho_{mn}) \cos 2m\phi}{(\eta_{mn}^2 - 1)} \right]$$

Pitching about the y-axis, $\theta = \theta_0 e^{i\omega t}$

$$\zeta = -\frac{\omega^2}{g} \theta_0 e^{i\omega t} \left\{ \frac{hr}{2} \cos \phi - \sum_{m=0}^{\infty} \sum_{n=0}^{\infty} \left[\bar{A}_{mn} \cosh \left(\frac{\kappa_{mn}}{2} \right) + \bar{B}_{mn} \sinh \left(\frac{\kappa_{mn}}{2} \right) \right] J_{2m}(\rho_{mn}) \cos 2m\phi \right\}$$

Table A-9. Liquid Displacements

Quarter-Sectored Tank	Excitation: Harmonic Roll
-----------------------	---------------------------

Roll about the z-axis, $\phi = \phi_0 e^{i\omega t}$

$$\zeta = \frac{\omega^2}{g} \phi_0 e^{i\omega t} \left\{ r^2 \left(\phi - \frac{\pi}{4} \right) + \frac{2r^2}{\pi} \left[\ln \left(\frac{r}{a} \right) + \frac{1}{2} \right] \cos 2\phi \right.$$

$$- \sum_{m=1}^{\infty} \frac{2a^2 \cos [(4m-2)\phi]}{\pi(2m-1)[(2m-1)^2 - 1]} \left[\left(\frac{r}{a} \right)^{4m-2} - \frac{r^2}{a^2(2m-1)} \right] + \sum_{n=0}^{\infty} \frac{(2f_n - e_n) J_2(\rho_n) \cos 2\phi}{\pi(\eta_n^2 - 1)}$$

$$- \sum_{m=1}^{\infty} \sum_{n=0}^{\infty} \frac{2 \left[f_{2m-1,n} - (2m-1) e_{2m-1,n} \right] J_{4m-2}(\rho_{2m-1,n}) \cos [(4m-2)\phi]}{\pi(2m-1) \left[(2m-1)^2 - 1 \right] (\eta_{2m-1,n}^2 - 1)}$$

REFERENCES

1. Chu, W-H., "Free Surface Condition for Sloshing Resulting from Pitching and Some Corrections", ARS Journal, (Nov. 1960), 1093-1094.
2. Schmitt, A. F., "Forced Oscillations of a Fluid in a Cylindrical Tank Oscillating in a Carried Acceleration Field--A Correction", Convair Rep. ZU-7-074, (Feb. 1957).
3. Bauer, H. F., "Theory of Fluid Oscillations in Partially Filled Cylindrical Containers", MSFC, Rept. No. MTP-AERO-62-1, (Jan. 1962).
4. -----, "Fluid Oscillations in the Containers of a Space Vehicle and their Influence Upon Stability", NASA-TR R-187.
5. Chu, W., "Sloshing of Liquids in Cylindrical Tanks of Elliptic Cross-Section", Southwest Research Institute, Technical Report No. 2, Contract DA-23-072-ORD-1251, (Sept. 1958).
6. Okhotsimskii, D. E., "Theory of the Motion of a Body with Cavities Partly Filled with a Liquid", NASA-TT, No. F-33, (May 1960)--
Translated from Prikladnaia Matematika: Makhanika, Vol. 20, No. 1, (Jan.-Feb. 1956).
7. Bauer, H. F., "The Moment of Inertia of a Liquid in a Circular Cylindrical Tank", ABMA Report No. DA-TR-5-58, (April 23, 1958).
8. Zhukovskii, N. E., The Motion of a Rigid Body with Cavities Filled with a Homogeneous Flowing Liquid. Collected Works (in Russian) (Gostekhizdat, M.-L., 1949), Vol. II. Translated by Consultants Custom Translations, Inc., 227 West 17th Street, New York 11, N.Y.
9. Lamb, H., Hydrodynamics. Sixth ed., Dover Publications, 1945.
10. Rayleigh, Lord, "On Waves", Phil. Mag., Series 5, Vol. 1, (1876) Seite 257-279.
11. Bauer, H. F., "Fluid Oscillations in a Circular Cylindrical Tank", ABMA Report No. DA-TR-1-58, (April 18, 1958).
12. Eulitz, W., "The Sloshing Phenomenon and the Mechanism of a Liquid in Motion in an Oscillating Missile Container", Rep. No. DS-R-31, DOD, ABMA, (Oct. 1957).
13. Abramson, H. N., and Ransleben, G. E., Jr., "Simulation of Fuel Sloshing Characteristics in Missile Tanks by Use of Small Models", Tech. Rep. No. 3, Contract DA-23-072-ORD-1251, SWRI, (March 1959).
14. -----, "Some Comparisons of Sloshing Behavior in Cylindrical Tanks with Flat and Conical Bottoms", Tech. Rep. No. 4, Contract No. DA-23-072-ORD-1251, SWRI, (May 1959).

15. -----., "A Note on Wall Pressure Distributions During Sloshing in Rigid Tanks", Tech. Rep. No. 5, Contract No. DA-23-072-ORD-1251, SWRI, (June 1959).
16. McCarty, J. L. and Stephens, D. G., "Investigation of the Natural Frequencies of Fluids in Spherical and Cylindrical Tanks", Langley Research Center, NASA-TN, D-252, (May 1960).
17. Abramson, H. N., Chu, W. H., Ransleben, G. E., Jr., and Squire, W., "A Theoretical and Experimental Study of Fuel Sloshing", Quarterly Progress Report No. 8, Contract No. DA-23-072-ORD-1251, SWRI, (May 1960).
18. Koelle, H. H., Editor-In-Chief, Handbook of Astronautical Engineering. McGraw-Hill Book Co., Inc., New York, N.Y., 1961.
19. Bauer, H. F., "Theoretical Investigation of Propellant Sloshing in a Circular Cylindrical Ring Tank", ABMA, Quarterly Report No. 1, Redstone Arsenal, Alabama, (Dec. 20, 1959).
20. Lorell, J., "Forces Produced by Fuel Oscillations", Progress Report No. 20-149, Jet Propulsion Laboratory, (October 16, 1951).
21. Abramson, N. H., and Ransleben, G. E., Jr., "Liquid Sloshing in Rigid Cylindrical Tanks Undergoing Pitching Motions", SWRI, Technical Report No. 11, Contract No. DA-23-072-ORD-1251, (May 1, 1961).
22. Hutton, R. E., "Fluid Particle Motion During Rotary Sloshing", Space Technology Laboratories, Inc., (March 1963).
23. -----., "An Investigation of Resonant, Nonlinear Nonplanar Free-Surface Oscillation of a Fluid", Ph.D. Dissertation, University of California, Los Angeles, California, (October 1962).
24. Miles, J. W., "Free Surface Oscillations in a Rotating Liquid", The Physics of Fluids, Vol. 2 (1959), 297-305.
25. Miles, J. W. and Troesch, B. A., "Surface Oscillations of a Rotating Liquid", Journal of Applied Mechanics, (December 1961).
26. Bauer, H. F., "Fluid Oscillations of a Circular Cylindrical Tank Performing Lissajons-Oscillations", ABMA-TR, Huntsville, Alabama, (April 18, 1958).
27. -----., "Fluid Oscillations in a Cylindrical Tank with Damping", ABMA-TR, Huntsville, Alabama, (April 23, 1958).
28. Miles, J. W., "Ring Damping of Free Surface Oscillations in a Circular Tank", Journal of Applied Mechanics, (June 1958).
29. Bauer, H. F., "Tables and Graphs of Zeros of Cross Product Bessel Functions", MSFC Report No. MTP-AERO-63-50, (June 24, 1963).

30. Langner, C. G., "A Preliminary Analysis for Optimum Design of Ring and Partition Antislosh Baffles", SWRI, Tech. Rept. No. 7, Contract No. NAS8-1555, Project No. 6-1072-2, (April 30, 1963).
31. Bauer, H. F., "The Damping Factor Provided by Flat Annular Ring Baffles for Free Fluid Surface Oscillations", MSFC, Rept. No. MTP-AERO-62-81, (Nov. 13, 1962).
32. Garza, L. R. and Abramson, N. H., "Measurements of Liquid Damping Provided by Ring Baffles in Cylindrical Tanks", SWRI, Tech. Rept. No. 5, Contract No. NAS8-1555, Project No. 6-1072-2, (April 1, 1963).
33. O'Neill, J. P., "Semiannual Report on Experimental Investigation of Sloshing", TR-59-0000-00713, Space Tech. Labs., Inc., (Jan. 1-June 30, 1959).
34. Abramson, H. N., Garza, L. R., and Kana, D. D., "Fuel Sloshing Studies", SWRI, Quarterly Progress Rept. No. 3, Contract No. NAS8-1555, (Jan. 1, 1962).
35. Silveira, M. A., Stephens, D. G., and Leonard, H. W., "An Experimental Investigation of the Damping of Liquid Oscillations in Cylindrical Tanks with Various Baffles", NASA TND-715, Langley Research Center, (May 1961).
36. Abramson, H. N. and Ransleben, G. E., Jr., "Some Studies of a Floating Lid Type Device for Suppression of Liquid Sloshing in Rigid Cylindrical Tanks", SWRI, Tech. Rept. No. 10, Contract No. DA-23-072-ORD-1251.
37. -----, "A Note on the Effectiveness of Two Types of Slosh Suppression Devices", SWRI, Tech. Rept. No. 6, Contract No. DA-23-072-ORD-1251, (June 15, 1959).
38. Garza, L. R., "A Brief Comparison of Ring and Asymmetrical Baffle Characteristics", SWRI, Tech. Rept. No. 6, Contract No. NAS8-1555, (April 15, 1963).
39. Cole, H. A., Jr., and Gambucci, B. J., "Tests of an Asymmetrical Baffle for Fuel-Sloshing Suppression", NASA TN D-1036, (July 1961).
40. Eulitz, Dr. W., "A Can-Type Anti-Slosh Device Derived from Basic Slosh Studies", ABMA, D.O.D. Rept. No. D SD-TR-4-58, Redstone Arsenal, Alabama, (August 12, 1958).
41. Cole, H. A., Jr., and Gambucci, B. J., "Measured Two-Dimensional Damping Effectiveness of Fuel-Sloshing Baffles Applied to Ring Baffles in Cylindrical Tanks", NASA-TN-D-694, Ames Research Center, Moffett Field, Calif., (Feb. 1961).

42. Eulitz, W. R., and Beduerftig, H., "Experimental Investigation of the Responses of a Liquid in an Oscillating Container", Office of Ordnance Research, Proceedings of the Third Conference on the Design of Experiments in Army Research Development and Testing, Duke Station, Durham, North Carolina, (1958).
43. Kachigan, K., "Forced Oscillations of a Fluid in a Cylindrical Tank", Convair Rept. ZU-7-046, (Oct. 1955).
44. Schmitt, A. F., "Forced Oscillations of a Fluid in a Cylindrical Tank Undergoing Translation and Rotation", Convair Rept. ZU-7-069, (Oct. 1956).
45. Miles, J. W., "On the Sloshing of Liquid in a Cylindrical Tank", Ramo-Wooldridge Rept. AM6-5, (April 1956).
46. Abramson, N. H., Chu, W-H., and Ransleben, G. E., Jr., "Representation of Fuel Sloshing in Cylindrical Tanks by an Equivalent Mechanical Model", SWRI, Tech. Rept. No. 8, Contract No. DA-23-072-ORD-1251, (June 30, 1960).
47. Abramson, H. N., and Ransleben, G. E., Jr., "Simulation of Fuel Sloshing Characteristics in Missile Tanks by Use of Models", SWRI, Tech. Rept. No. 7, Contract No. DA-23-072-ORD-1251, (April 25, 1960).
48. Buckingham, E., "Model Experiments and the Form of Empirical Equations", Trans. ASME, Vol. 37, (1915), 263-296.
49. Bauer, H. E., "Mechanical Model of Fluid Oscillations in Cylindrical Containers and Introduction of Damping", MSFC, MTP-AERO-62-16, (February 26, 1962).
50. Abramson, H. N., Martin, R. J., and Ransleben, G. E., Jr., "Application of Similitude Theory to the Problem of Fuel Sloshing in Rigid Tanks", SWRI, Tech. Rept. No. 1, Contract No. DA-23-072-ORD-1251, (May 23, 1958).
51. Scanlan, R. H., and Mendelson, A., "Structural Damping", AIAA Journal, Vol. 1, No. 4, (April 1963).
52. Bauer, H. E., "Mechanical Analogy of Fluid Oscillations in Cylindrical Tanks with Circular and Annular Cross Sections", MSFC, MTP AERO-61-4, Huntsville, Alabama, (January 12, 1961).
53. Miles, J. W., "Stability of Forced Oscillations of a Spherical Pendulum", Quarterly of Applied Mathematics, (1962); also, Space Tech. Labs., No. EM 11-2, (March 1960).
54. Stephens, D. G., and Leonard, H. W., "The Coupled Dynamic Response of a Tank Partially Filled with a Liquid and Undergoing Free and Forced Planar Oscillations", NASA TN, D-1945, Langley Research Center, (August 1963).

55. Abramson, H. N., Garza, L. R., and Kana, D. D., "Fuel Sloshing Studies", SWRI, Quarterly Progress Report No. 2, Contract No. NAS8-1555, (Oct. 1, 1961).
56. -----, "Fuel Sloshing Studies", SWRI, Quarterly Progress Rept. No. 1, Contract No. NAS8-1555, (July 1, 1961).
57. Abramson, H. N., and Ranselben, G. E., Jr., "Total Force Response Resulting from Liquid Sloshing in a Rigid Cylindrical Tank with a Vertical Center Wall Baffle", SWRI, Tech. Rept. No. 9, Contract No. DA-23-072-ORD-1251, (May 1, 1961).
58. Garza, L. R., "Measurements of Liquid Natural Frequencies and Damping in Compartmented Cylindrical Tanks", SWRI, Tech. Rept. No. 8, Contract No. NAS8-1555, (Feb. 5, 1964).
59. Bowman, F., Introduction to Bessel Functions. New York: Dover Publications.
60. Walls, J., Ryan, J., and Mooney, J., "Torsional Pendulum Analogy for Quarter and Eighth Sectored Cylindrical Tanks Subjected to Roll Oscillation", Northrop Space Labs., Tech. Memo. No. 9, (Feb. 21, 1964).
61. Abramson, H. N., Garza, L. R., and Kana, D. D., "Some Notes on Liquid Sloshing in Compartmented Cylindrical Tanks", SWRI, Tech. Rept. No. 1, Contract No. NAS8-1555, (Feb. 15, 1962); also, ARS Journal, (June 1962).
62. Abramson, H. N., Chu, W., and Garza, L. R., "Liquid Sloshing in 45° Sector Compartmented Cylindrical Tanks", SWRI, Tech. Rept. No. 3, (Nov. 1, 1962).
63. Bauer, H. F., "Theory of the Fluid Oscillations in a Circular Cylindrical Ring Tank Partially Filled with Liquid", NASA-TN-D557, (Dec. 1960).
64. Mooney, J., Ryan, J., and Walls, J., "Slosh Handbook", NSL Tech. Memo. No. 10, (Feb. 21, 1964).
65. Mooney, J., Walls, J., and Ryan, J., "Liquid Natural Frequencies of a Tank with Partially Submerged Sector Walls", NSL Tech. Memo. No. 14, (April 7, 1964).
66. Bauer, H. F., "The Effective Moment of Inertia in Roll of Propellant and Roll Damping", ABMA Report DA-TM-67-59.
67. -----, "Propellant Sloshing", Rept. No. DA-TR-18-58, C-AB-71091, Dev. Operations Div., Army Ballistic Missile Agency, Redstone Arsenal, Alabama, (Nov. 5, 1958).
68. Ransleben, G. E., Jr., "A Theoretical and Experimental Study of Fuel Sloshing", Progress Rept. No. 1, Contract DA-23-072-ORD-1251, Southwest Research Institute, (May 1, 1958).

69. Keulegan, G. H., and Carpenter, L. H., "Forces on Cylinders and Plates in an Oscillating Fluid", National Bureau of Standards, Report No. 4821, (Sept. 5, 1956).
70. Brown, J., "Laboratory Test of Fuel Sloshing", Rept. No. SM-Dev. 783, Douglas Aircraft Co., Inc.
71. Case, K. and Parkinson, W. C., "The Damping of a Liquid in a Right Circular Cylindrical Tank", Ramo-Wooldridge Rept. GM 45-75, (Sept. 1956).
72. Howell, E., and Ehler, F. G., "Experimental Investigation of the Influence of Mechanical Baffles on the Fundamental Sloshing Mode of Water in a Cylindrical Tank", Ramo-Wooldridge Rept. GM 45, 3-87, GM-TR-69, (July 1956).
73. Langhaar, H. S., Dimensional Analysis and Theory of Models. John Wiley, 1953.
74. Epperson, T. B., Pengelley, C. D., Ransleben, G. E., Jr., Wilson, L. E., and Younger, D. G., "Nonstationary Airload Distributions on a Straight, Flexible Wing Oscillating in a Subsonic Wing Stream", (Title Unclassified), WADC TR-55-323, (January 1956).
75. Mooney, J., Basurto, E., Kincaid, J., Ryan, J., and Walls, J., "Slosh Handbook", Progress Report No. 2, Northrop Space Labs., Tech. Memo No. 18, (May 25, 1964).
76. Graham, E. W., "The Forces Produced by Fuel Oscillation in a Rectangular Tank", Douglas Aircraft Company, Inc., Report No. SM-13748, (April 1951).
77. Lorell, J., "Forces Produced by Fuel Oscillations", Jet Propulsion Laboratory, Progress Report No. 20-149, Contract No. DA-04-495-Ord 18, (October 1951).
78. Graham, E. W., and Rodriguez, A. M., "The Characteristics of Fuel Motion which Affect Airplane Dynamics", Douglas Aircraft Company, Inc., Report No. SM-14212, (November 1951).
79. Luskin, H., and Lapin, E., "An Analytical Approach to the Fuel Sloshing and Buffeting Problems of Aircraft", Journal of the Aeronautical Sciences, (April 1952).
80. Cooper, R. M., "Dynamics of Liquids in Moving Containers", ARS Journal, (August 1960).
81. Lawrence, H. R., Wang, C. J., and Reddy, R. B., "Variational Solution of Fuel Sloshing Modes", Jet Propulsion, (November 1958).
82. Ring, E., Rocket Propellant and Pressurization Systems. Prentice-Hall, Inc., Englewood Cliffs, N. J., 1964.

83. Liu, F. C., "Pressure on Baffle Rings due to Fuel Sloshing in a Cylindrical Tank", MSFC, R-AERO-4-64, Huntsville, Alabama, (January 17, 1964).
84. O'Neill, J. P., "Final Report on an Experimental Investigation of Sloshing", STL/TR-59-0000-09960, Contract No. AF-04(647)-309, (March 4, 1960).